A multi-proxy palaeoenvironmental reconstruction from sediment cores, offshore Iran – natural hazards and climatic change within the Late Holocene

A thesis submitted for the degree of

Master of Philosophy

July 2010

Charlotte S. Miller

BSc. Hons (University of Leeds)

Supervised by: Prof. Suzanne Leroy & Dr Philip Collins

Institute for the Environment, Brunel University, Kingston Lane, Uxbridge, West London, UB8 3PH

Abstract

During the last millennia, North African and Arabian palaeoclimatic records indicate a number of important climatic transitions. As a direct consequence, terrestrial ecosystems experienced significant changes. Although palaeoenvironmental records do exist in proximity to the north-western Arabian Sea, they remain sparse and provide little insight into environmental and climatic change of this region during the Late Holocene (the dating here is from 2300 cal. yr BP to present). Additionally, the north-western Arabian Sea is prone to natural disasters including recent cyclones and tsunamis such as the Makran tsunami, 1945 and Cyclone Gonu, 2007, which may leave a signal in the sediment.

This thesis presents the results of detailed pollen and dinoflagellate cyst analysis in concert with a range of sedimentological techniques from sediment cores recovered from southern Iran (Chabahar Bay, Sea of Oman, Iran, 25° 20'N, 60° 30'E).

The data reveal the patterns of vegetation and oceanographic response to climatic change during the Late Holocene in the north-western Arabian Sea. Zonation on pollen and dinoflagellate results divides the last 2300 years into three distinct climatic phases: a wet period (2300 - 1830 cal. yr BP), a dry period (1830 - 1500 cal. yr BP) and a wet period (1500 - 120 cal. yr BP). The wet period (2300 - 1830 cal. yr BP) corresponds with well-known phases of intensive agriculture, including the Sassanid Period. The dry period (1830 – 1500 cal. yr BP) corresponds well with the end of the Beyşehir occupation phase in southern Turkey. Moreover, an abrupt event is preserved in a single core and is dated at AD <1808. Palynological evidence constrains the source of the sediment to be inner-continental but not of coastal origin, with a fluvial flood being the most likely mechanism of transportation.

Acknowledgements

Contents page

List of figures

List of tables

List of equations

1. Introduction

In the northern Arabian Sea, tsunamis, cyclones and coastal storms are known historically to have had shattering effects on local population centres. However, the absence of *a posteriori* evidence means that the recurrence times of these events remain unclear. Numerous historical records are available but, due to the biases involved in subjective human observations, the need for palaeo-tsunami research in this region is clear. In the northern Arabian Sea, palaeo-event records (*e.g.* Brookfield *et al.*, 2006; Donato *et al.*, 2009) reveal the preservation of distinct events. However the pattern of events over time has never been recorded from an oceanic record.

In regions depending on monsoonal rains for agriculture, small climatic changes may easily affect large numbers of people. Globally, marine records provide detailed information on the behaviour of both ocean and terrestrial systems. Previous studies have shown that pollen and dinoflagellate cyst analysis of well-dated continental and marine records allow the reconstruction of past environmental conditions on the continents (Hooghiemstra and Agwu, 1988; Lézine and Hooghiemstra, 1990; Gasse and Van Campo, 2001). Prior to this study no record existed which provided evidence of the terrestrial response to global climate change from sediment taken along the southern Iranian coastline (in the Baluchistan Province of Iran), the region selected for this study.

Rapid economic growth on the Makran coastline consequently brings population increase. In addition, in 2006 93% of all oil exported from the Persian Gulf was transported by oil tanker through this area as there are few alternative routes and most of these are closed due to geopolitical or economic concerns in the region. The area's crucial location means that it is becoming increasingly necessary to assess palaeoclimatic and environmental change within the region, as well as to reconstruct palaeo-events.

The aims of this project are therefore twofold; to reconstruct the effects of tsunami and storms in the northern Arabian Sea and to provide insight into the ocean and vegetation response to global climate change along the southern Iranian coastline in the Late Holocene. Five cores were taken offshore Iran (Fig. 1.1), of which, two were selected for further study using fossil pollen and dinoflagellate cyst analysis plus grain-size investigations to provide insight into

the effects of past tsunami and cyclones on the Makran coastline and to assess both vegetation and oceanographic changes (salinity, temperature, upwelling strength) over the last 2300 cal. yr BP.
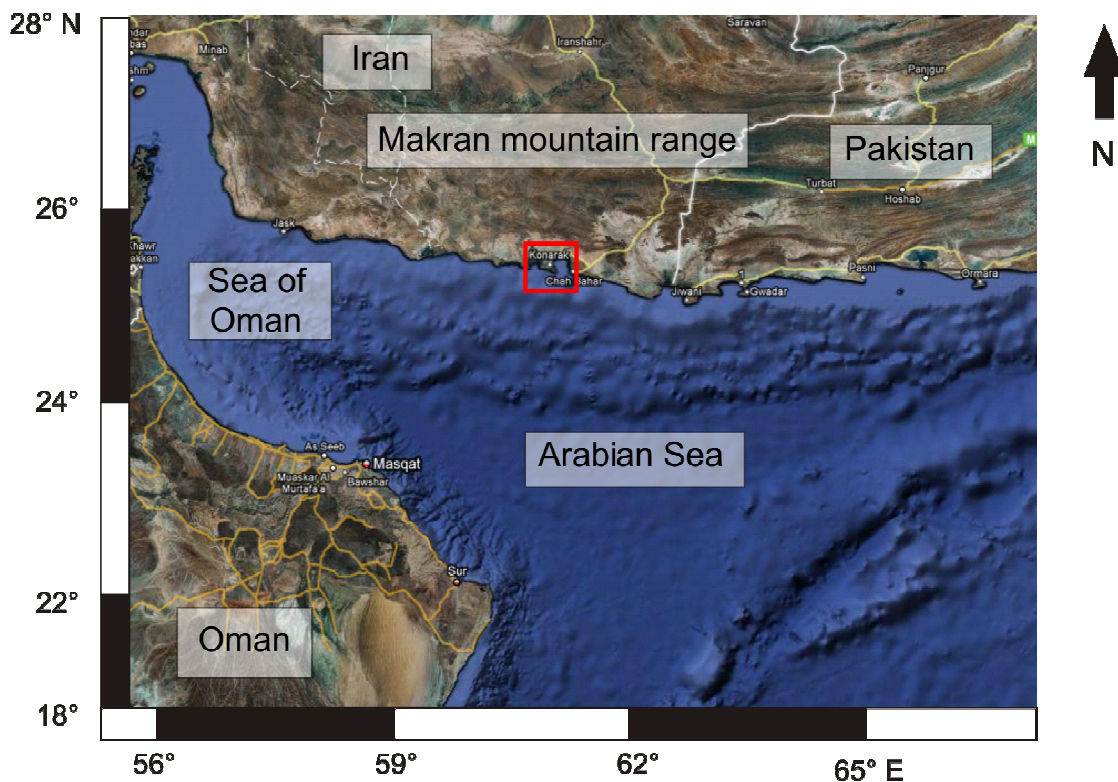
Fig. 1.1. Location of study region along the Makran coastline, southern Iran (Google Earth Image). Red box highlights the study region.

1.1 Tsunamis, cyclones and coastal storms

Tsunamis, cyclones and coastal storms are amongst the most devastating and frequent events to affect population centres and economic infrastructures. Although these events are short-lived, they often cause death and destruction, especially in low-lying coastal regions.

Recent catastrophic tsunamis, such as that of the Indian Ocean (Sumatra-Andaman) in 2004 where 237,000 people lost their lives and in Papua New Guinea in 1998 (McSaveney *et al.*, 2000) where over 2000 people died, have focused scientific attention on ways to predict the frequency, intensity and possible effects of these future disastrous events. Cyclone Gonu (2007), the strongest tropical cyclone on record in the Oman Sea, caused $4 billion in damages and nearly 50 deaths in Oman (Fritz *et al.*, 2010). It then went on to affect Iran where flooding caused 23 deaths and $215 million in damage (Fritz *et*

al., 2010). To derive the frequency and intensity of these events requires extending the historical record back using palaeo-event analysis within the stratigraphic record.

Over the recent years much research has focused on distinguishing tsunami and storm deposits in the geological record (Kortekaas, 2002; Tappin, 2007; Morton *et al.*, 2007; Dawson and Stewart 2007; Kortekaas and Dawson, 2007). Tsunami events are well documented from recent times but looking back in the geological record they are seldom described. There are two explanations for this obvious rarity of tsunami deposits in the geological record put forward by Dawson and Stewart (2007). Firstly the evidence may indicate a tendency for tsunami deposits to be easily eroded as they typically affect regions which undergo constant reworking for example floodplains, coastal regions and submarine canyons (Einsele *et al.*, 1996; Clifton, 1998; Dawson and Stewart, 2007). Secondly, tsunami deposits may have geological characteristics which are similar to those produced by other high energy phenomena (Shiki, 1996; Shiki *et al.*, 2000; Dawson and Stewart, 2007). This problematic issue requires additional sedimentary evidence from recent tsunamites in the stratigraphic record.

The growing body of literature concerning tsunamites and tempestites criteria including grain size, grading, deposit thickness and number of beds will be used to distinguish the event horizons in the marine cores. Tsunami and storm deposits are simple to differentiate when the depositional features are for very extreme events such as the emplacement of mega-blocks where a tsunami is the most likely explanation. The study of mega-blocks emplaced by tsunami may be achievable east of Chabahar Bay where caves are located offshore. However, in some regions, for example Chabahar Bay and the surrounding coastline, the material available for reworking is restricted to sand and silts which makes the deposits produced by high energy events difficult to differentiate without some *a priori* evidence (Morton *et al.*, 2007).

The southern Iranian coastline has been affected by numerous historical natural disasters in the recent past both in terms of tsunamis and tropical cyclones. Previous studies in the vicinity on the coasts of Pakistan and Oman have highlighted the preservation potential and occurrence of tsunami and storm deposits both in recent times and in the geological past (Brookfield *et al.*, 2006;

Donato *et al.*, 2009), therefore it is possible that tsunami and storm deposits may also be preserved in the sediment cores taken offshore southern Iran.

1.2 Past vegetation, dinoflagellate cysts and climate change

Past climate change is mainly the result of variations in the Earth's orbital parameters, feedbacks and on longer scales, tectonic activity (Zachos *et al.*, 2001). The earth has experienced continuous climatic change moving from extremes of ice-free polar regions to extensive continental ice-sheet build up. The majority of the high-frequency change in climate is caused by oscillations in the earth's orbital parameters, eccentricity, obliquity and precession that affect the distribution and amount of incident solar energy (Zachos *et al.*, 2001). A comprehensive understanding of the factors controlling climate change of the recent geological past is crucial as knowledge of how the earth's environment has transformed the heat input from the sun into climate variations will assist in the prediction of future global climate change. Of particular importance in the tropics are shifts in the latitudinal position of the intertropical convergence zone (ITCZ). The position of the ITCZ is controlled by the amount of incoming solar radiation and has been associated with climate variability in both Africa and Asia (Dupont *et al.*, 2008).

Vegetation in the tropics is very sensitive to precipitation change both in terms of the amount and distribution (Arens, 2001; Hoek, 2001; Shichi *et al.*, 2007; Zhao *et al.*, 2009; Bonnefille, 2010). Increases in the frequency, duration and severity of drought are well known to alter the structure, composition and biogeography of vegetation in many regions not only in the tropics, but globally (Allen *et al.*, 2010). Fluctuations in climate can affect not only the terrestrial but also the oceanographic systems. Investigation of ocean sediments for their dinoflagellate cyst assemblages can be used to provide evidence for the palaeo-environmental characteristics of the overlying water column, in terms of salinity, pH and oxygen content, possibly indicating changes in monsoonal strength and associated upwelling intensity.

1.3 Research objectives

A review of the literature highlighted several gaps in the current knowledge, such as:

1. The impact of past tsunamis and storms is unknown on the southern Iranian coastline
2. Late Holocene vegetation change along the southern Iranian coast is unknown

The palaeoenvironmental history of the southern Iranian coastline is poorly understood, possibly associated with political tensions in Iran resulting in a lack of adequate records available for palaeoenvironmental study. Access to sediment cores off southern Iran make it possible in this project to advance the understanding of past environmental change in present day arid systems.

Specific scientific aims:

1. To use published literature to assess whether tsunamis and/or cyclonic storms have had an effect on sediment accumulation in Chabahar Bay in the late Holocene.
2. To correlate any abrupt marine events found in the cores with events found in historical archival data.
3. To reconstruct the vegetation history of the region over the late Holocene, using pollen analysis and a range of sedimentological techniques.
4. To reconstruct the oceanographic history (upwelling intensity fluctuations) of the region over the late Holocene, using dinoflagellate cyst analysis and a range of sedimentological techniques.
5. To relate the palaeoenvironmental implications of this thesis to wider-scale studies.

1.4 Thesis structure

Following this introduction chapter there are six further chapters. In chapter 2, the background and study region are discussed. The background includes the geography and present day environmental conditions (including atmospheric and oceanic circulation and current day climatic settings). The geology of the region and how this generates earthquakes is presented as well as the historical record of

earthquakes and tsunamis in the Makran region. The mechanism of cyclone generation is examined in addition to historical records within the Arabian Sea. Additionally, present day vegetation and palaeoenvironmental change since the end of the Holocene Humid Period are stated as well as key phases of human occupation. Chapter 3 contains information on the practical methodology used in this investigation. Each method is discussed individually, giving information on the technique and equipment used. The results are presented in chapter 4. The results are comprised of stratigraphy and core description, the Iranian National Centre for Oceanography (INCO) data, magnetic susceptibility, grain-size and geochemistry results. The chronological profiles of ^{210}Pb and radiocarbon dating are presented in addition to pollen and dinoflagellate cyst data for two cores, OS55 and OS73. Chapter 5 contains an interpretation of the results presented. Chapter 6 discusses the results and compares the findings of this study with the wider literature. Finally, chapter 7 summarises the major findings and assesses how well the thesis has met the original research objectives and aims of the study. Potential areas for further study are also discussed.

2. Study region

In chapter 1 it was established that it is important to derive an accurate palaeoenvironmental reconstruction of the southern Iranian coastline. This section investigates the suitability of the coring region, Chabahar Bay, southern Iran (Fig. 1.1; 2.1) for such a study. The section begins by explaining the significance of Chabahar Bay and its geographical location. The tectonics of the region and consequent tsunami are then discussed. Atmospheric and oceanic circulation of the northern Arabian Sea is explained and how this gives rise to the production of cyclones in the region. Historical tsunami and cyclones and their probability of occurrence are then critically examined. The section then details the present day vegetation and palaeoenvironmental change from the end of the Holocene humid period to present. The section ends by stating the key phases of human occupation over the last 2300 cal. yr BP.

2.1 The significance of Chabahar Bay (Baluchistan Province, southern Iran)

The study area was selected because of its significance in terms of industry and trade in Iran. Since Chabahar Bay was declared a free-trade zone in 1992, it has undergone rapid economic growth (Pak and Farajzadeh, 2007). It is also the closest and best access point of Iran to the Indian Ocean. Large economic sectors of fishing and commercial industries exist in the port of Chabahar, compared to the rest of the relatively unpopulated southern coast of Iran. Through the development of transit routes to countries situated around the Indian Ocean and in central Asia, Chabahar has become the focal point of the south of the country. Identifying the frequency and intensity of past natural disasters in the region is crucial in terms of Chabahar's future development. The assessment of tsunami, cyclone frequency and/or extraordinary monsoonal rains and their consequences is becoming increasingly necessary as little has been done relating to disaster research in the region.

Additionally, the Arabian Sea region was selected for study because it experiences a monsoonal climatic regime, with people depending on rainfall to develop essential irrigation infrastructure for agriculture. In addition, the reversing monsoons generate upwelling. Unusually high seasonal primary productivity in the

ocean makes it an ideal locality for dinoflagellate cyst analysis (Quasim, 1982; Sen Gupta and Naqvi, 1984; Cowie and Levin, 2009). The export of organic debris to depth combined with limited deep water ventilation (Wyrtki, 1973; Cowie and Levin, 2009) result in well preserved pollen and dinoflagellate cyst assemblages and laminations with little evidence of bioturbation from benthic organisms. Good pollen and dinoflagellate preservation will help assess changes in sedimentation rate for palaeoevent reconstruction and also help elucidate changes in palaeoclimatic/environmental conditions.

2.2 Geographical location

Pozm and Chabahar Bays are found on the coast of the Baluchistan province in SE Iran (Fig. 1.1), north of the Arabian Sea (latitude 25.348, longitude 60.253). Both Pozm and Chabahar (Fig. 1.1 and 2.1) are situated on the narrow semi-desert Makran coastline. The coastline consists of low-lying alluvial plains which then rise quickly into the Makran mountain range (Fig. 2.2), trending east-west parallel to the Iranian coastline (Page *et al*., 1979). The Makran region is a 1000 km section of the Eurasian-Arabian plate boundary, where continental-oceanic collision has caused uplift of around 1800 m and in a small number of places to over 2400 m. This continuous consumption of the oceanic crust since the Early Cretaceous along the northerly dipping subduction zone has caused the topography seen in Iran, Pakistan, India and Afghanistan today (Fig. 2.2). The Makran coastline stretches from the Strait of Hormuz in Iran to the Indus River in Pakistan (Page *et al.,* 1979).

The Makran coastal plains are 5-20 km wide and occur where the ephemeral streams have eroded into the siltstone and claystone bedrock of the area (Page *et al.*, 1979). Locally the coastal plains are covered over by sand dunes. The Makran coast consists of uplifted terraces and at least nine of these have been preserved on the south side of Konarak headland (Fig. 2.3). The headland separates Pozm and Chabahar Bays and is connected to the mainland by a tombolo (Page *et al.*, 1979). The terraces on Konarak are associated with wavecut platforms (which have subsequently been covered by marine coquina), sandstones, wave-cut cliffs, boulder breccias and swash troughs.
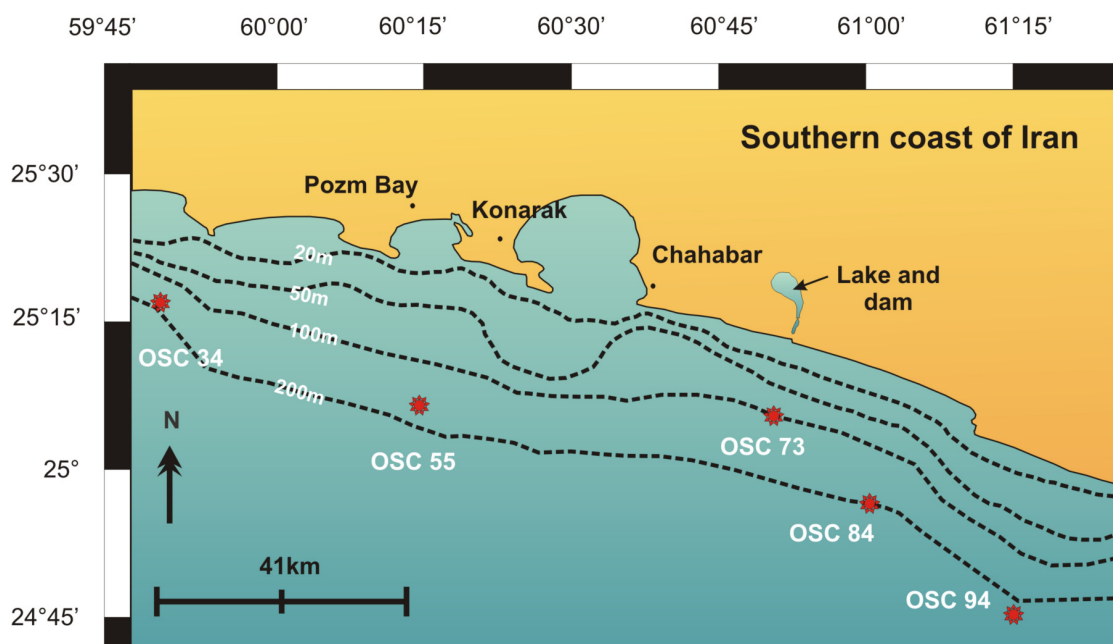
Fig. 2.1. Location and bathymetry of Oman Sea Cores taken offshore southern Iran.
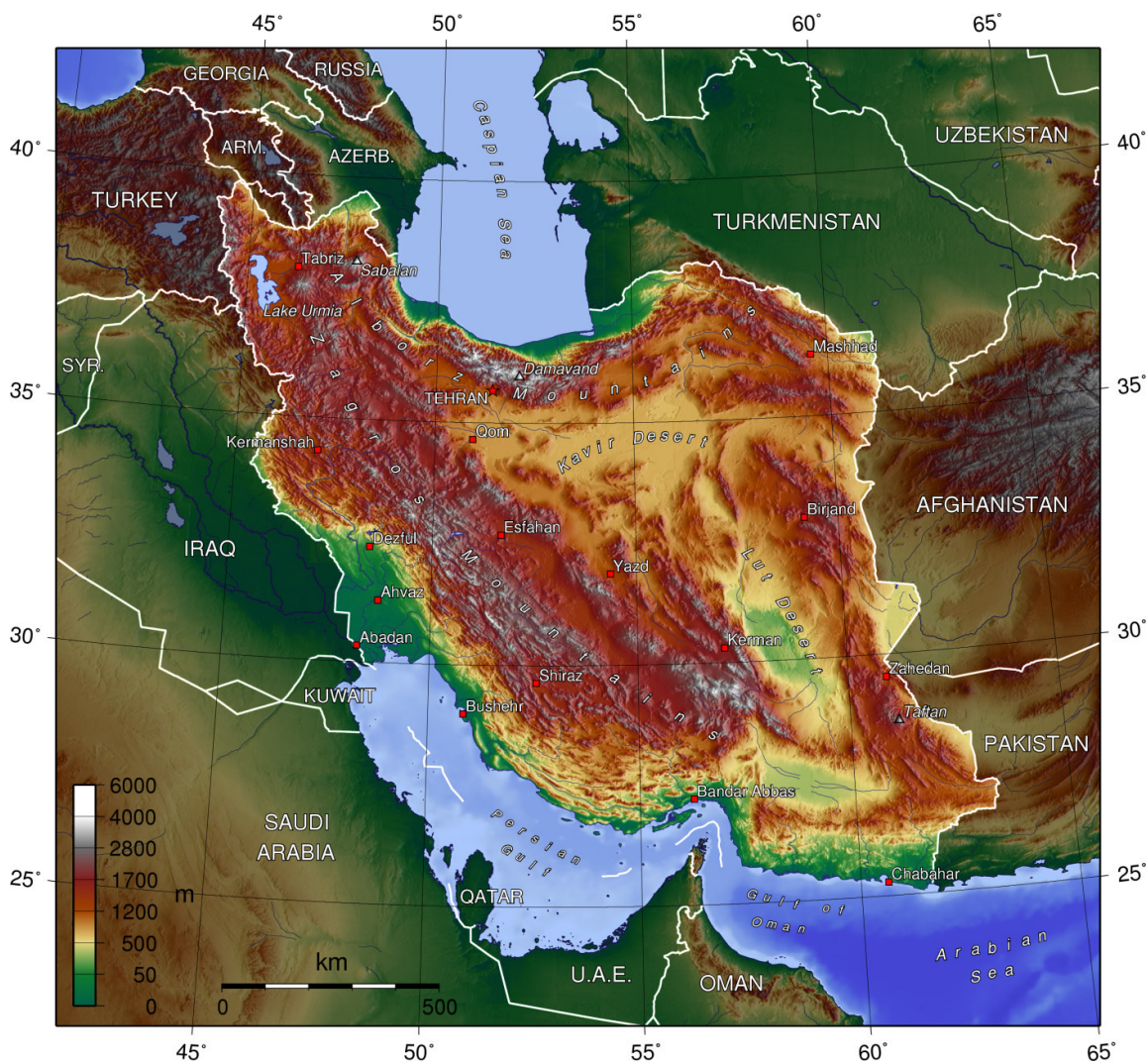
Fig. 2.2. Topographic relief of Iran (Generic Mapping Tools: http://gmt.soest.hawaii.edu/)
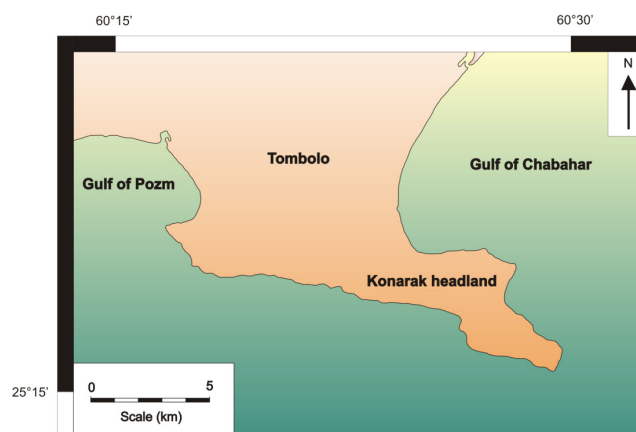
Fig. 2.3. Map of Konarak headland and tombolo, separating Pozm and Chabahar Bay (Modified from Page *et al*., 1979).

2.3 Geology

The Makran mountain range forms the leading region of crustal deformation along the southern edge of the Eurasian plate above the Makran Subduction Zone (MSZ) (Fig. 2.4). Crustal faults within this zone typically trend east-west and have both thrust and strike-slip components. The compressional deformation and resulting seismicity are widespread and not limited to a few major faults (Chen and Scawthorne, 2002).

The tectonics of the region are governed by the convergence of the Arabian and Eurasian plates (Jackson & McKenzie 1984). The majority of seismicity associated with this collision occurs at depths less than 20 km (Jackson and McKenzie, 1984). A subduction zone off the Makran coast that formed the margin between the Eurasian and the Arabian plate was first proposed by Stoneley (1974). Shearman (1976), Farhoudi and Karig (1977) and Page *et al.* (1979) then presented data to support Stoneley's hypothesis. Page *et al.* (1979) used the existence of raised beaches and created models of uplift along the Makran coastal region to estimate the average rate of uplift (1-3 m) (Heidarzadeh *et al.*, 2008).

The Makran accretionary prism (MAP) (Fig. 2.4) associated with the MSZ is regarded as one of the most extensive subduction complexes in the world, and is thought by many as an ideal example of an accretionary prism to study the processes related to subduction at plate boundaries (Grando and McClay, 2007).
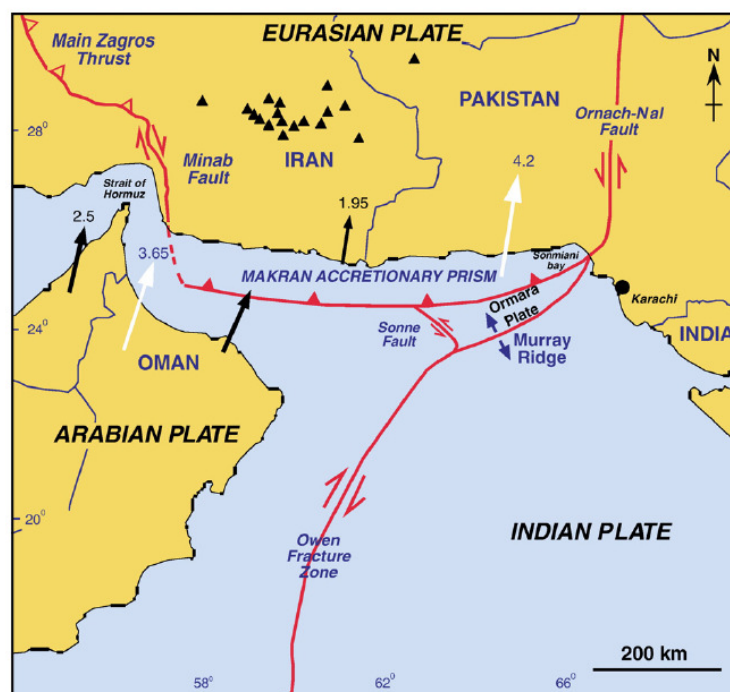
Fig. 2.4. Tectonic map of the Arabian, Indian and Eurasian plates, showing the location of the Makran Accretionary prism in southern Iran and Pakistan. Black triangles indicate the position of Pleistocene volcanoes related to subduction of the Arabian Plate underneath the Eurasian Plate. White arrows indicate convergence velocities and black GPS velocities. From Grando and McClay (2007).

The MAP has grown by frontal accretion where the sediments have been scraped off the subducting crust at the trench or formed by the result of underplating (partial melting of subducted sediment and subducted oceanic crust). This accretionary prism extends for approximately 1000 km from 57°30′ E in south eastern Iran to approximately 66°30′ E in southern Pakistan (Fig. 2.4). The topography of the prism fluctuates from <3000 m below sea level to heights of 1500 m above sea level (Grando and McClay, 2007). Active thrust faulting occurs within the MAP and the prism contains structures such as the imbrication of sediments scraped off the subducting Arabian Sea plate and underthrusting of sediments carried beneath the prism (Platt *et al.*, 1985) and accreted to its underside (Grando and McClay, 2007).

Subduction of the Arabian oceanic plate underneath the Eurasian continental plate is not simple and uniform along the entire subduction zone (Fig. 2.5) At either ends of the zone exists a complex tectonic array of differing subduction systems (Fig. 2.4, 2.5). The eastern boundary of the Makran system is a zone of major transpressional strike-slip systems (Ornach-Nal and the Charman fault regions), which accommodates the motion between the Eurasian plate and the

Indian plate (Byrne *et al.*, 1992). Sinistral slip and thrusting along these fault zones is well documented by Quittmeyer and Jacob (1979). At the western boundary of the MSZ is the Zendan-Minab fault system (Fig. 2.4). This is the transition zone between the Zagros continental collision and the Makran oceanic subduction (Heidarzadeh *et al.*, 2008). According to Gordon and DeMets (1989), the Murray Ridge delineates the Arabian-Indian plate boundary and extends from the northern tip of the Owen Fracture Zone to the eastern MSZ (Byrne *et al.*, 1992) (Fig. 2.4 and 2.5).
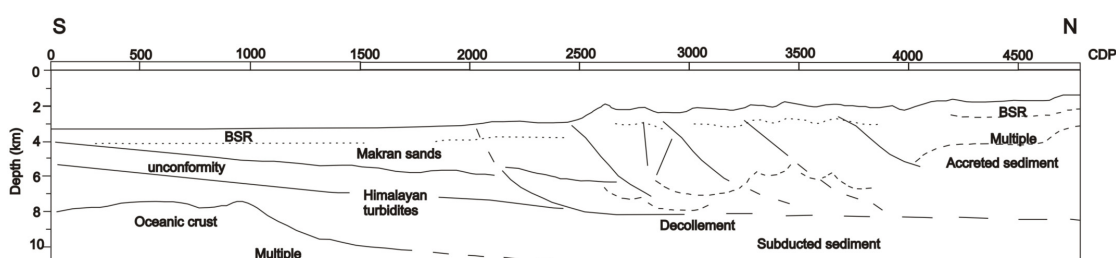
Fig. 2.5. Interpretation of the Makran subduction zone based on the seismic signature of sedimentary reflectors in the abyssal plain from Kopp et al. (2000) cdp = common depth point.

The convergence velocity along the MSZ (assuming completely rigid plate motion) varies from east to west. It increases from around 36.5 mm yr^{-1} near the Strait of Hormuz to 42 mm yr^{-1} in the east (DeMets *et al.*, 1990). A recent study by Vernant *et al.* (2004) used 27 global positioning satellite (GPS) sites in Iran and northern Oman to measure displacements in this region of the Alpine-Himalayan mountain belt. The results show that east of 58°E, most of the shortening is accommodated by the MSZ (at a rate of 19.5 ±2 mm yr^{-1}) and west of 58°E, the deformation is been distributed in fold and thrust belts separate from the main MSZ (Vernant *et al.*, 2004).
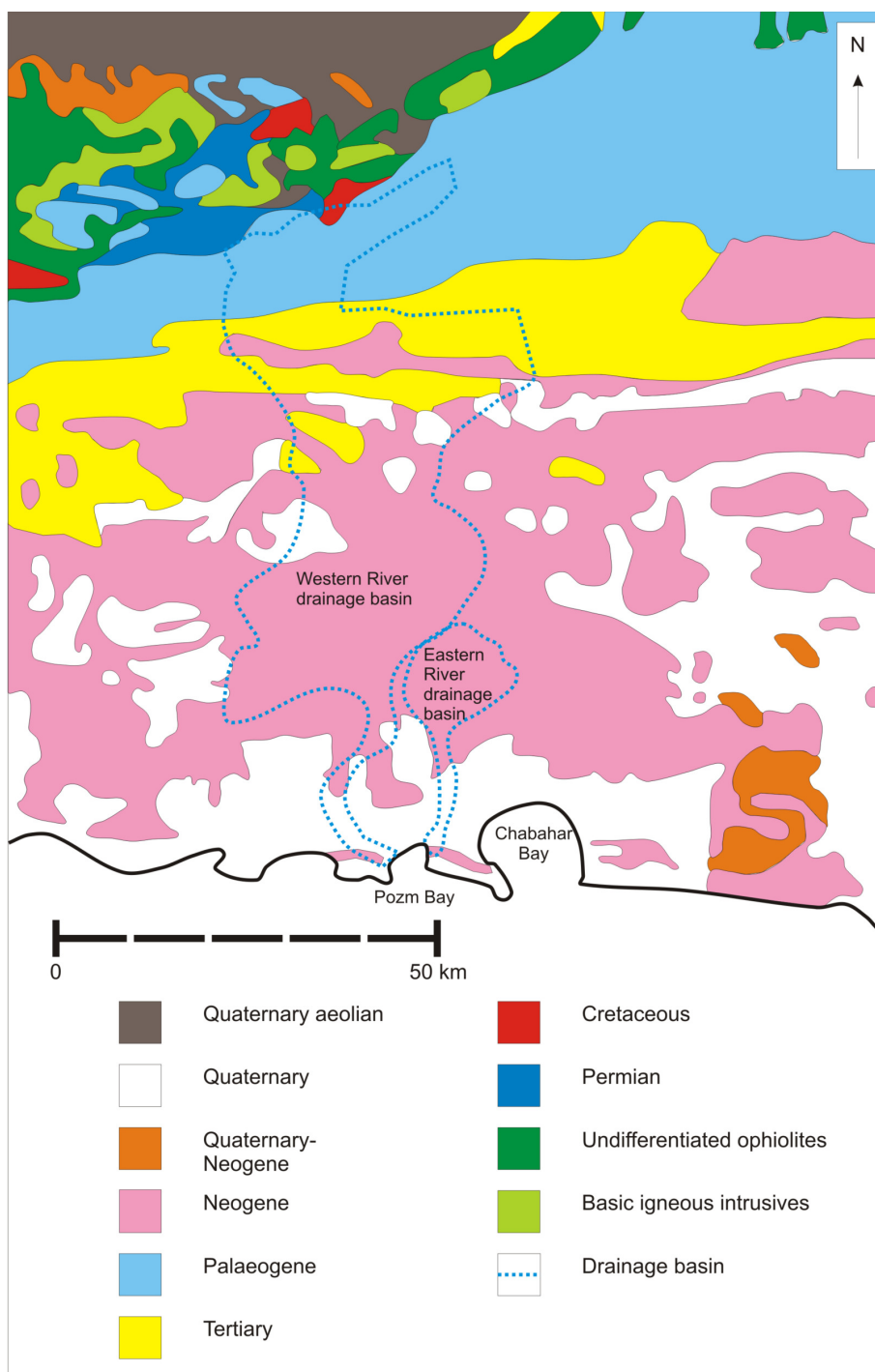
Fig. 2.6. Geological map showing rock ages, types and the eastern and western drainage basins draining into Pozm Bay, modified from Pollastro *et al*. (1997).

The geology of the Makran coast consists of low lying alluvial plains of Quaternary-Neogene age (Fig. 2.6). The Makran mountain range rises irregularly from the coastal plain in a series of ridges underlain by folded sedimentary rocks (Page *et al*., 1979). Highly resistant metamorphic and igneous rocks make up the central mountain chain creating exceptionally irregular topography (Fig. 2.2).

2.3.1 Tsunamigenesis

Tsunamis are generated by large and shallow earthquakes at many subduction zones around the world (*e.g.* 1960 Valdivia-Chilian tsunami; 1945 Makran tsunami). The risk of a widespread tsunami is low for earthquakes with an M_w <8.5 and then becomes significantly higher for earthquakes with a large moment magnitude of >9 (Stein and Okal, 2007). In the past 30 years there has been around one magnitude >8 earthquake and approximately 10 magnitude 7 submarine earthquakes per year around the world. However, only around 20 of these have induced a noticeable tsunami (Synolakis, 2003; Heidarzadeh *et al.*, 2008). Tsunamigenesis can only occur under certain geological and oceanographic conditions. One of the factors needed for a tsunami to be generated is that the earthquake occurs at a relatively shallow depth of <30 km (Synolakis, 2003). A deeper earthquake generally does not provide enough crustal deformation to produce a tsunami as tsunamis are only generated when great segments of the sea floor elevate or subside. Large displacements of the earth's crust can occur on any plate margin but subduction zones are particularly effective at generating tsunami (Furumoto and Fukao, 1985).

Raised beaches and elevated wave cut platforms on the Makran coast were first observed by Blanford (1872). By taking into account eustatic sea level during the Late Quaternary along the Makran, rates of episodic uplift along the Iranian and Pakistan coastlines were calculated (varying incremental uplift of 1 - 3 m resulting from the November 28, 1945 earthquake). This was achieved by observing present elevation above sea level (asl), previous elevations of marine terraces and raised beaches and by using ^{14}C and U-Th dates obtained on shells from the elevated wave-cut terraces (Page *et al.*, 1979). During the 1945 Pasni-Ormara earthquake (epicentre located just sea-ward of the village of Pasni) the the uplift occured as discrete increments along different parts of the coast at different times. Page *et al.* (1979) estimate that the recurrence time of a magnitude >8 earthquake along the Makran coast is approximately 125-250 years with the east end of the coastline appearing more likely to have a large-magnitude earthquake than the west. Reviewing the seismicity of the MSZ undoubtedly demonstrates that large and shallow earthquakes (those ideal for tsunami generation) are common within the Makran region.

2.4 Bathymetry

It proved especially difficult to find a bathymetric map of the study region, with the only map available unable to provide full, extensive coverage of the coring region. A bathymetric map of the coastline provided by the Iranian National Centre for Oceanography (INCO) is shown in Fig. 2.1. It provides a general coastal bathymetry, however does not show any possible small-scale local bathymetric lows or highs in the topography.

2.5 Present day climatic settings

The coring sites (Oman Sea; latitude 25.348, longitude 60.253) are positioned below the northernmost extent of the ITCZ (Fig. 2.7b), placing it in the zone of climatic transition between the system from Indian summer monsoon (ISM) and the Mediterranean depressionary system (Fig. 2.7a), giving it a highly monsoonal climatic regime consisting of wet and dry seasonal rainfall generally occurring between November and May and between June and October, respectively. The climate of Iran as a region is defined as subtropical with hot and dry weather in the summer, with the primary cause of annual rainfall variability been the changing position of synoptic systems and year-to-year variation of the frequency of cyclones passing through the region (Modarres and Rodrigues, 2007). Dinpashoh *et al.* (2004) estimated the average annual precipitation (Fig. 2.8) of Iran from 1956-1998 to be around 241 mm (using the isohyetal method). Over half of the country receives less than 200 mm yr^{-1} with over 75 % receiving less than 300 mm yr^{-1} giving most of the country an arid to sub-arid climate (Dinpashoh *et al.*, 2004).

Iran's two main mountain chains the Alborz and Zagros ranges (Fig. 2.2) play a crucial role in the non-uniform spatial and temporal distribution of precipitation in the whole country (Dinpashoh *et al.*, 2004). The Alborz mountains lie from the northwest to northeast rimming the Caspian Sea (Fig. 2.2), preventing Mediterranean moisture bearing systems crossing through the region to the east (Modarres and Rodrigues, 2007). The Zagros mountains (Fig. 2.2) extend from the northwest to southwest and are responsible for the majority of rain producing air masses which enter the region from the west and northwest, giving these regions reasonably high rainfall values (Sadeghi *et al.*, 2002; Alijani *et al.*, 2006).
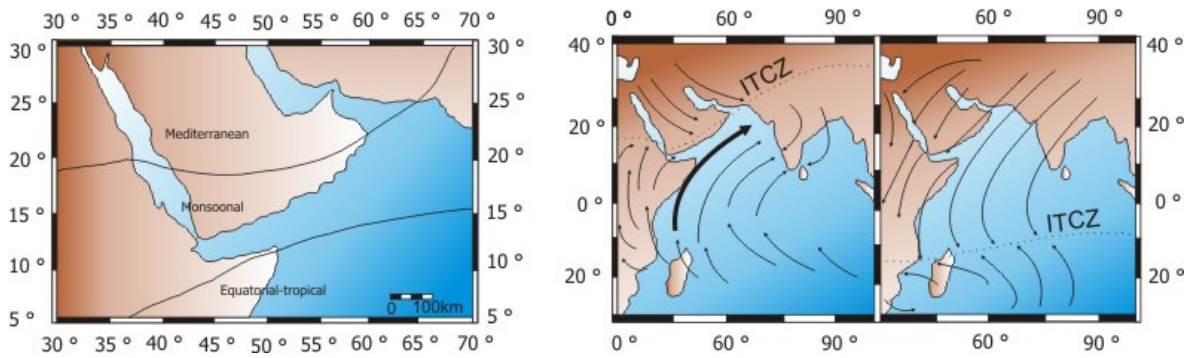
Fig. 2.7. a) Precipitation regimes (modified from Gasse, 2000 and Fleitmann *et al.*, 2007). Mediterranean = winter rainfall; Monsoonal = summer monsoonal rainfall; Equatorial = spring and autumn rainfall. b) Position of ITCZ during boreal summer (ISM season). c) Position of ITCZ during boreal winter (NE monsoon system). Bold arrow = Findlater jet.
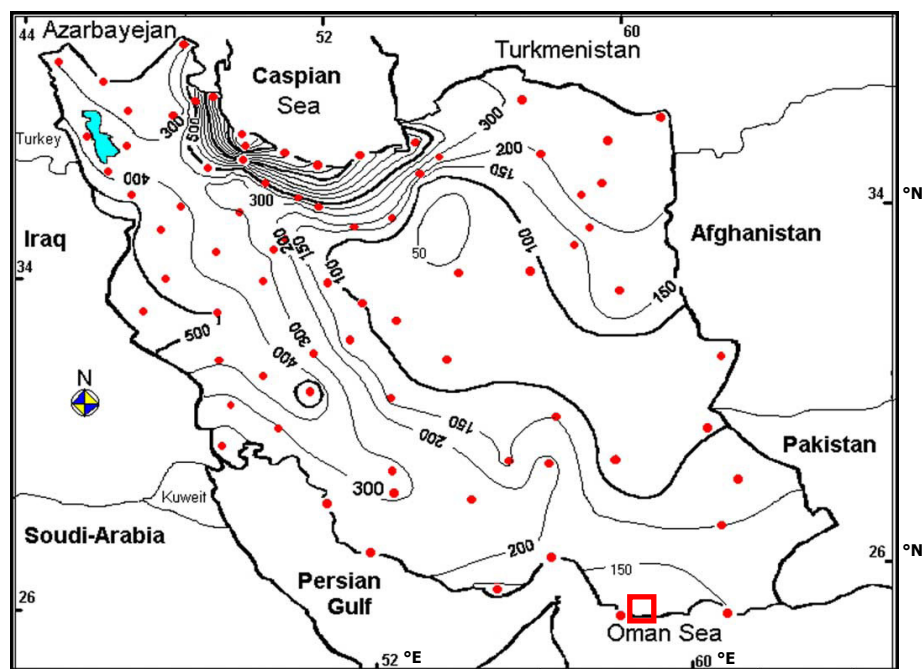
Fig. 2.8. Mean annual precipitation (mm). Data series taken from 77 weather stations over Iran, gathered from 1956 to 1998 (adapted from Dinpashoh *et al.*, 2004). Red box marks study region.

The temporal variability of precipitation in Chabahar and the surrounding regions produces significant hazards, including both droughts and floods. The hot summers along the southern Makran coasts are almost void of rain due to 'capping' by subtropical high pressure. Occasionally, the subtropical high weakens and the warm moist air at the surface rises to generate extremely strong convective rains (Alijani, 1997 in Dinpashoh *et al.*, 2004).

From 1960 to 2003 the annual precipitation around Chabahar averaged at approximately 100 mm per year and does not appear to have a trending increase or decrease during these years. The average annual temperature dataset is

incomplete. However, there is a peak at 1980, with annual temperatures rising to 33.5°C (data from the Iranian Meteorological Organisation website). Seasonal precipitation is shown in Fig. 2.9, which clearly demonstrates the seasonality of the region, with low summer/autumn precipitation and high winter/spring precipitation (New *et al*., 2000).
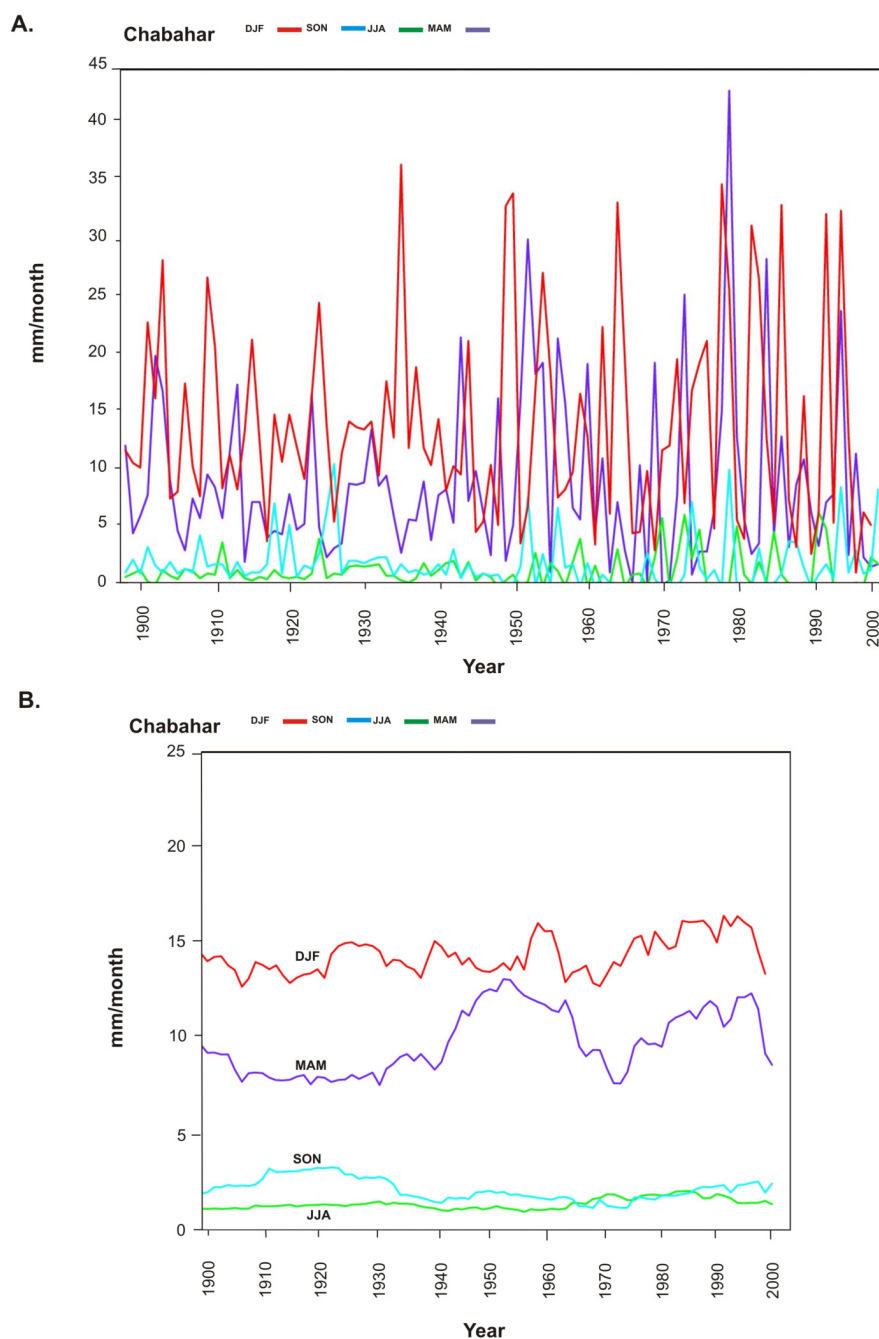
Fig. 2.9. A.) Monthly precipitation records in Chabahar from 1898 yr BP to present (2000). B.) Monthly precipitation records in Chabahar from 1898 yr BP to present (2000) with curve smoothed (data from New *et al*., 2000).

As a consequence of the semi-arid to arid climatic regime around both Chabahar and Pozm Bay, the southern Iranian coastline is made up of ephemeral

streams and rivers, flowing only in times of torrential downpour during the monsoon months. The intense 'baking' of sediments during the dry months greatly influences the porosity and permeability of the channel beds and in many ephemeral channels a layer of fines is found in the upper few centremetres of riverbed sediments reducing the hydraulic conductivity of the channel bed (El-Hames and Richards, 1998). The lack of fluvial input into the northern Arabian Sea, indicates that most of the sediment deposited in the coastal regions is of aeolian origin, or initially of aeolian origin and subsequently redeposited by infrequent flash floods.

2.6 Atmospheric and oceanic circulation of the Arabian Sea

The atmospheric and oceanic circulation of the Arabian Sea is strongly influenced by the seasonal migration of the intertropical convergence zone (ITCZ), a narrow region of wind convergence and precipitation. The position of the ITCZ determines the onset and the termination of the monsoonal systems in the tropics and sub-tropics (Fleitmann *et al.*, 2007). The Indian summer monsoon (ISM) interacts closely with the ITCZ and it is the conventional view that the ISM is driven by the land-sea thermal contrast between the Eurasian landmass and the southern Indian Ocean creating a 'giant sea breeze' (Webster *et al.*, 1998). Recent studies have suggested that the ITCZ and ISM are more coupled than previously thought and that the ISM is a manifestation of the seasonal migration of the ITCZ (Chao and Chen, 2001; Gadgil, 2003). The seasonal migration of the ITCZ and the associated semi-annual reversal of wind patterns, the SW monsoon in the boreal summer, and NE monsoon in the boreal winter (Zonneveld, 1997a) are key components of the climatology in the Indian Ocean. In the boreal summer (Fig. 2.7b and 2.10a), the ITCZ moves to its northernmost position and differential heating of continental and oceanic regions leads to the development of areas of low atmospheric surface pressures over Pakistan, India and Oman and relatively high surface pressures over the cooler Indian Ocean. A wide region of south westerly wind develops (Fig. 2.10a) with the prominent east African coastline intensifying the wind near the surface and directing it parallel to the coasts of Somalia, Yemen, and Oman (Honjo and Weller, 1997). This intense wind (Findlater Jet) causes the ocean to respond with the development of the Somali Boundary Current (Fig. 2.10b), with a north-northeastward current speed of about 150 cm s^{-1} (speed decreasing to about 10 cm s^{-1} at 100 m depth) (Schott *et al., 1990*; Brock *et al.,* 1991). The

Somali Boundary Current transports high salinity water from the equator northward (Schott *et al.,* 1990; Zonneveld, 1997a). The current induces the upwelling of cool, nutrient rich water along the Somali and Arabian coasts (Brock *et al.,* 1991; Zonneveld, 1997a). The nutrients introduced into the euphotic zone with the cold upwelling waters enhance levels of primary productivity which ranges from <2.5 gC m^{-2} day^{-1} in near-coastal waters to <0.3 gC m^{-2} day^{-1} in oligotrophic waters outside the region of upwelling (Qasim, 1982; Brock *et al.,* 1991; Zonneveld, 1997a). Chlorophyll *a* concentration, indicating planktonic activity, within the surface waters of the NW Arabian Sea are highest during the SW monsoon (Qasim, 1982). The observation of Chlorophyll *a* and the distribution of pigments were estimated using Coastal Zone Colour Scanner images (Brock *et al.*, 1991). The high level of planktonic productivity induces the development of an oxygen minimum zone (between 150 - 1200 metres in depth) which exists because of the tectonic situation of the northern Arabian Sea where it is closed to the north limiting ocean circulation (Schulz *et al.*, 1996). Low oxygen concentrations (0.05 ml^{-1}) limit any biological productivity to the sediment-water interface (Von Rad and Schulz, 1995). The Somali/Findlater Jet (Fig. 2.7b and 2.10b) transports a large quantity of moisture northward which is deposited as precipitation over southern Arabia and the India subcontinent (Fleitmann *et al.*, 2007). This latent heat release strengthens and further maintains the low pressure situation over the Arabian landmass (Webster *et al.*, 1998).

In midwinter (Fig. 2.7c) the ITCZ moves southwards (25°S in January) and the Eurasian continent cools, consequently a high pressure region develops on the seasonally snow-covered Tibetan plateau and northeast winds (Fig. 2.7c) persist over southern Asia and the Arabian Sea, cooling the NW Arabian Sea surface temperature to 23°C (Wyrtki, 1973). The relatively dry NE monsoon is not as strong as the summer monsoon flow and has an observed net northward flow of 20 - 30 cm s^{-1} (Schott *et al.,* 1990). Nevertheless, combined with a high amount of surface cooling, the NW monsoonal flow causes a deepening of the mixed layer in the central and western Arabian Sea (Honjo and Weller, 1997). The cool winds from the north-east (Fig. 2.10c) induce increased mixing and cooling of the ocean near the Gulf of Oman and on the Pakistan shelf (Makran coast), which results in exceptionally high bioproduction in these regions (Fig. 2.10d) (Qasim, 1982; Zonneveld, 1997a).
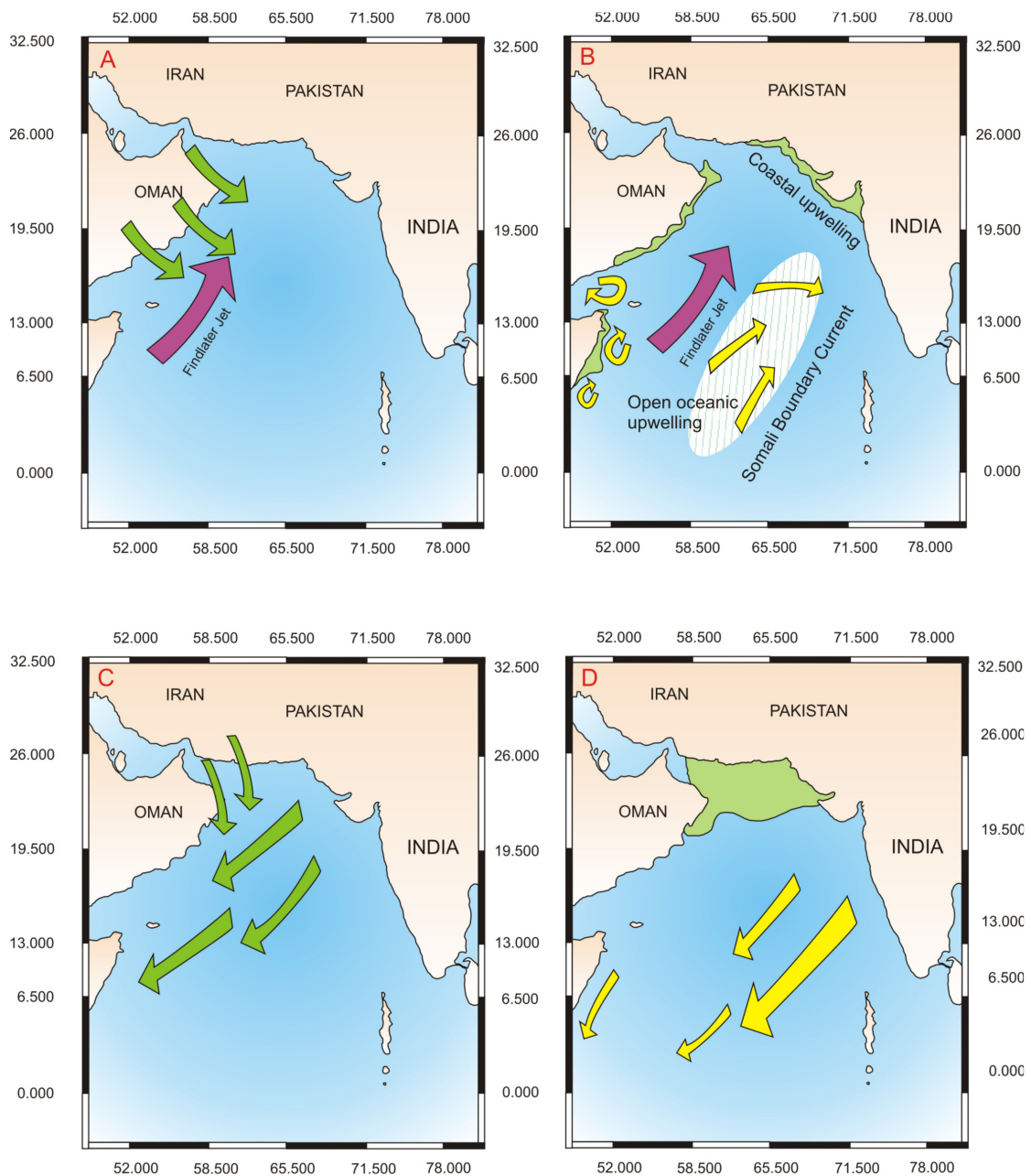
Fig. 2.10. (a). General wind pattern in the Arabian Sea area during the SW monsoon - compiled and modified from Zonneveld (1997a); McCreary and Kundu (1989) and Brock *et al.*, (1991). (b) General surface-water circulation of the Arabian Sea during the SW monsoon - compiled and modified from Zonneveld (1997a); Quraishee (1984); Schott *et al.*, (1990). (c) General wind pattern in the Arabian Sea area during the NE monsoon - modified from Zonneveld (1997a); McCreary and Kundu (1989). (d) General surface-water circulation of the Arabian Sea during the NE monsoon - compiled and modified from Zonneveld (1997a); Wyrtki (1973), McCreary and Kundu (1989), Schott *et al.*, (1990) and Naidu (1993). Green arrows show wind patterns. Yellow arrows show surface water circulation. Purple arrows show Findlater Jet. Green regions show areas of coastal upwelling. White striped region shows areas of open ocean upwelling.

The Arabian Sea contains a variety of waters including both the Gulf of Oman and the Red Sea outflow waters, which dissipate gradually southwards at a depth of 600-800 m and then mix with the other water masses (Wyrtki, 1973; Gründlingh, 1985; Shapiro and Meschanov, 1991). Furthermore water enters the Arabian Sea

from the south as bottom waters into the Somali Basin (Wyrtki, 1973; Barton and Hill, 1989; Johnson *et al.,* 1991a; 1991b; Zonneveld, 1997a). It is conceivable that some of these bottom waters in the Somali Basin splay out, travelling north past the Owen Fracture Zone and becoming incorporated into the currents along the Carlsberg Ridge (Zonneveld, 1997a). Additionally the Arabian Sea flows into the Persian Gulf via a significant current flowing westerly along the Iranian coast. This current is driven by density differences caused by river outflow having a comparatively low density (baroclinic forcing) (Reynolds, 1993). The inflow into the Persian Gulf is weakened by the Sharmal winds in the winter, but strengthened in the summer (Reynolds, 1993).

2.6.1 Cyclogenesis

Tropical cyclones are storm surges which gain energy by the release of large amounts of latent heat from water vapour condensing at high altitudes, with solar heating the initial source for evaporation. The development of a tropical cyclone depends on sea surface temperatures (at least 26.5°C), a strong decrease of air temperature with altitude and low wind shear in the upper troposphere, permitting strong convection and condensation (Krishna, 2009 and Arpe and Leroy, 2007).

There are several ocean basins which support tropical cyclone development for example; North Atlantic (90° to 20°W, 5° to 25°N), western North Pacific (120° to 180°E, 5° to 20°N), eastern North Pacific (90° to 120°W, 5° to 20°N), South Indian (50° to 115°E, 5° to 20°S), North Indian (55° to 90°E, 5° to 20°N), and Southwest Pacific (155° to 180°E, 5° to 20°S) (Webster *et al.,* 2005). It is the eastern part of the Arabian Sea that generates tropical cyclones and none are generated in the western part of the Arabian Sea (Fig. 2.11). There are two cyclone seasons in the Arabian Sea namely the pre-monsoon (April, May, June) and the post-monsoon (October, November and December). Intense tropical cyclones like Cyclone Gonu, 2007 (Fig. 2.11) are relatively rare over the Arabian Sea, with approximately four times more cyclones occurring in the Bay of Bengal (Singh *et al.*, 2001). The Bay of Bengal has experienced several large cyclones with devastating socio-economic impacts, for example Cyclone Nargis (2008) in Myanmar where damage estimates were over $10 billion and official death toll estimates exceeded 138,000 fatalities, making it the eighth deadliest cyclone ever recorded worldwide (Fritz *et al.*, 2010).
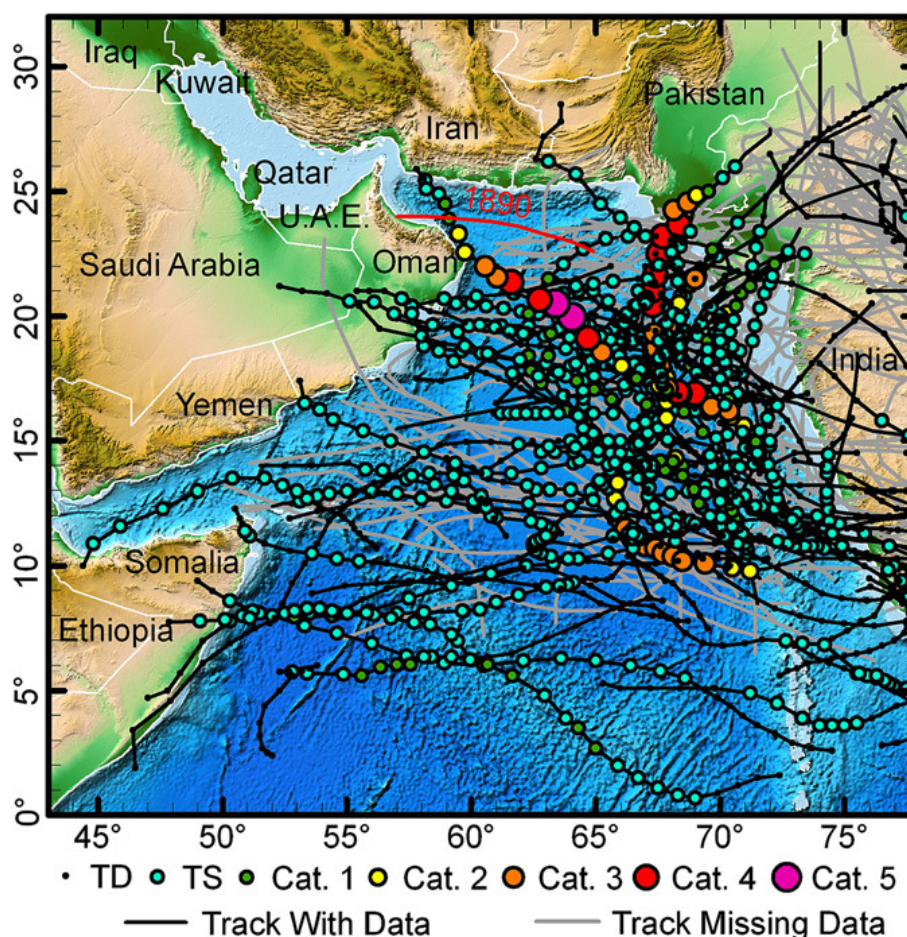
Fig. 2.11. Storm track data from the Arabian Sea from Fritz *et al.* (2010), modified from the IBTrACS database. The track of the 1890 cyclone is based on historical documents. Cyclone Gonu in 2007 is the only confirmed, instrumentally recorded category 5 storm on record. (TD=tropical depression, TS=tropical storm).

2.7 Historical earthquakes and cyclones in the Makran region

2.7.1 Historical earthquakes in the Makran region

The desert coast of Makran (southern Iran and Pakistan) has remained a remote region from the early Islamic period, AD 500 (and presumably before) through to the seventeenth and eighteenth centuries. This has lead to a short historical record of earthquakes in this region compared to that of adjacent civilizations to the east and west (Ambraseys and Melville, 1982; Byrne *et al.*, 1992). Even today the population of the Makran remains small with an even smaller population to be found inland. The first telegraph cables across the Makran regions were laid in AD 1864 and the coastal towns were connected to the international telecom network in the First World War (Byrne *et al.*, 1992). Although the populations have been small and communication was poor, large earthquakes over the past 500 years have been recorded in the region with large-

magnitude earthquakes reported from the more populated east end of the Makran (Page *et al*., 1979 and references therein). Ambraseys and Melville (1982) state that since the middle of the nineteenth century the historical record appears to be complete for large (M_s>7) earthquakes. However, looking back over the last millennia the historical record is clearly not complete indicating the need for palaeotsunami research. In a review of Makran seismicity, Heidarzadez *et al.* (2008) have compiled references of tsunami studies of the Makran (Table 2.1). Table 2.1 shows locations of the tsunami events, the confidence factor (CF), year of event and the recorded loss of life. This confidence factor has been assigned to each event after a review of the literature by Heidarzadez *et al.* (2008).

Table 2.1. Historical tsunamis recorded from MSZ from Heidarzadez *et al.* (2008).

Year	Longitute (°E)	Latitude (°N)	Moment magnitude	Type of source	CF	Deaths
326 BC	67.30	24.00	?	Earthquake	1	?
1008	60.00	25.00	?	Earthquake	2	1000
1524	?	?	?	Earthquake	1	?
1897	62.30	25.00	-	Volcanic	1	?
1945	63.00	24.50	8.1	Earthquake	3	4000

CF = Confidence factor: (1) probable tsunami; (2) definite tsunami but the type of tsunami source or its location is not certain; and (3) instrumentally recorded tsunami.

The following is a detailed discussion of each individual tsunami event recorded over the past 3000 years in the Makran (Fig. 2.12).
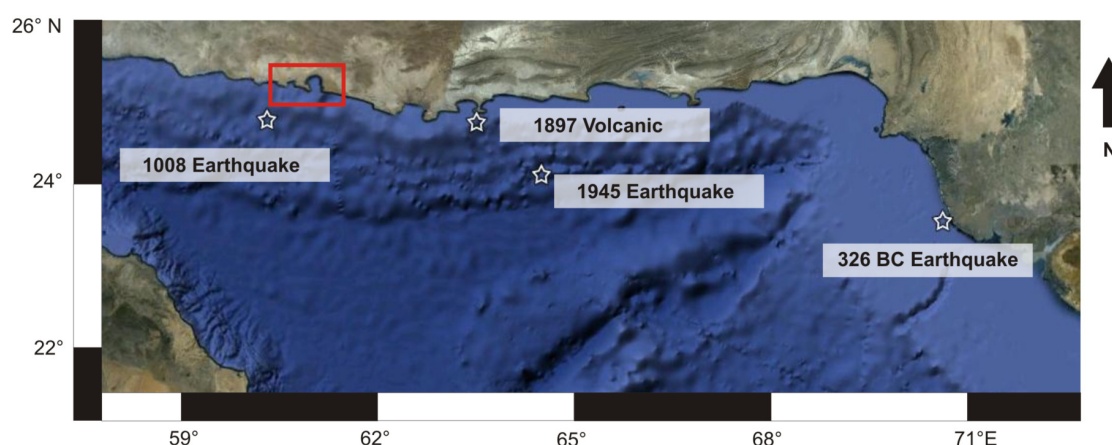
Fig. 2.12. Location of historical tsunamis recorded from MSZ locations mapped from Heidarzadez *et al.* (2008). Red box highlights Pozm and Chabahar Bay (study region).

2.7.1.1 Makran tsunami of November, 326 BC

The tsunami event of 326 BC (Table 2.1) (Fig. 2.12) possibly generated on the Makran subduction zone is historically fascinating as it involves the activities of Alexander the Great (Dominey-Howes *et al.,* 2006). It is significant to the research because it was said to have generated a large enough wave to destroy an entire navy fleet, therefore it is possible that it could be preserved within the sediment record of the cores. However, there is little documentary evidence for the tsunami of 326 BC thus Heidarzadez *et al.* (2008) have assigned a confidence factor of 1 to the event (Table 2.1). No information is available on the location or type-source of the earthquake. Confusion surrounds this event with arguments both for and against the classification of this event as a tsunami. Lisitzin (1974) has given an entry for the event as:

> *'World famous strategists were also unable to escape it. Various historical authors have mentioned the amazement of Alexander the Great and his army, when during the illustrious campaign to India in 325 BC they experienced for the first time in their lives sea-level variations caused by tide and noted the disastrous consequences of this phenomenon on the Macedonian fleet, anchored in the estuary of the River Indus'.* (Lisitzin, 1974, pp. 259–260).

Lisitzin (1974) appears to be describing the event of tidal variations on the Macedonian fleet and not the occurrence of a tsunami event, making it illogical to classify this event as a tsunami event. This view is supported by Dominey-Howes *et al.* (2007), who believe that tidal variations would have been an entirely new experience for Alexander the Great and his Macedonian fleet because they would have been more familiar with regions of restricted tidal variation for example the Aegean Sea. The normal tidal range within the Arabian Sea is extremely variable, but in Pakistan and along the Iranian coastline the difference between high and low tide is 3.7 m (National Ocean Survey, 1973). This value is large considering the tidal range of the Aegean Sea is far smaller, for example in Bodrum (southwestern Aegean Region of Turkey) the mean spring tidal range is 11.3 cm and only 20.3 cm at Bozcaada (Alpar and Yüce, 1996). Heidarzadez *et al.* (2008) disagree with the interpretation of Dominey-Howes *et al.* (2007) and believe that regular tides do not have the potential to destroy a military fleet and have used

another reference which is an account of Alexander the Great's military expedition to western India.

> *'About dawn they put out to sea and were met by so violent [sic] ebb that three of the ships ran ashore and were held hard and fast on dry land and the rest only just sailed through the surf and got safe into deep water. The ships, however, which ran aground, were floated off when next flood came, and arrived next day where the main fleet was'.* (Robson, 1933).

Although, it is possibly too early to regard the event of 326 BC as a non-tsunami event (Heidarzadez *et al.,* 2008), it is clear that more palaeo-event analysis must be done in the region to find possible evidence for this tsunami event.

2.7.1.2 The Makran tsunami AD 1008

Murty and Bapat (1999) and Ambraseys and Melville (1982) report a tsunami in the Indian Ocean affecting the southern coast of Iran, from an earthquake in AD 1008 (Fig. 2.12). The earthquake is said to have sunk ships and killed a number of people in the area. Rastogi and Jaiswal (2006) report that the epicentre of the earthquake was at 25°01' N, 60°01' E (western MSZ). If this report is correct then the earthquake occurred just 50 km from Chabahar Bay (study site).

2.7.1.3 The Dabhol tsunami of AD 1524

The tsunami catalogues of the Indian Ocean have listed this event, but do not include any detail. For example, nothing is known regarding the generation mechanism or epicentre location. Numerical modelling by Heidarzadez *et al.* (2008) has shown that the MSZ is most likely to have been the source locality for the Dabhol tsunami, giving it a low confidence factor of just 1. Owing to the large distance from epicentre (MSZ) to Dhabul (over 1000 km) Heidarzadez *et al.* (2008) speculate that an earthquake source would be a reasonable explanation (Synolakis and Okal, 2005).

2.7.1.4 The Makran Tsunami of AD 1897

The Makran tsunami of AD 1897 (Fig. 2.12) differs from the other tsunamis in that it was generated not by an earthquake but probably from a volcanic source. This tsunami provides evidence of the potential for tsunami generation from volcanic sources along the Makran coastline. None of the Indian Ocean tsunami catalogues show any record for the event of 1897. Ambraseys and Melville (1982) do not class the event of 1897 as a tsunami and state that the large ocean waves produced could perhaps be the result of just oceanic storms near Gwadar in December 1897. It is reported that the event caused substantial damage to coastal regions of the Makran with the waves transporting hundreds of tonnes of fish onto the Makran coast (Heidarzadez *et al.,* 2008). No evidence for earthquake activity around 1897 exists, thus Heidarzadez *et al.* (2008) speculate a volcanic source for the tsunami, with the death of the fish attributable to volcanic gas emissions from mud volcanoes present all along the MSZ. It seems unreasonable to be certain of the existence of a tsunami event in 1897, with only speculations from Heidarzadez *et al.* (2008) and no real evidence found. It seems other causes may be responsible for the death of tonnes of fish, for example a harmful algal bloom resulting in the production of neurotoxins or oxygen depletion of the water column from cellular respiration and bacterial degradation, both causing mass mortalities in fish populations. Algal blooms are possibly associated with strong monsoonal winter rainfall resulting in enhanced river run-off, thus higher oxygen and nutrient availability in the shallow seas.

2.7.1.5 Makran tsunami AD 1945

This tsunami (Fig. 2.12) is the first instrumentally recorded in the Indian Ocean, thus Heidaradez *et al.* (2008) has assigned it a confidence factor of 3. The tsunami occurred on 28th November 1945, from an *Mw* 8.1 earthquake with the epicentre just off the southern coast of Pakistan in the town of Pasni at 25°15' N, 63°48' E (Quittmeyer and Jacob, 1979). A study of p-wave motion, s-wave polarisation and surface wave amplitude ratios conclude a normal faulting focal solution was responsible for the earthquake of 1945 (Laane and Chen 1988 and Byrne *et al.,* 1992). The earthquake caused widespread damage along the sparsely populated coast and generated a large tsunami. On the coasts adjacent to the epicentre at Pasni, the tsunami wave heights are estimated to be 5-10 m

high. The tsunami wave heights vary, with the city of Karachi (360 km away) experiencing 1.5 m high waves, and Bombay (1100 km away) having a 2 m high wave (Ambraseys and Melville, 1982). It was reported that the transoceanic cable between India and England broke in eight places and a portion of the town of Pasni moved 100 m as a result of submarine slumping (Byrne *et al.,* 1992). In addition, intense mud-volcano activity and reactivation was recorded, which also resulted in the creation of four new volcanic islands (Byrne *et al.,* 1992 and references therein). This volcanic activity resulted in a large volume of methane escaping and igniting near Hinglaj (Byrne *et al.,* 1992). Only a small number of aftershocks were measured associated with the earthquake of 1945 according to the International Seismological Summary. Just five additional events were recorded, the largest of these events occurred in 1947, with an epicentre immediately south of the main 1945 shock (Quittmeyer and Jacob, 1979).

2.7.1.6 Synopsis of the historical tsunami in the Makran region over the last 2.5 ka cal BP

The research of Heidarzadez *et al.* (2008) indicates the recognition of five historical tsunamis with varying confidence factors assigned to each event. Due to the lack of evidence supporting most of the events, the need of more palaeo-tsunami research is clear. There is a requirement for field evidence to support the listed tsunamis and most of the evidence currently obtained is from relatively subjective historical documents. The Makran 1945 earthquake indicates that the MSZ has great potential for generating large destructive earthquakes. However, the lack of convincing evidence for the earthquakes prior to 1945 makes generating an average tsunami return period for the region problematic. Although dubious, using the list of the five earthquakes above, the average return period for a tectonic tsunami is approximately 800 years (Heidarzadez *et al.,* 2008). However, the lack of evidence for these tsunami indicates the need for more field evidence.

2.7.2 The historical record of cyclones in the Arabian Sea

Most storms which do occur over the Arabian Sea tend to be small and dissipate quickly. However, historically, large, highly destructive cyclones have

occurred in the Arabian Sea, the most recent, Cyclone Gonu in 2007 (2.12).

2.7.2.1 Arabian Sea cyclone AD 865

Limited information is available about this cyclone, although just like the cyclone of 1890, the AD 865 storm affected areas in Oman between Gobrah and Sohar and is said to have been comparatively devastating (Bailey, 1988; Blount *et al.,* 2009; Fritz *et al.,* 2010).

2.7.2.2 Arabian Sea cyclone AD 1890

The storm of 4th and 5th June 1890 (Fig. 2.12) is the deadliest natural disaster in Oman's history with a reported 727 fatalities (Bailey, 1988). The storm inundated the coastline from Soor to Suwayq and caused extensive inland wadi flooding. The hardest hit regions were Matrah and Muscat, where numerous ships were wrecked and agriculture losses were huge (Blount *et al.,* 2009).

2.7.2.3 Cyclone Gonu, 2007

From 2nd to the 6th June 2007, Cyclone Gonu, the strongest tropical cyclone on record in the Arabian Sea developed affecting India, Oman and Iran (Fig. 2.11). It developed from a persistent area of convection in the eastern Arabian Sea, strengthening to category 5 strength on 4th June with a pressure of 909 mbar and sustained winds of 263 km h^{-1} approximately 475 km east of Masirah Island off the coast of Oman (Fritz *et al.,* 2010). Gonu reached the Arabian Peninsula on the 5th June with winds of 164 km h^{-1}, reaching the Makran coast of Iran as a tropical storm on the 7th June. The cyclone caused immense damage costing up to \$4 billion in Oman and \$250 million in Iran. It resulted in 49 fatalities in the Sultanate of Oman and 23 deaths in Iran. In Oman, Gonu caused heavy rainfall reaching up to 610 mm in places, resulting in flooding and heavy damage, especially to infrastructure. Along the Omani and Iranian coastlines storm surge caused a large amount of damage (Fritz *et al.,* 2010). In addition, it was reported that the strong winds associated with the cyclone induced phytoplanktonic blooms, caused by storm induced mixing and intense upwelling along the coastlines (Wang and Zhao, 2008). Both Oman and Iran contain mountainous and arid terrain in close proximity to the coastline. High amounts of rainfall generated by the cyclone in a relatively short period of time falling on the mountainous regions resulted in wadi flooding,

this, combined with storm surge, posed an additional threat to the populations on the coastline (Fritz *et al.,* 2010).

2.8. Vegetation and sources of pollen

Little research has been conducted concerning vegetation reconstruction along the southern Iranian coastline, it may have always been presumed a dry environment, with little vegetation change. Most vegetation-environmental research focuses on northern Iran (Kazancı *et al*., 2009; Arpe and Leroy, 2007; Leroy *et al*., 2007; Djamali *et al*., 2008).

In 1963, Zohary published a general account of the vegetation of Iran (Leonard, 1993) (Fig. 2.13). With the study region consisting of Acacieta flavae iranica and Nubo-Sindian classes as well as pockets of littorial saltland vegetation.

Fig. 2.14 shows the modern-day vegetation settings for Pakistan from Ivory and Lézine (2009). It is useful to have a broad overview of the regional vegetation, as monsoonal winds may transport pollen thousands of miles into the study region. Large variations in seasonal precipitation and elevation over the region have a strong impact on vegetation distribution. The western slopes of the Himalaya in the east receive up to 2000 mm of rain per year, with the Balochistan plateaus and the Makran coast, too far north for summer rain, and receive extremely little rainfall (less than 200 mm per year) during the winter months (Ivory and Lézine, 2009) and around 100 mm per year in Chabahar (Iranian Meteorological Organisation, 2009).

In close proximity to the study region are mangroves, extending E-W along the Makran coastline, occurring in restricted pockets. The majority of the mangrove trees are *Avicennia marina*, a species well adapted to high salinity and dry environments (Spalding *et al.,* 1997). *Rhizophora mucronata*, *Ceriops tagal*, and *Bruguiera conjugata* occur closer to the mouth of the Indus River, and are adapted to more brackish waters and wetter environments. Two species of mangrove, (*Avicennia marina* and *Rhizophora mucronata*) have been recorded as far west as the Strait of Hormuz, 137 km east of Bandar Abbas (Danne-kar, 2005) and 410 km west of Chabahar. It has been reported that these mangroves found in the Strait of Hormuz were cultivated (Majid Akhani, pers. com.). In addition, Google Earth images indicate the modern day presence of *Avicennia* in Pozm Bay. Mangrove species found in the study region would provide evidence for the native characteristic of *Rhizophora* in the region.

Fig. 2.13. A simplified sketch map adapted from Zohary (1973) detailing present day pollen zones in Iran. The study site is highlighted by red box, with pollen zones and vegetation types coded according to key.
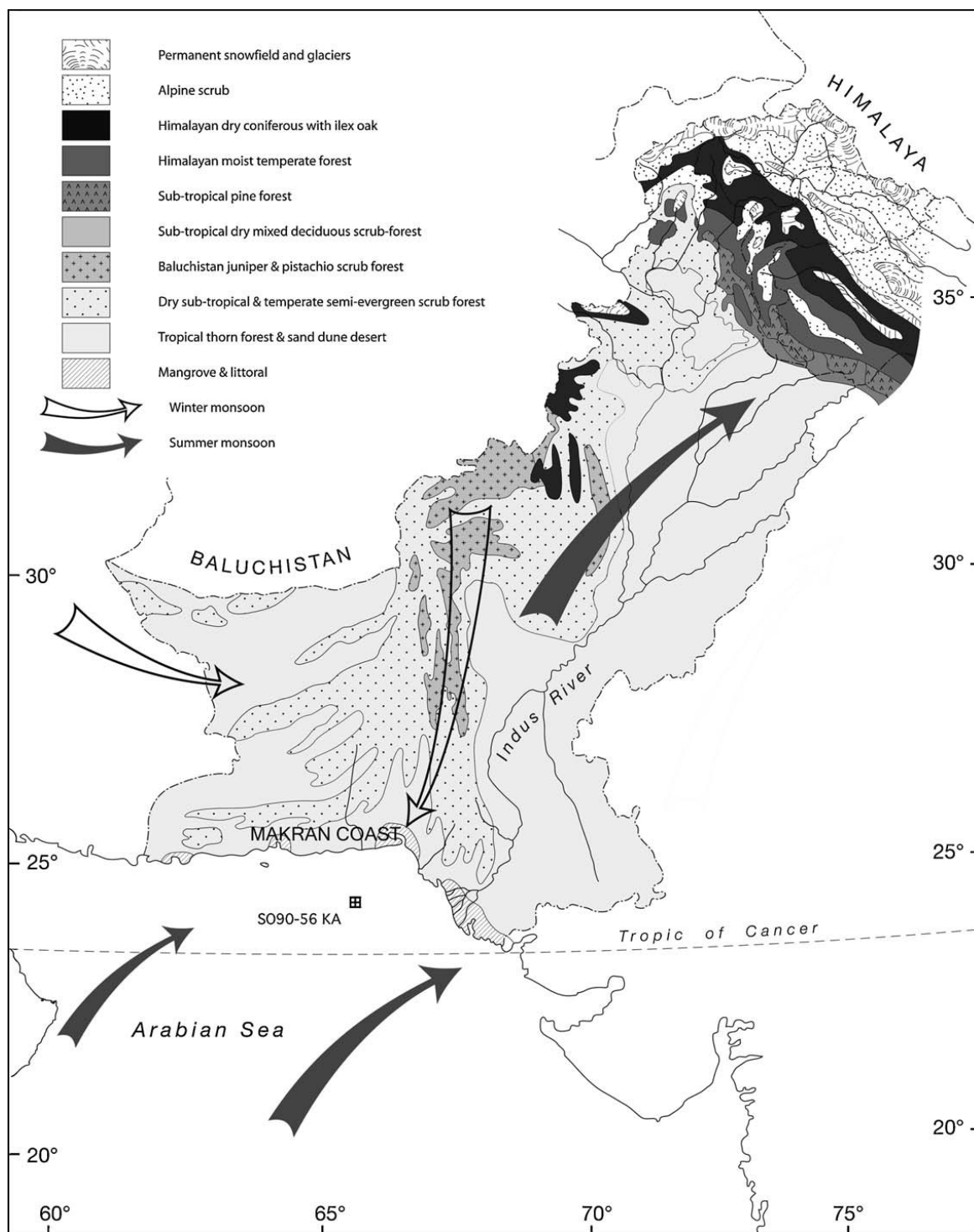
Fig. 2.14. Present-day vegetation zones in Pakistan (adapted from Ivory and Lézine, 2009 and Roberts, 1991). Seasonal monsoonal winds and location of study region are shown in relation to the Indus Delta and Himalayan Mountains.

Directly north of Chabahar Bay, in the Himalayan foothills (below 1200 m) and along the Balochistan Plateau, tropical thorn forests are present (Roberts, 1991). These regions, subject to extremely dry desertic conditions, contain typical species such as *Olea ferruginea* (Indian olive), *Acacia modesta*, species of *Artemisia*

(Ansari and Vink, 2007), *Acacia sp.*, *Prosopis cineraria*, *Tamarix dioica*, and *Salvadora persica*, associated with *Euphorbia* sp., xerophytic species of Amaranthaceae, *Calligonum polygonoides*, *Cassia sp.*, and halophytes such as *Suaeda fruticosa* and *Salsola foetida* (Ivory and Lézine, 2009).

The Himalayas contain four main vegetation belts, related to altitude and precipitation received. At 1000 - 1500 m asl the vegetation consists of dry subtropical scrub forest largely composed of *Olea cupidata*, *Acacia sp.,* and *Dodonaea viscose.* Additional components include sub-tropical pine forest and Himalayan moist temperate forest with *Pinus gerardiana*, *Cedrus deodorata*, *Picea morinda*, and *Abies pindrow* (sometimes associated with *Quercus incana, Quercus dilatata* and *Quercus semecarpifolia*). *Alnus sp.*, and other broad-leaf deciduous trees occur between 1500 and 3300 m asl. Dry coniferous forest begins above 3300 m asl and contains *Cedrus deodorata, Picea morinda, Pinus gerardiana*, evergreen oak (*Quercus ilex*) and *Betula*. The final zone, above the tree-line consists of alpine scrubs with *Juniperus* sp., *Artemisia sp.*, and *Ephedra intermedia* (Ivory and Lézine, 2009).

The coring sites are situated 15 - 35 km off the Makran coastline (Fig. 2.1) and receive some sediment input from rivers draining the Makran mountains and the Makran coastline (Fig. 2.6); thus any pollen in the rivers would be mostly tropical thorn forest, sand dune desert, dry sub-tropical and temperate semi-evergreen scrub forest vegetation type. Mangrove vegetation may provide an additional pollen input to the coring locations.

Buring boreal winter (Fig. 2.7c), the strong NE monsoonal winds may transport pollen across Pakistan, to the study region. However, a reversal occurs in boreal summer (Fig. 2.7b) when SW monsoonal winds are more prominent possibly transporting pollen from Oman across the Gulf of Oman. While arid conditions prevail throughout the mountain ranges of northern Oman, studies at several different elevations within the mountain ranges such as, Balad Seet (950 – 1020 m asl), Maqta (930 – 1180 m asl) and Al Jabal al Akhdar (1750–1930 m asl.), have shown that the mountains of northern Oman contain several different agro-climatic conditions (Gebauer *et al.,* 2007) with over 107 diverse crop species belonging to 39 families. Due to the hyper-aridity of the Arabian Peninsula, the agriculture of Oman depends heavily on intense irrigation (Norman *et al.,* 1997). Amongst the 39 families of cultivated species identified, Leguminosae, Gramineae, Rosaceae,

Rutaceae and Solanaceae were the most common (Gebauer *et al.,* 2007). Grazing pressures on the desert have increased across the whole Arabian Peninsula over the past decades (Oatham *et al.*, 1995) and now overgrazing is considered to be a serious problem (Ghazanfar, 2003). Goats, sheep, cattle and camels in northern Oman preferentially browse on certain plant species, resulting in a decline in some species, with those species avoided by the livestock increasing (Ghazanfar, 2003).

The natural vegetation of Oman is extremely sparse and is characterised by communities dominated by tree and shrub species such as *Acacia ehrenbergiana*, *Acacia tortilis*, *Nerium mascatense*, *Prosopis cineraria*, *Ziziphus spina-christi*, *Acridocarpus orientalis*, *Dyerophytum indicum*, *Ficus palmata*, *Grewia erythraea*, *Moringa peregrine*, *Dodonaea Viscose*, *Juniperus excelsa*, *Olea europaea*, *Sageretia thea* and *Sideroxylon mascatense* (Gebauer *et al.,* 2007).

2.9 Palaeoenvironmental change from the end of the Holocene humid period (9 - 5.5 ka cal BP) to present (~5.5 ka cal BP)

In extremely arid environments, continuous records of past environmental change are exceptionally rare with most continental records often discontinuous, with hundreds of years missing at the top of some lacustring sedimentary cores. Long continental sedimentary cores are rare, due to the lack of permanent lakes in these extremely arid regions. Frequently the top of lacustrine sedimentary sequences are absent, or hiatuses may exist in speleothem isotopic records (Fleitmann *et al.,* 2003). It appears that the only continuous records available come from marine sedimentary sequences (Ivory and Lézine, 2009). Most of the studies concerning environmental reconstructions have focused on Africa and pollen data from both lake and ocean records have proved a useful tool for reconstructing both vegetation and hydrological conditions. Records focusing on large-scale changes in the Holocene will be used to assist in the interpretation of small scale fluctuations seen offshore southern Iran in the late Holocene record.

2.9.1 The Atlantic monsoonal system and its influence on vegetation and upwelling in the Holocene

Considerable changes in vegetation have occurred on the African continent coinciding with the end of the HHP (Holocene Humid Period), with discrepancies in timing from West Africa to the northern Sahara desert. The HHP is attributed to a

strengthening of the African monsoon due to gradual orbital increases in summer seasonal insolation. However, the onset and termination of the HHP (whether abrupt or gradual) remains controversial. Results from ODP 658c (offshore Cap Blanc, Mauritania, Fig. 2.15) show that the onset and termination of this humid period were extremely abrupt, occurring within decades (deMenocal, 2000). Results have shown that during the period between 4500 to 1300 cal. yr BP forests between 4°S and 7°N were gradually replaced by open landscapes and grasslands (Lézine, 2009). The timing of this event varies locally depending on local hydrological conditions, with some lakes experiencing total desiccation, *e.g.* Lake Sinnda (Congo, Fig. 2.15) whilst other regions, *e.g.* Lake Bosumtwi (Ghana, Fig. 2.15) remaining forested, showing little change in vegetation (Talbot *et al*., 1984; Maley, 1991). In Mesopotamia, the event was abrupt and caused the aridification of the flood plains and is recorded by Aeolian and archaeological deposits accumulated in the Gulf of Oman (Weiss *et al*., 1993). The lack of long lacustrine material preserved on the African continent limits high-resolution palaeoenvironmental reconstruction over the Holocene period. However, Lake Yoa (N. Chad, Fig. 2.15) provides a high-resolution record showing the gradual step-like transition of aridification from 4700 to 2700 cal. yr BP (Kröpelin *et al*., 2008). The results show that after 2700 cal. yr BP progressive drying has taken place with an abundance of dry steppic vegetation, *e.g*. Amaranthaceae/Chenopodiaceae, *Artemisia* and *Ephedra* (Lézine, 2009). The results from Africa indicate a general gradual aridification from the end of the HHP until present.

Evidence is available to support enhanced productivity associated with intensified upwelling during glacial periods off the NW African margin (Berger *et al*., 1978). The upwelling phenomenon is related to a decrease in sea-surface temperatures associated with glacial periods (Van Zinderen Bakker, 1982 in Marret and Turon, 1994).
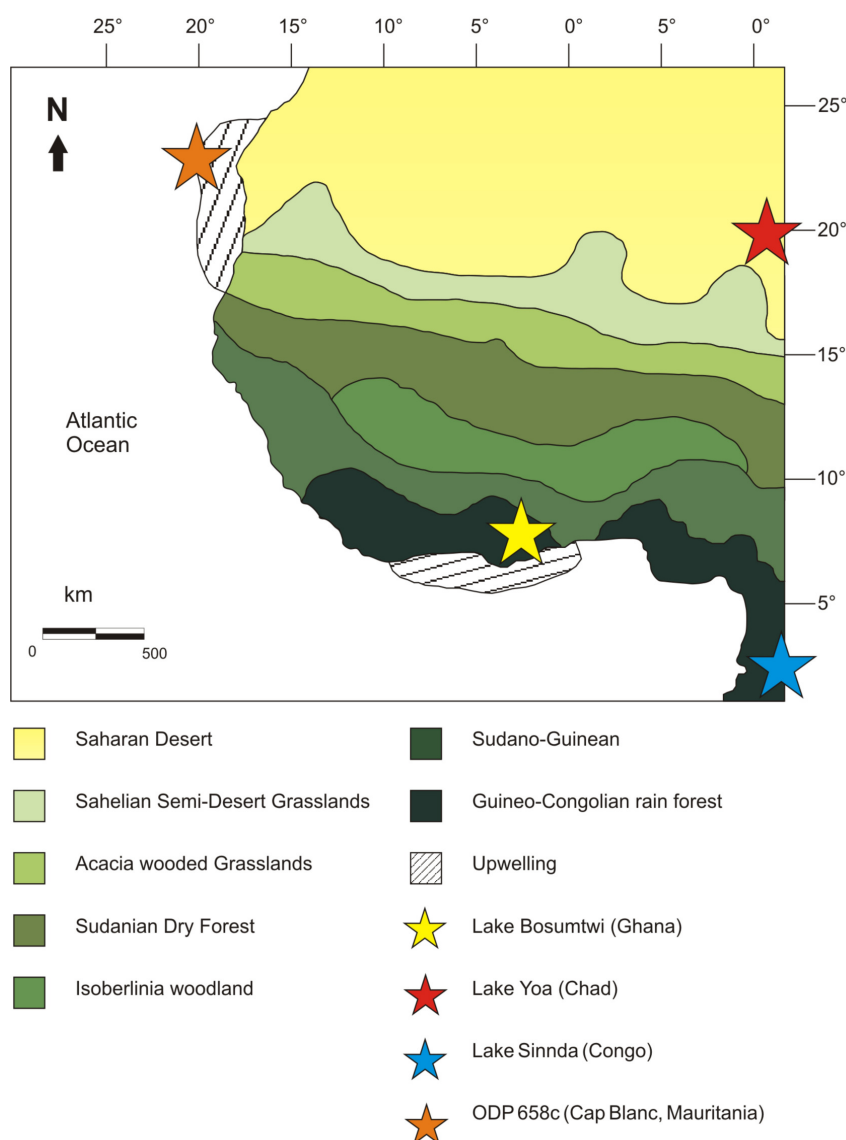
Fig. 2.15. Main latitudinal belts of vegetation zonation across south-west Africa and the location of Lake Bosumtwi (Ghana), Lake Yoa (Chad), Lake Sinnda (Congo) and ODP core 658c (offshore Mauritania). Modified from (White, 1983) and (Lezine and Vergnaud-Grazzini, 1993).

2.9.2 The Indian monsoonal system and its influence on vegetation and upwelling in the Holocene

In a comparison between the African and Indian monsoons, recent results show that variations in continental aridity (on time scales of 10^4 years) for both Africa and China have been roughly synchronous over the last 140 ka. Similarities include dry intervals recorded both in Africa and China between 7000 and 5600 yr BP and the onset of severe aridity at 4000 yr BP. These droughts were caused by weakenings of both the African and Indian monsoonal systems resulting in conditions almost emulating those experienced during glacial intervals (Guo *et al*., 2000).

An abrupt weakening in the Asian monsoonal strength occurred at 5000 - 4500 cal. yr BP (Morrill *et al.*, 2003). Vegetation change associated with this abrupt shift has recently been documented by Lézine (2009) in a 6000 year long sedimentary sequence from the eastern Arabian Sea, Kwar al Jaramah (Fig. 2.16 and 2.17).
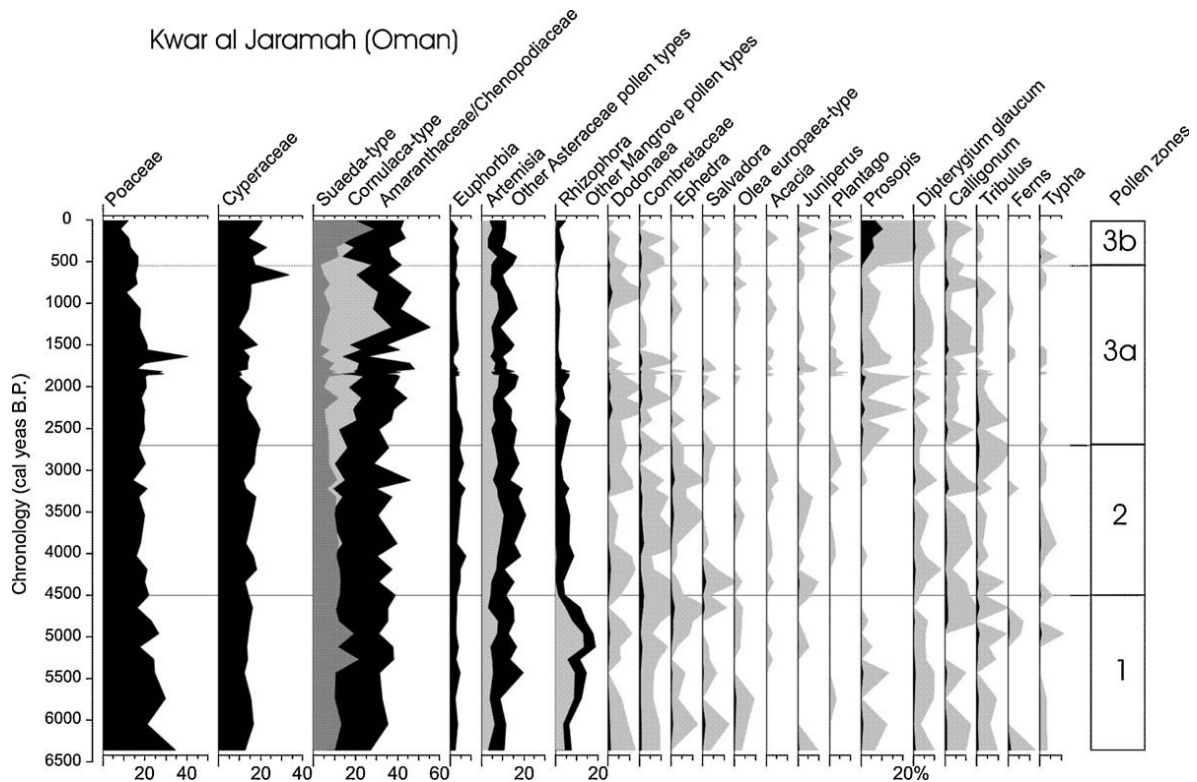
Fig. 2.16. Simplified pollen diagram for Kwar al Jaramah (Oman). This diagram shows percentages for the main pollen types. In grey x 10 exaggeration. From Lézine, 2009.

The pollen results undoubtedly display the dry conditions which have characterised the region over the last 6000 years with a dominance of semi-desert herbaceous plants from semi-desert communities (Chenopodiaceae, *Artemisia*, Asteraceae and Poaceae). Marine records encompassing the end of the transition from wet to dry at the end of the HHP show a gradual change associated with the decline of summer insolation and convective forcing by the surrounding highlands (Lézine *et al.*, 2010). The results are contrary to those observed off West Tropical Africa in core ODP 658c (Fig. 2.15) where an abrupt humid-arid transition marks the end of the HHP (deMenocal *et al.*, 2000). This abrupt transition was the result of summer seasonal insolation crossing a threshold value which was 4.2 % greater than the present (deMenocal *et al.*, 2000).
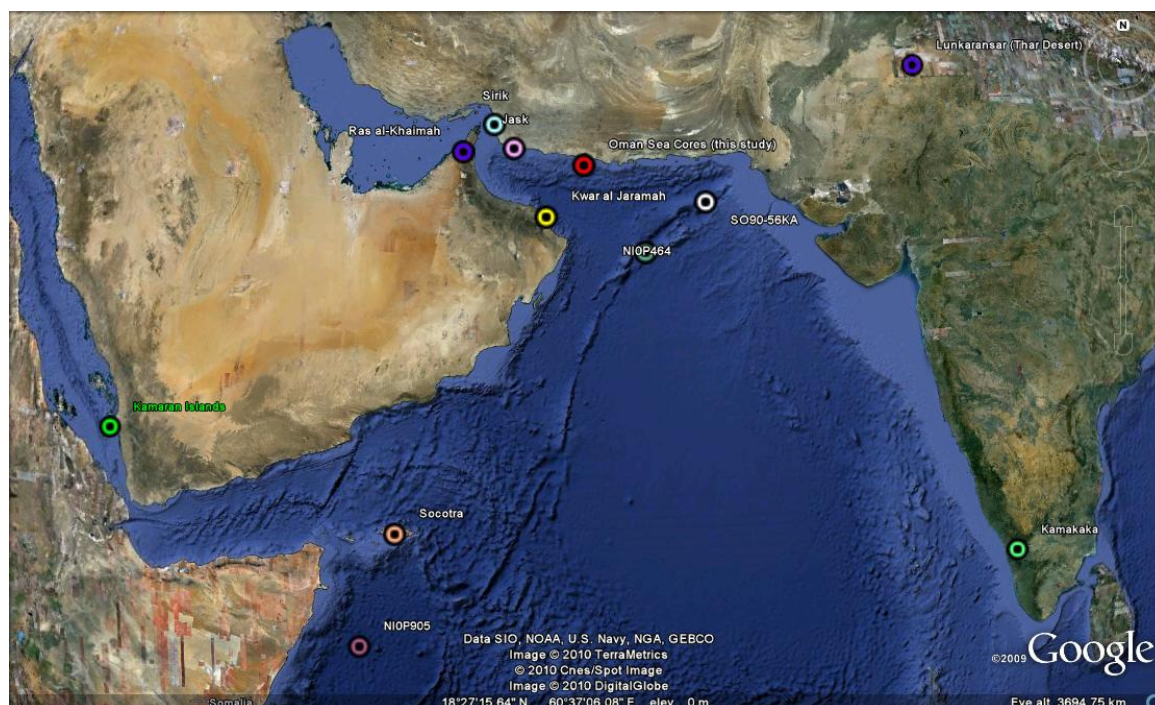
Fig. 2.17. Localities around Arabian Sea mentioned in discussion (Google Maps).

Core SO90-56KA situated off the Pakistan coast (Fig. 2.17) has been studied for geochemical, sedimentological and palynological information and provides us with small-scale fluctuations in climatic/environmental change from 5400 cal. yr BP to present. The pollen record of this core indicates that semi-arid conditions prevailed in the Makran region from the beginning of 5400 cal BP to the present, with the occurrence of steppic herbaceous pollen species (Ivory and Lézine, 2009). From 5400 - 4200 cal. yr BP, there was an increase of freshwater algae and mangrove vegetation such as *Rhizophora* to the coring locality, suggesting increases in river influx. Between 3200 and 2890 cal. yr BP, 1830 and 1090 cal. yr BP, and approximately 615 cal. yr BP the lack of freshwater indicators suggest lower influxes of freshwater flow (Ivory and Lézine, 2009). The aridification observed in core SO90-56KA (Fig. 2.17) is consistent with other palaeoenvironmental records of the region, showing complete desiccation of lakes after 5500 cal. yr BP in southern Arabia (Lézine *et al.* 2009), the Thar Desert (Fig. 2.17) north western India (Enzel *et al.* 1999) and geochemical and sedimentological records in the region of the expansion of dry environmental conditions (Ansari and Vink, 2007). The results indicate that the aridification to modern environmental conditions was gradual and mirrored the orbitally-induced long-term decrease of summer monsoon fluxes (Ivory and Lézine, 2009). The aridification was not

localised to Arabia and India as African records also show the end of the humid stage and the onset of more arid conditions. The lowering of lake levels also occurred at approximately 5.5 ka cal BP (Gasse and Van Campo, 1994; deMenocal *et al.* 2000; Gasse, 2000). The timing of the contraction of lake basins are roughly dispersed between 6 - 5 ka cal BP, but show some basin-to-basin variability (deMenocal *et al.,* 2000 and references therein).

In the NW Arabian Sea intense upwelling is directly related to boreal summer SW monsoonal winds. Past research has primarily focused on large-scale changes in the Holocene for example the Last Glacial Maximum. These changes will be used to assist in the interpretation of small scale fluctuations seen offshore southern Iran in the late Holocene record. Previous studies have suggested that during the Last Glacial Maximum biological productivity in the NW Arabian Sea was reduced and productivity maxima were reached during the early Holocene when sea surface temperatures (SST) increased (Overpeck *et al*., 1996). Records from the NE Arabian Sea show similar glacial-productivity relationships with maximum productivity reached during interglacial periods (von Rad et al., 1999) and minima occurring during the Younger Dryas and Heinrich Events H1 - H3. However this differs in the SE Arabian Sea where increased strength in the winter monsoonal winds during glacial periods lead to enhanced convective ocean mixing, nutrient injection and resulting in an increase in primary productivity (Thamban *et al*., 2000). In the SE Arabian Sea a reduction in surface planktonic productivity is identified during the early Holocene. This may have been the result of the complex oceanic circulation patterns existing along the SW coast of India (Thamban *et al*., 2001).

Over the last 3000 years it has been reported that upwelling conditions in the Arabian Sea have remained relatively constant. Long-chain 1,14-alkane diols, specific lipids of diatoms of the genus *Proboscia*, were used by Rampen *et al*. (2008) as new proxies to reconstruct upwelling conditions in the Arabian Sea. A diol index record was obtained from a piston core taken on the Somali slope (site NIOP 905, Fig. 2.17). The records show a dramatic increase in upwelling following the Younger Dryas, supporting previous findings of Overpeck *et al*. (1996), with upwelling remaining stable until 8.1 cal. ka BP. Upwelling increased again from 8.1 until 6.7 cal. ka BP. Levels of upwelling have remained at this high level from 6.7 cal. ka until the present day (Rampen *et al*., 2008).

2.10 Archaeological and historical context from 2300 cal. yr BP to present

The eastern Mediterranean, Africa, Persia, Mesopotamia and Arabia have a long history of human occupation and exploitation of the natural environment (Eastwood *et al*., 1998). Human occupational phases will be narrowed down to those present over the last 2300 cal. yr BP since this study focuses on palaeoenvironmental change on these timescales (Fig. 2.18).
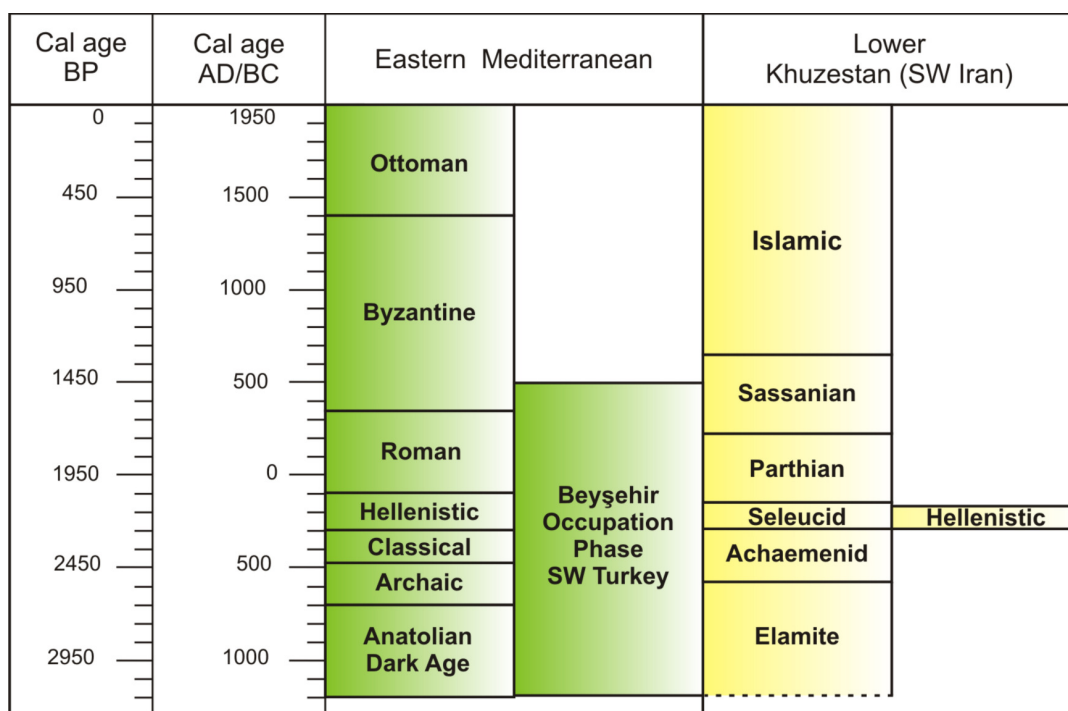
Fig. 2.18. Archaeological and historical timescale over last 4000 years (chronologies from Eastwood *et al*., 1998 and Djamali *et al*., 2008).

The Seleucid Empire (312 – *c*. 140 BC) (Fig. 2.18) encompassed modern Afghanistan, Iran, Iraq, Syria and Lebanon together with Turkey, Armenia, Turkmenistan, Uzbekistan and Tajikistan (Kuhrt and Sherwin-White, 1993). The Parthian Empire (160 BC – AD 221) (Fig. 2.18) was a major cultural and political power in Mesopotamia. Parthian history is only known through external sources, including Greek, Roman and Chinese documents of trade.

The Sassanid Period (AD 224 – 651) (Fig. 2.18) was the last pre-Islamic Persian Empire ruled by the Sassanian Dynasty. This period witnessed the peak of ancient Persian civilisation. The Sassanian kings made a large effort to extend settlement and cultivation and managed to construct irrigation systems on Mesopotamian floodplains which provided them with a wealthy material base

(Christensen, 1998). Pollen diagrams from Lake Almalou (northern Iran) indicate a phase of intensive tree cultivation which coincides with the Sassanid Empire (Fig. 2.18). Extensive infrastructure and irrigation management hugely increased crop productivity. The collapse of the Sassanid Period was a result of Islamic invasion, leading to the expansion of the Islamic Empire (Fig. 2.18). The invasion had a negative effect on the local agricultural system at the time with radical changes in the modes of food production (agriculture to pastoralism) (Djamali *et al.*, 2008).

The Beysehir Occupation Phase (Fig. 2.18) from roughly 3200 cal. yr BP to 1500 cal. yr BP (Eastwood *et al.*, 1998) is seen in pollen diagrams from southwest Turkey. The phase is an episode of increased anthropogenic activity and it is named after Beyşehir site where it is clearly expressed. The phase shows evidence of increased crop cultivation (cereals) and aboriculture (olives, manna and vines) and associated forest clearance. The Beyşehir Occupation Phase is better expressed in the palynological record than in the archaeological one. Pollen diagrams from N-W Turkey (Leroy *et al.*, 2010) and from the Levant (Leroy, 2010) show similar signals. In addition, regional pollen diagrams supported by facies change show that the Roman Byzantine Period 2100 – 600 cal. yr BP had a wet climate (Leroy, 2010, Neumann *et al.*, 2010). The wet period allowed intensive arboriculture around the Dead Sea region (Leroy *et al.*, 2009). The wet period was followed by a change to pastoralism at the Byzantine - Islamic transition (Leroy, 2010).

Both archaeological and historical documents provide qualitative agreement that moister conditions prevailed in the Mediterranean, Mesopotamia and northern Africa during Roman times, around 2000 cal. yr BP during the Roman Classical Period (Reale and Shukla, 2000) (Fig. 2.18). Previous research has suggested that the moister climate resulted in the wealthy agricultural economy of pre-Roman and Roman Africa in the areas of present northern Morocco and Algeria, Tunisia and Egypt (Reale and Shukla, 2000).

3. Methodology

3.1 Introduction

Palaeoenvironmental and palaeotsunami research requires a 'multi-proxy' approach to successfully identify and distinguish possible tsunamites and tempestites within geological record. The methods employed in this study were used to identify abrupt marine events and to reconstruct the past environmental history off and on southern Iran. The proxies used include: magnetic susceptibility, visual core logging, digital core photography, total organic carbon (TOC) analysis, total inorganic carbon (TIC), grain size analysis, palynology (pollen and dinoflagellate cyst analysis) combined with dating methods (^{210}Pb and ^{14}C) allowing the temporal evolution of these characteristics to be constrained.

3.2 Coring

The acquisition of the core material was performed by INCO (Fig. 3.1) in 2006 before to the start of this research project. The core locations were selected in water depths in excess of 50 m in order to distinguish between fine background sedimentation and any coarser abrupt marine invasions (Fig. 2.1, Table 3.1 and Fig. 4.1). The acquisition of undisturbed sediment cores was of fundamental importance since marine cores provide a good archive yielding great potential for providing information on seabed character, depositional history and environmental change (Rothwell and Rack, 2006).

The Oman Sea (OS) cores were collected using a gravity corer (Fig. 3.1 and 3.2), with all the cores being taken off the southern coast of Iran during a cruise in 2006 (Fig. 2.1, Table 3.1 and Fig. 4.1). Although a number of different methods of obtaining core samples exists, for this study gravity coring was selected. Despite being a relatively simple method of coring, its robust nature and low cost/maintenance make the gravity coring method particularly appealing. The cores collected were 67 mm in diameter and ranged in length depending on the sediment properties and the velocity of the corer when it intersects the sediment to be penetrated (*e.g.* Nevissi *et al.*, 1989).

Fig 3.1. Colleagues from INCO collecting sediment cores using a gravity corer in the Oman Sea (source: Majid Naderi per. com, 2007).

Table 3.1. Water depth, length and location of Oman Sea Cores.

Name	Water depth (m)	Length (cm)	Longitude	Latitude
OS34	190	90	59° 48.97' E	25° 14.27' N
OS55	170	88	60° 15.36' E	25° 07.41' N
OS73	100	141	60° 49.95' E	25° 08.20' N
OS84	200	61	61° 00.06' E	25° 01.20' N
OS94	214	34	61° 15.04' E	24° 52.01' N

Despite the simplicity of gravity coring, recent studies have highlighted a number of inherent problems, caveats including: vertical mixing of the top layers of sediment with those stratigraphically lower; shortening of the core relative to the *in situ* sediments it represents; bulk sediment loss; and general disturbance of unconsolidated material collected during the coring procedure (*e.g.* Nevissi *et al.*, 1989). Sediment disturbance may arise from a number of sources; however, the majority of disturbance is evidenced at the core top. This phenomenon arises either from the shock wave of the water preceding the corer, or from the impact of the downward movement of the corer through the sediment (Sachs and Raymond, 1965). To minimise the impact of sediment disturbance and potential contamination/dilution effects this disturbance may cause, sub-samples were taken from the middle of the core and a thorough visual inspection was conducted to avoid sampling close to any obvious disturbed intervals of unconsolidated sediment.
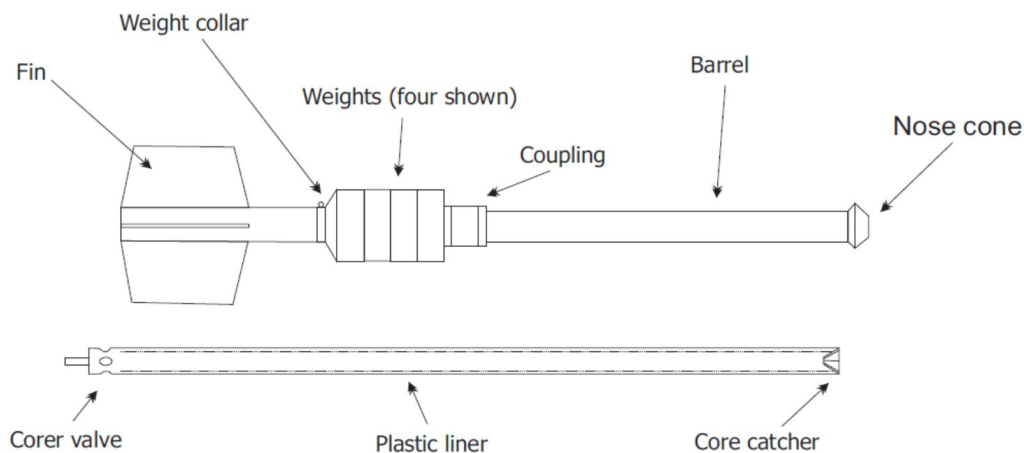
Fig 3.2. Schematic of gravity corer, adapted from Lee and Clausner (1979).

3.3 Visual description & core photography

Standard visual core description was performed using a Munsell colour chart, handlens, and a Geo grainsize card. Detailed descriptions were recorded detailing: sedimentary structures, mineralogy and the nature of the contacts (whether sharp or gradual). Sediment description was achieved following the ODP method and guidelines (Mazullo *et al.*, 1988). First the bedding variations were described noting variations in lithology, colour, sedimentary structures and any other significant characteristics. Subsequently, major characteristics of each bed were described, including thickness, sedimentary structures, degree of bioturbation, contacts separating bedding places and also the degree of any noticeable drilling disturbance (Mazullo *et al.*, 1988). The cores were described immediately after core photography prior to any destructive sampling and analysis.

Individual cores were photographed using a Kodak EasyShare Z1275 camera (12 mega-pixels), with separate images compiled to form high-resolution digital images. Larger-scale photographs were also taken using a Nikon D3 camera with a speed of ISO 200 and an f22 aperture to highlight the gross similarities/differences between the cores.

3.4 Magnetic susceptibility

The magnetic susceptibility of a sample is given by the ratio of induced (temporary) magnetization acquired by the sample in the presence of a weak magnetic field. It is, in essence, the capability of the minerals within a material to be attracted to a magnet (Sandgren and Snowball, 2002). The origin of the magnetism

lies in the orbital spin motions of the electrons and how they interact with one another. All material is magnetic however some material is more magnetic than others. When the material contains a strong interaction between atomic moments it has a high degree of magnetic susceptibility. The magnetic behaviour of all materials can be classified into five major groups; diamagnetism (atoms which have no net magnetic moments *e.g.* quartz, calcite, water), paramagnetism (*e.g.* biotite, pyrite, siderite), ferromagnetism (*e.g.* cobalt, iron, nickel), ferrimagnetism (*e.g.* magnetite) and antiferromagnetism (*e.g.* hematite) (Sandgren and Snowball, 2002). Sedimentary deposits generally contain a range of minerals of different magnetic properties belonging to the groups above. The technique measured the retrospective contributions of the above groups to the bulk susceptibility signal.

Magnetic susceptibility can indicate palaeoclimatic and palaeoenvironmental change in both oceanic (*e.g.* Bloemendal, 1983; Robinson, 1990; Robinson *et al*., 1995) and terrestrial settings (*e.g.* Heller *et al*., 1993; Maher *et al*., 1994; Hounslow and Maher, 1999). To link palaeoenvironmental change to fluctuations in the magnetic susceptibility requires an identification of the origin of the magnetic minerals. Susceptibility variations can occur due to changes in 1) the abundance in detrital magnetic minerals, 2) the abundance and mineralogy of magnetic materials formed in situ by authigenic processes, 3) the preservation/dissolution of magnetic grains and 4) the amount of diamagnetic minerals (*e.g.* increased abundance of silica or carbonates can dilute the remaining magnetic material) (Hounslow and Maher, 1999). These factors affecting magnetic susceptibility values can indicate various environmental phenomena, for example, fluctuations in aeolian dust influx (Shackleton *et al*., 1984), changes in oceanic upwelling, productivity and monsoon intensity and variations in erosion and weathering intensity (Shimmield *et al*., 1990; Clemens and Prell, 1990; Weedon and Shimmield, 1991). Measurements of magnetic susceptibility can be made rapidly and with little expense. It is a non-destructive technique which leaves the core available for much more proxy analysis. In addition the technique was used as it identifies magnetic phases within the sediment core independently from grain size. Magnetic susceptibility was measured on all cores at 1 cm intervals for environmental and palaeomagnetic investigation using a Bartington MS2 magnetic susceptibly system with the MS2C whole-core logging sensor (Fig. 3.3). The technique is also important as it can allow correlation between cores.
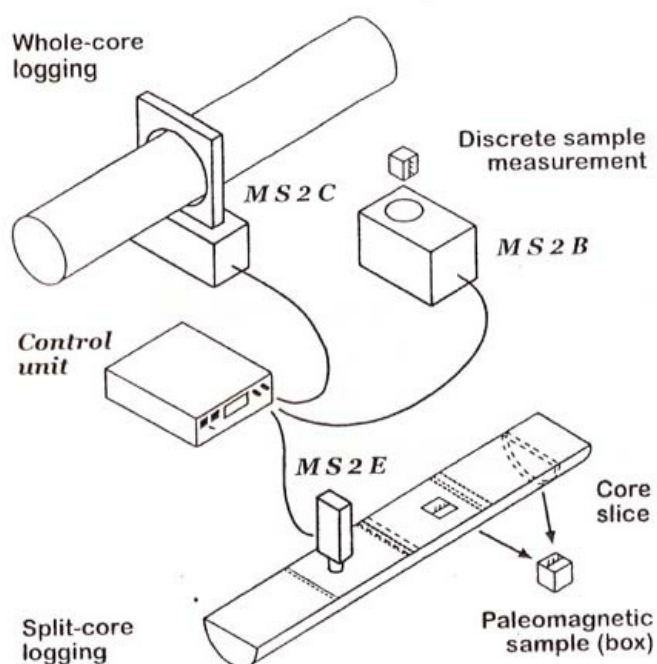
Fig 3.3. Various magnetic susceptibility sensors from Bartington (Nowaczyk, 2001; Costa, 2006)

3.5 Grain size analysis

Grain size analysis was performed by INCO in Iran at regular 4 cm intervals throughout each of the cores. Due to the coarse resolution of the sampling, grain size analysis was performed again at finer scale resolution on core OS55 and 73 using a Cilas 1064 laser particle size analyser for the interpretation of depositional processes and sedimentary structures at Brunel University. The cores were sub-sampled for grain size every cm and prepared for analysis. Initially the samples were weighed to 0.05 g and soaked in 10 ml 10 % tetrasodium pyrophosphate to deflocculate. The samples were then added into the Cilas using the program Size Expert. Background measurements and rinsing were performed in between each sample measurement to keep the results consistent and reliable. Twenty seconds of ultrasound and fast-pumping was also used for each sample. Statistical analyses was carried out on the data produced including mean, median, skewness, kurtosis and standard deviation. The results were also plotted on a particle size distribution plot (Beierle *et al*., 2002).

3.6 Palynology (pollen and dinoflagellate cyst analysis)

Both micro and macro-fossils can be important tools to identify tsunamites within the stratigraphic record (Donato *et al*., 2009). Pollen and dinoflagellate cyst assemblages were analysed in order to assess any potential change in

sedimentation associated with abrupt marine events. In addition palynology is a good tool for reconstructing past ocean and terrestrial environments.

Although pollen and dinoflagellate preservation was good with almost all grains being in excellent preservation condition, pollen concentrations were relatively low and with time constraints it was challenging to count >300 grains per sample. Pollen concentration values were calculated by adding *Lycopodium* tablets to weighed sediment samples (Stockmarr, 1972).

Cores OS55 and 73 were sub-sampled for the palynological analysis. From grain size analysis and visual core description OS73 did not appear to contain substantial variations in sediment type and thus was sampled at regular intervals throughout the core. OS55 was sub-sampled around and through any suspected event beds. The samples were prepared for palynological analysis using the following procedure: 1) Volume of samples measured as precisely as possible (to 1/10 of ml) using the displacement method in tetrasodium pyrophosphate ($Na_4P_2O_7$) which acted as a defloculant. 2) Two *Lycopodium* tablets, of known concentration, were then added to determine concentrations of microfossils per millilitre of wet sediment. 3) 10 % HCL. 4) Concentrated HCL. 5) 60 % HF. 6) Concentrated HCL rinsing. 7) Sieving at 125 µm and 10 µm. 8) Residues transferred into vials using alcohol then mounted on glass slides with glycerol and sealed with nail varnish. Acetolysis was not used in the sample preparation as the process destroys dinoflagellate cysts.

Pollen and dinoflagellates were counted under a light microscope at a routine magnification of 400 X and 1000 X for special identifications. Pollen grains were identified using Faegri and Iversen (1989), Reille (1995), the online African Pollen Database (http://medias.obs-mip.fr/apd/) and PalDat (www.paldat.org). Dinoflagellates were identified using the papers of Zonneveld (1997a; 1997b), Zonneveld and Jurkschat (1999), Rochon *et al*. (1999) and Fabienne Marret, Robert Fensome and Henk Brinkhuis (pers. com. 2009). Pollen and dinoflagellate concentrations were calculated using the following equation (Equ 3.1).

Equation 3.1. Concentration calculation, using *Lycopodium* marker spores.

Concentration =

$$\frac{\text{number of counted pollen or dinos x number of } \textit{Lycopodium} \text{ added}}{\text{number of counted } \textit{Lycopodium} \text{ x volume of sample}}$$

3.7 Dating methods (^{14}C and ^{210}Pb)

Precise dating of the sediment cores was imperative in order to match potential abrupt marine events to historical events recorded in the literature and to establish accurate environmental reconstructions. Two dating methods were used in this study: ^{210}Pb and ^{14}C dating. ^{210}Pb and ^{137}Cs for core OS55 were performed by Andrew Cundy and Phillip Teasdale at University of Brighton in 2009. ^{210}Pb dating for core OS73 was performed at Brunel University.

Radiometric dating methods have proved their reliability in a large number of studies of lacustrine environments, whether sediment accumulation rates are uniform or non-uniform (French *et al*., 1994; Cundy *et al*., 2000; Arnaud *et al*., 2002). In the past 15 years the use of ^{210}Pb to date relatively modern sedimentary sequences has become an increasingly common approach. Although the majority of work to date has been carried out on lake deposits, the application of such isotope methods to the marine environment is becoming increasingly important (French *et al*., 1994; Schwab *et al*., 2009).

Unfortunately dating of the most recent part of the geological timescale presents us with considerable challenges (Gale, 2009). Several techniques are available which can be used for dating of the recent past, with ^{14}C, ^{210}Pb and ^{137}Cs been the only widely available procedures, with each procedure having its disadvantages. ^{14}C methods are made complex by a plateau in the calibration curve between AD 1650 and AD 1950. ^{210}Pb appears to be capable of resolving the chronological challenges of the most recent past, giving high resolution dates with uncertainties varying from less than a year to around a decade at the chronological limit of the procedure (Gale, 2009). However the ^{210}Pb dating method is limited to sedimentary deposits less than approximately 120 to 150 years old (5–7 half lives of ^{210}Pb), which is taken as the period over which ^{210}Pb$_{excess}$ decays to negligible activities which cannot be measured (Cundy and Stewart, 2004). In addition, ^{210}Pb dating becomes more problematic if the ^{210}Pb has been mobilised within the sediment.

3.7.1 ^{210}Pb

^{210}Pb is a naturally occurring radionuclide in the ^{238}U decay series (Fig. 3.4). The major source of ^{210}Pb to rivers, lakes, peatlands, polar ices, and the ocean is direct atmospheric ^{210}Pb deposition (El-Daoushy, 1988). Atmospheric ^{210}Pb or 'unsupported' is created through the emanation of ^{222}Rn from continental lands

devoid of glaciers and permafrost (El-Daoushy, 1988) at an average rate of 4×10^{-17} Ci cm^{-2} sec^{-1} (Wilkening *et al*., 1974). Supported ^{210}Pb originates from the decay of ^{238}U in the sediments (Lund-Hansen, 1991). The amount of radon emanation from the land fluctuates and is mainly influenced by changing meteorological conditions (Pearson and Jones, 1966). Once in the atmosphere where it has a residence time of 9.6 days to few weeks (Burton and Stewart, 1960; Peirson *et al*., 1966; Francis *et al*., 1970) it is removed from the atmosphere in a process called wash-out. Upon entry to the water column eventually ^{210}Pb is removed by settling particulate matter at the sediment-water interface by sedimentation and exchange processes (Eakins and Morrison, 1978). In the marine environment there is an additional source of ^{210}Pb in the sediment coming from ^{226}Ra which is present in the overlying water column (Eakins and Morrison, 1978). Providing the input and residence time of ^{210}Pb remains constant and there is little migration within the sediment, the concentration of unsupported ^{210}Pb within the sediment will decrease as a function of depth due to radioactive decay enabling the age of the sediment at any particular depth to be calculated and thus the sedimentation rate.

Uranium-238 (α) (4,460,000,000 years)

Thorium-234(β) (24.1 days)

Protactinium-234 (β) (1.17 minutes)

Uranium-234 (α) (247,000 years)

Thorium-230 (α) (80,000 years)

Radium-226 (α) 1,602 years

Radon-222 (α) (3.82 days)

Polonium-218 (α) (3.05 minutes)

Lead-214 (β) (27 minutes)

Bismuth-214 (β) (19.7 minutes)

Polonium-214 (α) (1 microsecond)

Lead-210 (β) (22.3 years)

Bismuth-210 (β) (5.01 days)

Polonium-210 (α) (138.4 days)
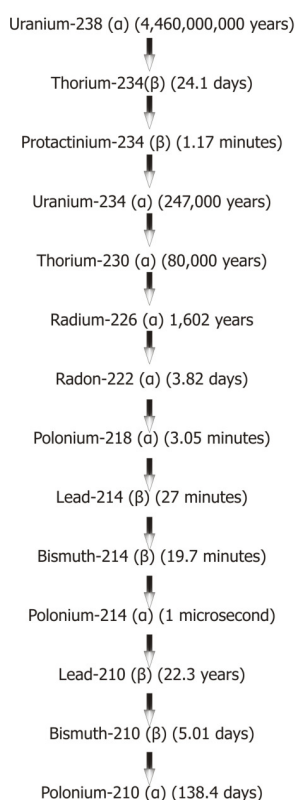
Fig 3.4. Uranium-238 decay series.

"The ^{210}Pb method relies on an estimation of the lingering radioactivity arising from the presence of unsupported ^{210}Pb in the

sediments derived from 'rain-out' onto the surface of the water body beneath which the sediments have accumulated" (Appleby and Oldfield, 1978).

Various laboratory techniques have been developed to estimate the residual unsupported ^{210}Pb content. Gamma emission can be used to measure total ^{210}Pb activity directly (Gäggeler *et al.*, 1976). Emissions can be measured indirectly by using either the beta emitting daughter isotope ^{210}Bi (Krishnaswamy *et al.,* 1971, Koide *et al.,* 1972; 1973, Robbins and Edgington, 1975) or the alpha emitting granddaughter isotope ^{210}Po (Eakins and Morrison, 1978).

In addition to ^{210}Pb, ^{137}Cs can also be measured. ^{137}Cs has a half-life of 30 years and is an artificially produced radionuclide. It is only present in the environment owing to atmospheric fallout from nuclear weapons testing, reactor accidents and deliberate discharges from nuclear facilities (Cundy and Stewart, 2004). Following the initial release of ^{137}Cs from nuclear weapons testing in 1954, atmospheric fallout maxima has occurred in 1958, 1963 and 1986 (from Chernobyl). Measurement of ^{137}Cs within a sediment core can be used to identify subsurface activity maxima and used to date the sediment column *e.g.* Ritchie and McHenry (1990), Cundy and Croudace (1996) and Cundy and Stewart (2004).

In this study samples were measured for ^{210}Pb using the Alpha Spectrometer at Brunel University, following the methodology of Flynn (1968) which was subsequently adapted by Teasdale (2005). ^{137}Cs was determined by using gamma spectrometry at the University of Brighton by Andrew Cundy and Phill Teasdale.

Detail of the ^{210}Pb dating method using the proxy method of ^{210}Po determination following acid leaching and auto-deposition on Ag discs is as follows. The top 30 cm of the core was sub-sampled at regular intervals where by 1 - 3 g sample were weighed and then dried at 60°C. 0.5 ml of ^{209}Po yield tracer was then added and the weight of the sample was recorded immediately. 30 ml of freshly prepared aqua regia was added to each sample and left to digest for 3 - 5 hours. A further 20 ml of aqua regia was added and the samples were covered with a watch glass and gently refluxed on a hotplate overnight. The samples were allowed to cool, filtered and the residue washed 3 times with distilled water. The supernatant was then collected and dried prior to been taken up in 5.5 ml of 6M HCL. Subsequently, the solution was transferred to a Po plating cell. 1.5 g of ascorbic acid was added to the cell and stirred until the solution changed to a pale green

colour. A pre-prepared silver disc was added to the Po plating cell and left to plate for 36 hours. The plating cell was washed with distilled water and left covered for 24 hours before counting on the Alpha Spectrometer. The samples were then analysed in an Ortec Alpha Spectrometer at Brunel University. The results obtained were then calculated based on the 'Constant Rate of Supply model' (Appleby and Oldfield, 1978). This assumes that the supply of unsupported ^{210}Pb to the sediment is the same for each time interval therefore the initial concentration C_0 (t) of unsupported ^{210}Pb in sediment of age (t) years must satisfy:

Equation 3.2. Constant Rate of Supply (Appleby and Oldfield, 1978).

$$C_0(t)\, r(t) = const$$

3.7.2 Radiocarbon (^{14}C)

Carbon has three natural isotopes, ^{12}C and ^{13}C (stable), with relative abundances of 98.9 % and 1.1 %, and ^{14}C or radiocarbon (radioactive), which occurs only in minute amounts (*e.g.* 1.2 x 10^{-10} % in the troposphere) (Hua, 2009). Radiocarbon is produced continuously within the atmosphere by the interaction between atmospheric ^{14}N and cosmic rays:

Equation 3.3. The production of radiocarbon within the atmosphere (Hua, 2009).

$$^{14}N + n\ (neutron) = {}^{14}C + p\ (proton)$$
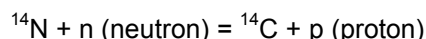
Radiocarbon is then taken up by living organisms through the food chain and via metabolic processes. Metabolic fixation of ^{14}C is continuous throughout the lifetime of an organism. However, when the organism dies, the fixation of radiocarbon ceases and the ^{14}C within the organism starts to decay at rate termed the half-life (5730 years for ^{14}C - Godwin, 1962). The time elapsed since the organism has originally formed can be calculated from the following equation:

Equation 3.4. Calculation of the time since the formation of an organism (Hua, 2009).

$$T = -\frac{T_{1/2}}{1n2} 1n\left(\frac{N(t)}{N_0}\right)$$

Whereby $T_{1/2}$ is the radiocarbon half-life, N_0 is the original ^{14}C concentration in the organism and N (t) is its residual ^{14}C concentration at time t (Hua, 2009).

Three radiocarbon dates were attained for core OS73. A 15 g sample was collected at the bottom of the core at 147.5 - 149.5 cm. The sample was sieved

using 125 µm mesh and gastropods were picked. The largest gastropod was sent to Beta Analytic (Florida, USA) for analysis. Additional gastropods were picked at 86.5 and 120.5 cm and sent to the Chrono Centre at Queens University, Belfast for radiocarbon dating. It was reported that all the gastropods provided plenty of carbon for an accurate measurement and the analysis proceeded normally. Before the samples were processed for dating, any contaminants (material containing carbon that did not belong to the original sample) were removed. Without this pre-treatment step incorrect ages may have been determined. According to Hedges (1992), the removal of contamination can be carried out using various strategies. In this case, acid etching was used. The calibration database MARINE04 was used and the dates were adjusted for the local reservoir correction from the Marine Reservoir Correction database.

There are two methods used for radiocarbon dating; radiometric dating and accelerator mass spectrometry (AMS) (Tuniz *et al*., 1998; Jull and Burr, 2006). The AMS method counts ^{14}C atoms directly (relative to the stable carbon isotopes ^{13}C and ^{12}C) while the radiometric method involves measuring ^{14}C by either gas proportional or liquid scintillation counters (Taylor, 1987). In this study AMS dating was used, due to its advantages in terms of measurement time (from minutes to a few hours for AMS compared to days for the radiometric method) and the smaller quantity of material required for dating (Hua, 2009).

3.8 Geochemical analysis (organic matter and calcium carbonate content) and oceanographic data

Geochemical analysis was performed by INCO colleagues in Iran at regular 4 cm intervals throughout each of the cores. Whilst coring INCO also recorded several oceanographic parameters. The data was obtained using an Ocean Seven 316 CTD (conductivity, temperature, depth) probe (Idronaut, Italy). The CTD can measure a variety of parameters for example pressure, temperature, conductivity and dissolved oxygen content. It was ensured that the CTD probe passed pre-calibrations and laboratory procedures prior to the survey in order to achieve precise estimates of conductivity ($\pm$0.003 ms cm^{-1}), temperature ($\pm$0.003 °C), and pressure (0.05 % full scale) in deep water. Dissolved oxygen measurements were made using a routinely calibrated polarographic oxygen sensor which is insensitive to nitrogen, nitrous oxide, carbon dioxide and other gases. In addition, the probe was equipped with ancillary sensors such as chlorophyll a and pH. CTD profiling

was carried out at some stations and cores were obtained within some of the transects (Muna Hossein Dust, pers. com.).

3.8.1 Total organic carbon

Total organic matter (TOC) was determined by wet digestion in hydrogen peroxide (using the method described in Schumacher, 2002). This method destroys organic matter in the sample through oxidation and involves the addition of concentrated hydrogen peroxide (30 % or 50 %) to a known weight of sediment (Schumacher, 2002). The samples were heated to around 90°C whilst hydrogen peroxide was continually added to the sample until the reaction ceased. This addition of heat increases the speed of peroxide digestion. After digestion the sample is dried at 105°C in a desiccator and then weighed. The percentage of organic matter is determined gravimetrically and is calculated as the difference between the initial and final sample weights divided by the initial sample weight times 100 % (Schumacher, 2002).

Several limitations exist for the hydrogen peroxide digestion method, which reduce its effectiveness, rendering the method as semi-quantitative at best (Schumacher, 2002). Prior to analysis, whilst collecting and handling the samples loss of organic compounds may occur for several reasons including microbial degradation, oxidation, volatilisation, sample drying and sample processing biases (*e.g.* selective removal of carbon-bearing components) (Schumacher, 2002). The main limitation of the method is that organic matter oxidation can be incomplete and the degree of the oxidation can vary depending on the sediment type (Robinson, 1927). The loss of volatile organic compounds when samples are oven dried prior to digestion is also a potential source of error.

3.8.2 Calcium carbonate

Total inorganic carbon (TIC) was determined rather than $CaCO_3$ %. The TIC content of sediments was determined by simple decarbonation. To achieve this, aliquots of dried sample were weighed into a series of pre-weighed beakers and reacted with a stoichiometric excess of 10 % HCl (vol. %) in the reaction below.

Equation 3.5. Debcarbonation reaction.

$$CaCO_3(s) + 2HCl(aq) \rightarrow CaCl_2(aq) + CO_2(g) + H_2O(l)$$

These beakers where left overnight, to ensure a complete reaction and dissolution

of more resilient carbonate minerals (e.g siderite). The excess supernatent fluid was pippetted off before the residues were dried thoroughly, prior to being reweighed. Simple subtraction allowed the mass lost to be calculated, which assuming the HCl only attacked carbonate phases, allowed the calculation of the TIC content expressed as a weight percent (wt %):

TIC was determined rather than $CaCO_3$ because the HCl attacks the CO_3 anion, in an acid-base reaction, and hence it is not particular about whether it attacks $CaCO_3$ (calcite/aragonite + exotic species), $CaMg(CO_3)_2$ (dolomite) or $FeCO_3$ (siderite). It is assumed that $CaCO_3$ is the most prevalent phase in the majority of cores, nevertheless there will always be other CO_3 baring phases within the sample.

4. Results

4.1 Coring

A series of cores were collected by INCO in 2006 for oceanographic research, of which, five gravity cores were provided to Brunel University in 2007 (Fig. 4.1).
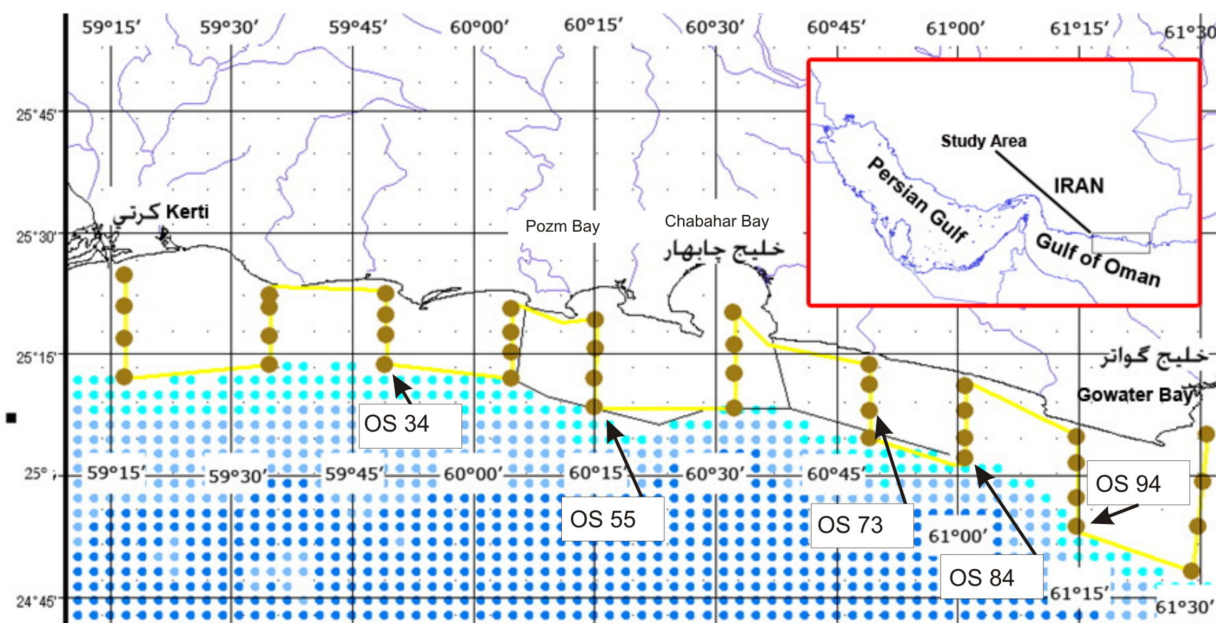
Fig. 4.1. Spatial distribution of INCO coring locations in the northern Arabian Sea (Map provided by INCO).

Two of these cores were subsequently selected for further study and are described in detail, core OS55 and 73 (Table 3.1). Core OS55 was selected because it contained a variety of sediment types (Fig. 4.2). As the material available for reworking in core OS55 was not restricted to muds and fine silts, it was hoped that the changes in sedimentology may be more evident and possibly be related to abrupt marine events. Core OS73 was selected for further study because it was the longest core in the region and also contained minimal changes in sediment type (Fig. 4.2), therefore any changes in pollen and dinoflagellate assemblage would be related to palaeoclimatic signals and not the changing sedimentary regime. Subsequent to coring, the cores were stored in PVC pipes and were halved and analysed for % of organic matter and % of calcium carbonate at the INCO laboratory in Chabahar. The cores were also subjected to grain-size analysis using a particle size analyser at 4 cm intervals. Half cores were then sent to Brunel University and on arrival the cores were visually inspected and stored at

5°C for the duration of this study, preventing the oxidation of organic matter and re-equilibration under ambient conditions (modification of sedimentary structures and core length).
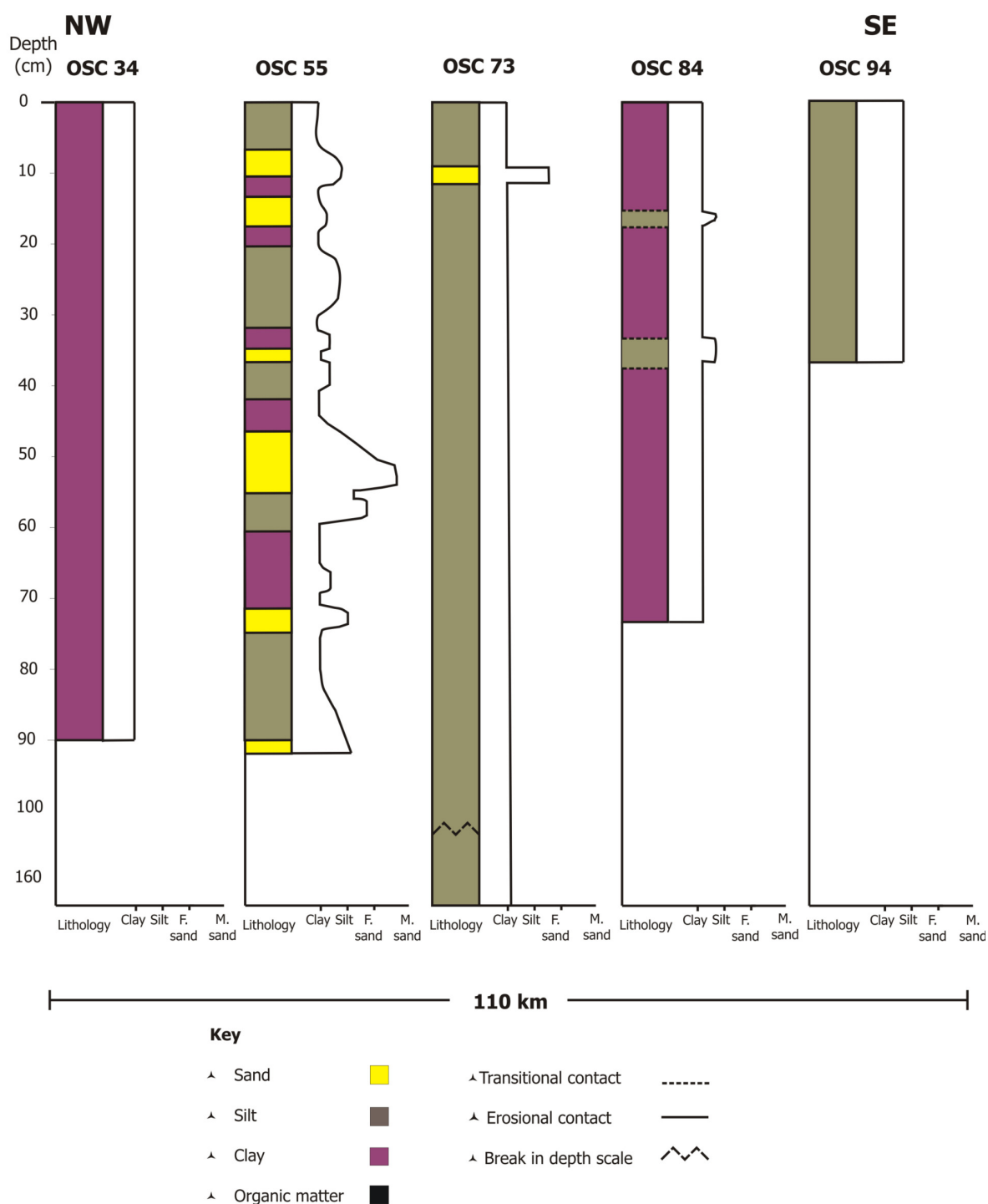
Fig. 4.2. Schematic lithostratigraphy of Oman Sea Cores.

4.2 INCO data

Whilst coring INCO also collected the following oceanographic data: temperature, salinity, oxygen saturation, dissolved oxygen, pH and chlorophyll a (blue-green pigment) at various locations along the Iranian coastline (Fig. 4.3).

Fig. 4.3. Spatial distribution of locations where INCO recorded oceanographic parameters.

Fig. 4.4a-c shows temperature, oxygen saturation and chlorophyll a decreasing with depth with both density (σt kg m^{-3}) and pH demonstrating an inverse relationship. Oxygen saturation (Fig. 4.4a.) shows exponential decrease with depth, with maximum values of 130 % between 10-20 m depth, decreasing to below 10 % after 90 m depth. Chlorophyll a (Fig. 4.4b) fluctuates greatly between 1 and 12.5 µg l^{-1} from 1 to 7 m depth. The values then remain low from 7 m to 250 m which appears to be rather unusual.

A.

B.

C.
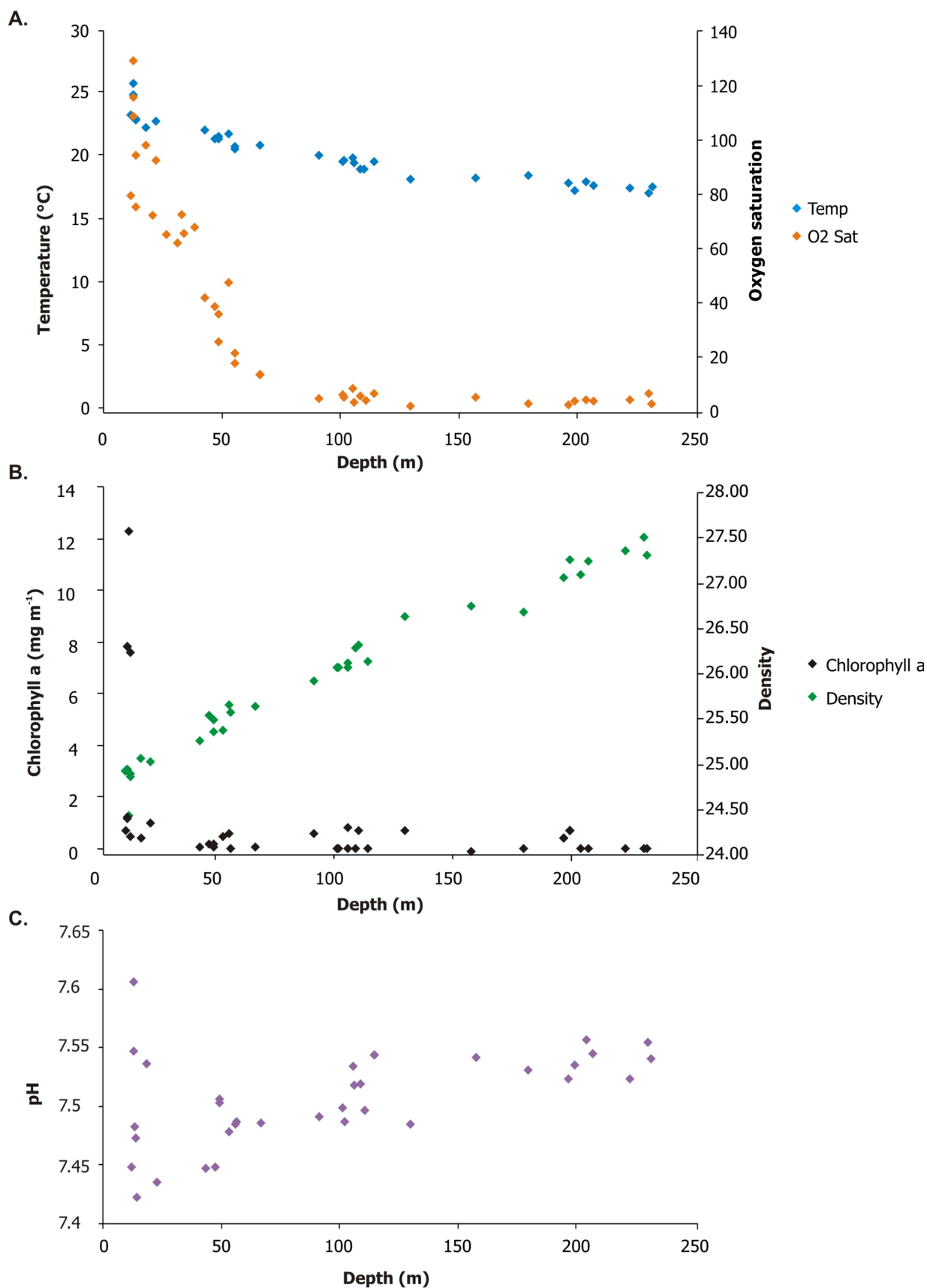
Fig. 4.4. A compilation of a) Temperature (°C) and oxygen saturation (%) of water samples taken by INCO. b) Chlorophyll a (µg l^{-1}) and density (σt) of samples taken by INCO. c) pH of samples taken by INCO during coring campaign along southern Iranian coastline (Fig. 4.3).

4.3 Sediment and core description

Standard visual core description was performed on all cores at Brunel University. The majority of cores consist of mostly silts and clays, with little depth variation.

Core OS34 and 94 (Fig. 4.2, 4.5 and 4.9) (the cores farthest to the east and west of the study region) contain laminated silts and clays containing no evidence of high energy events or any disturbance in sedimentation. Core OS84 (Fig. 4.2 and 4.8) consisted of very fine clay material but contained two slightly coarser horizons of silt at 17 and 35 cm with gradual transitional contacts. All three of these cores, which demonstrate primarily continuous homogeneous sedimentation were recovered in the deepest waters (>190 m).

Core OS73 (Fig. 4.2 and 4.7) consists of mostly silt with a single unit of sand, with both upper and lower erosional contacts. Core OS55 (Fig. 4.2 and Fig. 4.6) contains a large variety of sediment types, with fining upward deposition and erosional contacts below each sand bed. Both core OS55 and 73 were taken at water depths less than 170 m.

Core OS55, 73, 84 and 94 contain iron mottling staining. This is due to oxidation of iron minerals on the surface of the core subsequent to deposition and core aquisation and has no implications for palaeoenvironmental reconstruction.

Lithology key

- Sand ⬚ (yellow)
- Silt ⬚ (grey)
- Clay ⬚ (purple)
- Organic matter ⬚ (black)

Symbol key

- Cross laminations
- Cross bedding
- Massive beds
- Horizontal laminations
- Hummocky cross stratification
- Lenticular bedding

- Wave ripples
- Symmetrical wave ripples
- Drilling distu.
- Iron oxide mottling
- Bivalve
- Fragmented fossils
- Wood
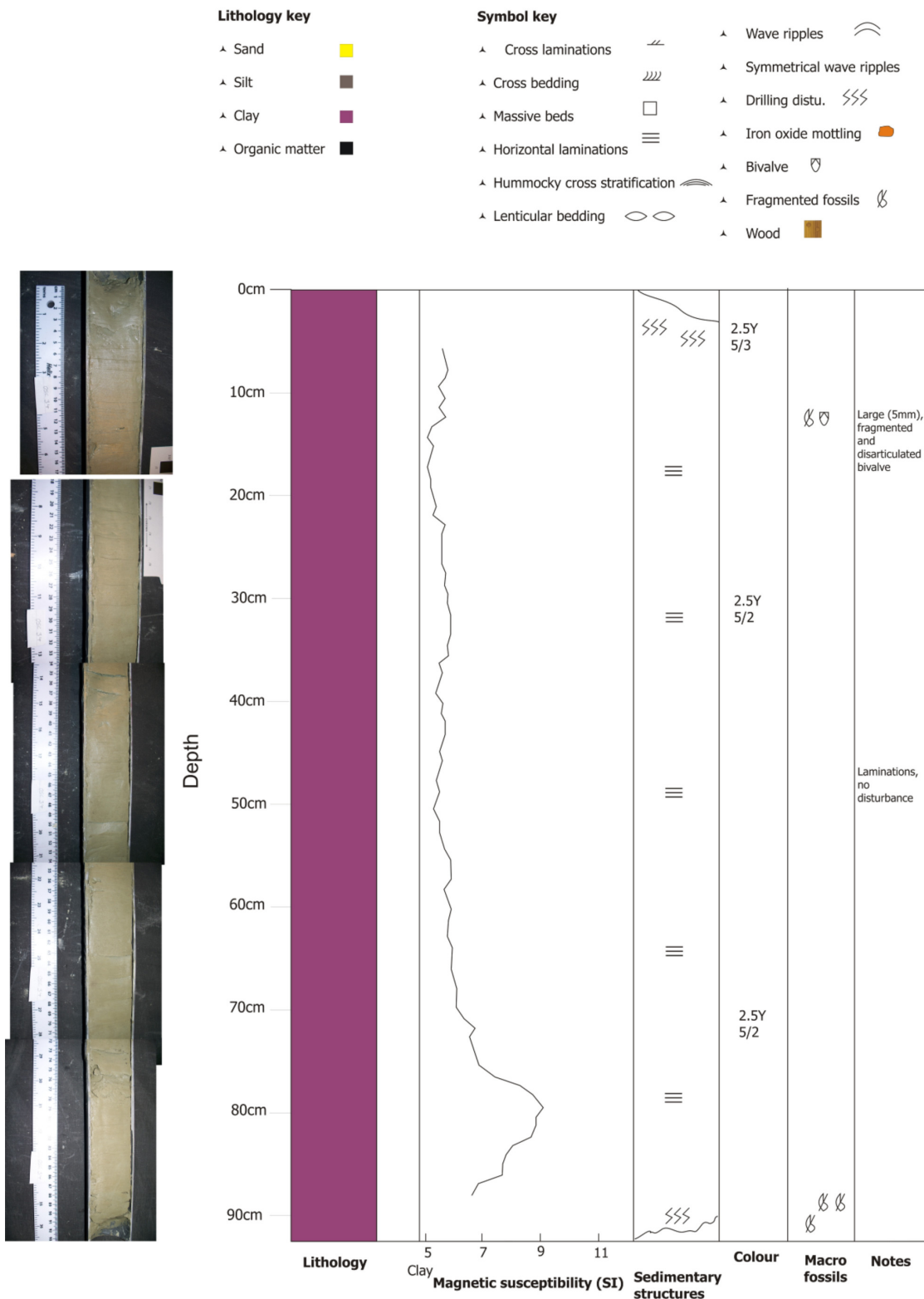
Fig. 4.5. Sedimentary log for OS34, displaying lithology, magnetic susceptibility (S.I), sedimentary structures (including evidence of drilling disturbance), colour (using Munsell colour chart) and the presence of macrofossils.
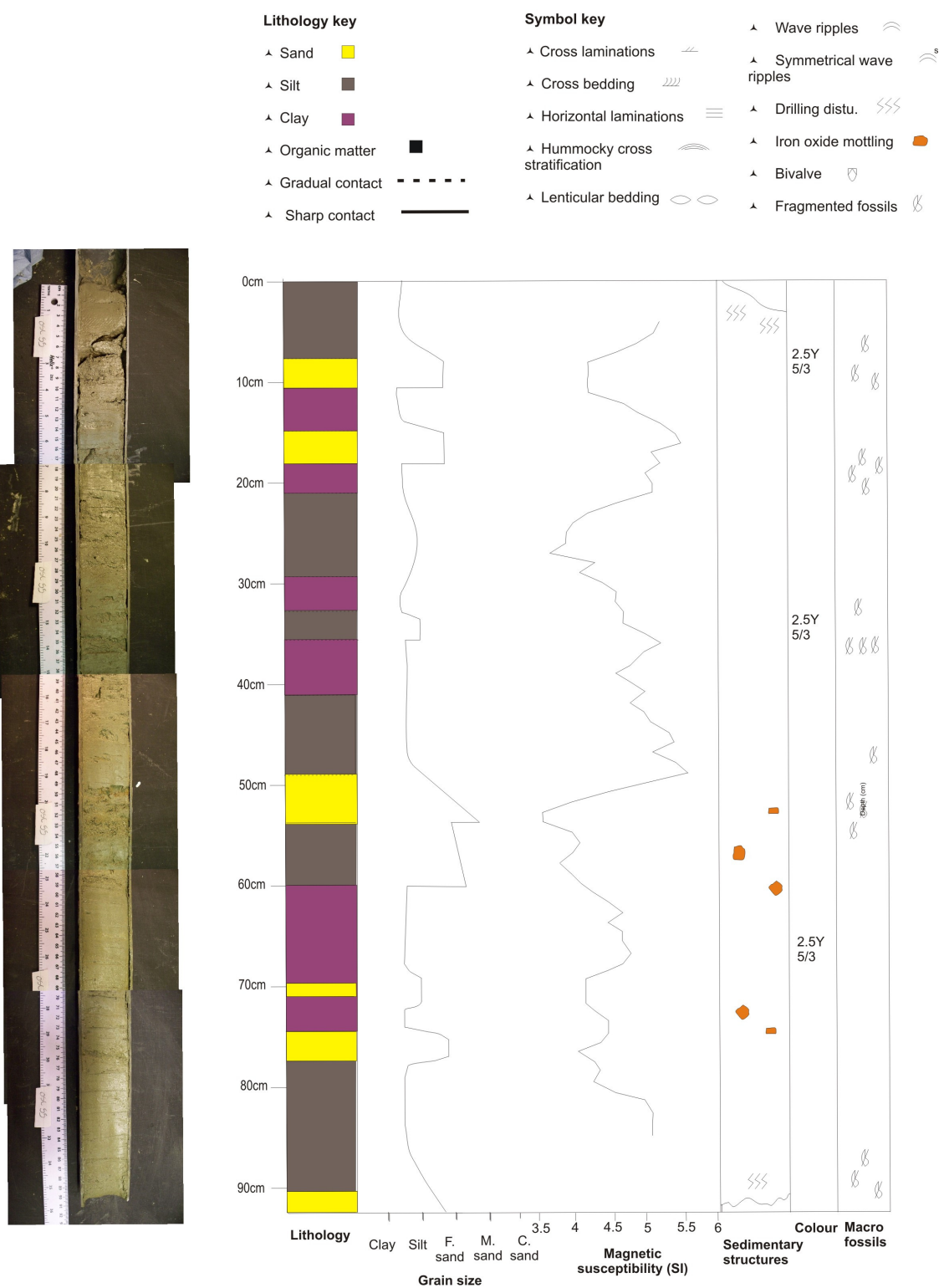
Fig. 4.6. Sedimentary log for OS55, displaying lithology, magnetic susceptibility (S.I), sedimentary structures (including evidence of drilling disturbance), colour (using Munsell colour chart) and the presence of macrofossils.

Lithology key

⌃ Sand 🟨
⌃ Silt ⬛
⌃ Clay 🟪
⌃ Organic matter ■
⌃ Sharp contact ▬▬▬
⌃ Gradual contact ▬ ▬ ▬

Symbol key

⌃ Cross laminations
⌃ Cross bedding
⌃ Horizontal laminations
⌃ Hummocky cross stratification
⌃ Lenticular bedding

⌃ Wave ripples
⌃ Symmetrical wave ripples
⌃ Drilling distu.
⌃ Iron oxide mottling
⌃ Bivalve
⌃ Fragmented fossils
⌃ Wood
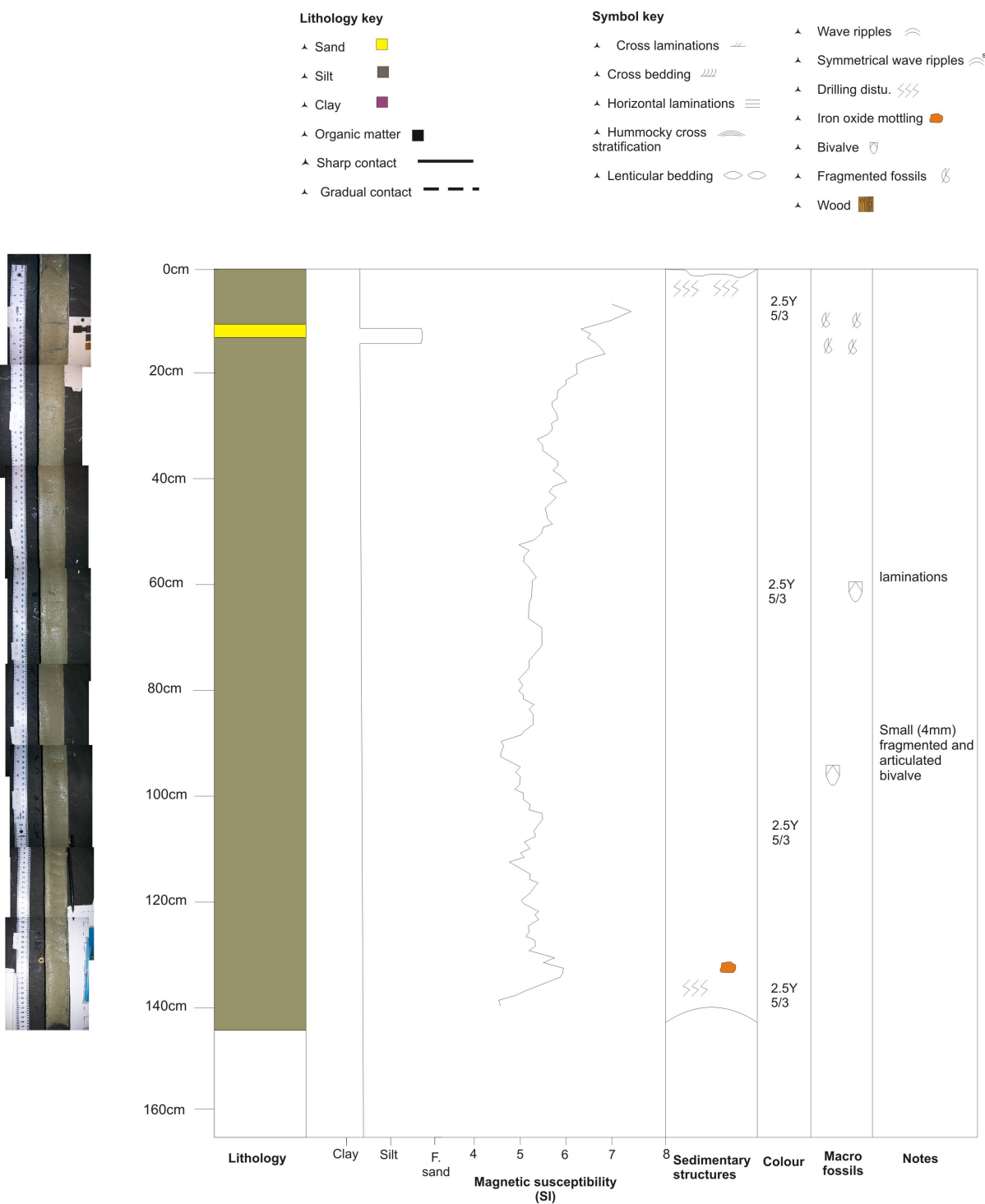
Fig. 4.7. Sedimentary log for OS73, displaying lithology, magnetic susceptibility (S.I), sedimentary structures (including evidence of drilling disturbance), colour (using Munsell colour chart) and the presence of macrofossils.
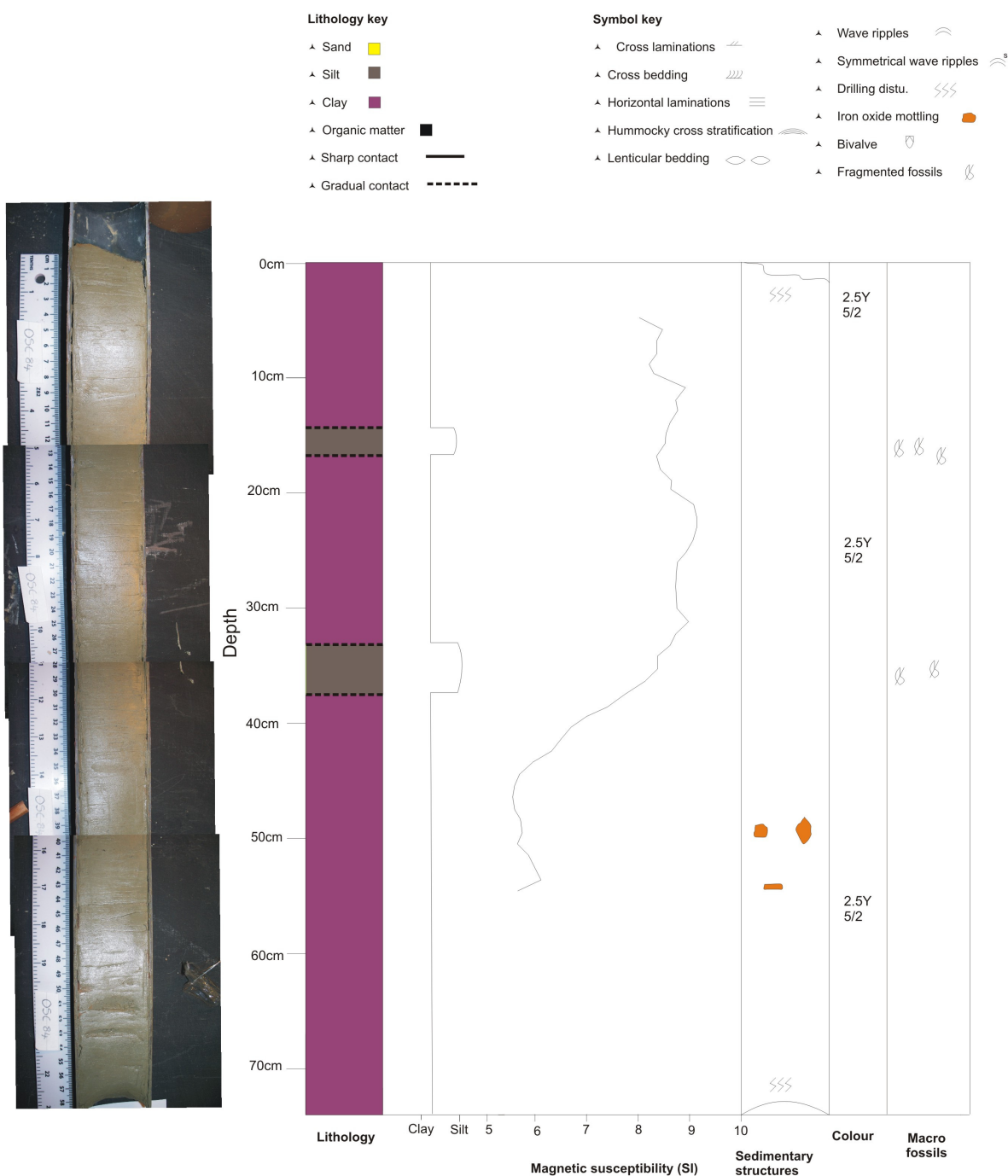
Fig. 4.8. Sedimentary log for OS84, displaying lithology, magnetic susceptibility (S.I), sedimentary structures (including evidence of drilling disturbance), colour (using Munsell colour chart) and the presence of macrofossils.
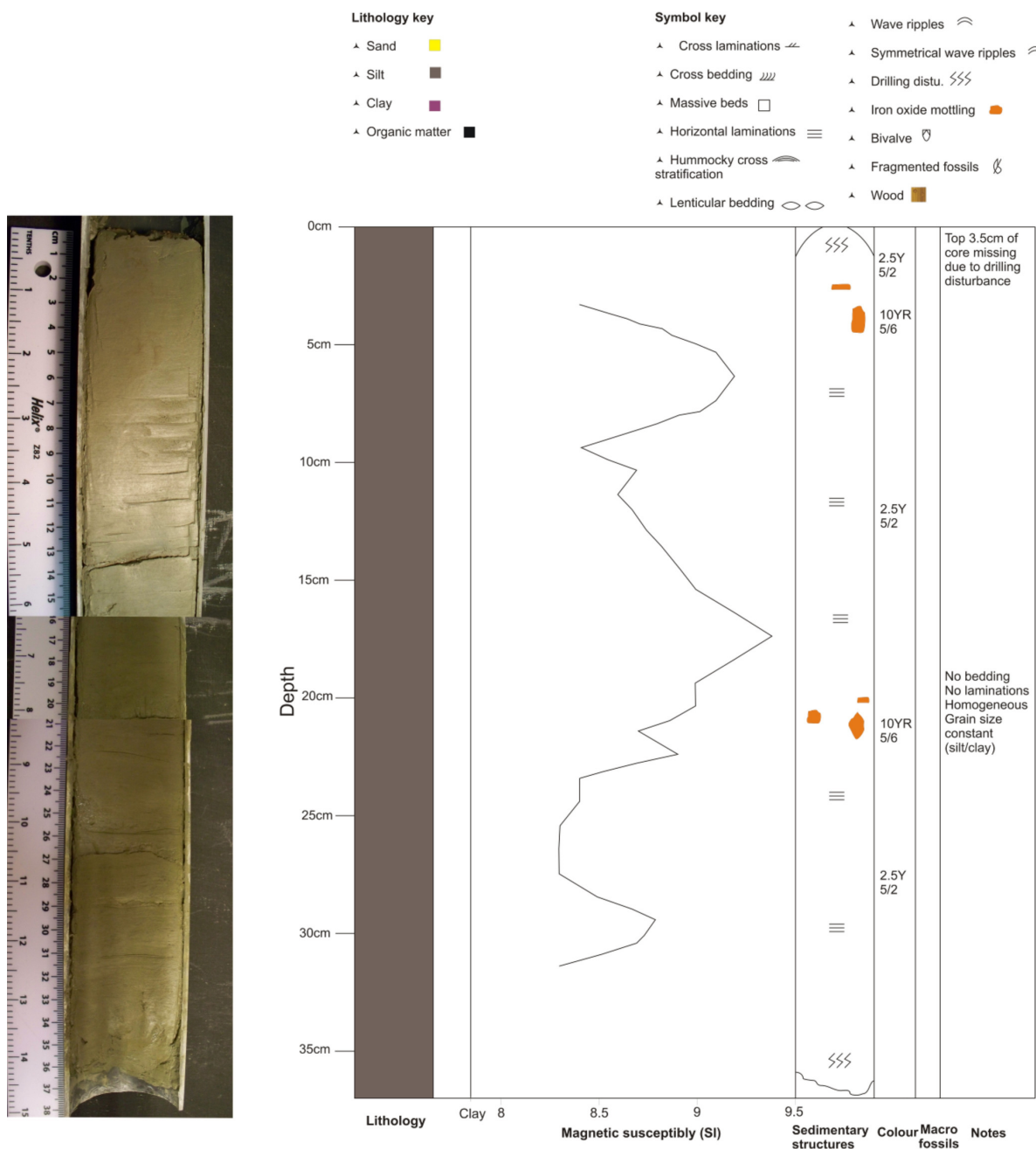
Fig. 4.9. Sedimentary log for OS94, displaying lithology, magnetic susceptibility (S.I), sedimentary structures (including evidence of drilling disturbance), colour (using Munsell colour chart) and the presence of macrofossils.

4.4 Chronological profiles

Both radiocarbon and ^{210}Pb were used to formulate an age-depth model for core OS73. Extrapolation of the results obtained with ^{210}Pb and radiocarbon dating enabled the sedimentation rate to be established.

4.4.1 Radionuclide analysis

^{210}Pb dating was performed on both cores, with core OS73 dated at Brunel University and core OS55 at the University of Brighton. In the latter core ^{137}Cs was also measured.

4.4.1.1 Core OS55 ^{210}Pb

^{137}Cs was measured on core OS55. However the levels reached were below the limit of detection. The ^{210}Pb specific activity curve shows a peak at 16.5 cm and a drop at 9.5 cm (Fig. 4.10a). The results of ^{210}Pb dating for core OS55 gave an average sedimentation rate of 2.3 mm yr^{-1} (Fig 4.10b). The dating results are discussed in Chapter 5.

4.4.1.2 Core OS73 ^{210}Pb

The OS73 ^{210}Pb profile (Fig. 4.11) peaks at 4.5 cm with activities of 101 Bq kg^{-1}. There is a drop in ^{210}Pb activities at 14.5 cm, with activities seemingly reaching background values of constant ^{210}Pb at depth. An anomalous peak in activities is observed at 15.5 cm (one sample). The sedimentation rate varies throughout the ^{210}Pb profile (0-18 cm) from 0.3-4.4 mm yr^{-1} (Fig 4.13).
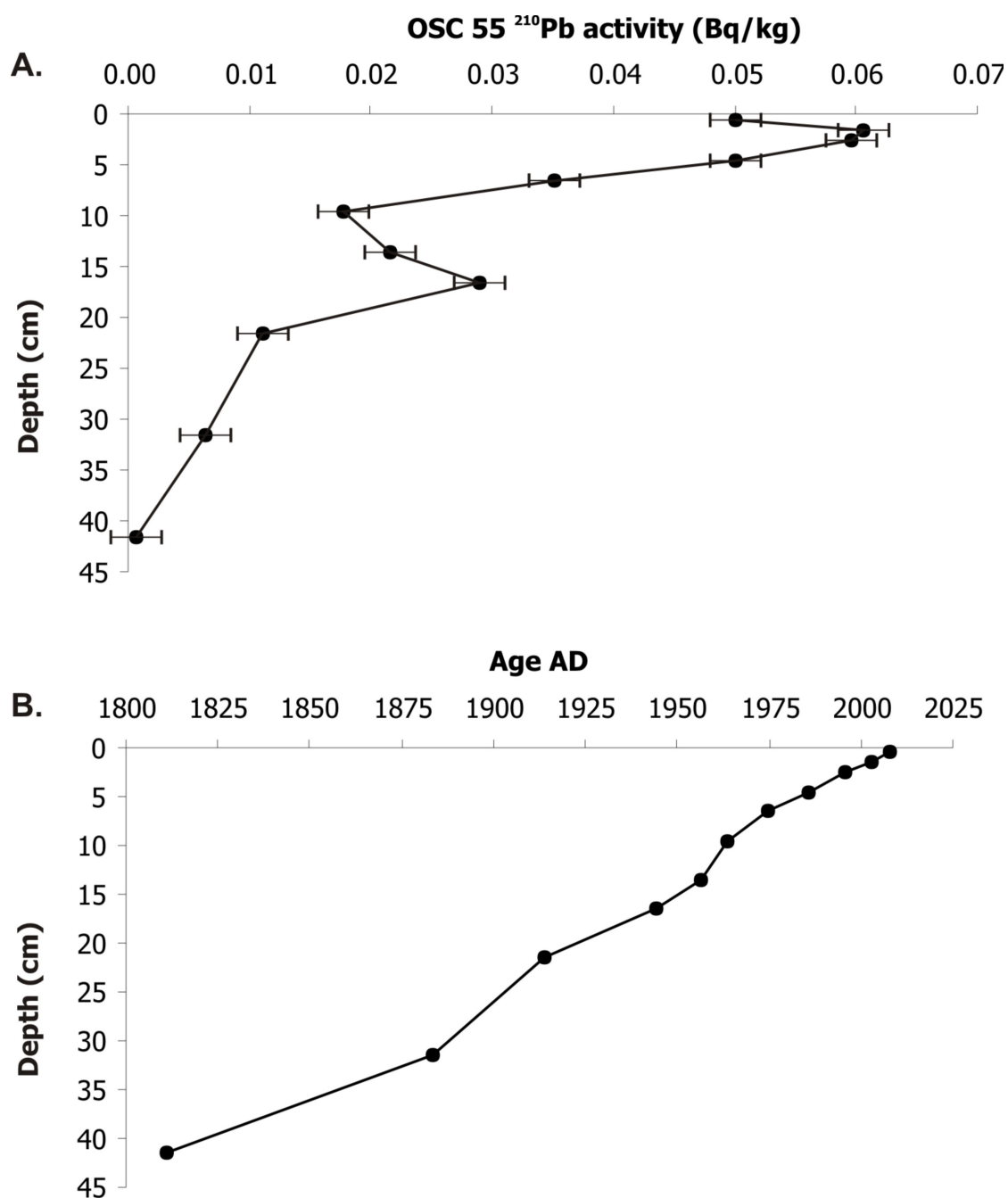
Fig. 4.10. Radionuclides profiles of ^{210}Pb of core OS55. A) Raw ^{210}Pb activity curve. B) Sedimentation rate. Error bars are expressed at 95% confidence levels. Activity values are given in massic activities (Bq kg^{-1} dry weight).
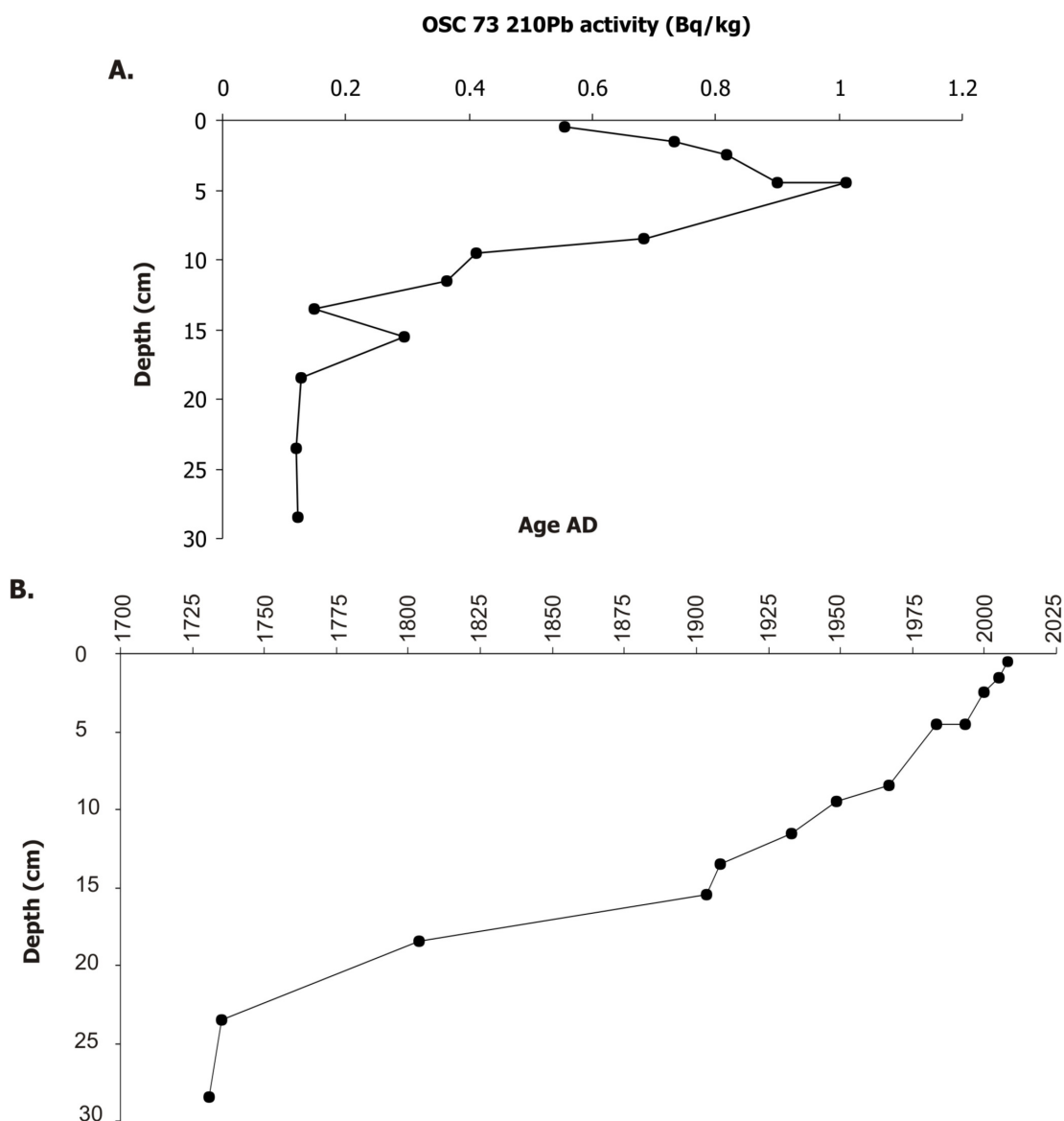
Fig. 4.11. Radionuclides profiles of ^{210}Pb of core OS73. A) Raw ^{210}Pb activity curve. B) Sedimentation rate. Activity values are given in massic activities (Bq kg^{-1} dry weight).

4.4.2 Radiocarbon analysis of core OS73

Within core OS73, three radiocarbon dates were attained from three gastropod shells picked at 86.5, 120.5 and 148.5 cm depth. Raw radiocarbon measurements were converted into calibrated ages using the calibration database MARINE04 and IntCal04. The ^{14}C ages were calibrated to calendar years defined by the 2σ envelope error (Stuiver *et al*., 1998). The calibrated radiocarbon ages attained were 1740 cal. yr BP (86.5 cm), 1880 cal. yr BP (120.5 cm) and 2280 cal. yr BP (148.5 cm). The data from Beta Anaytic is shown in Fig. 4.12. The conventional radiocarbon age was 2760 ±40 BP (2560 ±70 adjusted for local marine reservoir correction) (Fig. 4.12). The 2σ calibrated result was 400 to 110 BC

(2350 to 2060 cal. BP) at 95% probability (Fig. 4.12). The interception of the radiocarbon age with the calibration curve (Fig. 4.12) occurred at 330 cal BC (2280 cal. yr. BP). The sedimentation rate from the radiocarbon results varies from 0.7 to 2.42 mm yr^{-1} accumulation which is slightly lower than the assumed sedimentation rate from ^{210}Pb (Fig. 4.13), as is often the case due to ^{210}Pb producing age overestimation (Leroy *et al*., 2007).

CALIBRATION OF RADIOCARBON AGE TO CALENDAR YEARS

(Variables: C13/C12=0.1:Delta-R=200±60:Glob res=-200 to 500:lab. mult=1)

Laboratory number: Beta-246519

Conventional radiocarbon age: 2760±40 BP

(2560±70 adjusted for local reservoir correction)

2 Sigma calibrated result: Cal BC 400 to 110 (Cal BP 2350 to 2060)
(95% probability)

Intercept data

Intercept of radiocarbon age
with calibration curve: Cal BC 330 (Cal BP 2280)

1 Sigma calibrated result: Cal BC 370 to 190 (Cal BP 2320 to 2140)
(68% probability)
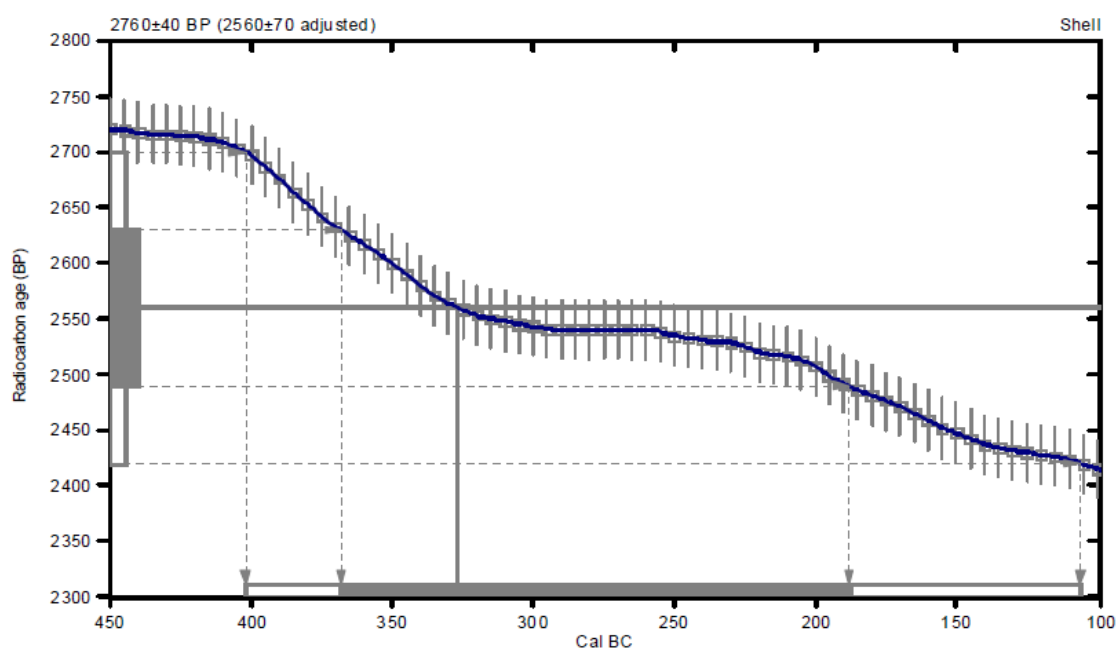
References:
Database used
MARINE04
Calibration Database
INTCAL04 Radiocarbon Age Calibration
IntCal04: Calibration Issue of Radiocarbon (Volume 46, nr 3, 2004).
Mathematics
A Simplified Approach to Calibrating C14 Dates
Talma, A. S., Vogel, J. C., 1993, Radiocarbon 35(2), p317-322

Fig. 4.12. Calibration of radiocarbon age to calendar years. Radiocarbon age obtained (2560 ±40 BP) and the interception with calibration curve at 330 cal BC, obtained from calibration database IntCal04 (directly from Beta Analytic Radiocarbon Dating Laboratory, Florida).
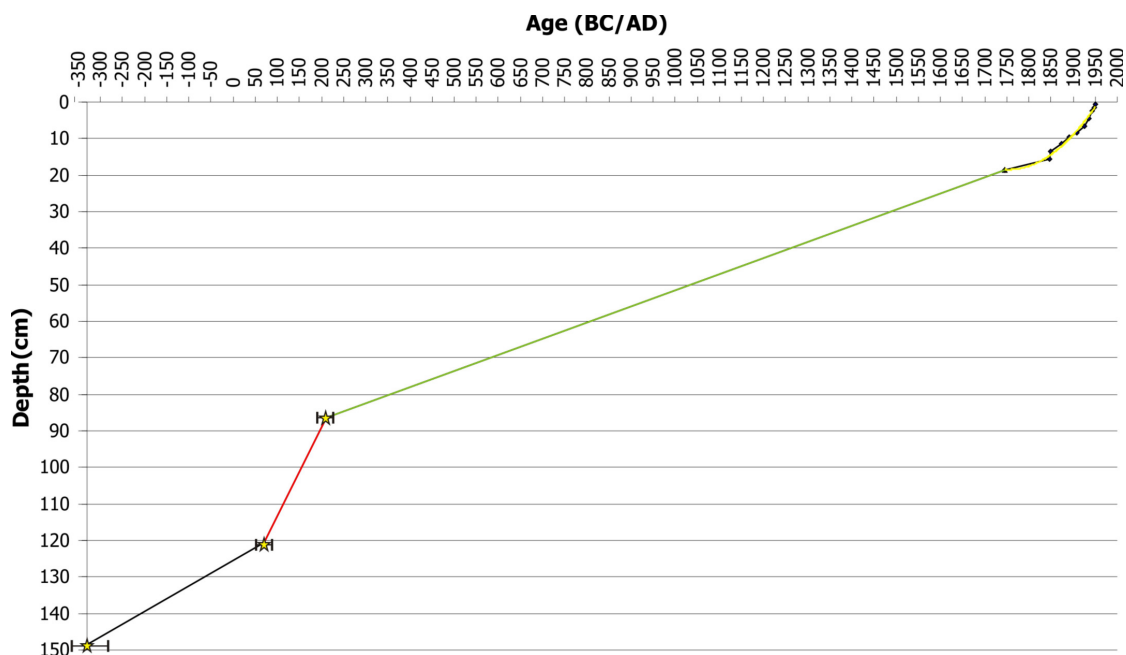
Fig. 4.13. ^{210}Pb and radiocarbon results from core OS73. Age-depth curve has been constructed using one 2nd order polynomial curve through ^{210}Pb dates (yellow line), and three linear trend lines (green, red and black lines). (NB. X-axis: BC to left, AD to right).

4.5 Magnetic susceptibility

Magnetic susceptibility was conducted on half cores using the method described in Chaper 3. Results of the magnetic susceptibility showed large variation both within individual cores and between cores, preventing inter-core correlation. OS34 (Fig. 4.5) showed a large peak in magnetic susceptibility at approximately 80 cm (Fig. 4.5 and 4.14). This large peak did not correlate with any change in sedimentation type in the log (Fig. 4.5). OS55 consisted of substantial variations in magnetic susceptibility (Fig. 4.6 and 4.14), which could, as a first order approximation be correlated with the sedimentary log (Fig. 4.6). Large peaks in magnetic susceptibility roughly correlate with decreases in grain-size. Core OS73 (Fig. 4.7 and 4.14) demonstrates a gradual decrease in magnetic susceptibility throughout, showing no evidence for the event seen in the log (Fig. 4.7 and 4.14). OS84 and 94 (Fig. 4.8, 4.9 and 4.14) show relatively high magnetic susceptibility values (Fig. 4.8, 4.9 and 4.14) compared to the cores further to the west. OS84 contains a sharp decrease in magnetic susceptibility at 30 cm, but again this decrease is not witnessed in the sedimentary log as a change in mineraology (Fig. 4.8).
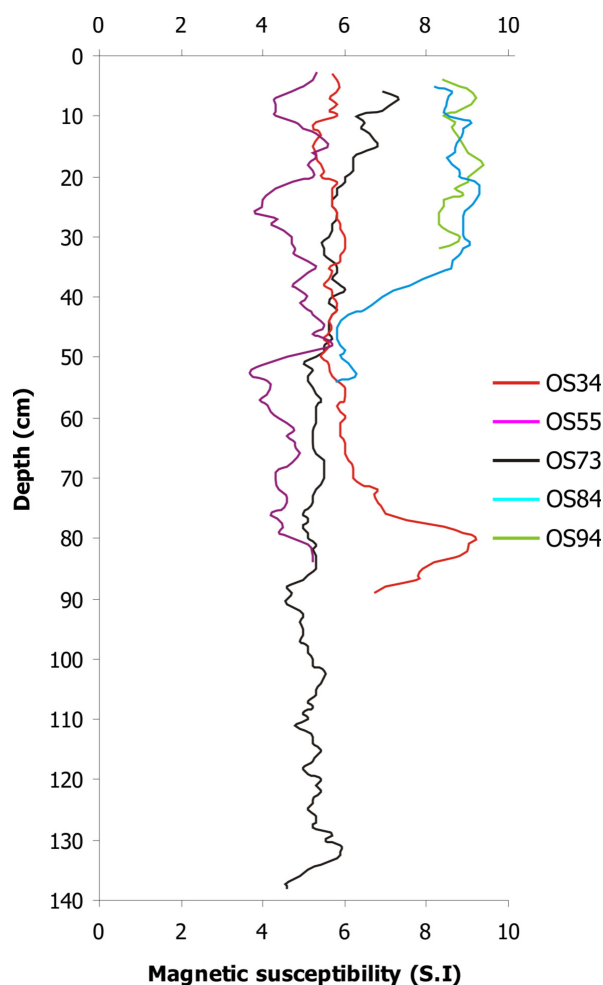
Fig. 4.14. Magnetic susceptibility of all Oman Sea cores obtained by INCO, 2006.

4.6 Geochemical analysis

4.6.1 Total organic carbon

TOC remains constant throughout core OS34 (Fig. 4.15), 84 (Fig. 4.18) and 94 (Fig. 4.19) fluctuating somewhat from 10 - 25 %. TOC in core OS55 shows a small peak in organic matter at 76 cm and a second peak at around 13 cm (Fig. 4.16). Analysis of OS73 exhibited small persistent fluctuations in TOC throughout the core ranging from 5 to 20 % (Fig. 4.17).

4.6.2 Calcium carbonate

Total inorganic carbon (TIC) was determined by INCO using the same sampling resolution as for the TOC. TIC remains relatively constant for core OS34 (Fig. 4.15), 73 (Fig. 4.17) and 94 (Fig. 4.19), showing no apparent peaks or troughs throughout the cores. In core OS55 (Fig. 4.16) TIC increases gradually at around 57 cm and peaks again at 70 cm. Core OS84 (Fig. 4.18) shows extremely stable

TIC concentrations throughout the core showing only one gradual peak in TIC at 25 cm.

4.7 INCO grain-size analysis

In addition to TOC and TIC, INCO also provided grain-size data. This data was gathered by using a particle size analyser, similar to the equipment used at Brunel University, but at a coarser resolution of 4 cm throughout the cores. The data is presented in percentages of sand, silt, and clay. The majority of cores show deviations in grain-size which appear to approximately correlate with the visual core descriptions made at Brunel University.

Laser particle size analyser results for core OS34 (Fig. 4.15) shows no depth variation in grain-size, and contains no sand. This observation is mirrored in the visual grain-size descriptions. Core OS55 (Fig. 4.16) shows little variation in silt and clay percentages, but sharp peaks in the percentage of sand at 53, 41 and 25 cm. These observations are also seen in the visual core descriptions. Core OS73 (Fig. 4.17) shows a small increase in the percentage of silt at 26 cm, which coincides with a decrease in clay at this level. The remainder of the core contains slight fluctuations in clay and relatively stable silt percentages throughout. The percentage of sand in OS73 varies from 5 - 25 %. At 117 cm, there is a gradual increase in sand percentage toward the bottom of the core. There is a gradual decrease at 42 cm, with the percentage of sand from 117 to 46 cm been very low and stable at around 8 %. Between 42 and 9 cm, the percentage of sand is relatively high compared to the rest of the core and shows fluctuations between 20 - 25 %. None of these sand percentage fluctuations are reflected in the visual stratigraphic log. Core OS84 (Fig. 4.18) which contains no changes in silt and clay percentages however shows large changes in sand percentage throughout. There is a gradual increase in grain-size from 52 to 40 cm and a peak in grain-size from 32 to 25 cm. These changes were not evident in the visual core descriptions, with the changes observed in the core not correlating with the changes in grain-size recorded by INCO.

Laser particle size analyser results for core OS94 (Fig. 4.19) shows stable silt and clay percentages throughout, but a gradual increase in sand percentage between 13 cm and the core top. This gradual increase is not seen in the visual

description of the core, where visually the core was recorded as clay-silt throughout, with no variations in grain-size.
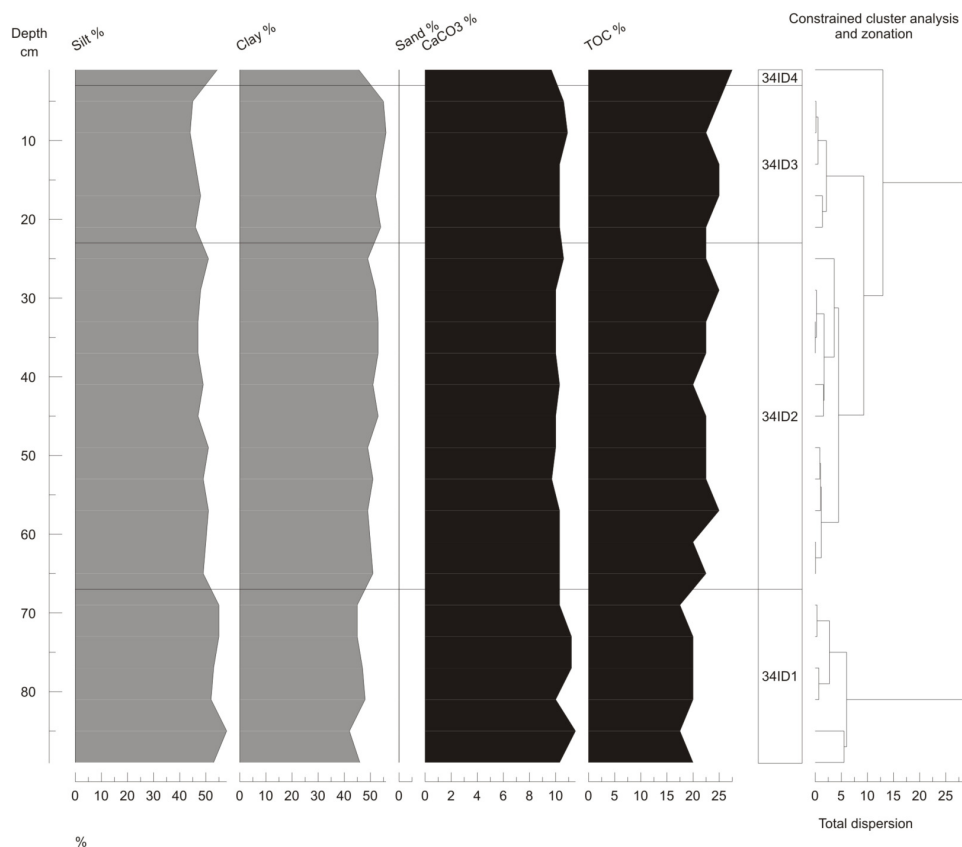
Fig. 4.15. Oman Sea Core 34- INCO data, acquired in 2006.
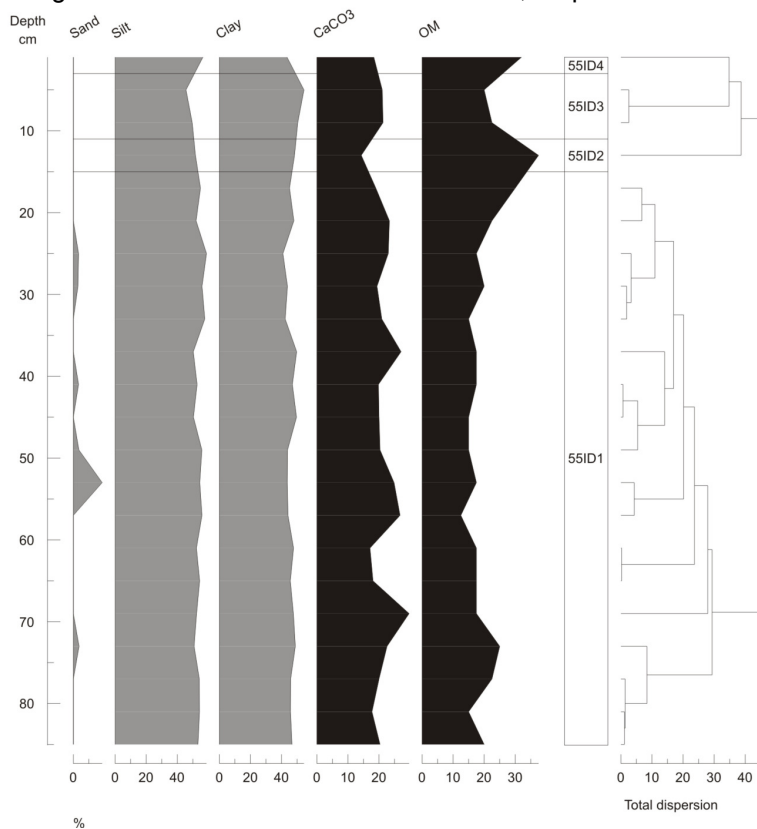
Fig. 4.16. Oman Sea Core 55 – INCO data, acquired 2006.
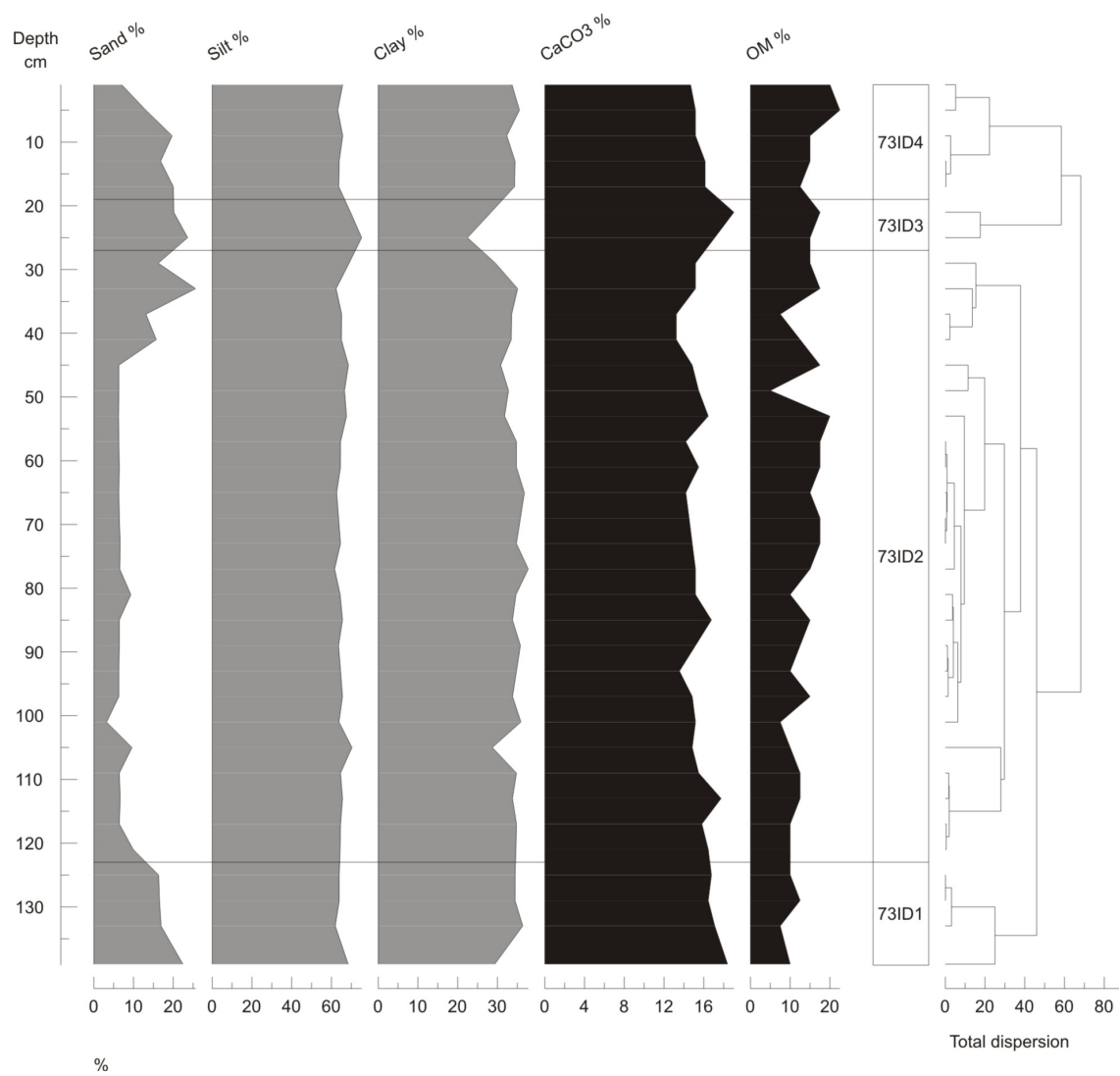
Fig. 4.17. Oman Sea Core 73– INCO data, acquired 2006.
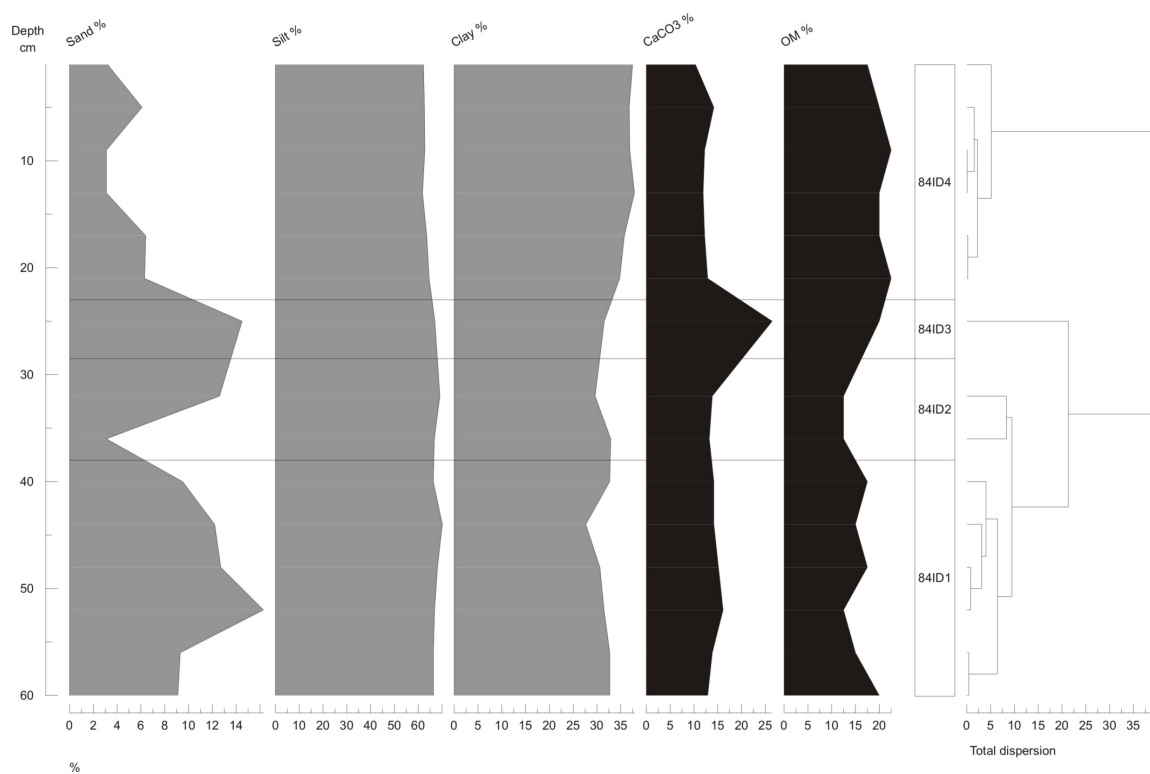
Fig. 4.18. Oman Sea Core 84– INCO data, acquired 2006.
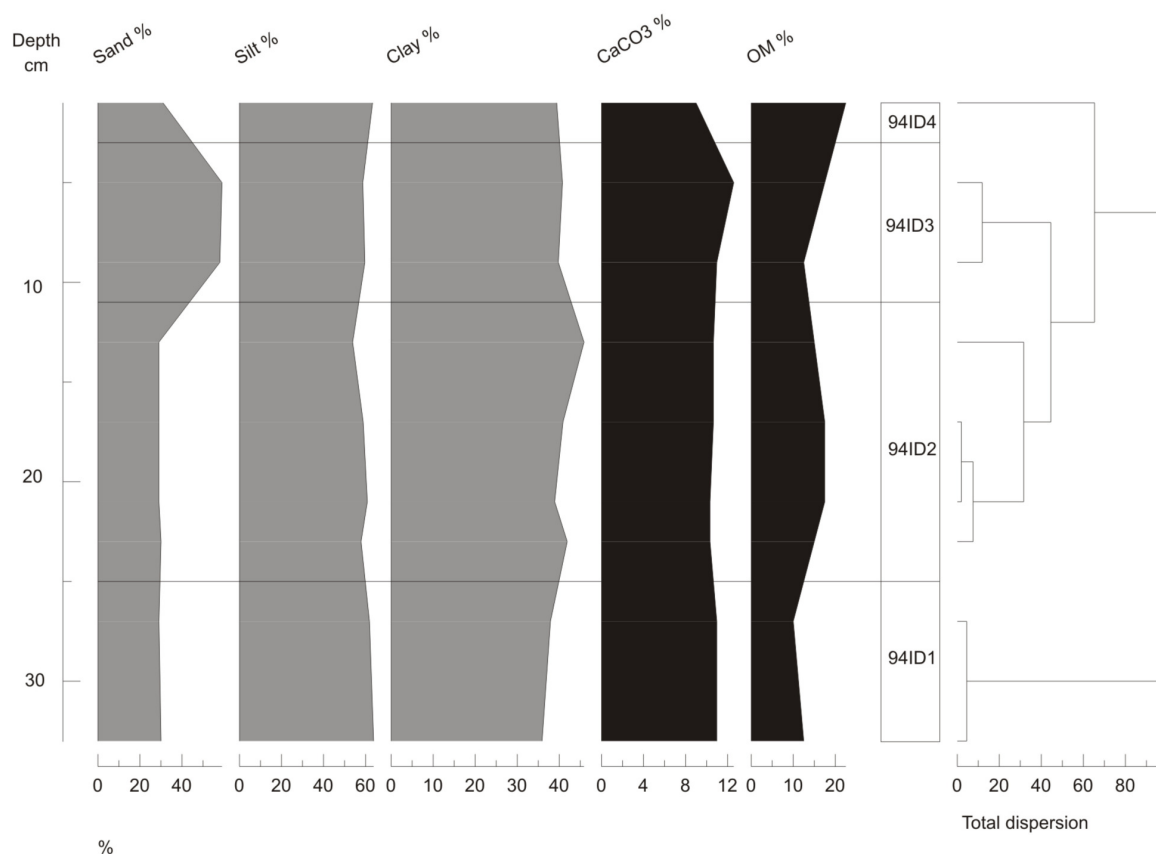
Fig. 4.19. Oman Sea Core 94– INCO data, acquired 2006.

4.8 High resolution grain-size analysis of core OS55 and OS73

Grain-size analysis was performed at Brunel University on core OS55 and 73 only, using a Cilas 1064 laser particle size analyser (technique described in section 3.5). The two cores were analysed at 1 cm resolution throughout, increasing the resolution of the preliminary data provided by INCO in section 4.7. For both cores median (D50), mean, skewness, kurtosis, standard deviation (SD), D10 and D90 were plotted. The results for each variable were plotted as a percentage of the total sum.

4.8.1 Core OS55 – grain-size

The results for OS55 (Fig. 4.20, 4.21 and 4.22a) indicate a series of abrupt increases in grain-size superimposed on top of continued background sedimentation dominated mostly by silts and clays. The grain-size results indicate four major changes in particle size, with sharp increases in grain-size at the bottom of each bed and a gradual fining upwards throughout each of the beds. The grain-size analysis demonstrates five events at 77-75, 71-70, 60-43, 17-15 and 11-8 cm depth.

It is difficult to establish whether the coarse horizon at a depth of 60-43 cm represents a single change in sedimentation or a series of transient changes punctuated by a return to background sedimentation. The visual core description (Fig. 4.6) indicates a sharp increase in grain-size, followed by a second increase containing a gradual fining upwards sequence. The grain-size analysis shows possibly two coarse beds, the first truncated by the second with the latter characterised by a more pronounced fining upward sequence which appears to be truncated by the next coarse horizon.

These statistical summary methods (mean, D50, kurtosis, D75 and D90) have been used previously to describe the particle size distribution (PSD) of sedimentary deposits, with the assumption that one or more of these parameters will precisely describe the key components of a given distribution assisting in the interpretation of the depositional environment (Beierle *et al.*, 2002).

In addition to the standard statistical methods, the grain-size results were also presented on a particle size distribution plot (PSD) (Fig. 4.20) (Beierle *et al.*, 2002). The benefit of a distribution plot is that it presents the raw grain-size data in its entirety, plotting three variables on one chart (frequency, grain-size (µm) and

depth) (Fig. 4.23) as is the normal practice with other palaeoenvironmental proxy data such as diatoms or pollen. The PSD plot indicates fluctuations in grain-size throughout the core, showing the four events as increasing grain-size and decreasing finer material at 76, 50 – 60, 18 and 10 cm (Fig. 4.20).
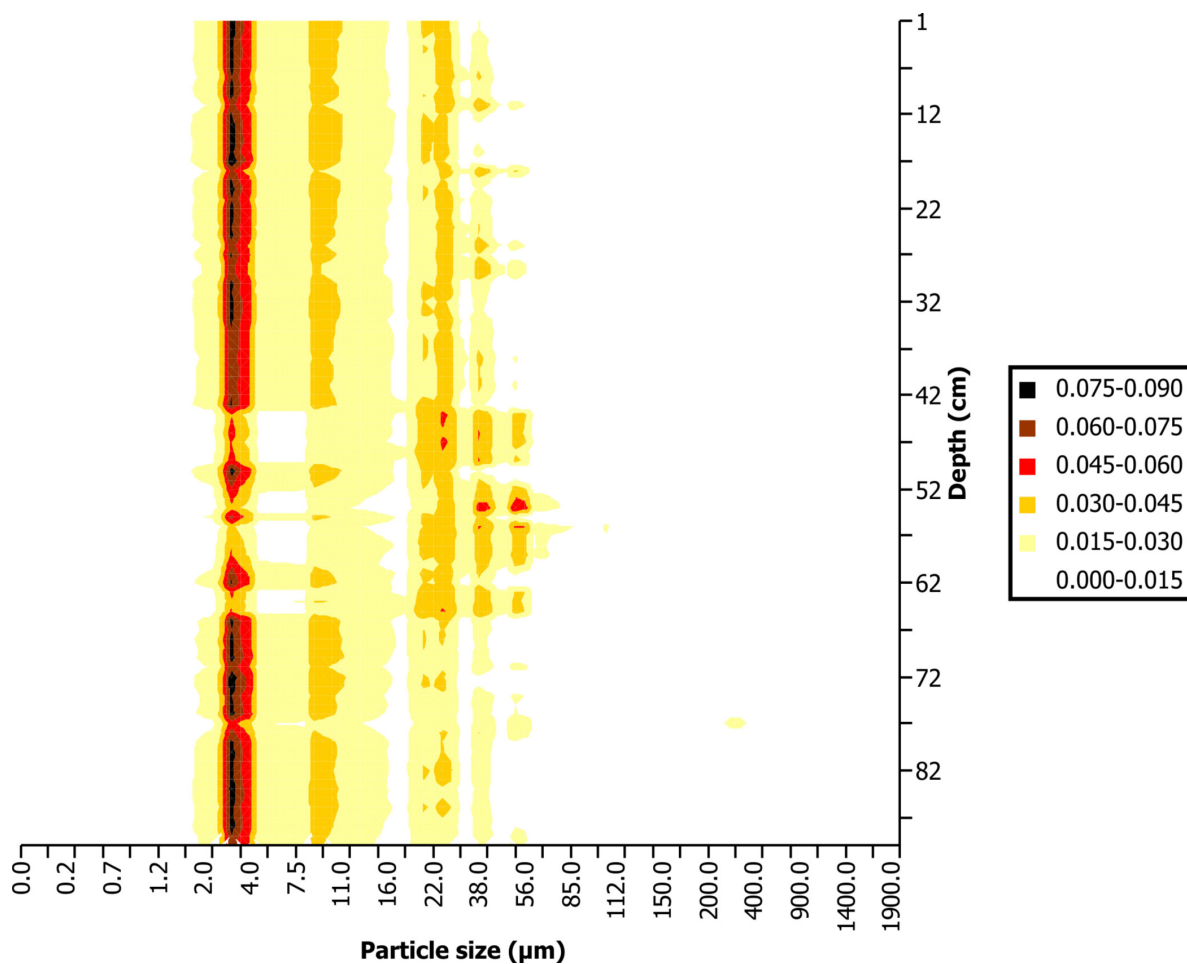
Fig. 4.20. Particle size distribution plot for OS55 indicating fluctuations in grain-size throughout the core. The coarsest horizons occur at 76, 50 - 60, 18 and 10 cm depth.
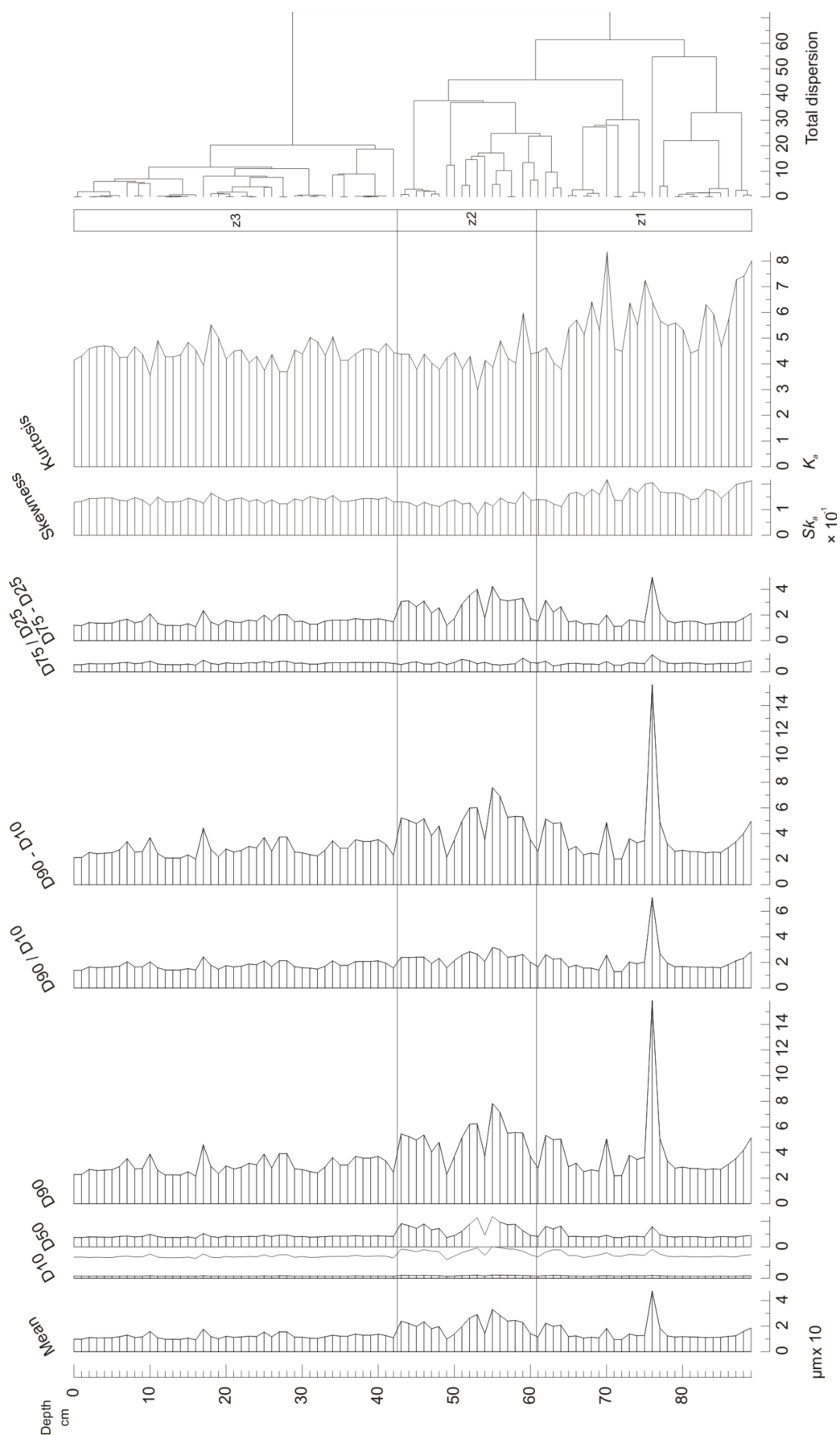
Fig. 4.21. Statistical grain-size analysis of core OS55. Median with x 10 exaggeration curve. CONISS performed on all statistical methods.
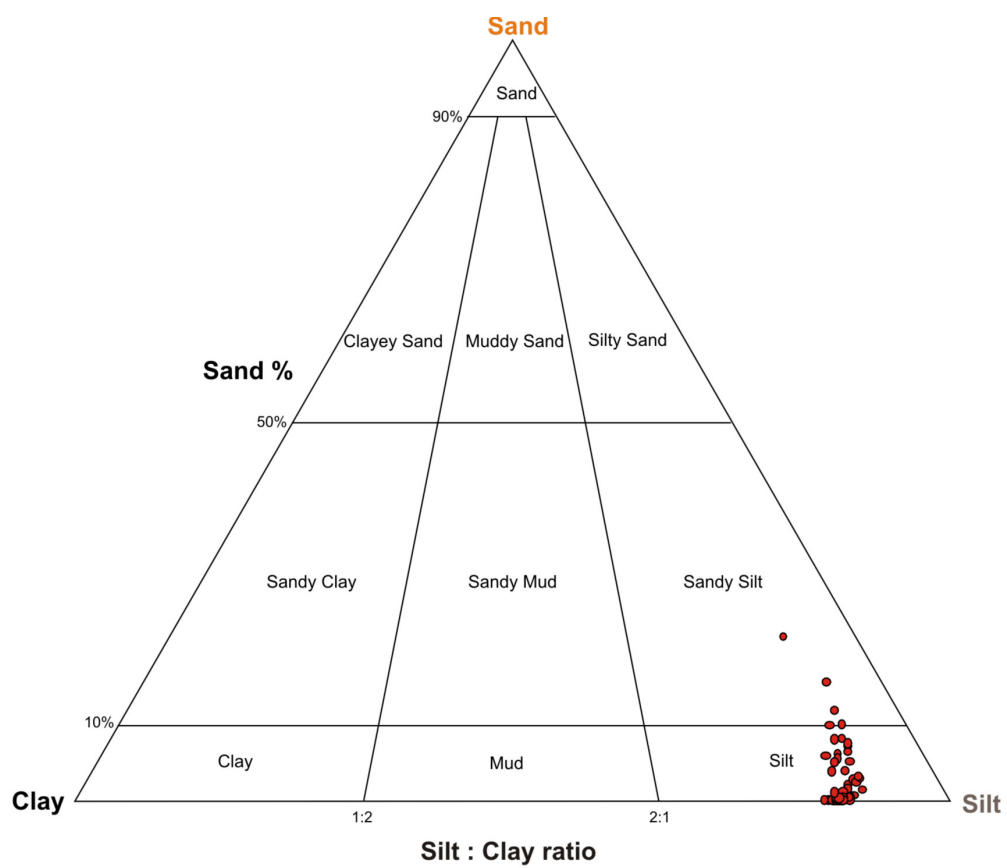
Fig. 4.22. Sand-silt-clay triangular plot for grain sizes recorded from core a.) OS55 and b.) OS73.
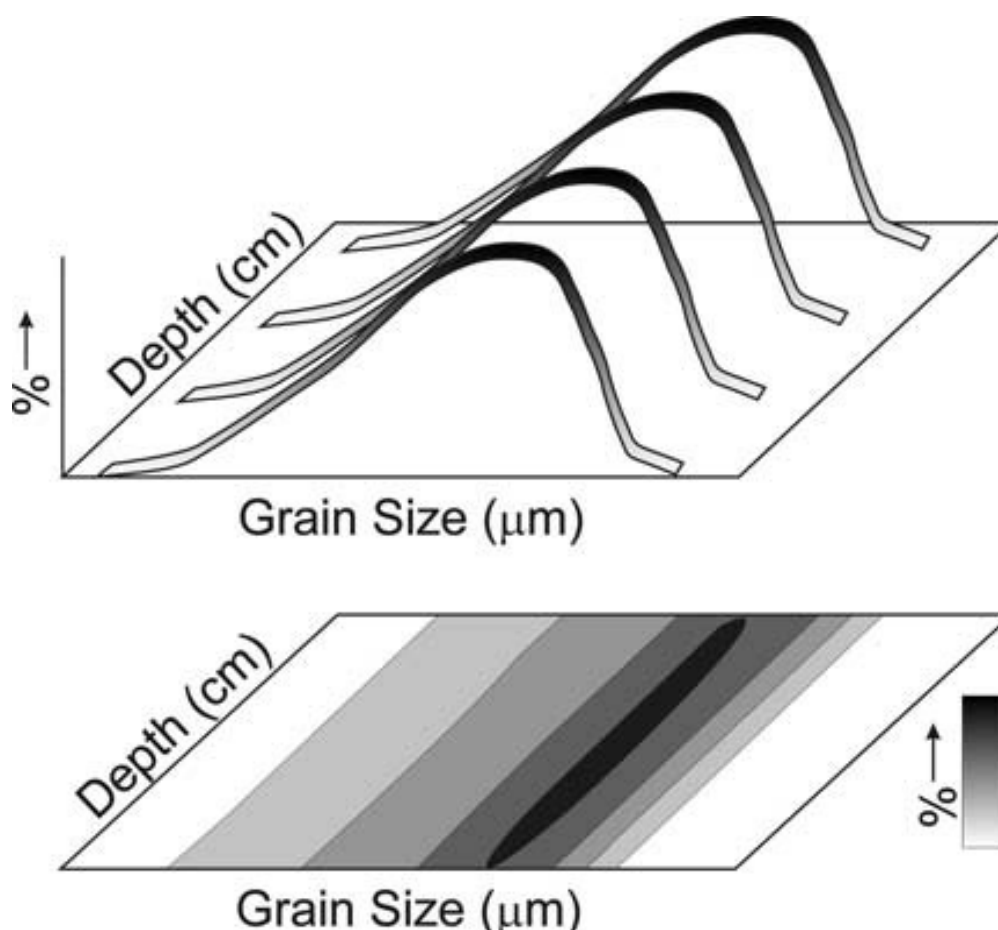
Fig. 4.23. Schematic diagram of the relationship between a PSD plot and the frequency distribution obtained from each sample. NB. Vertical scale in percentage (or frequency). Figure taken from Beierle *et al*. (2002).

4.8.2 Core OS73 – grain-size

The grain size results for OS73 are shown in Fig. 4.22, 4.24 and 4.25. Statistical methods were used to determine grain size changes throughout the core and are shown in Fig. 4.25. The results for OS73 indicate the core is dominated mostly by fine silts and coarse clays with a notable absence of the coarse horizons witnessed in core OS55.

Once again in addition to the standard statistical methods, the grain-size results were also presented on a particle size distribution surface plot (Beierle *et al*., 2002) (Fig. 4.24). The particle size distribution plot highlights the transition from coarser to finer grained sedimentation at 17 cm. Both the particle size distribution plot and the statistical grain size analysis indicate that the majority of core OS73 consists of fine grained sedimentation with no coarser horizons.
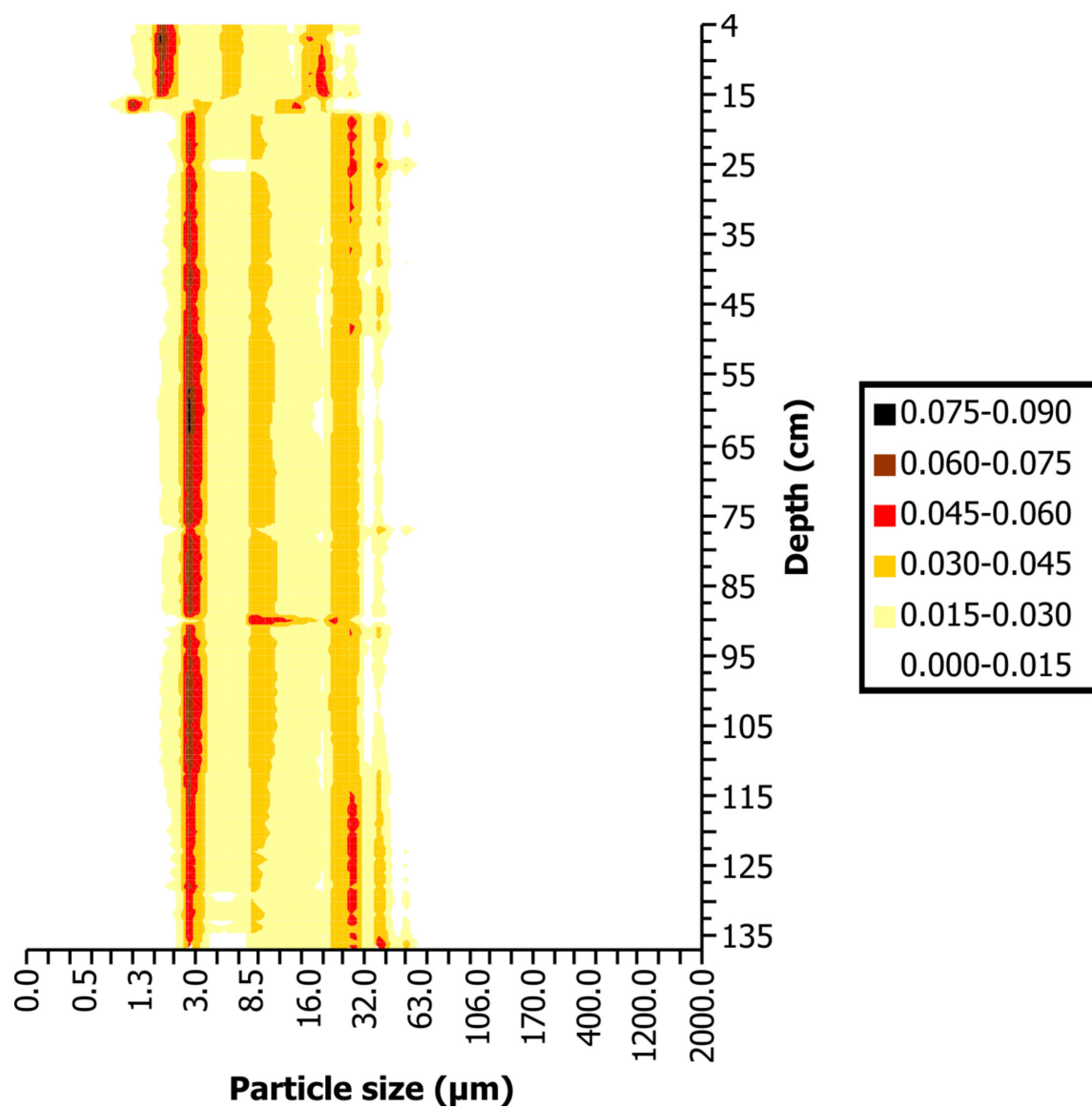
Fig. 4.24. Particle size distribution plot for OS73 showing that the core is mostly comprised of fine silts and coarse clays with a noticeable shift in sedimentation around 17 cm.
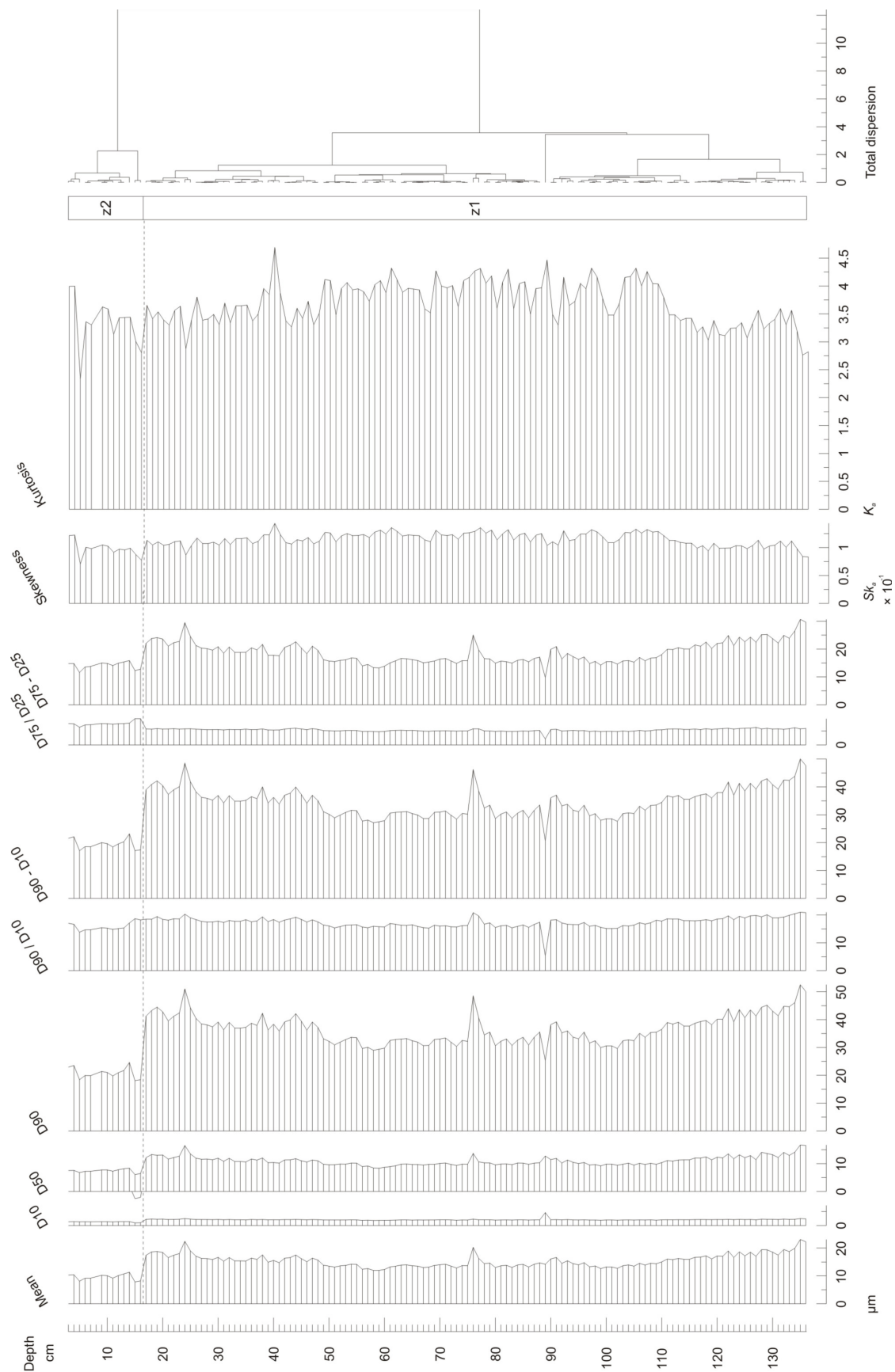
Fig. 4.25. Statistical grain-size analysis of core OS73.

4.8.3 Core OS55 and OS73 – grain-size comparisons

Grain size was plotted on a sand-silt-clay triangular plot which enabled overall comparisons between the two cores using Gradistat, the grain size analysis program (Blott, 2001) (Fig. 4.22). It is evident from the triangular plot that core OS55 contains samples containing a larger percentage of sand, with core OS73 containing more clay sized material. Overall samples from core OS55 lie in the sandy silt and silt regions of the triangular plot, with samples from core OS73 remaining in the mud and silt regions. A greater spread of grain sizes is evident in core OS55.

4.9 Palaeontology

Macrofossil abundance and preservation was visually assessed throughout core OS34, 55, 73, 84, and 94 (Fig. 4.5-4.9). OS55 demonstrated increased fragmentation and disarticulation of shell material (mostly bivalves) in discrete horizons correlated with the coarser intervals throughout the core (Fig. 4.6). No apparent change in the preservation of shell material was evident throughout core OS73 (Fig. 4.7).

4.10 Palynology (pollen and dinoflagellate cyst analysis)

Pollen and dinoflagellate cyst assemblages were analysed to assess any potential change in sedimentation rate associated with abrupt marine events in core OS55 and to search for overall trends in core OS73. Diagrams are presented containing zonations obtained by CONISS (constrained cluster analysis by sum of squares). First pollen percentages, pollen taxa concentrations, dinoflagellate percentages, dinoflagellate taxa concentrations and finally pollen and dinoflagellate total concentrations are presented. The ratio between these two concentrations (P:D) are also shown for both cores.

Owing to time restrictions and extremely low average pollen (~2230 grains per ml of sediment) and dinocyst (~3320 grains per ml of sediment) concentrations within both core OS55 and OS73, the statistically significant number of 300 pollen grains could not be counted in the limited time available. More pollen counts will be counted for future publication. A minimum of 100 pollen grains were ensured for each sample in OS55 and 200 pollen grains in OS73. This involved counting two slides for every sample and up to four slides in several. Percentages of individual

taxa were calculated as a percentage of the total sum of pollen or dinocysts counted (excluding varia and aquatic pollen).

4.10.1 Core OS55 – pollen analysis

In core OS55, 17 taxa were identified within the 30 samples that were counted throughout the core (Fig. 4.26). Samples were taken before, within and after coarser, presumed, event horizons, to assess any changes in taxa abundance and concentrations, associated with changes in depositional environment. Overall the diagram is dominated by Chenopodiaceae, *Artemisia* and Poaceae. The sequence was divided into four pollen zones (55Pz) by CONISS.

55Pz1 (base to 63 cm)

This zone is clearly characterised by maximal values of *Artemisia* (35 - 40 %) forming a bell shaped curve, maximal values of *Calligonum* (10 %) and decreasing values of Chenopodiaceae. Other taxa remain constant or show little change. *Rhizophora* is present, at a constant rate throughout this zone and is the only component of the mangrove species within OS55.

55Pz2 (63 to 43 cm)

This zone is characterised by high values of Chenopodiaceae (35 - 40%), total arboreal pollen (AP), *Betula* and maximal values of *Typha-Sparganium* (3 - 4%). This zone is taxonomically diverse compared to the subsequent zone, with a high level of undeterminable grains. A minor decrease in Poaceae was observed compared to the previous zone. Both *Rhizophora* and Cyperaceae are low within this zone. Both zones 55Pz1 and 55Pz2 show fluctuations in trees species, with high values of *Ephedra* and Brassicaceae (cf.).

55Pz3 (43 to 13 cm)

55Pz3 contains a decrease in general percentage variability within individual taxa, with *Artemisia* showing minimal fluctuations in percentage from 43 cm to the top of the core. The percentage of Chenopodiaceae gradually increases towards the top of the core but drops sharply at 13 cm. The onset of 55Pz3 shows a clear progressive development of taxa such as Cyperaceae, Poaceae, Apiaceae and *Calligonum*. *Betula* and Pinaceae percentages decrease through this zone.
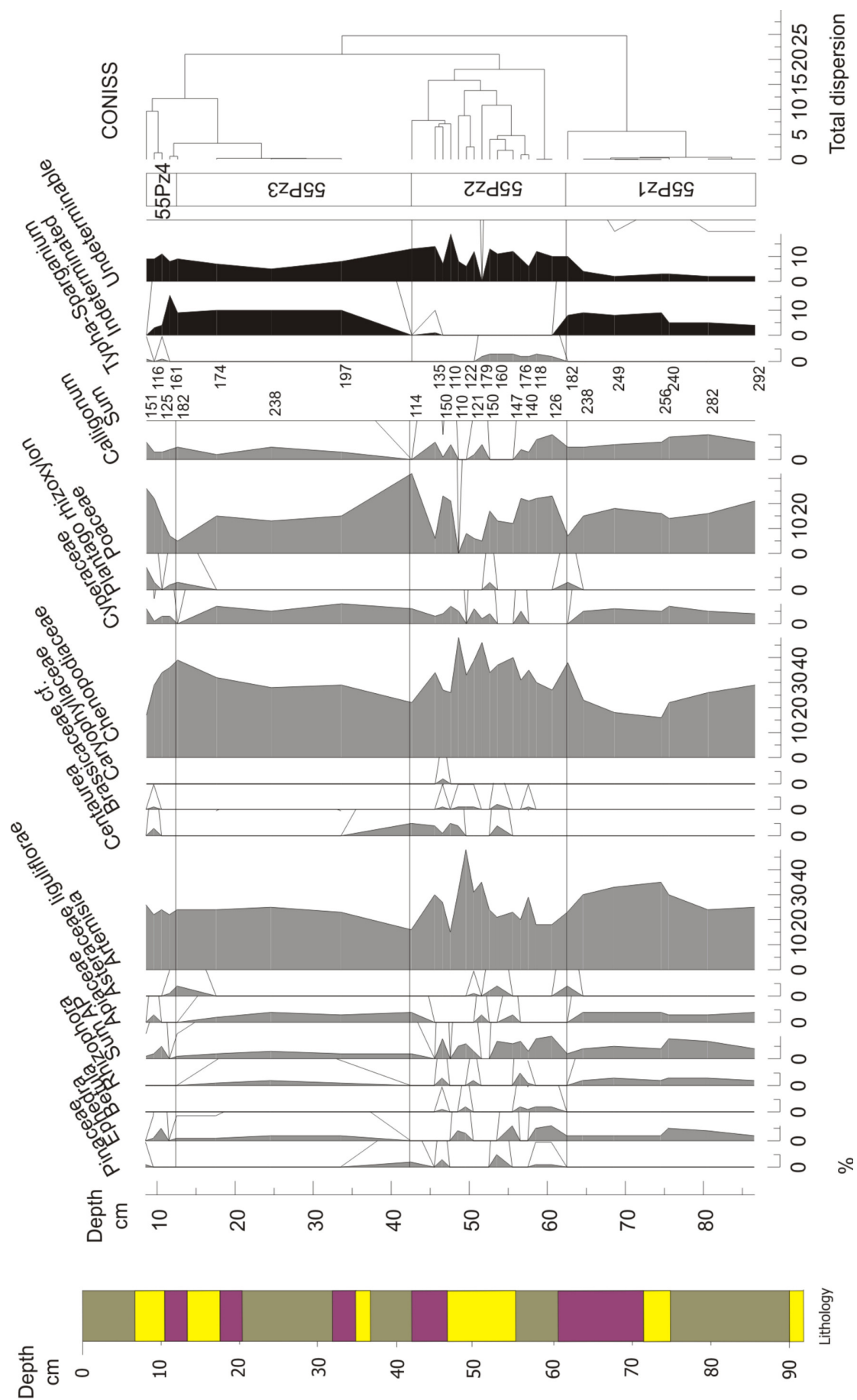
Fig. 4.26. Pollen percentages for core OS55. With 10 x exaggeration curve. Legend for lithology shown in Fig. 4.6.

55Pz4 (13 cm to top)

Minimal values of Poaceae are reached at approximately 13 cm. Many of the taxa including *Ephedra*, Apiaceae, *Centaurea*, Poaceae, *Plantago rhizoxylon* and *Calligonum* peak at around 10 cm, which also coincides with a small increase in indeterminable and undeterminated grains.

Core OS55 pollen taxa concentrations

Individual pollen counts were plotted as concentrations (Fig. 4.27) as biases often exist in percentage data, as large increases in certain taxa percentages often mark a significant decrease in other taxa percentages resulting in incorrect interpretations. CONISS has given slightly different zonations for the pollen taxa concentration (55PCz) data than for the percentage data for core OS55 (Fig. 4.26).

55PCz1 (base to 63 cm)

This zone is similar to 55Pz1 as it is clearly characterised by maximal concentrations of *Artemisia* at 900 grains ml^{-1}. The zone is characterised by maximal concentrations of *Calligonum* at 378 grains per ml^{-1}. Chenopodiaceae concentrations first decrease from 1000 to 600 grains ml^{-1} and then stabilise at 75 cm. The concentrations of other taxa remain constant or show little change. The concentration of *Rhizophora* remains at a constant rate throughout this zone.

55PCz2 (63 to 52 cm)

This zone is characterised rapid decreases and increases in the concentration of various taxa throughout. Concentrations of Apiaceae decrease to 0, whilst concentrations of *Artemisia* decrease sharply and then increase again at 57 cm to 500 grains per ml^{-1} but do not reach pre-55PCz2 values. Chenopodiaceae peaks at the beginning of 55Pcz2 to almost 1000 grains per ml^{-1} and then decreases again to 400 grains per ml^{-1}. This zone contains high variability in most of the taxa. The zone contains maximal concentrations of *Typha-Sparganium* (10 grains per ml^{-1}) and low concentrations of *Rhizophora* and Cyperaceae. Concentration data shows the zone to be more taxonomically diverse compared to the subsequent zone. Concentrations of Poaceae decrease substantially across the zone and remain low around 200 - 400 grains per ml^{-1}.

55PCz3 (52 to 48 cm)

CONISS divided the pollen concentration diagram and has produced this zone which differs from the percentage diagram (Fig. 4.26). 55PCz3 contains peaks in the concentrations of most taxa with *Artemisia* displaying the largest peak from 300 to 800 grains per ml^{-1}. Concentrations of Chenopodiaceae also increase from 400 to 800 grains grains ml^{-1}. A decrease in the concentration of *Typha-Sparganium* is apparent falling to 0 grains per ml^{-1}. Concentrations of AP rise to 100 grains per ml^{-1} and then fall back to 0 grains per ml^{-1} across this zone.

55PCz4 (48 cm to top)

At the start of zone 55PCz4 most taxa increase in concentration including *Artemisia*, Chenopodiaceae, Poaceae and *Calligonum*. At 43 cm Poaceae reaches high concentration values of 800 grains per ml^{-1}. After the initial peak at the beginning of the zone, all taxa appear to stabilise. A peak in Chenopodiaceae concentrations is evident at 13 cm with values reaching 1000 grains per ml^{-1}. All taxa appear to peak in concentration at 10 cm with the exceptions of Asteraceae, Cyperaceae, *Plantago rhizoxylon* and *Calligonum.*
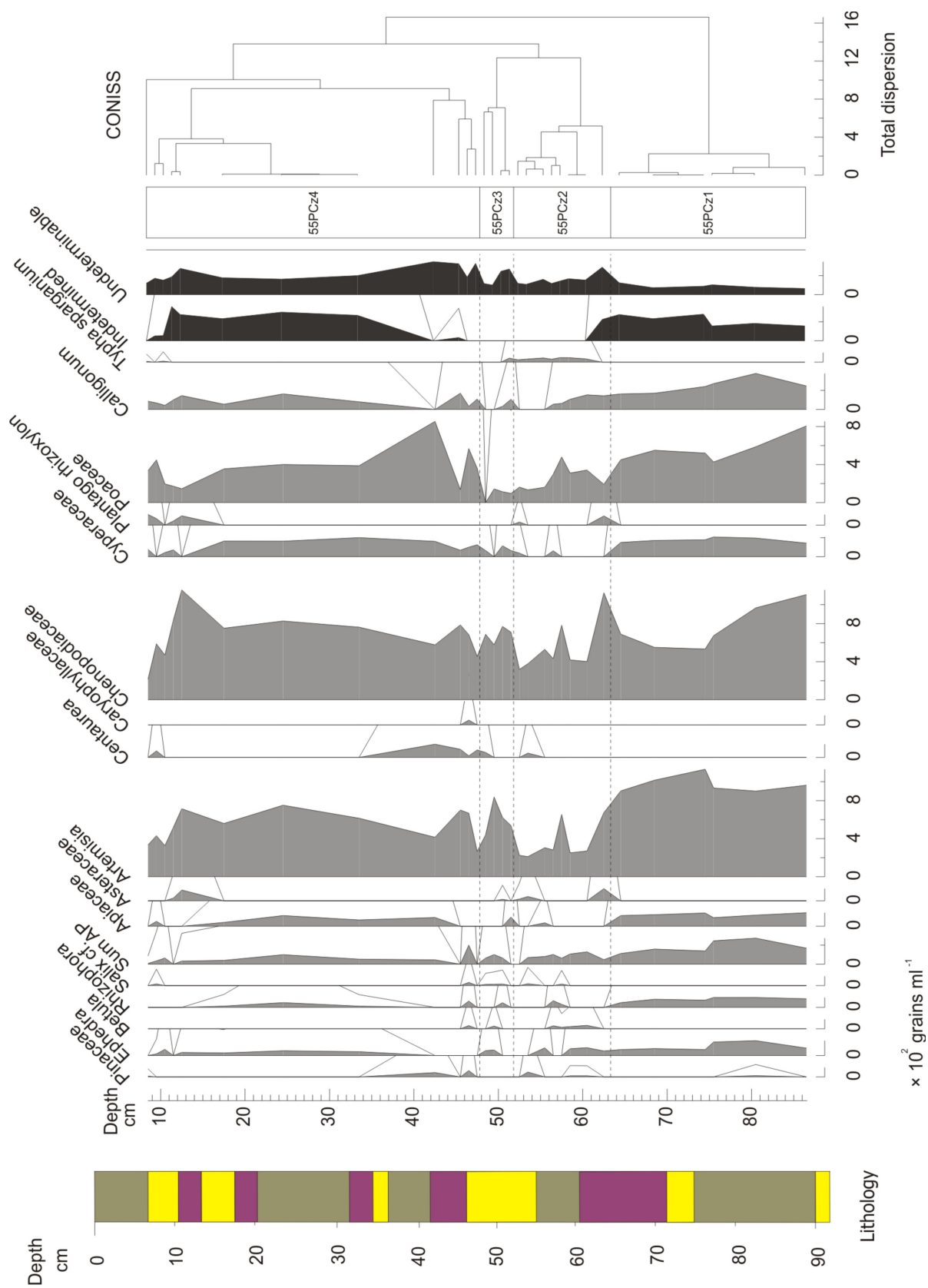
Fig. 4.27. Pollen taxa concentrations for core OS55. With 10 x exaggeration curve. Legend for lithology shown in Fig. 4.6.

4.10.2 Core OS55 – dinoflagellate cyst analysis

Overall 30 species of dinoflagellate cysts were identified within 30 samples (Fig. 4.28). Compared to pollen, the concentration of dinoflagellates within the samples was relatively high, resulting in more dinoflagellates per sample been counted (predominantly over 200 cysts) than for the pollen. On the whole the assemblage is dominated by *Bitectatodinium spongium*, *Spiniferites ramosus* and *Brigantedinium* sp. with lesser amounts of *Echinidinium granulatum, Echinidinium delicatum* and *Operculodinium centrocarpum*. CONISS suggested dividing the diagram into four dinoflagellate cyst zones (55Dz).

55Dz1 (base to 61 cm)

This zone is stable, with values of individual species remaining constant throughout.

55Dz2 (61 to 44 cm)

This zone consists of large variations in most taxa especially *Brigantedinium* sp., *B. spongium* and *S. ramosus*. The zone is characterised by the continuous occurrence of *Echinidinium aculeatum, Echinidinium transparantum* and *Protoperidinium stellatum*. Several maxima are reached within this zone including, *O. centrocarpum*, *S. ramosus* and *B. spongium.*

55Dz3 (44 to 12 cm)

This zone is characterised by the continued occurrence of the dominating species: *B. spongium*, *S. ramosus* and *Brigantedinium* sp. Several species re-emerge at the base of 55Dz3 including Spiniferites *belerius, E. aculeatum, E. transparantum, P. stellatum* and *Quinquecuspis concreta, Selenopemphix nephroides* and *Tuberculodinium vancampoae*.

55Dz4 (12 cm to top)

12 cm is highlighted by a sharp decrease in *B. spongium* and an increase in *S. ramosus, Brigantedinium* sp. *Impagidinium aceulatum* and *paradoxum* show a minimal increase from the previous zone. The majority of species decrease at 12 cm and then recover to the levels before 12 cm.
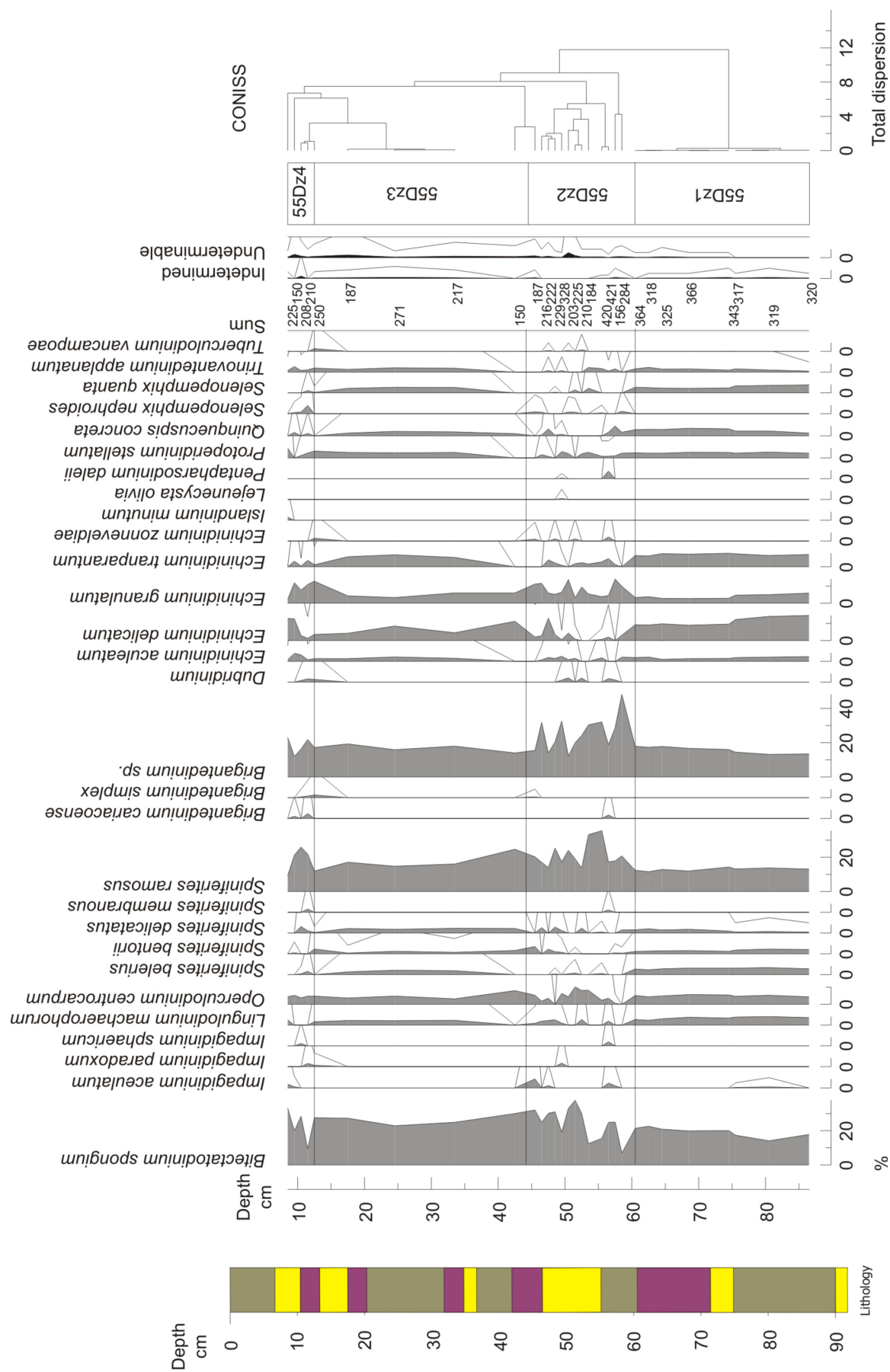
Fig. 4.28. Dinoflagellate percentages for core OS55. With 10 x exaggeration curve. Legend for lithology shown in Fig. 4.6.

OS55 dinoflagellate taxa concentrations

Individual dinoflagellate counts were plotted as concentrations (Fig. 4.29). CONISS has given similar zonations for the dinoflagellate taxa concentration data (55DCz) and for the dinoflagellate percentage data for OS55 (Fig. 4.28).

55DCz1 (base to 60 cm)

This zone is very much the same as 55Dz1. All concentrations of individual taxa remain stable throughout the zone. Concentrations of *E. delicatum* decrease slightly from 1500 to 900 grains ml^{-1} throughout the zone.

55DCz2 (60 to 45 cm)

This zone consists of large variations in the concentrations of most taxa especially *Brigantedinium* sp., *B. spongium* and *S. ramosus*. Concentrations of *Brigantedinium* sp., reach maximal values of 5000 grains per ml^{-1} in this zone at 58 cm. Concentrations of *B. spongium* decrease at the beginning of this zone from 2000 to 800 grains ml^{-1}. Several other concentration maxima are reached within this zone including, *O. centrocarpum*, *S. ramosus* and *B. spongium.*

55DCz3 (45 to 12 cm)

This zone is characterised by high concentrations of the dominating species: *B. spongium*, *S. ramosus* and *Brigantedinium* sp. There are increases in the concentrations of several species including *Spiniferites belerius, E. aculeatum, E. transparantum, P. stellatum* and *Quinquecuspis concreta, Selenopemphix nephroides* and *Tuberculodinium vancampoae*.

55DCz4 (12 cm to top)

12 cm is highlighted by a sharp decrease in the concentration of *B. spongium* which decreases from 3000 to 1000 grains ml^{-1}. The concentration of *S. ramosus* increases from 1200 to 2800 grains ml^{-1}. The majority of taxa concentration decrease at 12 cm and then recover to the levels before 12 cm within this zone.
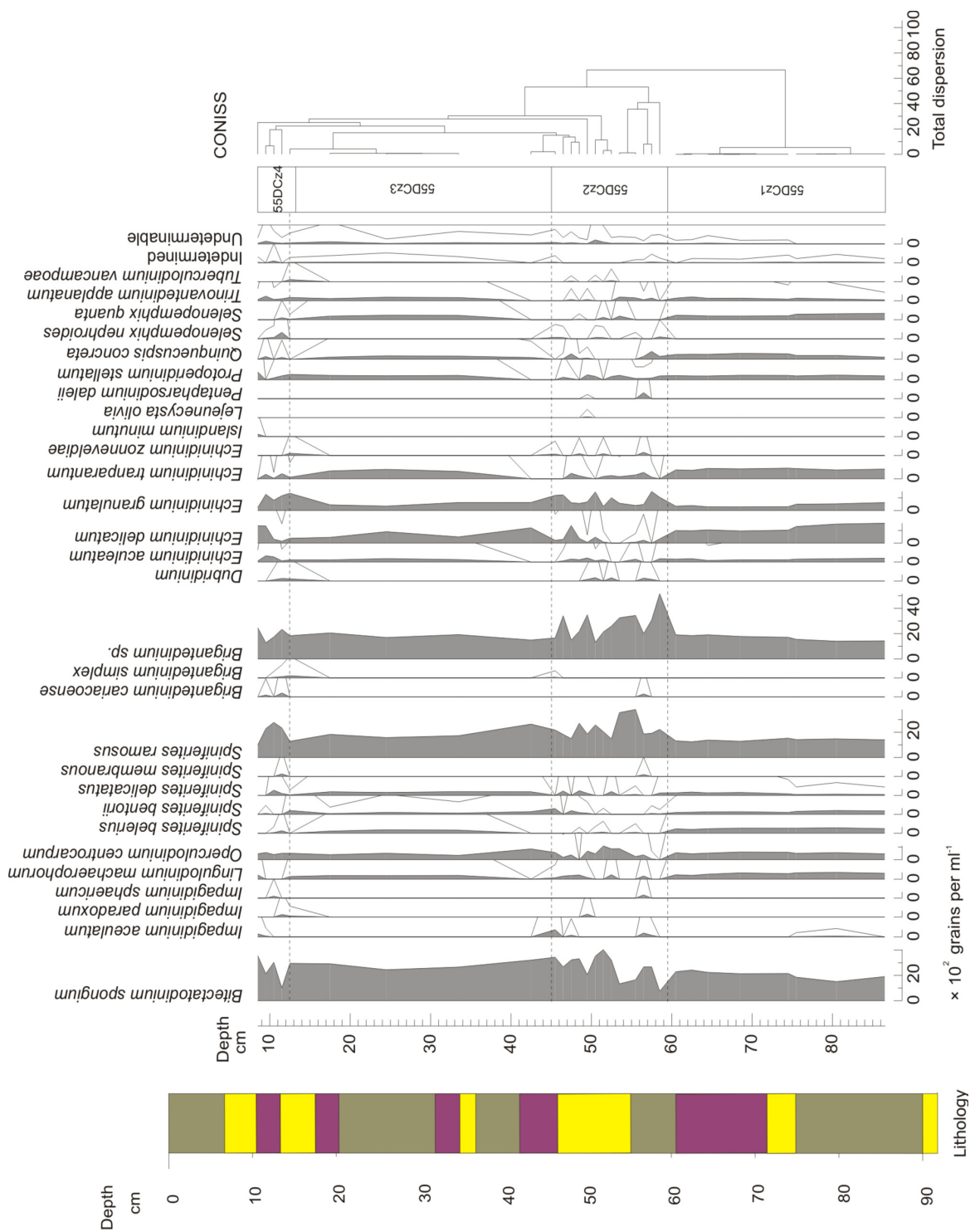
Fig. 4.29. Dinoflagellate taxa concentrations for core OS55. With 10 x exaggeration curve. Legend for lithology shown in Fig. 4.6.

4.10.3 Core OS55 – pollen and dinoflagellate cyst concentrations

Pollen and dinoflagellate concentrations were calculated using Equ 3.1, and the results are shown in Fig. 4.30. Pollen (55Pz), dinoflagellate (55Dz) and the pollen dinoflagellate ratio (55PDz) zonations correlate well, with four 55Pz, 55Dz and 55PDz zones. 55PDz1 from base to 62 cm show a relatively stable dinoflagellate concentration throughout, with a decrease in pollen concentration. This zone is characterised by a gradual decrease in P:D (pollen: dinoflagellate ratio). The start of 55PDz2 is marked by a sharp decrease in both pollen and dinoflagellate concentrations, with dinoflagellates decreasing more gradually. P:D also decreases gradually at this level. 55PDz2 is characterised by fluctuating pollen, dinoflagellate and P:D concentrations throughout, with fluctuating pollen and dinocysts displaying a positive correlation. Overall 55PDz2 displays a drop in both pollen and dinocyst concentrations, with minima of both reached in this zone. At the top of 55PDz2, both pollen and dinoflagellate concentrations show significant increases into 55PDz3. Dinoflagellate and pollen concentrations within 55PDz3 both show a slight fluctuation. Dinoflagellate concentrations show a continuous decrease until 17 cm, whereas pollen concentrations remain relatively constant. At 17 cm both concentrations increase progressively until 13 cm, where concentrations of dinoflagellates drop sharply from 4000 to 2500 grains per ml^{-1} and pollen concentrations from 2500 to 1500 grains per ml^{-1}.
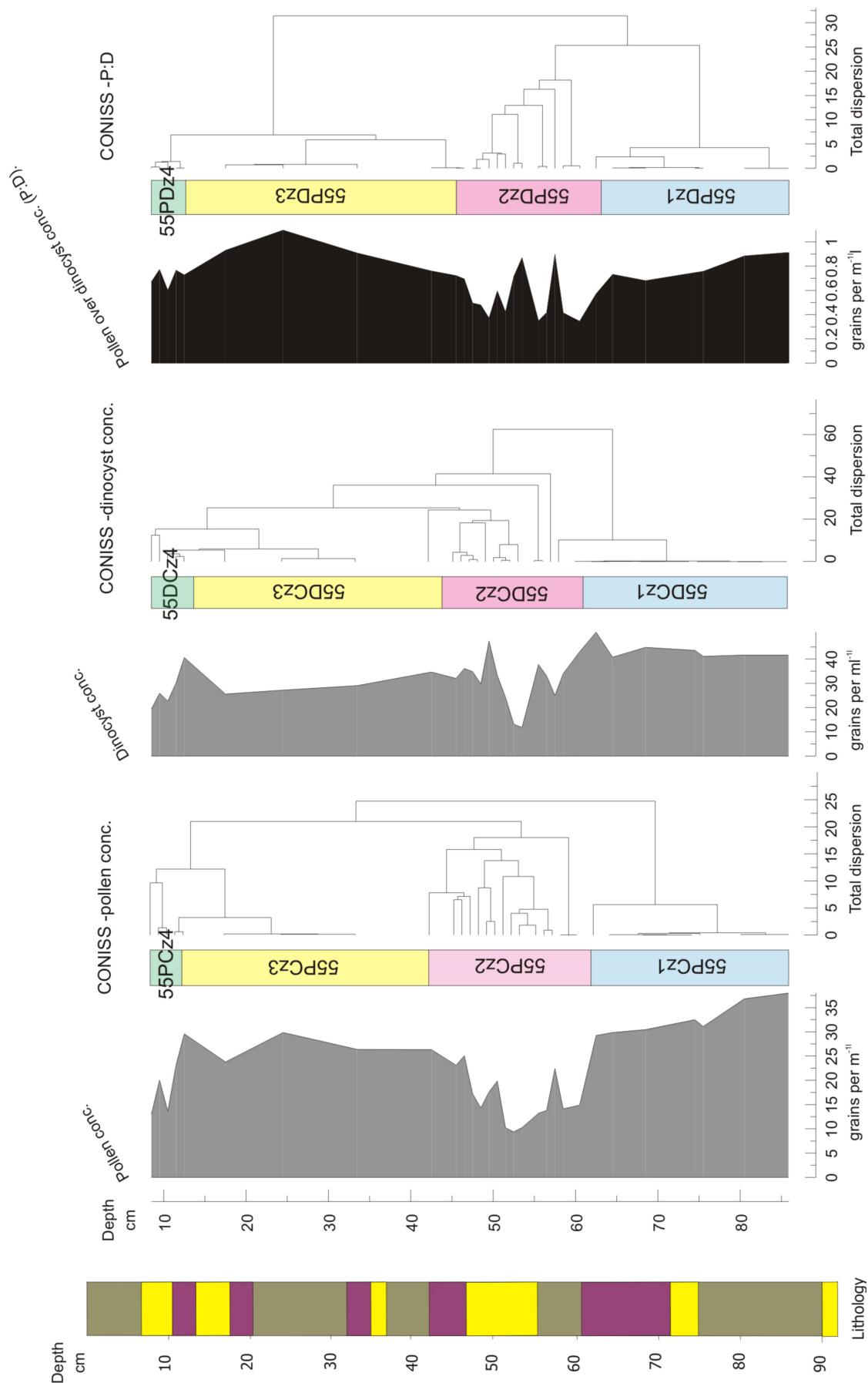
Fig. 4.30. Pollen and dinoflagellate concentrations and the P:D ratios for core OS55. Concentrations are per ml of wet sediment. Conc = concentration. Legend for lithology shown in Fig. 4.6.

4.10.4 Core OS73 – pollen analysis

In core OS73, 19 taxa were identified within the 17 samples that were counted throughout the core (Fig. 4.31).
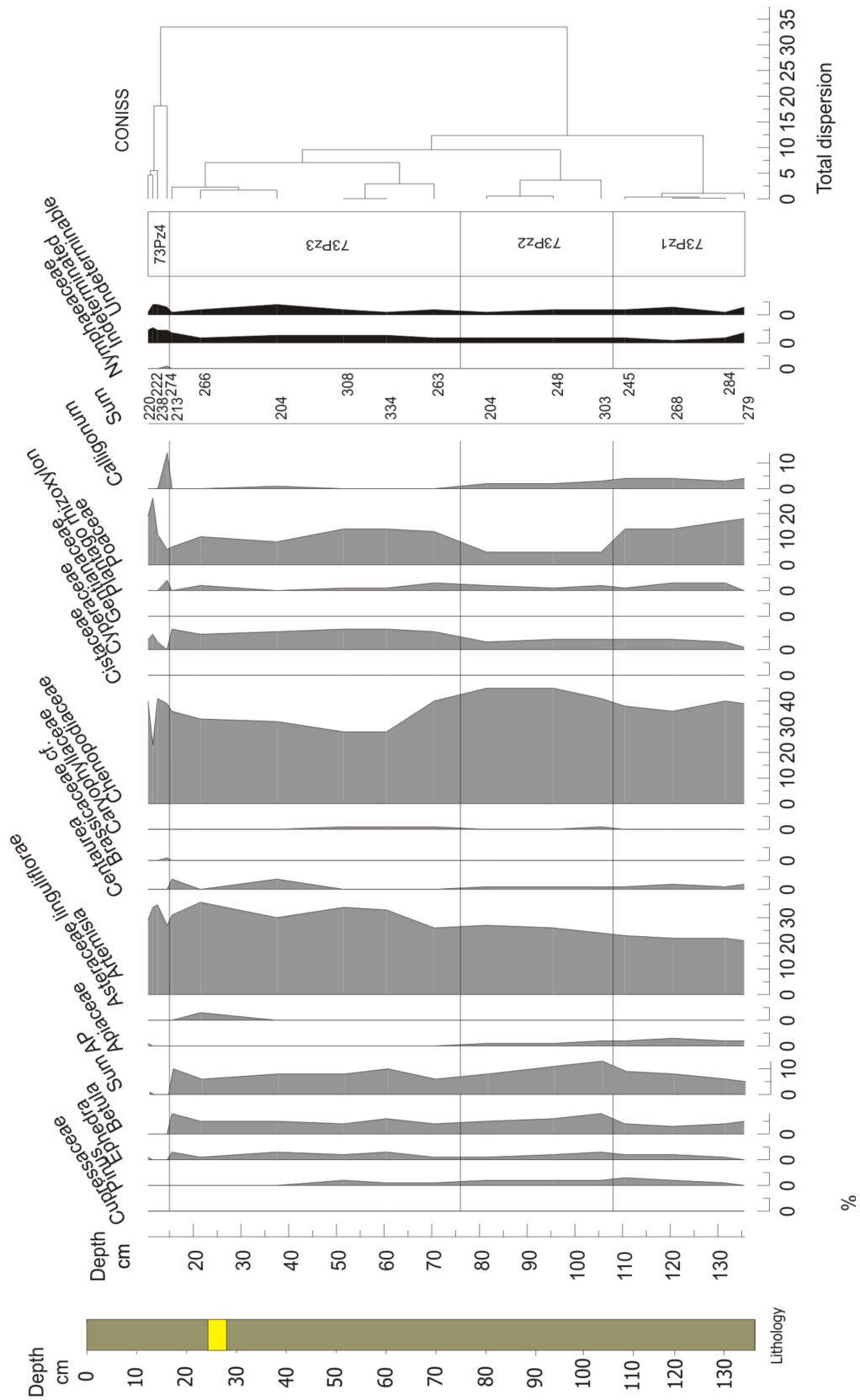
Fig. 4.31. Pollen percentages for core OS73. Legend for lithology shown in Fig. 4.7.

Owing to the core containing no obvious coarse horizons, samples were taken spread throughout the core. Within this core, observations were made to assess any long-term (over the last 2.3 ka) changes in vegetation. Once again the diagram (Fig. 4.31) for core OS73 is dominated by Chenopodiaceae, *Artemisia* and Poaceae. Unlike core OS55, OS73 contains no *Rhizophora*. The sequence was divided into four pollen zones (73Pz) by CONISS.

73Pz1 (base to 108 cm)

73Pz1 (Fig. 4.31) contains a minor increase of arboreal pollen from the base to 108 cm, increasing by just 5 %. There is evidence for a small increase in the percentage of *Pinus* throughout the zone. The percentage of Chenopodiaceae is high in this zone fluctuating between 35 and 45 % of the total pollen sum. Poaceae shows a gradual decrease from base to 110 cm, dropping sharply from approximately 15 to 5 %. The amount of indeterminated and undeterminable grains remain constant through the entirety of the zone. Overall the percentages of the majority of taxa remain constant throughout this zone.

73Pz2 (108 to 76 cm)

73Pz2 is characterised by a gradual increase to a maximum and subsequent decrease in Chenopodiaceae throughout the zone. *Artemisia* displays a progressive increase, whilst other taxa for example *Betula* sp., arboreal pollen, and *Calligonum* all decreasing within this zone, with *Calligonum* reaching 0 % by the end of 73Pz2.

73Pz3 (76 to 15 cm)

Overall, 73Pz3 shows little internal variation for most taxa. The zone is characterised by the continued occurrence of *Ephedra, Betula* sp*.* and *Artemisia.* Percentages of *Artemisia*, Chenopodiaceae and Poaceae remain high, dominating any other species. There is a decrease in Chenopodiaceae from 73Pz2 into 73Pz3 with percentages dropping around 15 %. Percentages of both *Artemisia* and Chenopodiaceae fluctuate but show an overall increase through the zone. *Pinus*, Apiaceae and *Calligonum* all decrease to 0 % in 73Pz3.

73Pz4 (15 cm to top)

The termination of 73Pz3 and the onset of 73Pz4 shows a sudden decrease in arboreal pollen, with percentages of *Betula* and *Ephedra* falling rapidly to 0 %. Cyperaceae also appears to decrease rapidly at the end of 73Pz3. In addition both Poaceae and *Artemisia* percentages fall at the end of 73Pz3, but at a gradual rate. Within 73Pz4 percentages of Poaceae and *Artemisia* appear to recover reaching percentages greater than at any other time within the core sequence. There is a peak in *Calligonum* (37 grains) from 0 to 10 % with a lesser peak in *Plantago rhizoxylon* (10 grains). The percentages of indeterminated and undeterminable grains peak across the three zones.

Core OS73 pollen taxa concentrations

Individual pollen counts were plotted as concentrations (73PCz) and are shown in Fig. 4.32.

73PCz1 (base to 107 cm)

Like 73Pz1 (Fig. 4.32), 73PCz1 contains a minor increase in the concentrations of arboreal pollen to 280 grains per ml^{-1} from the base to 108 cm. The concentration of Chenopodiaceae and *Artemesia* increases throughout this zone up to 800 and 1200 grains per ml^{-1}. Poaceae shows a gradual decrease from base to 110 cm, dropping sharply from 400 to 200 grains per ml^{-1}. The concentrations of indeterminated and undeterminable grains remain constant through the entirety of the zone.

73PCz2 (107 to 76 cm)

73PCz2 is very similar to 73Pz2, however Chenopodiaceae displays generally decreasing values throughout but continues to remain dominant dropping from 1200 to 1100 grains per ml^{-1}. Poaceae concentrations are very low in this zone decreasing from 400 to 200 grains per ml^{-1} at 107 cm.

73PCz3 (76 to 15 cm)

73PCz3 is again very similar to 73Pz3 and shows a gradual decrease in the concentrations of Chenopodiaceae. The decrease in Chenopodiaceae is pronounced dropping from 1100 to 600 grains per ml^{-1}. Poaceae concentrations increase in this zone to 400 grains per ml^{-1}.

73PCz4 (15 cm to top)

The onset of 73PCz4 shows an exaggerated peak in *Artemisia* reaching maximal concentrations of 1000 grains per ml^{-1}. Chenopodiaceae and Poaceae also peak at 15 cm to 1200 and 600 grains per ml^{-1}. Certain taxa decrease for example all AP drop to negligible values.
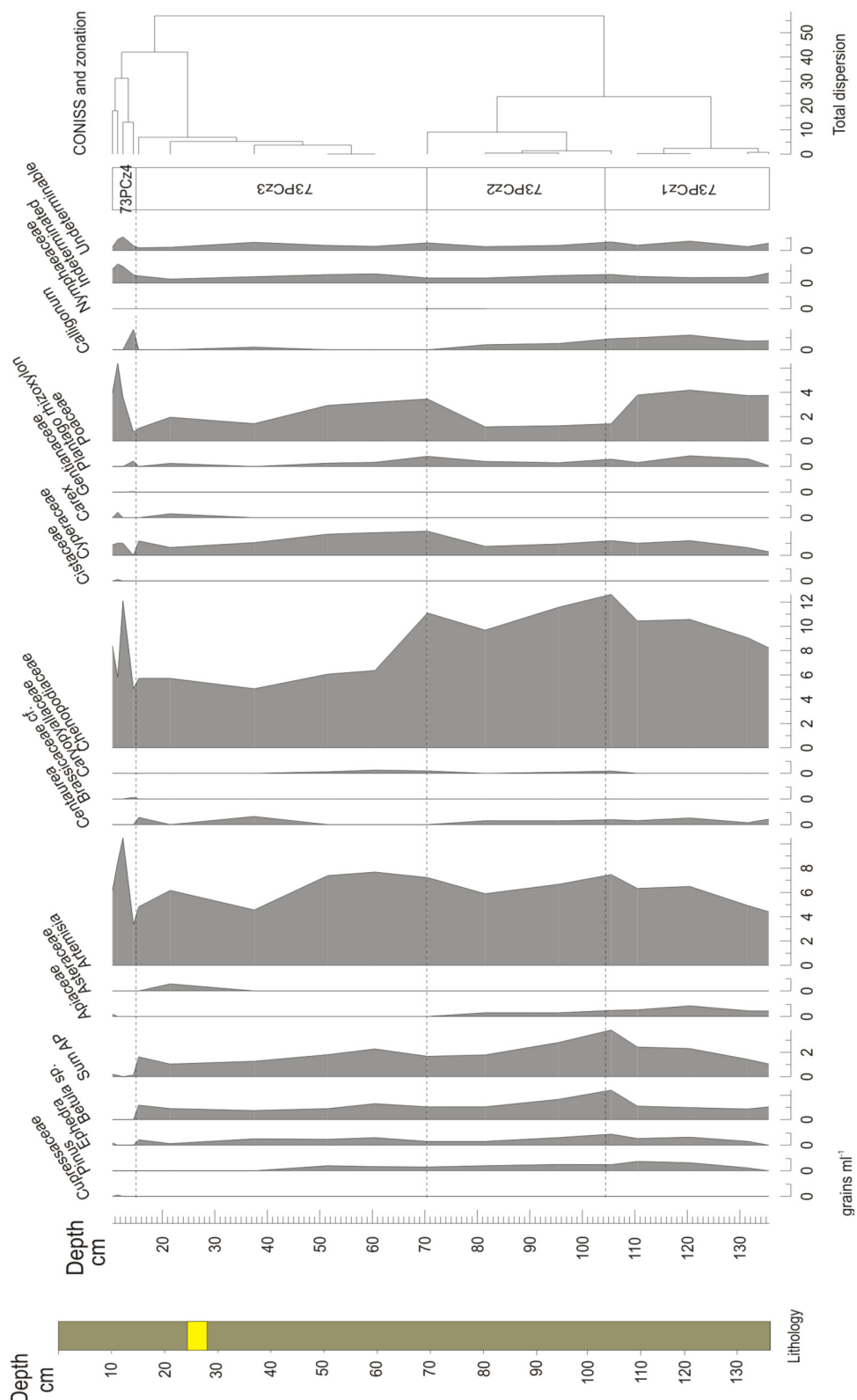
Fig. 4.32. Pollen taxa concentrations for core OS73. Legend for lithology shown in Fig. 4.7.

4.10.5 Core OS73 – dinoflagellate cyst analysis

Overall 26 species of dinoflagellate cysts were identified within 17 samples (Fig. 4.33).
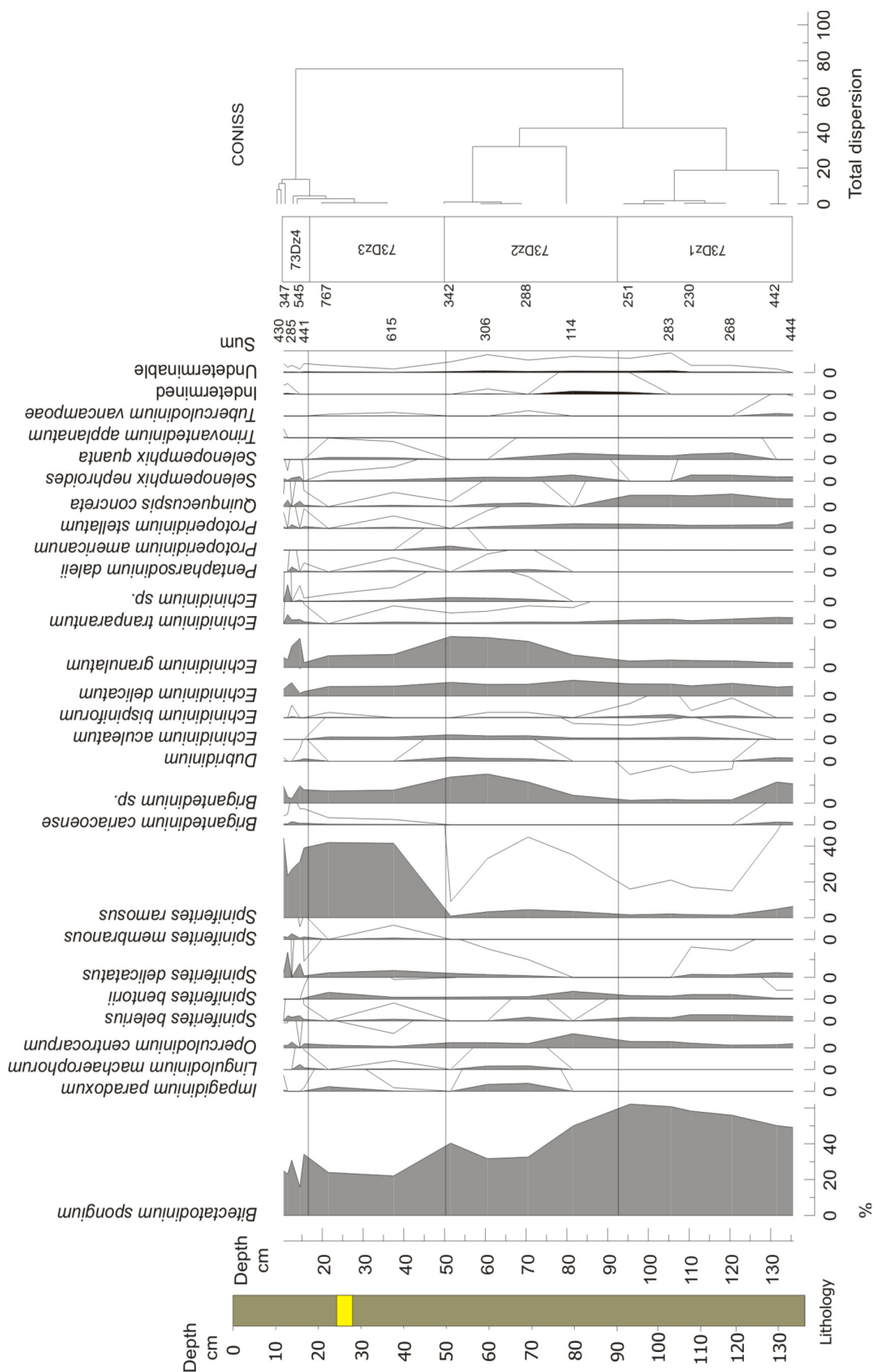
Fig. 4.33. Dinoflagellate percentages for core OS73. With 10x exaggeration curve. Legend for lithology shown in Fig. 4.7

Again, analogous to OS55 the concentration of dinoflagellates was high in comparison to the pollen found in the same samples. Thus sums of dinoflagellates counted per sample are greater. In general the assemblage is dominated by *B. spongium*, *S. ramosus*, *Brigantedinium* sp. and *E. granulatum,* with lesser amounts of *E. delicatum.* The dinoflagellate percentage diagram was divided into 4 zones (73Dz).

73Dz1 (base to 94 cm)

This zone is characterised by relatively stable dinoflagellate cyst percentages within individual species. Small fluctuations are observed however with *B. spongium* increasing from 50 to 55 % between base and 110 cm. A diminutive overall decrease in percentage is present throughout the zone in a number of species for example *S. belerius*, *S. ramosus*, *Brigantedinium* sp. and *P. stellatum.* Some species appear to increase throughout the zone for example *O. centrocarpum, S. bentorii, E. granulatum, S. nephroides* and *S. quanta.*

73Dz2 (94 to 50 cm)

This zone appears to become more taxonomically diverse. It shows a clear progressive development of *I. paradoxum, L. machaerophorum* and *E. aculeatum.* 73Dz2 highlights slight changes from the previous zone with *B. spongium* the most obvious change overall. The percentage *B. spongium* decreases gradually between 96 and 71 cm depth, stabilising then increasing by around 5 % from 60 to 50 cm. Values of *B. spongium* change from 50 to 40 % through the zone. Values of both *O. centrocarpum* and *E. delicatatum* first increase and then decrease towards the end of the zone. Percentages of *Brigantedinium* sp and *E. granulatum* both increase through this zone. Percentages of *S. ramosus* remain extremely low throughout 73Dz2.

73Dz3 (50 to 17 cm)

73Dz3 shows continued abundance of *B. spongium*, with it first decreasing and then becoming stable. *S. ramosus* demonstrates a dramatic increase in percentage abundance throughout this zone. Many species show continuous presence within the zone, e.g. *S. delicatatus, Brigantedinium* sp., *E. delicatum* and *E. granulatum.*

73Dz4 (17 cm to top)

73Dz4 shows a sudden decrease in percentage at 15 cm of most taxa, especially those that have been so abundant previously such as *B. spongium, S. ramosus,* and *Brigantedinium* sp. Several species are observed to increase at 15 cm depth: *E. granulatum*, *E. tranparatum, Q. concreta* and *S. quanta.* From 15 cm to core top there is a continued dominance of *B. spongium* and *S. ramosus* and there is evidence for a recovery of all species after the sudden decrease at 15 cm.

OS73 dinoflagellate taxa concentrations

Individual dinoflagellate counts were plotted as concentrations (Fig. 4.34) in the same way as the pollen to minimise any possible biases within the percentage data (Fig. 4.33).

73DCz1 (base to 81 cm)

This zone appears quite different to 73Dz1 with *B. spongium* decreasing throughout the zone from 1600 grains per ml^{-1} dropping to 500 grains per ml^{-1}. There is an overall decrease in concentration throughout the zone in a number of species for example *S. belerius*, *S. ramosus*, *Brigantedinium* sp. and *P. stellatum.*

73DCz2 (81 to 50 cm)

This zone shows an increase in numerous taxa with concentrations of *S. ramosus*, *I. paradoxum, L. machaerophorum* and *Echinidinium* sp. increasing. *B. spongium* concentration remains low and stable at 500 grains per ml^{-1}. Concentrations of *S. ramosus* are extremely low throughout at 40 grains per ml^{-1}.

73DCz3 (50 to 17 cm)

73DCz3 shows the concentration of *B. spongium* remaining stable throughout the zone at around 1200 grains per ml^{-1}. Concentrations for *I. paradoxum* first decrease and then increase again at the beginning of the zone but do not reach more than 130 grains per ml^{-1}. *S. ramosus* demonstrates a dramatic increase in concentration in this zone reaching values of up to 200 grains per ml^{-1}.

73DCz4 (17 cm to top)

73DCz4 shows a decrease in the concentration of all taxa except *S. delicatatus*, and species of *Echinidinium. S. ramosus* shows the most dramatic

decrease with concentration values falling from 1200 to 1000 grains per ml^{-1}.
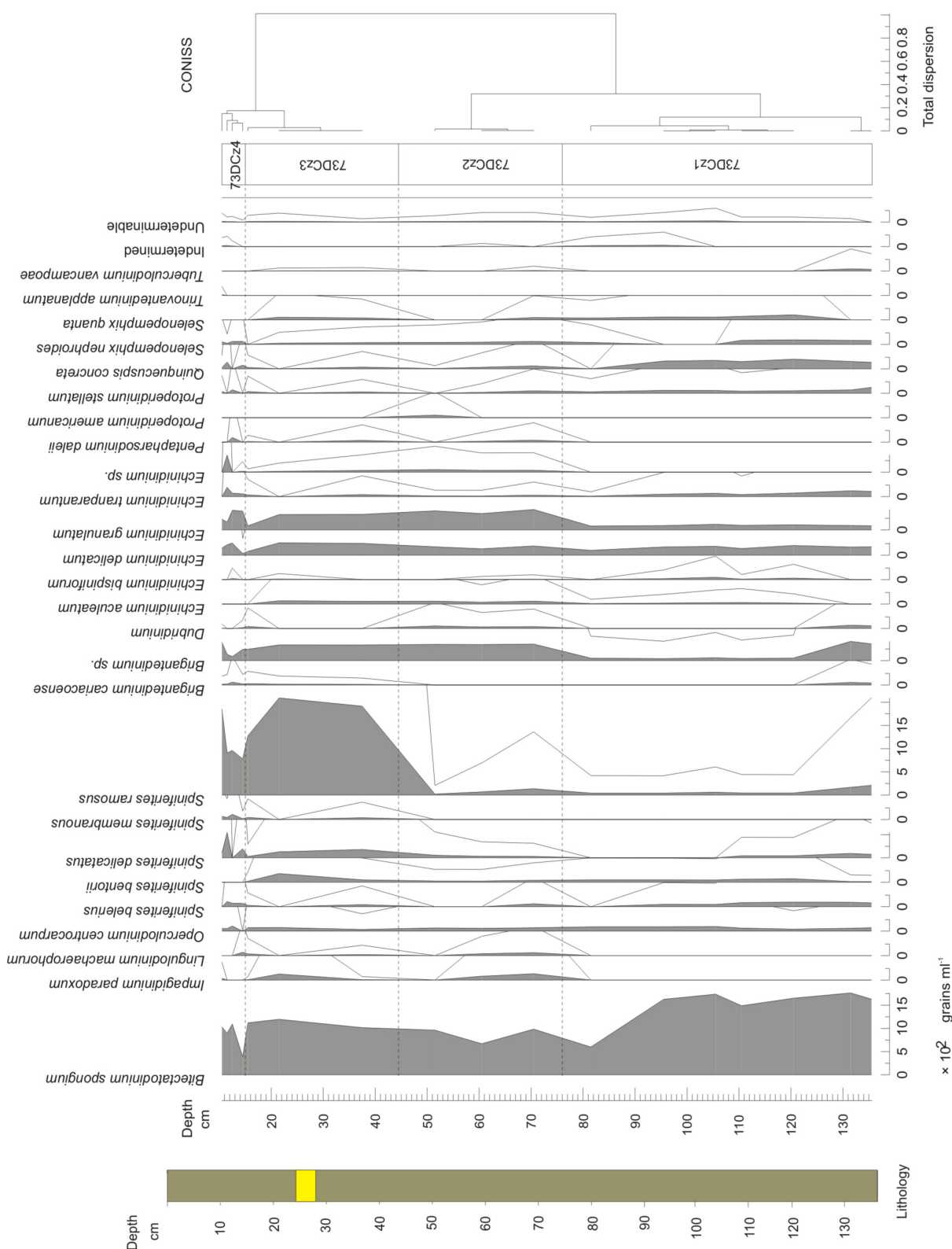
Fig. 4.34. Dinoflagellate taxa concentrations for core OS73. Legend for lithology shown in Fig. 4.7.

4.10.6 Core OS73 – pollen and dinoflagellate cyst concentrations

Pollen and dinoflagellate concentrations were calculated using Equ 4.1, and the results are shown below in Fig. 4.35.
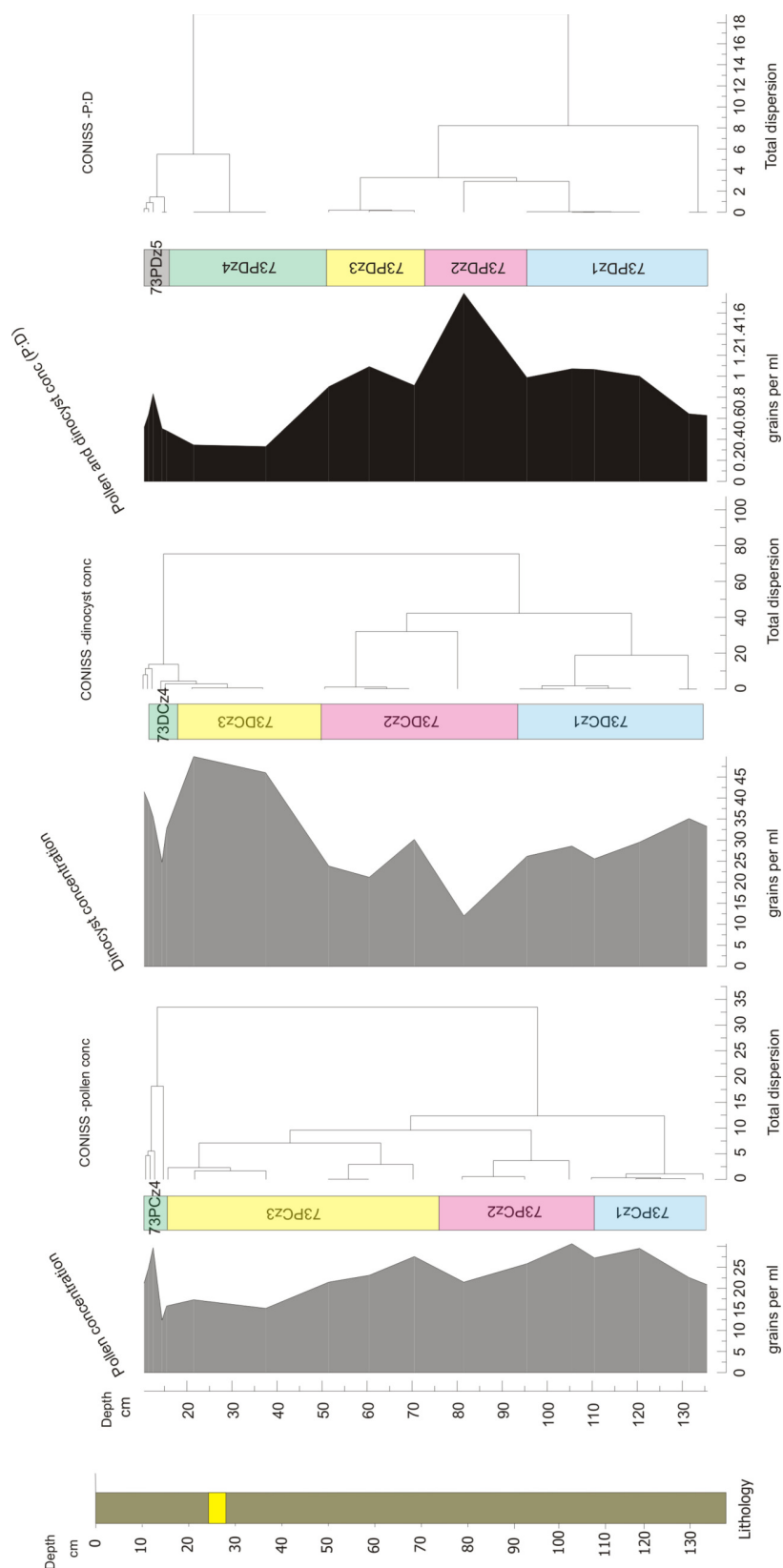
Fig. 4.35. Pollen and dinoflagellate concentrations and the P:D ratios for core OS73. Concentrations are per ml of wet sediment. Legend for lithology shown in Fig. 4.7

In general the pollen concentration appears relatively stable throughout the core showing only slight fluctuations. Dinoflagellate concentrations appear to display more variation throughout the core. Seemingly, the slight fluctuations in the pollen are exaggerated in the dinoflagellates. 73PDz1 from base to approximately 96 cm contains a decrease in dinoflagellate concentration throughout. The pollen concentration increases until 106 cm then falls slightly towards the end of 73PDz1. 73PDz2 involves a decrease in both pollen and dinoflagellate concentrations until 82 cm when levels begin to increase once more into 73PDz3. 73PDz2 is characterised by a sharp peak in P:D concentrations at 82 cm. Pollen concentrations peak at 72 cm to 2500 grains per ml. Dinoflagellates show a more prominent peak, displayed as a decrease in P:D at 72 cm. 73PDz3 involves a decrease in pollen concentrations throughout. Dinoflagellates increase within 73PDz4 until 22 cm. 73PDz4 is characterised by low pollen concentrations at approximately 1500 grains per ml. Dinoflagellates rapidly decrease within 73PDz5, falling from 5000 to 2500 grains per ml. The remainder of 73PDz5 from 15 cm to top displays both increases in pollen and dinocyst concentrations, and increasing P:D values.

5. Interpretation

The results obtained indicate that abrupt marine events are not present in all cores across the region, with core OS34 and 94 showing no change in sediment succession. It is reasonable to presume that the depth of water at these coring sites was high enough (or the slope angle was insufficient) to limit the impact of high-energy events on the sedimentation regime. Alternatively the sediment supply may be of limited grain size. Significant variations in sedimentology and magnetic susceptibility both within cores OS55 and 73 and between cores, prevented any reliable inter-core correlation. Each of these two cores will be discussed individually.

5.1 Core OS55

The majority of proxies used in this study indicate that core OS55 was subject to several abrupt events which have left sedimentological and palaeontological signatures within the deposits. These event deposits make acquiring an accurate age-depth estimation for core OS55 problematic. The dating results and the associated problems encountered will be addressed in more depth in section 5.1.7.

5.1.1 Grain-size results

It is clear from the grain-size data obtained at Brunel University that the sedimentation within core OS55 was not homogeneous. It contained the most varying lithologies compared to the other cores available. The sequence in core OS55 consists of a series of abrupt events (Fig 4.6) superimposed on top of continuous clay-silt sized background sedimentation.

Grain-size results obtained using the Cilas Particle Size Analyser generally correlate well with the visual core descriptions made at Brunel University. The grain-size data from core OS55 shows a polymodal distribution, indicating different transport or depositional processes (abrupt events superimposed on top of background gradual fine grained sedimentation). Grain size parameters of the bulk sediment sample cannot be used as environmental indicators given that the grain size component in polymodal sediments reflect different transportation or depositional processes (Sun *et al*., 2002).

The visual core descriptions and particle size distribution plot for core OS55 (Fig. 4.6, 4.20, 5.1) indicate an increase in grain size at 91 cm, however at this

depth the core is highly disturbed as a result of the drilling and exhumation, therefore it is unreasonable to class this horizon as a unit. The visual core descriptions and particle size distribution plot indicates a coarse horizon from 77 - 75 cm (unit A). From the measured grain-size data it is reasonable to presume that unit A consists of one single event, with no evidence of any internal fining upward sequences.
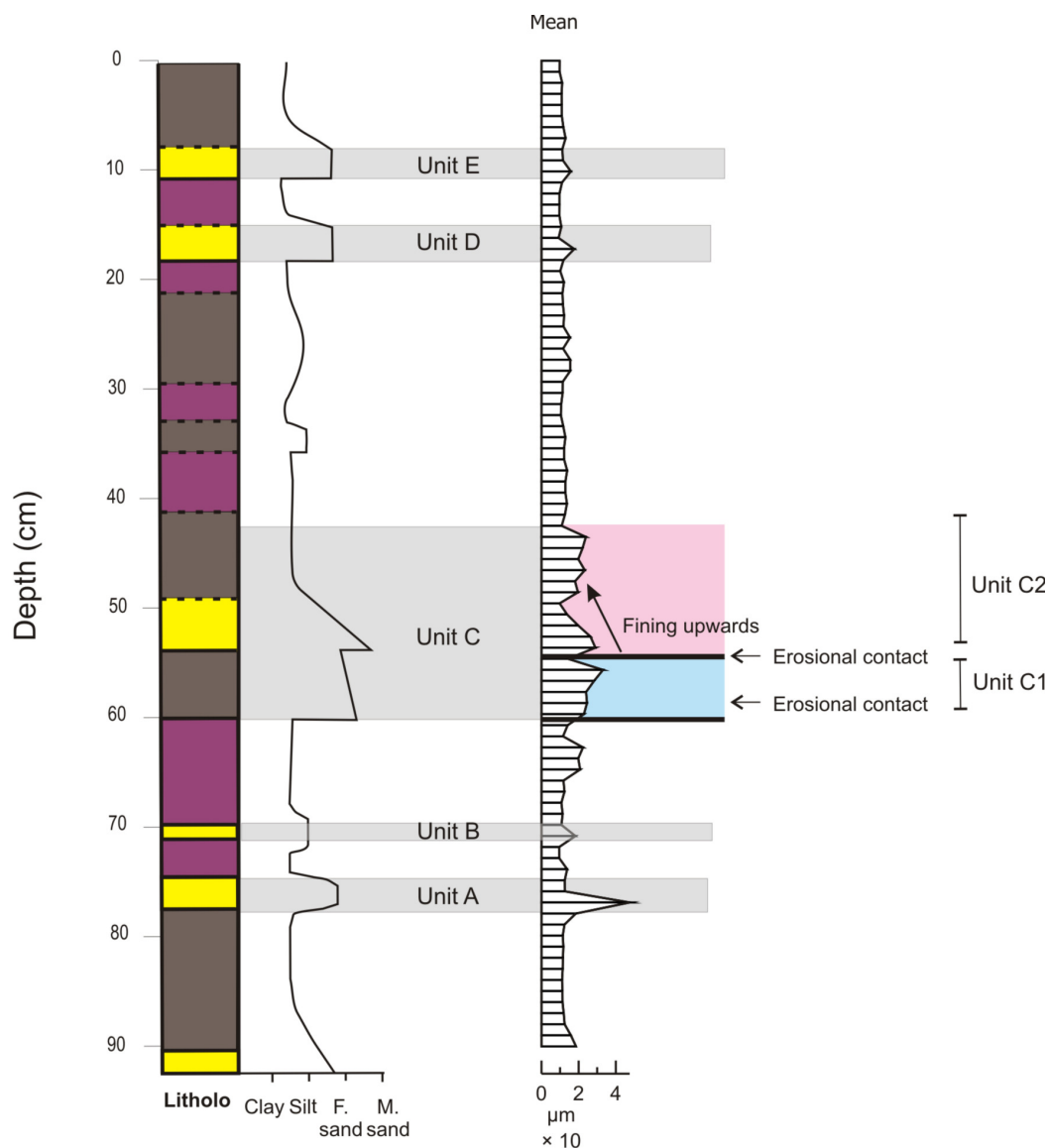
Fig. 5.1. To left: schematic of lithology of core OS55. Legend on Fig. 4.6. Right: event unit C and sub-divisions C1 and C2. Highlighting erosional contacts and fining upward sequence. A-E correspond to units described.

Unit B (Fig. 5.1) consists of a slight increase in grain-size from 71 – 70 cm. The event is represented in the visual grain size log (Fig. 4.6) and the Cilas particle size results (Fig. 4.20). The horizon is marked as an increase in $CaCO_3$ in the INCO grain size results (Fig. 4.16)I k. This is evidence that the horizon consists of abundant fragmented shell material, the cause of the increase in $CaCO_3$.

According to the Cilas particle size results there also seems to be a small peak in grain size at around 66 – 63 cm. This peak is not visible in the visual sedimentary log or in the INCO grain size results.

Unit C (Fig. 5.1) consists of a significant increase in grain-size, which does not correspond with a major increase in skewness or kurtosis. In contrast to preliminary data provided by INCO, unit C (Fig. 5.1) appears to consist of two separate events, one at 60 - 55 cm (unit C1) and the other at 55 - 43 cm (unit C2). Additionally, unit C1 is marked by an erosional base and consists of coarser material, containing no laminations or other sedimentary structures, interpreted as a high-energy deposit. Unit C2 also has an erosional base and consists of a fining upward sequence where laminations are re-established towards the upper surface, interpreted as normal graded bedding. This bed represents a depositional environment with a decrease in transport energy throughout, where dense, coarser sediment are deposited initially, and then finer sediments follow as the current weakens.

If unit C is indeed a turbidite bed, it is far from the ideal Bouma sequence (Fig. 5.2) as most beds appear to be missing (Bouma, 1962). This is often the case in reality where only the vertical ordering of sequences remains constant. Bouma divisions seen in unit C1 probably only include a small section of Ta, consisting of massive beds with no internal structure, however the characteristic graded bedding is missing from the sequence. Unit C2 contains a fining upwards sequence and may also represent a section of Ta in the next turbidite. A range of indicative sedimentary structures of the Bouma sequence such as climbing ripples, convoluted laminae, flute casts and dewatering features are also missing from unit C (Bouma, 1962).

As unit C does not contain all the characterists of a turbidite deposit it is reasonable to assume that the horizon represents a fine sand from the shelf generated by energy increase possibly from storms.

Units D and E are marked by an increase in mean and median at 17 - 15 cm and 11 - 8 cm respectively. The peak in standard deviation marks an increase in the spread of grain-sizes at these depths. The grain-size results do not indicate fining upward sequences within the deposits, but during visual core description erosive basal contacts were observed within both unit D and E (Fig. 5.1).

	Grain size	Bouma (1962)		Middleton and Hampton (1973)	Lowe (1982)	Shanmugam (1997)
Mud		Te	Laminated to homogeneous	Pelagic and low-density turbidity current	Pelagic and hemipelagic	Pelagic and hemipelagic
Sand /silt		Td	Upper parallel laminae	Turbidity current	Low-density turbidity current	Bottom-current reworking
		Tc	Ripples, wavy or convoluted laminae			
		Tb	Planar parallel laminae			
Sand (granule at base)		Ta	Massive, to fining upwards, flute marks, tool marks and ball and pillow structures at the base		High density turbidity current	Sandy debris flow (turbidity current if graded)

Fig. 5.2. Ideal Bouma Sequence showing Bouma (1962) divisions Ta-Te and facies change. Hemipelagic deposits are overlain by the deposits of the next turbidity current. Subsequent interpretation and subdivision given by Middleton and Hampton (1973), Lowe (1982) and Shanmugam (1997). Figure redrawn and adapted from Shanmugam (1997).

5.1.2 INCO Data

The oceanographic INCO data gives a clear idea of the conditions under which the most recent sediment was deposited. The oxygen saturation shows that core OS55 and OS73 were taken where oxygen levels at the sediment-water interface were low, OS55 (170 m depth) and OS73 (100 m depth) (Fig. 2.1). However, the sediments were not completely anoxic as the well-developed oxygen minimum zone (OMZ) lies between 200 – 1200 m water depth in this region leading to dysoxic or anoxic facies on the sea floor (von Rad *et al.*, 1995).

It should be noted that discrepancies in the grain-size data obtained by INCO and obtained by Brunel University are probably due to the coarse sampling resolution at INCO and the inherent subjectivity of visual description. The grain-size results of INCO for OS55 generally correlate well with the visual description and grain-size analysis made at Brunel. Due to the coarse resolution sampling, it was impossible to use INCO grain-size data to determine any small-scale changes in sediment type, such as graded bedding. Unit A (Fig. 5.1) is shown undoubtedly at 77 – 70 cm, as a marked increase in sand and a slight decrease in silt percentage. INCO has recorded unit B, as containing one sharp peak in sand percentage, with no fining upwards sub-units. Both the thin units C and D are not apparent within the INCO data, and they have recorded instead, a peak of sand from 33 to 21 cm. It was expected that CaCO$_3$ percentage would increase across the event horizons, with the peak caused by an increase of fragmented shell material brought into the region. Nevertheless it is difficult to associate small-scale

fluctuations in CaCO$_3$ obtained by INCO within their coarse resolution sampling with the event horizons found within the core, as they do not appear to correlate. It is odd that CaCO$_3$ percentages did not increase over the event beds, especially at 60 - 50 cm, where visually it was clear that the percentage of fragmented shell material increased dramatically. Additionally it was expected that there would be a slight increase in organic matter across the event horizons with organic rip-up clasts transported into the study regions by any high-energy event. A decrease in organic matter could also have been observed, from its dilution by siliceous sediment and/or fragmented shell material. Conversely, no real change in organic matter could be confidently associated with the grain-size changes within core OS55.

5.1.3 Magnetic susceptibility

Core OS55 displays the lowest and most fluctuating values of magnetic susceptibility, possibly due to the core containing both fine to coarse sediment. This core contains the most diamagnetic biogenic material in the form of both carbonate (shell material) and silica (increases in the percentages of sand). The increases in sand percentage and grain-size, correlate well in core OS55 with decreases in magnetic susceptibility, yet again due to magnetic susceptibility recording accurately the dilution of magnetic minerals with diamagnetic material.

5.1.4 Macrobiota

Fluctuations in macrofossil abundance as observed by visual inspection within core OS55 correlate well with increases in grain-size. Fragmentation was generally high throughout the core with the majority of shells found fragmented and disarticulated. A large increase in the concentration of shell material was observed within most of the event horizons, except in units A and B. The increase in concentration of fragmented shell material coupled with an increase in grain-size at the same level suggests that these deposits would originate offshore in shallow water. INCO data provides evidence that the sediment was deposited under dysoxic bottom water conditions, therefore benthic shell material must have originated from offshore in the shallower waters. The concentration of fossil material in these event horizons therefore represents a fossil death assemblage. The high level of fragmentation implies that shell material was either broken at the location where the animals dwelled, for example in the high energy rocky shore

region, or during the depositional process possibly a high-energy event. The type of fragmentation and shell breakage is evidence for the environmental processes responsible for depositing each unit (Fig. 5.3). The shell fragmentation found within units C to E resembles breakage linked with high-energy pounding suggesting deposition in shallow water in a high-energy environment, the shells were subsequently transported to the coring location. Although the method of transportation to the coring location is still unclear.
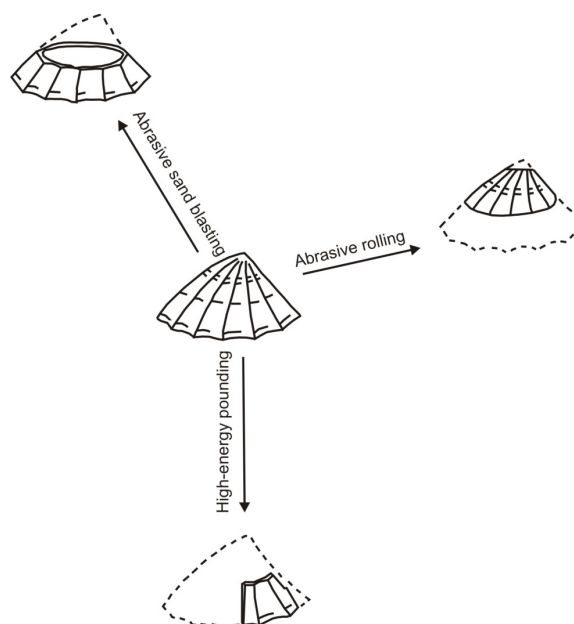
Fig. 5.3. Limpets showing an example of the processes of shell breakage. Abrasion (by sand blasting) leaves the shell fairly stable and only affects the exposed shell parts. Rolling along the sediment surface mainly abrades the shell extremities. Breakage on a high-energy rocky shore, or within a high-energy turbidity flow follows radial and concentric shell structure lines (modified from Zuschin *et al*., 2003 from Seilacher, 1973).

5.1.5 Palynology

Pollen and dinoflagellate percentages and concentrations within core OS55 were mainly used to assess changes in sedimentation rate and taphonomy rather than to elucidate changes in palaeoclimatic/environmental conditions. Palynological study, especially the ratio of pollen and spores to dinoflagellate cysts (P:D), *should* reflect increases in terrigenous sediment influx to the northern Arabian Sea (McCarthy and Mudie, 1998). However, the events only show slight increases in the the P:D ratio at these levels (Fig. 5.4). Smoothed pollen and dinoflagellate concentration curves appear to fall, peak, decrease then increase at the end of C1. The concentrations appear to fall further again at the beginning of the next event horizon B2 (Fig. 5.4). *Rhizophora,* a coastal tree, does not peak across the event horizons. In addition, percentages of *Betula* and *Typha Sparganium* increase across the event.
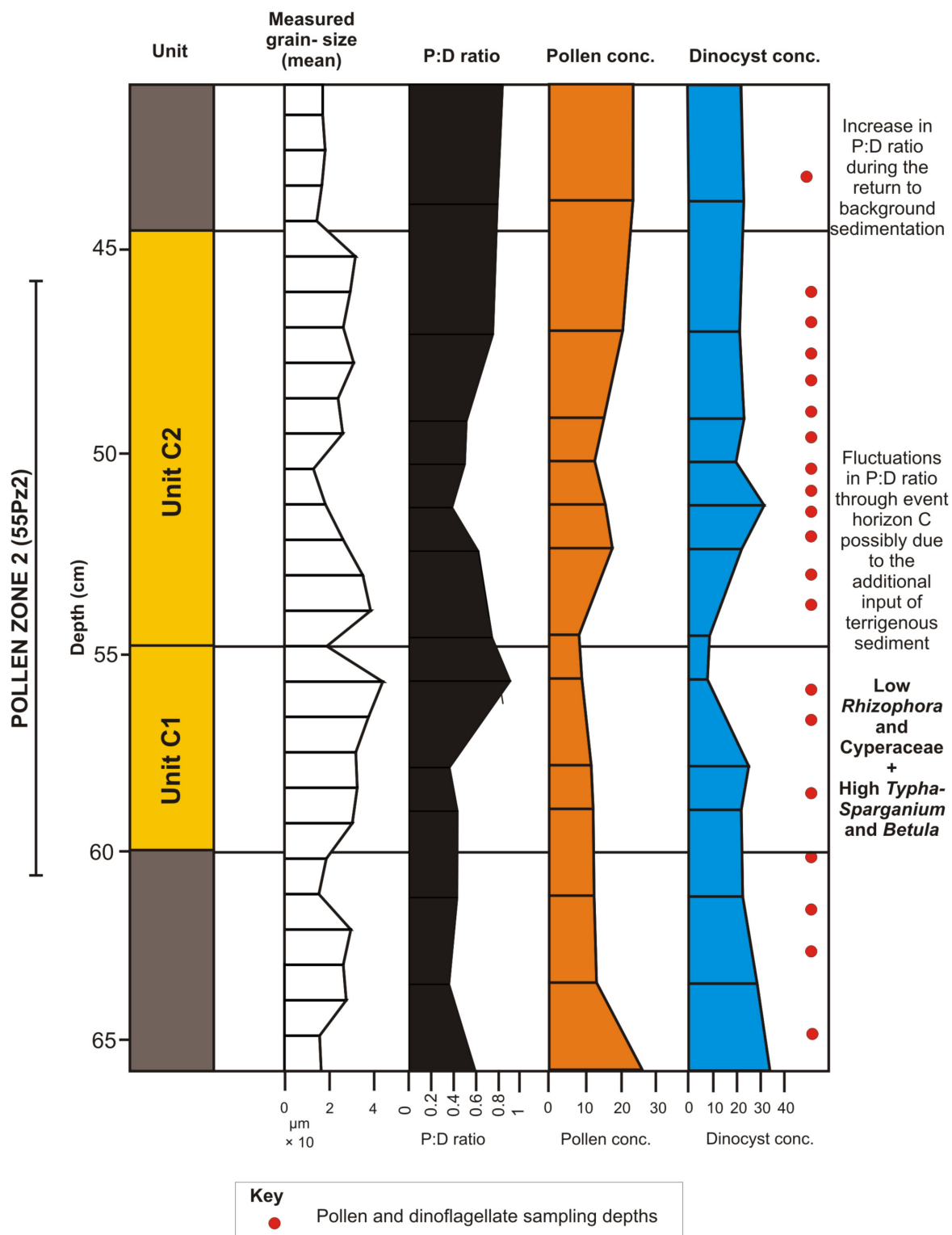
Fig. 5.4. Schematic of pollen and dinoflagellate concentrations and P:D ratios and their variation with grain-size within unit C. Pollen and dinocyst concentrations and P:D ratios are smoothed on 5 values, see Fig. 4.30 for correct values. Conc = concentration.

5.1.5.1 Hypothesis of source material of unit C

Possible hypotheses are offered to explain the mechanisms associated with the pollen and dinoflagellate concentrations and ratios within the event beds, with focus on unit C, the largest event within core OS55 (Fig. 5.1).

There are two hypotheses explaining the source of the sediment comprising event unit C:

Source material:
1. River deposited sediment (inner continental material)
2. Sediment deposited on the coast where *Rhizophora* does not grow

It is possible that the coarser sediment input does not originate from the shore line (coastal sediment), but from a sediment pile containing sediment from the inner continent. Increases in *Betula* (continental) and *Typha Sparganium* (freshwater) indicate that the sediment may have an inner continental origin rather than coastal. Evidence for this hypothesis also comes from the lack of *Rhizophora* (growing along the coastline) and Cyperaceae (marshy, coastal element) within the event horizon. A large event may have been responsible for bringing the sediment directly from the continent, for example, a tsunami backwash or a significant flood.

Largely, unit C shows a diversification in pollen and dinoflagellate taxa with percentages of *Ephedra, Betula, Salix* (cf.) and *Typha Sparganium* as well as percentages of *Impagidinium* species*, Brigantedinium* and *Echinidinium granulatum*., increasing. Taxa such as *Brigantedinium* have a higher abundance in relatively shallow and nutrient rich waters. Overall the percentages of arboreal pollen increase within the event beds, with significant increases in *Betula*. This amplification in taxa and preferential loss of marine derived palynomorphs could be due to the event units containing different source material than the background sedimentation. For example, the turbidite contains material sourced from pooling sediment, deposited on the shelf by episodic rivers. This material is likely to contain different pollen and dinoflagellate than the sediment deposited through background sedimentation processes within water column above the core location. There is substantial evidence to support hypothesis 1 that the likely source of the material comprising unit C is of river deposited sediment, from the inner continent. The second hypothesis can be rejected as if the source of the sediment was from material initially deposited on the coast then there would be no such increase in *Ephedra, Betula, Salix* (cf.) and *Typha Sparganium* over the event horizon. The

material has to be river deposited sediment, proving hypothesis 1 the most probable.

5.1.5.2 Hypothesis of transport mechanism depositing sediment of unit C:

There are three hypotheses that can be used to explain the transport mechanism for the sediment comprising event unit C:

Transport mechanism:
1. Episodic river flood
2. Tsunami backwash
3. Storm

There are numerous methods of shelf sediment destabilisation and the initiation of gravity flows. Core OS55 is situated 40 km from Pozm Bay (Fig. 2.1) which, in times of monsoonal rainfall contains a number of temporary rivers depositing a large amount of terrigenous sediment into the bay. This siliceous, continental river sediment could accumulate on the continental shelf, and simple over-steepening of the sediment pile could initiate a gravity flow.

For the duration of the traction phase of a tsunami, pulses of tsunami backwash may generate turbidity currents that move, under gravity, into the deep sea, following depressions and submarine gullies.

Alternatively, large storms may effect the unconsolidated sedimentary deposits on the shelf, resulting in a gravity flow.

Any mass shaking of the sediment by either a tsunami or storm would result in slope failure and a possible gravity flow. Build up of river deposited sediment on the slope will eventually lead to slope failure and a resulting density flow. As the fast moving density flow, containing a large concentration of particulate matter moves down slope it increases in speed.

Episodic flood, tsunami backwash and storm could result in the initiation of a gravity flow forming unit C. The method of self-acceleration involves the current entraining more sediment than it loses through deposition, resulting in the current becoming denser, consequently increasing the speed and eroding capacity of the flow, resulting in a self-reinforcing process (Parker *et al*., 1986). As the turbidity current moves down slope it entrains sediment from the seafloor, scouring the pre-deposited, unconsolidated sediment (Parker *et al*., 1986) (Fig. 5.5 b1). Evidence

for this scouring process in OS55 is the existence of erosional surfaces on the base of each event deposit (Fig. 5.1).

Within the mix of sediment transported by the high energy current were pollen and dinoflagellates cysts that were previously deposited from slow settling-out of the water column through time. The high-energy current could re-suspend the pre-deposited sediment and palynomorphs into the above water column (Fig. 5.5 b2).

Re-deposition of sediment occurs as the flow velocity decreases, with large particles being dumped quickly, then smaller ones entraining the pollen and dinoflagellates cysts. The very fine pre-deposited particles are taken further seaward as the particle-size distribution decreases with distance from land (Fig. 5.5 b3). This process may be responsible for the small peak in the pollen and dinoflagellates concentrations at approximately 52 cm within the coarse unit C1 (Fig. 5.4). Perhaps due to the differing settling velocities of pollen and dinoflagellates, the peak occurs at slightly different levels within the bed (Fig. 5.4). The process of self-acceleration within the turbidite only begins to slow as the angle of the seabed slope drops below a certain level. However, it has been noted that turbidity currents can flow on slope angles as low as 5° (Drago, 2002). The termination of the turbidity flow producing unit C1 results in the smoothed concentrations of pollen and dinoflagellates being slightly lower at this level (at approximately 55 cm see; Fig. 5.4) and this is possibly attributable to the bed below (58 – 56 cm) entraining most of the palynomorphs within the coarse sediment deposition below (Fig. 5.4; Fig. 5.5 b4).

Following the turbidity current, a return to normal background sedimentation resumes with pollen and dinoflagellates returning to pre-turbidity current levels (Fig. 5.5 b5). The second turbidity current (producing unit C2) truncates the first and represents a fluctuation in both pollen and dinoflagellate concentrations, possibly due to a dilution of the signals observed within the terrigenous material (Fig. 5.4).

The source of the sediment which comprises event unit C is well constrained. Pollen and dinoflagellate taxa provide evidence inner continental, but not of coastal origin. What remains controversial is the mechanism that brought the sediment into the coring location. There are three possible explanations including tsunami, storm or flood. The most likely explanation appears to be a flood (hypothesis 1). Both a tsunami (hypothesis 2) or storm (hypothesis 3) would incorporate coastal sediment into the deposit, bringing with it appreciable quantities of *Rhizophora* and

Cyperaceae. A flood would bring continental sediment and with it continental taxa (*Betula* and *Typha-Sparganium*) to the coring location, which is what is apparent in event unit C.
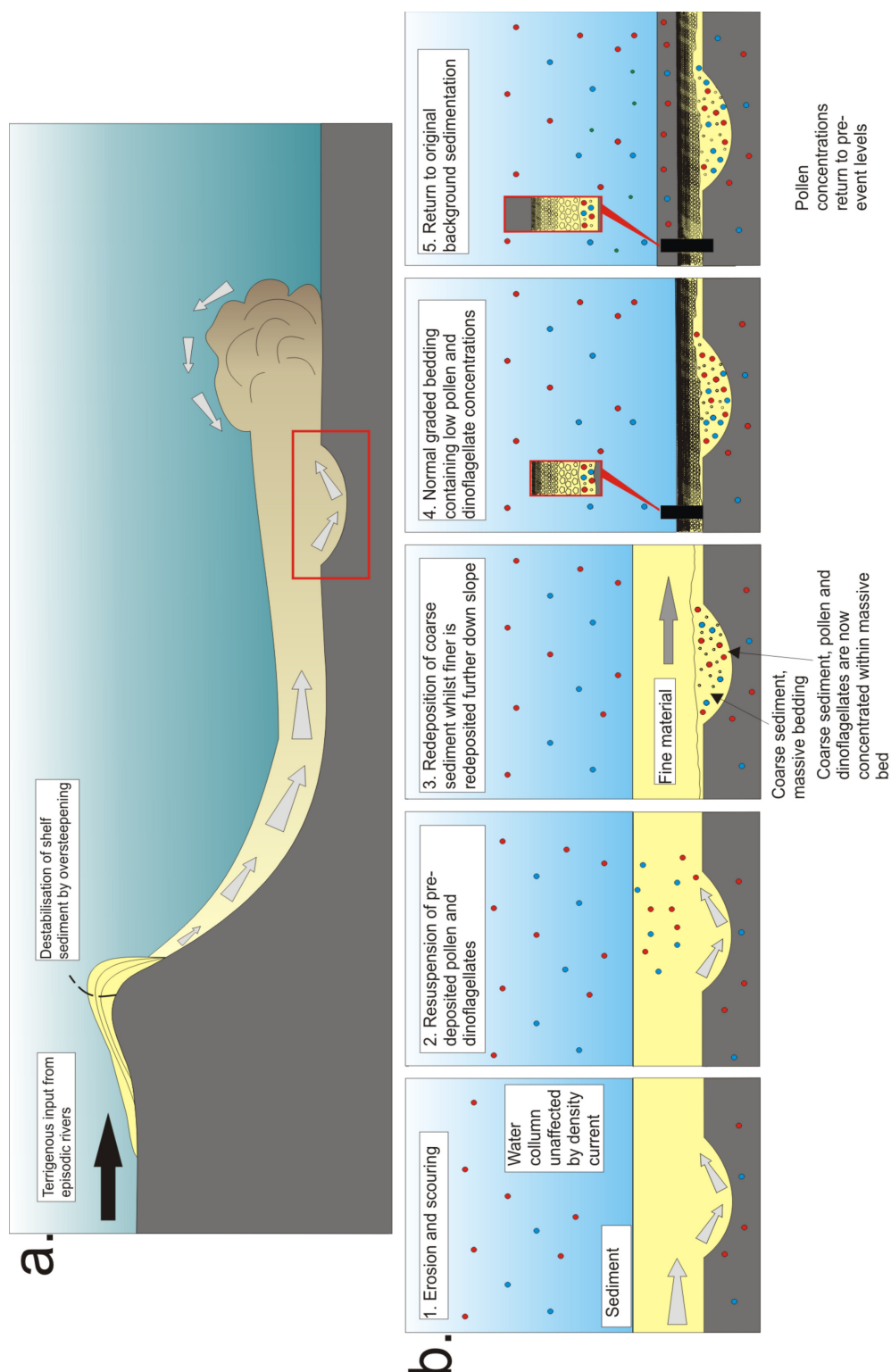
Fig. 5.5. A hypothetical model depicting a plausible mechanism for the fluctuations in pollen and dinocyst concentrations observed in core OS55. Dinocysts are illustrated using red circles and pollen blue. The enlarged sections (Fig. 5.5 b. 1-5) correspond to the red box detailed in Fig. 5.5 a. and are intended to give a pictorial representation of the hypothesised processes acting in a temporal progression (left to right). Enlargements within Fig. 5.6 b. 4-5 show stratigraphic variation and pollen and dinocyst abundance.

5.1.6 Core OS55 summary of sediment source interpretation

In conclusion, the grain-size results indicate five major changes in particle size, with sharp increases in grain-size at the bottom of each bed and a gradual fining upwards observed in unit C2 only. Each of the event units (A-E) within this core show several tsunamigenic, storm and flood characteristics. Fig. 5.6 gives an overview of the diagnostic criteria for tsunamis, storms and flood deposits from Kortekaas (2002) and Marren *et al*. (2002) and indicates whether each event unit within core OS55 displays the characteristic indicators.

Diagnostic criteria for tsunami		Event bed				
		Unit A	Unit B	Unit C	Unit D	Unit E
Stratigraphical	• Basal erosional /unconformable surface	YES	YES	YES	YES	YES
Sedimentological	• One or more fining upward sequence	NO	NO	YES	NO	NO
	• Intraclasts from underlying material	NO	NO	NO	NO	NO
	• Loading structures at base	NO	NO	NO	NO	NO
	• Bidirectional imbrication	NO	NO	NO	NO	NO
	• Poorly sorted	YES	YES	YES IN C1, NO IN C2	YES	YES
	• Lack of sedimentary structures	YES	YES	NO (graded bedding in C2)	YES	YES
Geochemical	• Increase in geochemical elements	YES	YES	YES	YES	YES
Palaeontological	• Marine fossils present	YES	YES	YES	YES	YES
	• Increased diversity	NO	NO	YES	NO	YES
	• Both well and poorly preserved fossils	YES	YES	YES	YES	YES
	• Plant fragments	NO	NO	NO	NO	NO
	• Shell rich unit	YES	YES	YES	YES	YES
	• Rafted material	NO	NO	NO	NO	NO
	• Buried plants at base	NO	NO	NO	NO	NO
SCORE (total 15)		**7**	**7**	**8**	**7**	**8**
Diagnostic criteria for storms		Event bed				
		Unit A	Unit B	Unit C	Unit D	Unit E
Stratigraphical	• Basal erosional /unconformable surface	YES	YES	YES	YES	YES
Sedimentological	• Fining upwards or homogeneous	NO	NO	YES	NO	NO
	• No intraclasts	YES	YES	YES	YES	YES
	• No load structures	YES	YES	YES	YES	YES
	• Unidirectional imbrication	NO	NO	NO	NO	NO
	• Well sorted	NO	NO	YES in C2, NO in C1	NO	NO
	• Sedimentary structures present	NO	NO	YES (graded bedding in C2)	NO	NO
Geochemical	• Increase in geochemical elements	YES	YES	YES	YES	YES
Palaeontological	• Marine fossils present	YES	YES	YES	YES	YES
	• Mixture of marine and freshwater fossils	YES	NO	YES	NO	YES
	• Poorly preserved fossils	YES	YES	YES	YES	YES
	• Plant fragments	NO	NO	NO	NO	NO
	• Shell fragments	YES	YES	YES	YES	YES
	• No rafted material	YES	YES	YES	YES	YES
	• Buried plants at base	NO	NO	NO	NO	NO
SCORE (total 15)		**9**	**8**	**11**	**8**	**8**
Diagnostic criteria for flood deposits		Event bed				
		Unit A	Unit B	Unit C	Unit D	Unit E
	• Poorly sorted	YES	YES	YES IN C1, NO IN C2	YES	YES
	• Massive bedding	NO	NO	YES IN C1, NO IN C2	NO	NO
	• Reverse grading	NO	NO	NO	NO	NO
	• Poor imbrication	YES	YES	YES	YES	YES
	• Floating clasts	NO	NO	NO	NO	NO
	• Traction carpets	NO	NO	NO	NO	NO
	• Cross bedding	NO	NO	NO	NO	NO
	• Erosional surfaces	YES	YES	YES	YES	YES
SCORE (total 8)		**3**	**3**	**4**	**3**	**3**

Fig. 5.6. Diagnostic criteria to recognise tsunamis and storms from Kortekaas, (2002) and flood deposits from Marren *et al*. (2002) and the assessment of whether each event bed contains each criteria.

It is difficult to compare the results of this research with the published diagnostic criteria (Fig. 5.6) as some of the criteria would not be evident in a deep water marine core (for example rafted material and buried plant deposits). It appears that most of the proxies used indicate that core OS55 was subject to several abrupt marine events which have left a sedimentological signature within the deposits. However the pollen and dinoflagellates show no evidence for event units A, B and D. The top of core OS55 contained abundant drilling disturbance therefore the certainty of unit E is also unclear. It is sensible to assume the certainty of only one large event within the core (containing 2 events), unit C. The existence of the graded bedding, erosive surfaces and fluctuations in pollen and dinoflagellate concentrations at this level provide strong evidence for this conclusion.

It is clear from the data that the core contains event units. However, it is evident from the P:D ratio and *Rhizophora,* Cyperaceae*, Betula and Typha Sparganium* percentages that the sediment is probably not from the coast but have being deposited by a river. All events consist of fragmented shell rich units rather than arbitrary shell fragments scattered throughout the beds, thus providing some evidence for tsunami source rather than storm. It is possible that a tsunami, storm or a flood may have been responsible for the event. However, if the deposit was of tsunami origin, coastal sediment would have been brought into the coring location during the traction phase of a tsunami (backwash), indicated by an increase in *Rhizophora*, however this is not the case. It is more plausible that an episodic flood, along one of the rivers flowing into Pozm Bay, brought continental sediment into the coring vicinity (Fig. 5.7).
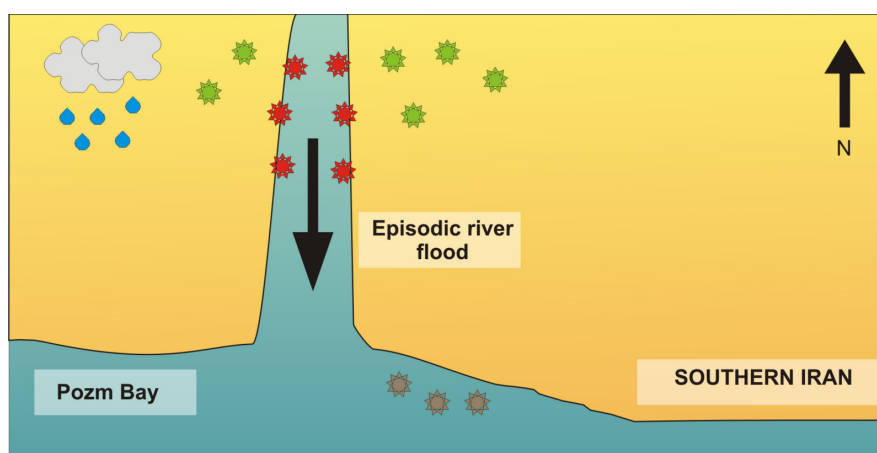
Fig. 5.7. River flood hypothesis from increased monsoonal precipitation. Green stars represent wind blow *Betula* from the continent, red stars *represent Typha Sparganium* and brown stars represent *Rhizophora* (coastal mangrove).

5.1.7 Dating of core OS55

Dating any storm or tsunami event deposit is complicated and the same was the case for those found within core OS55. Tsunamiites, tempestites and turbidites can incorporate older, reworked sediment within the event bed, therefore causing an over-estimation of the date. Within core OS55 dates were obtained for the sediment directly above unit C. The simple ^{210}Pb model assumes a constant rate of supply, and consequently it was impossible to date below when the event took place. Dates were however estimated for the top of the event as AD 1808, which cannot be accurately correlated with any recorded historical event. The tsunami of AD 1897 (section 2.7.1.4) may correlate with event unit C, however with the dating of this core problematic, certainty cannot be attained. Extrapolation of ^{210}Pb dates often produces age overestamination, therefore the end of the event (unit C) is no older than AD 1808 (*e.g.* Kazancı *et al*., 2004; Leroy *et al*., 2007). With the complexity of the sedimentation regime within the depositional basin for core OS55 and the various changes in lithological composition, it can be assumed that dates obtained by extrapolation of the sedimentation rate are relatively unreliable. The ^{210}Pb results show a decrease at 9.5 cm. This may be the result of an increase in grain-size at this level, associated with event unit E. The distribution of the accumulated fallout of ^{210}Pb demonstrates a significant preferential adsorption within fine grain-sizes (He and Walling, 1996). Thus, a sudden coarsening may result in a minor decrease in ^{210}Pb enrichment at this level. The peak in ^{210}Pb, within core OS55 at 16.5 cm, may also be grain-size induced, with finer grain-sizes conversely enriched with ^{210}Pb. It is problematic to use the ^{210}Pb dating technique on cores with differential grain-sizes containing numerous event beds, as failure to take into account such grain-size selectivity would lead to incorrect dates. Thus for core OS55, one can only speculate with the results. It has been suggested that radionuclide profiles can be used as additional indicators for disturbance event beds (Schwab *et al*., 2009). Deviations of excess ^{210}Pb activities from the decay curve were used to identify variations within the sedimentation rate which is characteristic of event deposits.

Radiocarbon dates for core OS55 may have firmed up the chronology to an extent. However, dating of the event beds still remains a considerable problem and has been reported in other studies, such as that of the early basin infill within Lake Bosumtwi (Shanahan *et al*., 2009; Tim Shanahan, pers. com. 2010). Other studies

on cores containing turbidite/mass movement deposits have shown that radiocarbon ages within event layers are commonly older than the overlying and underlying lake sediment and that numerous radiocarbon dates would be necessary to date individual events (Leroy *et al*., 2009).

5.2 Core OS73

The lithology of core OS73 is overall relatively homogeneous. Thus core OS73 is likely to hold a continuous record of any changing environmental conditions (temperature, precipitation, oceanic salinity *etc*.) on the southern Iranian coast.

5.2.1 Age-depth model for core OS73

Dating for core OS73 can be considered to be more reliable than that of core OS55, with no events throughout the laminated record back to the base at *c*. 2280 cal. yr BP. The top 5 cm of the core appears to display sediment mixing, with older ^{210}Pb dates incorporated within more recently deposited sediment. This sediment mixing may have been caused by recent bioturbating organisms, sediment reworking or perhaps simply due to drilling disturbances as seen in Fig. 4.7. The grain-size analysis of core OS73 also shows a shift to a finer regime at this level.

With 10 ^{210}Pb dates and three radiocarbon dates for the core an accurate sedimentation rate has been established for core OS73 (Fig. 5.8).

For the construction of the age-depth model (Fig. 5.8) for core OS73, the top 18 cm are dated by radionuclide dating (with an age of AD 1830), as ^{210}Pb dating can only be used for sediment younger than ~150 years. A second order polynomial was used to accurately fit the ^{210}Pb dates. The remainder of the core was dated by three radiocarbon dates. A linear extrapolation was used from the basal ^{210}Pb date to the first radiocarbon date (18.5 – 86.5 cm). Two additional linear trend lines were fitted between the radiocarbon date at 86.5 and 120.5 cm and 120.5 to the basal radiocarbon date at 148.5 cm.

$y = 0.5827x^2 - 0.7718x + 4.3891$

Depth (cm)

$y = 22.569x - 212.21$

$y = 4.1176x + 1383.8$

$y = 14.286x + 158.57$
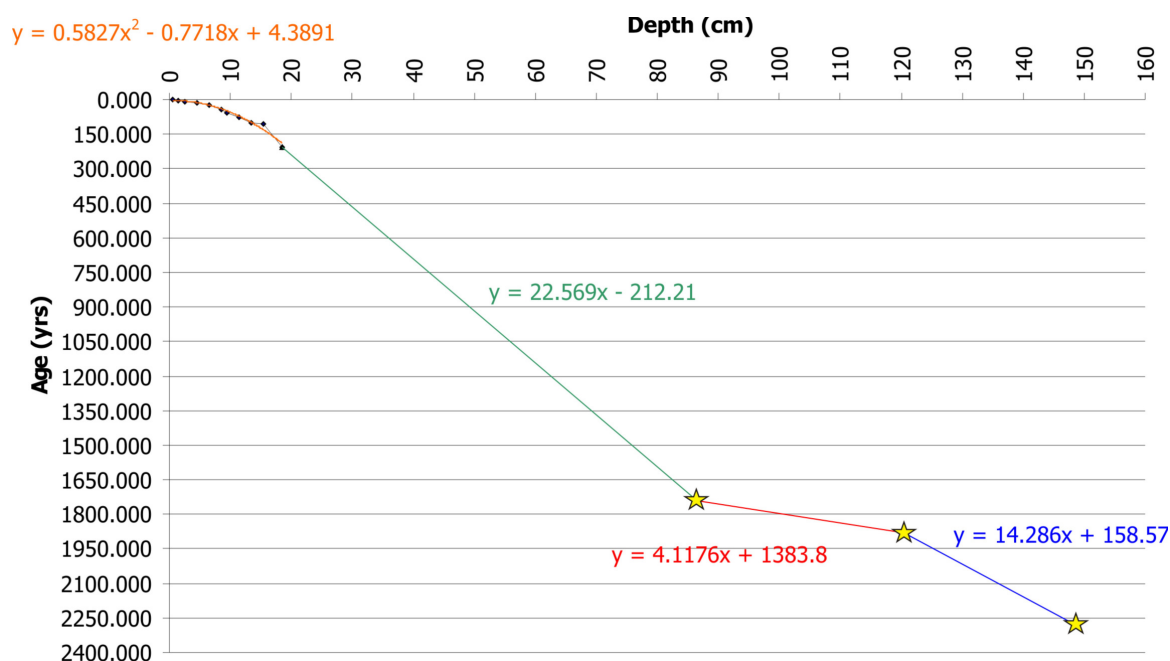
Fig. 5.8. Age-depth curve constructed using ^{210}Pb radionuclide dates (black points) and three calibrated radiocarbon dates (yellow stars). Separate trend lines make up age-depth curve. Second order polynomial trend line for ^{210}Pb dates (orange line), linear extrapolation between ^{210}Pb dates and radiocarbon date at 86.5 cm (green line), linear trend between 86.5 and 120.5 cm (red line) and linear trend between radiocarbon date at 120.5 and 148.5 cm (purple line) are also shown with the equations. NB. X-axis is in yrs BP.

5.2.2 Grain size

The grain-size data obtained at Brunel University show that the sedimentation within core OS73 was relatively homogeneous, with no event horizons as observed in core OS55. Small fluctuations were observed in sedimentation, but it is unreasonable to class these as event beds. A shift to finer sedimentation was detected at 17 cm, which is possibly due to a recent phenomenon in the region, for example a diversion of river deposition out of the coring vicinity, therefore only permitting fine-grained 'settling out' deposition, or the desiccation of the east and/or west rivers flowing into Pozm or Chabahar Bay (Fig. 4.1).

The grain-size results obtained using the Cilas Particle Size Analyser generally correlate with the visual core descriptions made at Brunel University, although slight grain-size deviations were not observed by eye. The shift in sedimentation to finer grains shown in the grain-size results was observed visually as a peak in sand and alternatively INCO data showed a peak in silt and a decrease in clay at this level. Due to the subjectivity of visual descriptions and the coarse resolution sampling of INCO, it would be sensible to presume the measured grain-size data obtained at Brunel to be the most reliable.

5.2.3 INCO sediment Data

As there are no clear event horizons recorded in core OS73 it was expected that $CaCO_3$ percentages would remain rather stable. This is mainly true, except for the small peak at 21 cm, which is not recorded in changes in the grain-size observed by INCO nor at Brunel. The small peak may be attributable to a single measurement of a large passing shell. The percentage of organic matter fluctuates throughout the core, with the intensity of the fluctuations increasing towards the core top, but being unrelated to any grain-size fluctuations.

5.2.4 Magnetic susceptibility

Magnetic susceptibility values remained rather constant throughout the entire core, which was expected due to just a slight variability in the sediment type throughout.

5.2.5 Macrobiota

Macrofossils within core OS73 were very rare. Two articulated bivalves were found within the core at 94 and 60 cm depth which were well preserved. The radiocarbon ages of these articulated bivalves are 1770 and 1140 cal. yr BP respectively. Fragmented shells were found in the top section of the core, coinciding with the shift in sedimentation to a finer regime at 17 cm (approximately AD 1791). It seems anomalous that a shift in grain-size, especially into fine sedimentation, could coincide with an increase in fragmentation. A rise in energy levels associated with increased fragmentation usually results in larger recorded grain sizes.

5.2.6 Palynology

As core OS73 contained no evidence for event units, pollen and dinoflagellate percentages and concentrations were used to assess any change in climatic/environmental conditions over the last 2300 years.

Although grain-size remains constant, and no event beds are present within the core, changes in pollen and dinoflagellate cyst percentages and concentrations are present throughout. The pollen is interpreted using the information derived from surface sediment samples collected offshore NW Africa from the Mediterranean to the Equator (Hooghiemstra *et al*., 2006) as both localities record

similar arid-adaptive taxa. Individual zones are discussed below. Dates are based on the sedimentation rate obtained by the age-depth model presented in Fig. 5.9.

5.2.6.1 Core OS73 - Pollen zones

The pollen zones within core OS73 are discussed in Table 5.1. The zones are associated with the pollen percentage diagram shown in Fig. 4.31. Pollen percentage data indicates that taxa such as *Artemisia* (steppic) and Poaceae (grassland) increase from base until 10 cm. This suggests that the climate has become progressively wetter over the last 2300 years. 73Pz3 is the wettest phase in the diagram (Fig. 4.31) over the last 2300 years displaying high levels of Poaceae and lower percentages of Chenopodiaceae. 73Pz2 is the driest phase with low levels of Poaceae and high levels of Chenopodiaceae (Fig. 4.31).

Pollen zone	Interpretation
73 Pz1 (2300 – 1830 cal. yr BP)	73Pz1 is characterised by relatively high percentages of Poaceae and lower percentages of Chenopodiaceae and *Artemisia*. It is possible that this zone is a manifestation of a wet phase in around Pozm Bay within the last 2300 years.
73 Pz2 (1830 – 1500 cal. yr BP)	73Pz2 is the driest phase within the last 2300 years on the southern Iranian coastline. The zone is characterised by low levels of Poaceae and high levels of arid-adaptive taxa such as Chenopodiaceae.
73 Pz3 (1500 – 120 cal. yr BP)	Within this period a decrease in desert vegetation, such as Chenopodiaceae and *Calligonum,* and an increase in grass percentages, possibly indicating a slight shift to grassland from desert vegetation occurs, implying a possible wetter period affecting the coring vicinity.
73 Pz4 (120 cal. yr BP - present)	The termination of 73Pz3 and the onset of 73Pz4 show a decrease in arboreal pollen, Cyperaceae and *Artemisia*. Certain taxa increase such as Poaceae and *Calligonum*. These dramatic changes in pollen percentages coincide with a shift in sedimentation. This shift could be due to recent human impacts in the region and it is unlikely to be associated with natural changes in the local precipitation as records from Chabahar Meteorological Station show no such changes (Fig. 2.9).

Table 5.1. OS73 pollen zones and interpretation based on Fig. 4.31.

5.2.6.2 Core OS73 – pollen taxa concentrations

Individual pollen counts were also plotted as concentrations as large increases in certain taxa percentages often mark a significant decrease in other taxa percentages, merely an affect of representing the data as a percentage. Thus pollen taxa were plotted as concentrations with each taxa plotted independent of

the next (Fig. 4.32). The individual pollen taxa concentrations zones within core OS73 are discussed in Table 5.2. The zones are associated with the pollen diagram shown in Fig. 4.32.

Pollen zone	Interpretation
73 PCz1 (2300 – 1820 cal. yr BP)	73PCz1 contains an increase in Chenopodiaceae and *Artemisia* throughout (Fig. 4.32). Pollen concentrations remain stable at around 400 grains per ml until the termination of 73PCz1 where concentrations drop to 200 grains per ml. The amount of arboreal taxa also remains relatively constant with only a small increase in *Betula* at the top of the zone. This zone is similar to zone 73Pz1 where percentages indicate this zone to represent a wet period in the coring vicinity (Fig. 4.31). The zone is marked by a slight increase in total pollen concentrations which become stable at approximately 1820 cal. yr BP. The small increase in concentration is possibly caused by the increase in the amount of Chenopodiaceae and *Artemisia*.
73 PCz2 (1820 - 1500 cal. yr BP)	Yet again plotting the taxa as concentrations gives similar results to the percentage data (Fig. 4.31). This zone is almost identical to 73Pz2, however Chenopodiaceae displays slightly decreasing values throughout the zone, whereas the percentage diagram showed Chenopodiaceae values as static (Fig. 4.32). Poaceae percentages are low thus this zone represents a dry period. An overall gradual decrease in total pollen concentration is evidenced in 73PCz2. This is possibly the result of a decrease in Poaceae.
73 PCz3 (1500 – 120 cal. yr BP)	This zone is similar to 73Pz3 and shows a decrease in desert vegetation (Chenopodiaceae, *Calligonum* and *Artemisia*) and an increase in grass percentages. 73PCz3 unlike 73Pz3 shows a gradual decrease in *Artemisia* throughout. The vegetation in the zone indicates a slight shift of grassland to desert vegetation, implying a possible wet period affecting the coring vicinity. The wet period in 73PCz3 may be more pronounced than that of 73PCz1 with 73PCz3 containing a more dramatic decrease of desert taxa (Chenopodiaceae). This zone is characterised by a decrease in total pollen concentration throughout which is mirrored by a decrease in the individual pollen concentrations.
73 PCz4 (120 cal. yr BP – present)	The onset of 73PCz4 shows a more exaggerated peak in Chenopodiaceae, *Artemisia* and Poaceae than 73Pz4 (Fig. 4.31). Decreases in arboreal pollen are evident, with all taxa decreasing. Again the changes in pollen concentrations coincide with the shift in sedimentation at this level.

Table 5.2. OS73 individual pollen taxa concentrations based on Fig. 4.32.

The pollen percentage and concentration results from OS73 indicate three climatic stages within the last 2300 years. 73Pz1 (2300 - 1830 cal. yr BP) is a wet period containing high percentages of Poaceae and low percentages of percentages of Chenopodiaceae and *Artemisia*. 73Pz2 (1830 – 1500 cal. yr BP) is relatively dry with Poaceae decreasing and desert taxa increasing. 73Pz3 (1500 - 120 cal. yr BP) is a wet period with decreasing percentages of desert taxa.

5.2.6.3 Core OS73 - dinoflagellate zones

The dinoflagellate zones within core OS73 are discussed in Table 5.3. The zones are associated with the dinoflagellate percentage diagram shown in Fig. 4.33.

Dinoflagellate zone	Interpretation
73Dz1 (2300 – 1770 cal. yr BP)	This zone is characterised by stable dinoflagellate cyst percentages with a relatively minor increase in B. *spongium* throughout. This increase in *B. spongium* from 2300 until 1770 cal. yr BP implies a gradual strengthening of the SW summer monsoon and an associated increase in upwelling intensity along the southern Iranian coastline. The zone contains no evidence of *I. paradoxum,* a species which dominates open-ocean, nutrient deficient, assemblages, therefore providing evidence for a strengthening of upwelling along the coastline.
73Dz2 (1770 – 920 cal. yr BP)	73Dz2 contains an overall increase in diversity and a decrease in *B. spongium* percentages. The decrease in *B. spongium* (a species associated with intense upwelling) and the slight increase in the percentages of *I. paradoxum* imply that 73Dz2 is a period of decreased upwelling.
73Dz3 (920 - 160 cal. yr BP)	73Dz3 is characterised by a gradual decrease in *B. spongium* and a significant increase in *S. ramosus* at 52 cm (960 cal. yr BP). *S. ramosus* is indicative of warm waters and warm SST in winter, spring, and autumn. Additionally it indicates relatively low nitrate and spring chlorophyll-a concentrations (Bouimetarhan *et al*., 2009). 73Dz3 may record a period of warmer SST giving rise to high percentages of *S. ramosus*.
73Dz4 (160 cal. yr BP - present)	A sudden drop in dinoflagellate percentages at 10 cm (approximately 50 cal. yr BP) is observed, where all taxa with the exception of *Echinidinium* sp. decrease. *Echinidinium sp.* is characteristically present in mesotrophic/eutrophic waters and is indicative of coastal upwelling and high productivity (Marret and Zonneveld, 2003). Records of precipitation taken at Chabahar meteorological station (Fig. 2.9) indicate that after approximately AD 1948 monthly rainfall records show high intensity fluctuations until present. These spikes in precipitation could explain an increase in surface run-off and the associated increase in oxygenation and oceanic nutrient content, resulting in the amplification of certain taxa favouring oxic, nutrient rich and high productivity environments. However, it is unclear why a decrease in other dinocysts relative to *Echinidinium* sp. occurs particularly if productivity in the region was high.

Table 5.3. OS73 dinoflagellate zones and interpretation based on Fig. 4.33.

5.2.6.4 Core OS73 – dinoflagellate taxa concentrations

The individual dinoflagellate taxa concentrations zones within core OS73 are discussed in Table 5.4. The zones are associated with the pollen diagram shown in Fig. 4.34. Total dinoflagellate concentration displays more variability than the pollen, declining to 2500 grains ml at 52 cm (960 cal. yr BP). This drop in concentration is associated with an increase in the percentage of *Brigantedinium sp*. and *B. spongium*, both species associated with coastal upwelling.

Dinoflagellate zone	Interpretation
73 DCz1 (2300 cal. yr BP – 1620 cal. yr BP)	This zone is similar to 73Dz1 where dinoflagellate values remain stable. However, plotting the individual taxa as concentrations highlights slight variations *B. spongium*, with values gradually decreasing throughout this zone. This decrease in *B. spongium* causes a decrease in the total dinoflagellate concentration throughout this zone. Previously data from Fig. 4.33 indicated increasing values of *B. spongium*, 73DCz1 shows this to be incorrect. This decrease in *B. spongium* implies a weakening of the SW summer monsoon and a decrease in upwelling intensity along the southern Iranian coastline. However the zone contains no *I. paradoxum,* therefore upwelling must still be sufficient to prevent the occurrence of the species along the coastline.
73DCz2 (1620 cal. yr BP – 920 cal. yr BP)	73DCz2 indicates a stable phase within the last 2300 years around Pozm Bay. By plotting the data as concentrations the apparent decrease in *B. spongium* seen in Fig. 4.33 is shown to be incorrect, and just an influence of changes in the percentages of other taxa. However, just like 73Dz2 (Fig. 4.33) *I. paradoxum* within 73DCz2 shows a slight increase indicating the zone may represent a period of decreased upwelling.
73DCz3 (920 cal. yr BP – 160 cal. yr BP)	The apparent gradual decrease in *B. spongium* seen in 73Dz3 (Fig. 4.33) is not seen in 73DCz3 (Fig. 4.34). Instead 73DCz3 displays exceptionally stable values of *B. spongium* throughout the zone. It seems the decrease in *B. spongium* seen in 73Dz3 is merely a consequence of the significant increase in *S. ramosus* in this zone. A large increase in total dinoflagellate concentration is observed associated with the increase in *S. ramosus*.
73DCz4 (160 cal. yr BP - present)	73DCz4 is identical to 73Dz4 with the decrease in concentrations of most taxa except *Echinidinium* sp. at 10 cm (approximately 50 cal. yr BP).

Table 5.4. OS73 individual dinoflagellate taxa concentrations based on Fig. 4.34.

B. spongium displays a general decrease indicating a gradual decrease in high summer SST from approximately 1770 cal. yr BP. The general decrease in the abundance of *B. spongium* over the last 2000 years implies a weakening of the summer SW monsoon. A slight increase in *I. paradoxum* from approximately 1590 - 1030 cal. yr BP may represent a minor decrease in the strength of upwelling along the Iranian coastline.

5.2.6.5 Core OS73 P:D concentration ratio zones

The P:D concentration ratio zones within core OS73 are discussed in Table 5.5. The zones are associated with the pollen diagram shown in Fig. 4.35.

P:D zone	Interpretation
73PDCz1 (2300 – 1780 cal. yr BP)	An overall increase in the P:D ratio occurs in 73PDCz1 which coincides with a gradual increase in the percentage of dry-adaptive taxa in 73PCz1 (Fig. 4.35).
73PDCz2 (1780 – 1480 cal. yr BP)	A peak in P:D at 82 cm (1640 cal. yr BP) is observed. Both pollen and dinoflagellate concentrations decrease at this level. However, dinoflagellate concentrations decrease more so, resulting in a peak in P:D ratio. Historical records of the region and Iranian climatic records (Fig. 2.9) do not extend far enough back in time to provide an explanation. The decreases in both pollen and dinoflagellates appear to correlate at the same interval, thus causes for each may be interconnected. It is plausible that several exceptionally dry years may result in a decrease in regional vegetation production. Alternatively, a simple explanation could be dilution of the pollen and dinoflagellates by an increase in the deposition of sediment. More samples around 82 cm would be needed in order to draw a firm conclusion.
73PDCz3 (1480 - 920 cal. yr BP)	73PDCz3 involves a decrease in pollen concentrations throughout. 73PDCz3 lies within 73Dz2 (Fig. 4.33) and correlates well with the increase in the percentage of *I. paradoxum* and the associated decrease in the percentage of *B. spongium* marking the period of decreased upwelling, cool temperatures and aridification (as seen in 73Pz2). An increase in both pollen and dinoflagellate concentrations occurs at 70 cm at the beginning of 73PDCz3 or 1200 cal. yr BP, with dinoflagellates displaying a larger magnitude of increase, and thus a decrease in P:D.
73PDCz4 (920 - 54 cal. yr BP)	Dinoflagellate concentrations increase within 73PDCz4 until 280 yr BP with pollen concentrations remaining low at 1500 grains per ml. 73PDCz4 correlates well with 73Dz3 (Fig. 4.33), where the increase in P:D is a result of a significant increase in the percentages of *S. ramosus*. This zone represents high SST and a warmer, wetter climate as indicated by a decrease in Chenopodiaceae and increase in Poaceae percentages. It is important to note that any changes in precipitation did not provide sufficient change to impact the sedimentary regime within the core vicinity. However, a peak in dinoflagellate cysts may imply an intensification of surface run-off and an increase in nutrient supply to the ocean.
73 PDCz5 (54 cal. yr BP - present)	Dinoflagellates rapidly decrease within 73PDCz5, falling from 5000 to 2500 grains per ml. The remainder of 73PDCz5 from 15 cm to top displays both increases in pollen and dinocyst concentrations, and increasing P:D values. The peak in P:D may imply more sediment coming from terrestrial sources due to human impacts and increased sediment supply around Chabahar Bay.

Table 5.5. OS73 P:D concentrations based on Fig. 4.35.

The higher ratio of pollen and spores to dinoflagellate cysts (P:D) *should* reflect increases in terrigenous sediment influx, but here they do not coincide with

any observed changes in grain-size. The P:D may in fact represent climatic changes on land that have not sufficiently impacted the marine environment or vice versa. For instance, if climate conditions have become suitably preferable for vegetation, more pollen would be produced, marking a significant peak in the P:D curve. It must be noted however that significant changes in rainfall usually result in fluctuations in sedimentation, but this is not observed within core OS73. The lack of sedimentation fluctuations may be because core OS73 is too far away from land to receive coarser material from the coast, or that the region surrounding the core is passed by gravity currents channelling the coarser material. More pollen is not necessarily required to mark a peak in the P:D ratio curve, a drop in dinoflagellate concentration relative to the pollen concentration would also be adequate. In addition, the P:D ratio perhaps indicates that there have been no strong climatic changes in the last 2300 years in the northern Arabian Sea.

5.3 Comparison between the OS cores

Although the cores were taken within a small region along the southern Iranian coastline they display numerous dissimilarities. The cores all differ in length, with core OS73 141 cm long and the shortest core OS94 just 37 cm long. OS55 is 88 cm long and is situated in front of Pozm Bay in a water depth of 170 m. Conversely core OS73 is situated approximately 45 km east of Chabahar Bay. Core OS73 was taken at a water depth of 100 m in a region with relatively little freshwater input from rivers.

The sedimentology of the cores differ dramatically displaying the complexity of the sedimentary regimes existing on the Makran coastline. OS55 showed the most variability in sediment type. Core OS35, OS73, OS84 and OS94 showed little change and consisted mostly of laminated silty-clays. The length and variations in sedimentology helped choose the cores suitable for further study for this research. Cores OS34, OS84 and OS94 would have been suitable for palaeoenvironmental study, with little variation in sedimentology. Although they do not encompass a long time period, it would be interesting to ensure the changes found within core OS73 are applicable to the wider region and not localised to the OS73 coring location. OS55 was ideal to reconstruct abrupt marine events as the material available for reworking was not restricted to just fine silts and clays. As OS73 was the longest core it was ideal for environmental reconstruction. Core OS55 contains a variety of sediment types and is dominated by silt and clay-sized material. It also contains

beds of sandier material which have erosive bases. These have been interpreted as event beds. The location of core OS55 (infront of Pozm Bay), the coarse material and the erosional surfaces provide evidence that OS55 lies in the path of gravity currents. The sediment within core OS73 is much more homogeneous. A slight coarsening of material occurs at approximately 12 cm; however the remainder of the core is mostly laminated and silt-sized. Therefore this core can be interpreted more directly in terms of environmental and climatic changes. It seems likely that core OS55 contains different sediment sources to that of core OS73, due to the large variety of sediment types it contains.

The magnetic susceptibility values showed large variations between and within the cores preventing any inter-core correlation. The average values for cores to the west (OS34, OS55, OS73) is around 5 (SI units), whereas the cores further to the east (OS84 and OS94) have relatively high magnetic susceptibility values (8.5-9 SI units). This may be related to the cores to the east receiving a different sediment supply than those to the west. The amount of variability within core OS55 is very high. This variation coincides with changes in sediment type. The increases in sand percentage and grain-size, correlate with decreases in magnetic susceptibility, due to proxy recording the dilution of magnetic minerals with diamagnetic material. Little variation in magnetic susceptibility within core OS73 is observed, with the core showing only a slight increase to the present day.

Sedimentology, magnetic susceptibility and the fact that dates could not be obtained evenly throughout each core inhibited accurate core correlation between any of the cores within the study. As core OS55 contained numerous event beds, dating was problematic and the results obtained possibly unreliable. A whole suite of radiocarbon dates would be necessary to date the event beds within the core. The dates obtained from core OS73 were more reliable. The sedimentology and dating profiles suggest that core OS55 experienced less surface mixing and incorporation of older sediment than core OS73.

Macrofossil preservation was visually assessed briefly on all cores. The results show that core OS55 contained variations in the degree of fragmentation and preservation state of shells throughout, with poor preservation recorded within the coarser event beds. No change in preservation state within core OS34, OS73, OS84 and OS94 was observed in the sparce accumuation of shells.

The pollen concentrations of core OS55 and OS73 are similar with average values of 2226 and 2276 grains ml^{-1} respectively. Dinoflagellate concentrations are

also very similar with core OS55 displaying a slightly elevated average concentration of 3318 grains per ml^{-1} against the dinoflagellate concentration within core OS73 of 3145 grains per ml^{-1}. Overall in both profiles the concentration of dinoflagellates was greater than that of the pollen. Less pollen samples were studied in core OS73 than in OS55, even though core OS73 was considerably longer, primarily due to time constraints. More pollen samples are required in core OS73 to draw any firm conclusions on any palaeoenvironmental change. Core OS73 is characterised by less indeterminated and undeterminable grains than in core OS55. This possibly relates to the better environment of deposition with core OS73 cored in low energy, deep water conditions. *Rhizophora* is abundant in core OS55 but absent in OS73. The results of this thesis provide evidence of the local variability of *Rhizophora* growth along the Iranian coastline. A possible explanation for *Rhizophora* found in core OS55 is that this core is located in front of Pozm Bay, which contains two small rivers. It is plausible that core OS55 experiences a considerable amount more freshwater input than core OS73 (which is situated along the coastline, within proximity of only one small river) permitting *Rhizophora* growth only in front of coring location OS55. Additionally, more *Betula* is present in core OS73, perhaps because OS73 has a slower sedimentation rate allowing for higher amounts of *Betula* to be transported by wind and deposited in the study region without it been diluted by additional terrigenous and biogenous material.

The dinoflagellate percentages between the two cores vary. In core OS55 no large increase in *S. ramosus* as seen in core OS73 can be observed. In addition, no gradual decrease in *B. spongium* in core OS55 can be seen as evidenced in core OS73.

It is possible that core OS55 is controlled mainly by the sedimentation regime with a high abundance of event beds and erratic changes in sedimentation. Core OS73 displays more constant sedimentation thus providing a better record of overall environmental change within the coring vicinity.

6. Discussion

As cores OS34, OS84 and OS94 were not subjected to high-resolution analysis (due to the time restrictions of the project), detailed conclusions cannot be attained and the results will not be discussed in depth.

6.1. Core OS55 – implications for abrupt marine events

Core OS55, although not suitable for palaeoenvironmental reconstruction provided some interesting results. The proxies used for core OS55 indicate that the area, in very close proximity to the coring region, was subject to abrupt events which left a distinct sedimentological and palynological signature within the core. It is sensible to assume the certainty of only one large event within the core, unit C (Fig. 5.1). Unit C has been interpreted as a turbidite deposit with evidence from grain-size, pollen and dinoflagellates results.

Deep cores (3095 – 1456 m depth) off the coast of Pakistan studied for turbidite characteristics contain turbidites showing Bouma sequence Tc, Td and Te displaying overall finer grain-size, upper parallel laminae and convoluted laminae (Lanfumey, 2008). Core OS55 was cored at a relatively shallow depth of 170 m, therefore may contain the deposition of coarser, proximal turbidites rather than distal turbidites identified in the study of Lanfumey (2008). Visual inspection indicated high levels of fragmentation of macrobiota within the core, with an increase in the concentration of fragmented material within the event horizons, indicating the occurrence of high-energy events. The date estimated for the top turbiditic bed unit C is <AD 1808. However this cannot be correlated accurately with any historical event in the region. The tsunami of AD 1897 (section 2.7.1.4) may correlate with event unit C. Nevertheless the dating of this core is problematic, with the lack of dates between 18.5 cm and 86.5 cm certainty cannot be attained.

A summary diagram of the interpreted pollen, dinoflagellate and grain size results seen in core OS55 is presented in Fig. 6.1. Unit C, the only certain event in core OS55 is highlighted with the termination of the event at <AD 1808. The presence of *Rhizophora*, Cyperaceae, *Typha-Sparganium* and *Betula* percentages throughout core OS55 is shown in Fig. 6.1. There is a decrease in *Rhizophora* and Cyperaceae across the event horizon supporting the hypothesis that the material comprising event unit C has a continental origin. Increases in the percentages of *Typha Sparganium* and *Betula* (typical inland taxa) provides additional evidence

that the material is formed from a sediment of inner-continental origin and not coastal. The results of this thesis provide evidence of the local presence of *Rhizophora* growth along the Iranian coastline, possibly related to local variations in salinity or sedimentary environments which are suitable for mangrove growth *e.g.* river mouths.
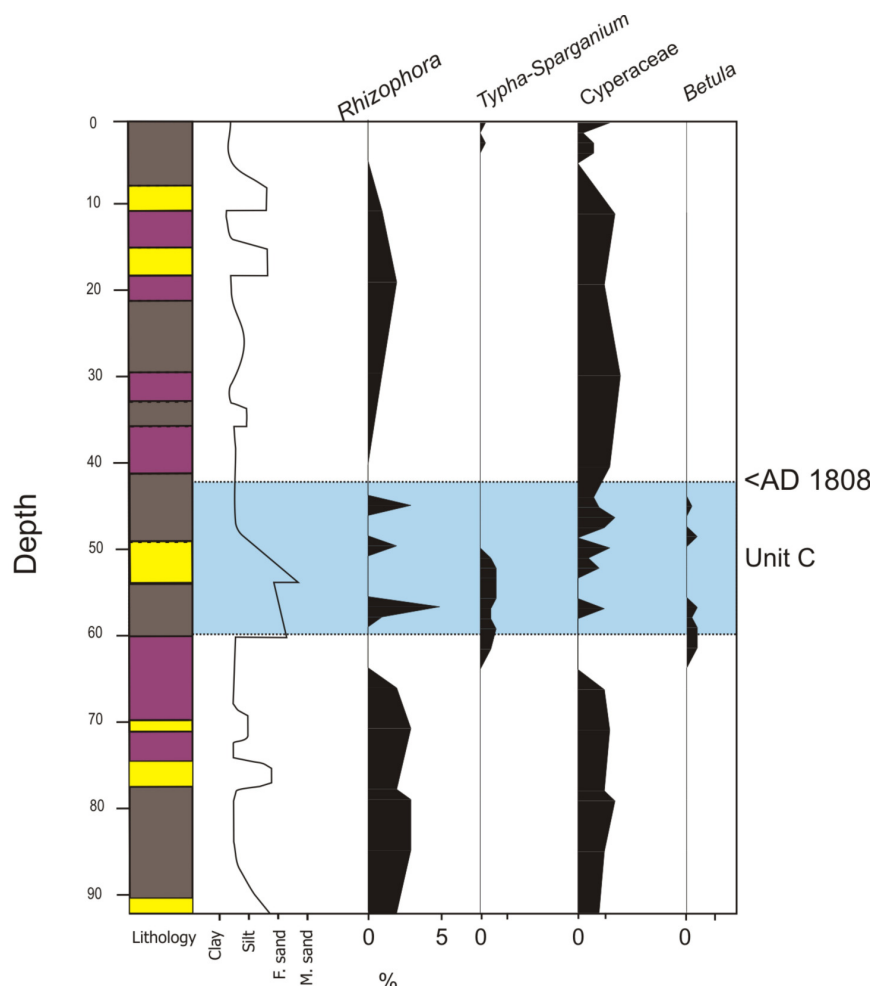
Fig. 6.1. Summary diagram indicating grain size and *Rhizophora*, Cyperaceae, *Typha-Sparganium* and *Betula* percentages throughout core OS55. Unit C is shown in blue with termination at <AD 1808.

In conclusion, the source of the sediment which comprises event unit C is well constrained. It is inner continental, but not of coastal origin. The mechanism that brought the sediment into the coring location remains controversial. Possible explanations include a tsunami, storm or a flood. A flood appears to be the most likely explanation (hypothesis 1, section 5.1.5.2), as both a tsunami (hypothesis 2) or storm (hypothesis 3) would incorporate coastal sediment into the deposit, bringing with it appreciable quantities of *Rhizophora* and Cyperaceae (coastal taxa). A flood would bring continental sediment and with it continental taxa (*Betula* and *Typha-Sparganium*) to the coring location, which is apparent in event unit C.

6.2 Core OS73 – comparison with other Holocene palaeoclimatic records in the region

As yet, few studies concerning the Makran region and its palaeoclimatic change over the most recent part of the Holocene are published in western literature. The majority of studies concerning environmental reconstructions of deserts have focussed on Africa, where lake level and pollen data have been widely used for reconstructing vegetation and hydrological conditions (Lézine *et al.*, 1998 and Gasse, 2000). Most studies have centred on large-scale changes at the end of the HHP around *c.* 5 ka ago and little is known regarding the most recent part of the Holocene. As more information is available regarding the large-scale changes during the mid-Holocene, the results are compared with the proxy data in core OS73 to assist with interpretation of the small-scale fluctuations seen in the core. The records are compared and contrasted within this section. Numerous palaeoenvironmental models have been used to connect climatic changes with orbital variations and to reconstruct atmospheric and vegetation feedback mechanisms (Kutzbach and Street-Perrott, 1985). In contrast less is known about the Arabian Peninsula and its surroundings, and most studies place emphasis on the early Holocene and larger scale Holocene monsoonal fluctuations (*e.g.* Lézine *et al.*, 1998; Neff *et al.*, 2001; Fleitmann *et al.*, 2003; Lézine *et al.*, 2007), paying little attention to recent records. In addition, possibly due to political conflicts and its remote location, southern Iran remains relatively poorly studied, with most palaeoenvironmental studies focusing on northern Iran. This thesis presents a record of vegetation and climate change in southern Iran based on sedimentological, palynological and geochemical records for the period 2280 cal. yr BP (330 BC) to present. Large-scale changes in vegetation during the Holocene for both the Atlantic and Indian monsoonal systems are presented in Chapter 2, which are relevant to the interpretation/discussion of the Iranian results presented in this study.

A high-resolution laminated sediment record (Kasten core SO90-56KA and box core 39KG) (Fig. 2.17) from the north-eastern Arabian Sea, off Pakistan (Fig. 6.2), were used as a reference to distinguish whether signals found in core OS73 were due to local or regional influences (Lückge *et al.*, 2001). The Pakistan core was studied to reconstruct past climatic variations and to understand the monsoon-driven moisture history in the northern Arabian Sea over the past 5000 years to

present. The results from core SO90-56KA show that the end of the HHP was linked to the weakening of the Indian monsoon which took place between 4700 - 4200 cal. yr BP. The pollen records show that there were two periods of strong summer monsoonal activity which occurred between 5400 - 4200 cal. yr BP and 2000 - 1000 cal. yr BP (Ivory and Lézine, 2009). During these two periods of intense monsoonal rainfall an increase in the percentage of montane taxa sourced from the Himalayas was recorded in the core due to increased fluvial activity of the Indus River.
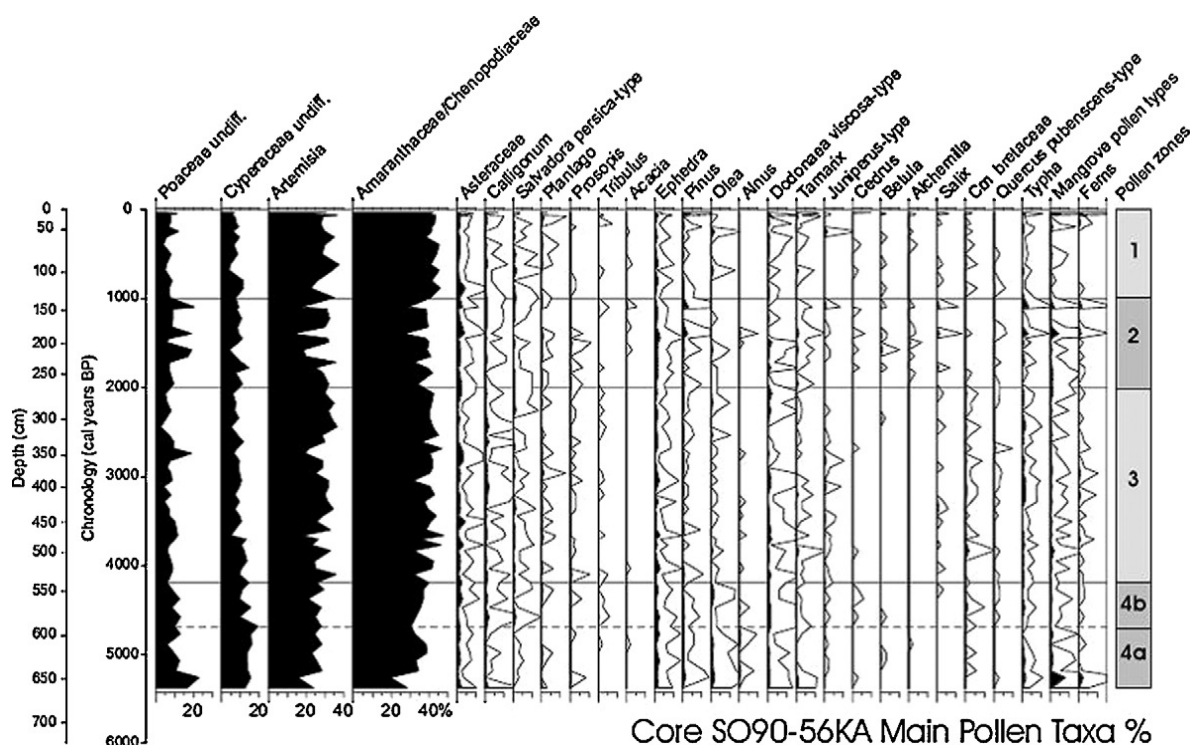
Fig. 6.2. Simplified pollen percentage diagram for core SO90-56KA offshore Pakistan. All white curves represent a x 10 exaggeration. From Ivory and Lézine (2009).

The laminated core SO90-56KA and 39KG displayed in Fig. 6.2 (Ivory and Lézine, 2009) shows an increase in montane vegetation from 2000 - 1000 cal. yr BP. This is not evidenced in the OS cores, with the maximum wet period from 1500 to 120 cal. yr BP in 73Pz3 (Fig. 4.31). A surge in mangrove taxa occurs between 2000 - 1000 cal. yr BP in SO90-56KA. However, arid taxa remain dominant with high percentages of Amaranthaceae-Chenopodiaceae and *Artemisia*. The results from 1000 cal. yr BP to present show a dominance of Amaranthaceae-Chenopodiaceae and *Artemisia* with low concentrations of freshwater taxa. Due to a high variability of *Salvadora persica*-type, *Calligonum* and *Ephedra* it is recognised that a high-resolution study would be necessary to clarify the effects of

short-term climatic events on the vegetation during this period (Ivory and Lézine, 2009).

6.2.1 *Rhizophora*

The taxa identified in SO90-56KA (Fig. 6.2) are extremely similar in type to those found in core OS55 and OS73. However discrepancies such as the lack of *Rhizophora* since 4500 cal. yr BP recorded in the Kwar al Jaramah core (Fig. 2.17) require further investigation (Lézine, 2009). Mangrove ecosystems are extremely sensitive to climatic change with their extent controlled by air temperature, aridity and salinity (Lézine *et al.*, 2002). Lézine *et al.* (2002) state that *Rhizophora* is currently absent from the Omani mangroves, where the highly saline conditions only permit *Avicennia marina* to survive (Lézine, 2009). *Rhizophora* is linked to brackish water conditions and an abundance of fresh water input. Lézine (2009) have reported that the nearest occurrence of natural *Rhizophora* populations are located to the south of both the OS and the Kwar al Jaramah coring locations at the Kamaran Islands (Fig. 2.17). This is evidently incorrect as the results of this study confirm the botanical observations reported from the Hormozgan Province in Jask and on Sirik Island (Fig. 2.17) that natural *Rhizophora* is present on the Iranian coastline.

As core OS55 is merely a short core covering the last centuaries, temporal changes in *Rhizophora* concentrations are not evident. It would be advantageous to have a long core in the vicinity of core OS55 to record the variations in *Rhizophora* abundance over the last 6000 yrs to assess the progressive drying event associated with the ecosystem response to the orbitally induced weakening of the Indian monsoon, as proposed by Lézine (2009). *Rhizophora* abundance within core OS55 is not high, but in the past when the Indian monsoon was stronger and associated with elevated amounts of rainfall, thus a greater freshwater supply to the mangrove system, *Rhizophora* concentrations may have been considerably greater. Lézine, (1997) recorded large fluctuations in the extent of mangrove populations during the Late Quaternary directly related to changes in monsoonal precipitation. The records suggest that the west of Africa has experienced relatively wet conditions from 13 ka BP until 2 ka BP, allowing for a wide expansion of mangrove along the West African coast up to 21°N. During the Last Glacial Maximum, the mangrove greatly reduced in response to dry, cooler conditions.

However, the mangrove did not disappear everywhere, with pockets existing near the Gulf of Guinea, indicating the presence of freshwater discharge despite the regional drought (Lézine, 1997).

6.2.2 *Betula*

Betula, sourced within upland forests of the Himalayan highlands (Ivory and Lézine, 2009), remains at a constant rate throughout core OS73 (and one peak in core OS55), providing evidence that the study region is distal and unconnected to the fluvial output of the Indus River. *Betula* transport to the study region must be by wind and the stable concentrations suggest little variation in wind strength over the last 2300 years.

6.2.3 Relevance of early Holocene (pre 2300 cal. yr BP) records

The majority of studies concerning the environmental reconstruction of Africa and Arabia focus on the large early Holocene climatic changes. By analysing these large scale climate changes and their effects on the environment, it is possible to compare this data with data presented in this thesis. The literature provides evidence for considerable changes in vegetation both on Africa and in Asia coinciding with the end of the HHP. This period is associated with an decrease in the strength of the Africa and Asian monsoonal systems. The early Holocene records provide evidence for both abrupt (deMenocal, 2000) and gradual step-like (Kröpelin *et al*., 2008) climatic changes. Aridification is known to result in the expansion of dry steppic vegetation for example Chenopodiaceae, *Artemisia* and *Ephedra* (Lézine, 2009), which can assist in interpretaing the data acquired from the OS cores. In addition, deminished productivity and upwelling is associated with cooler periods on the African margin.

6.3 Evidence for climatic fluctuations during the Late Holocene

The area of the NW Arabian Sea has experienced several episodes of climatic fluctuations during the Late Holocene and these episodes will be discussed in comparison with the interpretation of core OS73. The Late Holocene has been divided into its major climatic fluctuations from the available literature and the section will begin by discussing the earliest event within the last 2300 years recorded in the literature, a period of aridification from 3000 to 2000 cal. yr BP.

Some of the dates in this section are given as raw ^{14}C radiocarbon dates straight from the publication and have then been have been calibrated according to the IntCal04 terrestrial calibration curve (Reimer *et al*., 2004).

6.3.1 Dry period: 3000 to 2000 yr BP

Sr/Ca values from core SO90-56KA (Fig. 2.17 and Fig. 6.3) indicate an aridification period from 3000 to 2000 yr BP (3200 to 2000 cal. yr BP) (Lückge *et al*., 2001). Pollen records from Rajasthan (Thar Desert, India, Fig. 2.17) suggest that aridification began at 3500 and continued until 2000 yr BP (3700 – 2000 cal. yr BP) (Singh *et al*., 1974, 1990; Bryson and Swain, 1981; Swain *et al*., 1983 in Lückge *et al*., 2001). Core OS73 does not encompass the beginning but should show an end to the aridification at 2000 yr BP. Nevertheless, although sampling resolution is low, the data show no indication of an end of aridification at this stage. Numerous studies, both in Africa and Asia suggest aridification at 2000 yr BP (Gasse and Van Campo, 1994; Bryson, 1997). It is postulated that this decrease in precipitation may be due to a southward shift of the ITCZ, strengthening the winter and reducing the length of the summer monsoon. This shift in ITCZ would have impacted the Makran region (OS study region) by enhancing the rainfall during the winter season and causing diminished rainfall during the summer monsoon (Lückge *et al*., 2001). It would be expected that core OS73 should show overall diminished levels of precipitation during this aridification period. However the short length of this core inhibits investigation into this period. Owing to the large amount of evidence within the literature it can be concluded that the aridification period affected a broad region, occurring at the same time in both Africa and the Middle East and probably resulted from a weakening within the whole monsoonal system.

6.3.2 Wet period: 2300 to 1830 cal. yr BP

Core OS73 indicates the presence of a wet period from 2300 (at least) to 1830 cal. yr BP. On account of the variability of inorganic compounds (Ti/Al and Zr/Al), varve thickness, and δ^{18}O-values of *G. ruber,* Lückge *et al*. (2001) divided the last 2500 years into three periods (III-V), the wettest period from 2000 to 1500 yr BP (2000 – 1400 cal. yr BP) (Fig. 6.3). Reichart *et al*. (1998) used Sr/Ca ratios associated with pteropods to reconstruct monsoonal activity within the Arabian Sea using core NIOP464 on the Murray Ridge (450 km SE of OS coring locations – Fig. 2.17).

Sr/Ca ratios imply that the wettest period (IV) within the last 5000 years should occur between 2000 to 1500 yr BP (2000 – 1400 cal. yr BP), however the wettest period in core OS73 occurs between 1500-120 cal. yr BP (73Pz3). There is a wet period in the OS core from 2300 to 1830 cal. yr BP and this roughly correlates with the period of intense summer monsoonal rainfall from 2000 to 1400 cal. yr BP period IV (Fig. 6.3).
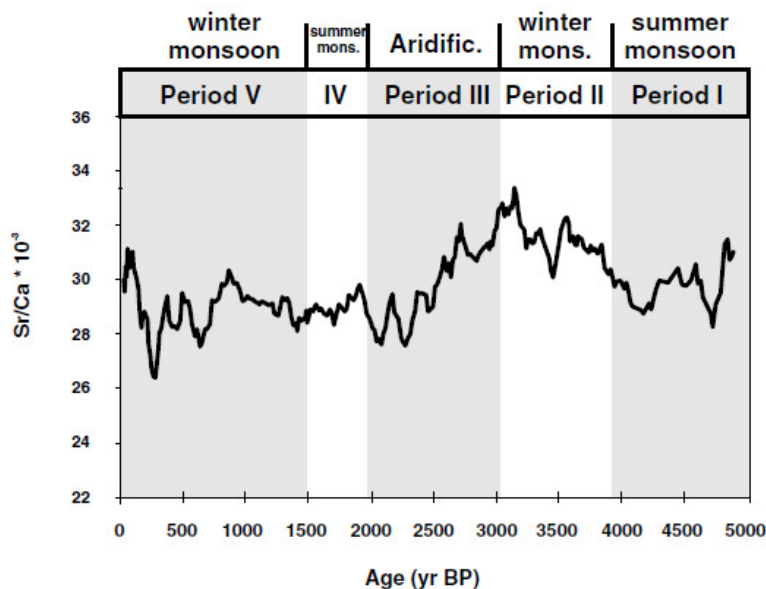
Fig. 6.3. Sr/Ca ratios of the last 5000 years at site SO90-56KA. Figure from Lückge *et al.* (2001).

6.3.2.1 Sassanid Period (AD 224 – 651)

The collapse of this Sassinid Empire at AD 651 coincides roughly with the end of the dry period recorded in the OS cores (~1500 cal. yr BP). The slight offset of the dates may be due to dating problems of the OS73 core. Low values of cereal-type, cultivated tree pollen and the collapse of the irrigation infrastructure after the Islamic conquest of Iran may indicate a change from the cultivation of fields to more nomadic pastoral cultivation. A combination of Islamic invasion and changing precipitation pattherns in Iran as recorded in the OS cores may have caused the change in farming at the collapse of the Sassinid Empire, although there is no archaeological evidence for this.

The 2300-1830 cal. yr BP wetter phase in S. Iran relates to the wetter phases in the Mediterranean and the Middle East. These wetter phases have been explained by warmer temperatures in southern Turkey (van Zeist *et al.*, 1975) and around the Dead Sea (Neumann *et al.*, 2010) and the northward displacement of the ITCZ in northern Africa (Reale and Shukla, 2000).

6.3.2.2 Beyşehir Occupation Phase (*c.* 3200 – *c.* 1500 cal. yr BP)

The dry period (1830-1500 cal. yr BP) found in the OS cores corresponds well with the end of the Beyşehir Occupation Phase (van Zeist *et al.*, 1975) in southern Turkey and the associated intensive agriculture. The collapse of the Beyşehir Occupation Phase varies spatially but it is generally thought to be at approximately 1600 – 1400 cal. yr BP (Eastwood *et al.*, 1998; Leroy *et al.*, 2002; Leroy *et al.*, 2009; Leroy, 2010). The timing of the Beyşehir Occupation Phase is considered to have involved a shift to more humid conditions, marked by an expansion of forest into previously steppic regions (Eastwood *et al.*, 1998). *Olea* (olive) pollen is common during the Beyşehir Occupation Phase from sites from southwest Turkey, indicating that climatic conditions during the Beyşehir Occupation Phase must have favoured *Olea* cultivation (Eastwood, 1998). Roberts (1990) calculated that winter and spring temperatures must have been 2 - 3°C higher than today. The humid conditions during the Beyşehir Occupation Phase correlates well with the wet phase from 2300 (at least) to 1830 cal. yr BP found in the OS cores. The collapse of the Beyşehir Occupation Phase marks a time of decreased precipitation and the aridification in the southern Iranian cores.

6.3.2.3 Roman-Early Byzantine Period (2100 – 820 cal. yr BP)

The wet period (2300 - 1830 cal. yr BP) found in the OS cores corresponds well with the start of the Roman-Byzantine period recorded in the Dead Sea sediments from six cores near Mount Sedom, Ein Boqueq, and Ein Gedi and from outcrops near Ze'elim and Ein Feshkha (Neumann *et al.*, 2010). The Roman Early Byzantine Period is characterised by higher lake levels in the Dead Sea implying humid climatic conditions. Increases in Olea, *Sarcopoterium spinosum,* and *Plantago* (anthropogenic indicators) and decreases in *Quercus* and *Pinus* (forests) imply increased agricultural activity and forest clearance (Neumann *et al.*, 2010). However there is not evidence for the dry period (1830-1500 cal. yr BP) as seen in the OS cores having an impact on the civilisations during the Roman Byzantine Period.

6.3.2.4 Roman Classical Period (2000 cal. yr BP)

The increase in humidity from 2300 – 1830 cal. yr BP recorded in the OS cores may be attributed to the northward displacement of the ITCZ, as recorded in

the Mediterranean and northern Africa. The increase in precipitation can be attributed to high surface warming that takes place in close proximity to the ITCZ (Reale and Shukla, 2000).

6.3.3 Onset of aridification in SW Asia at 1000 years BP

Within the southeast Arabian Pennisula, inter-dune dry lakes in Awafi, Ras al-Khaimah (UAE, Fig 2.17), show an intensification of aridification at ca 1000 cal. yr BP (Parker *et al*., 2004). Rapid dune accretion was recorded in Idhn, RAK (UAE), where 30 m of dune sand accumulated at ca 1000 cal. yr BP (Goudie *et al*., 2000). Other records around the northern Arabian Sea also show this intensification of aridification (Von Rad *et al*., 1999; Lückge *et al*., 2001). 73Pz2, the driest zone within core OS73, occurs between 1830 – 1500 cal. yr BP, earlier than the period of aridification recorded at approximately 1000 cal. yr BP.

6.3.4 Late Holocene weakening of monsoonal precipitation?

High-resolution δ^{18}O profiles of stalagmites from four caves in Oman and Yemen (Socotra, Fig. 2.17) provide information on fluctuations in precipitation during the Holocene period. The precipitation is reflected in the δ^{18}O values which are primarily controlled by the latitudinal position of the ITCZ (Fleitmann *et al*., 2007). The results show that during the middle to late Holocene, the mean latitudinal position of the summer ITCZ migrated southwards, leading to a decrease in the amount of precipitation, a weaker monsoon and a shorter summer monsoonal season. This migration of the ITCZ was a response to a decrease in the amount of solar insolation received. The results show no abrupt middle Holocene weakening of monsoonal precipitation (Fleitmann *et al*., 2007). Results from Gupta *et al*. (2003) on benthic foraminifera provide confirmation of the smooth nature of the wet-arid transition seen in the Oman speleothem record (Fleitmann *et al*., 2003; 2007), where upwelling-intensity related to summer monsoon circulation over the northern Indian Ocean has smoothly declined from the early Holocene until present.

The results of this thesis however show three main phases of climate change over the last 2300 years, with the vegetation recording first a wet phase (73Pz1) from 2300 – 1830 cal. yr BP, followed by a dry stage from 1830 – 1500 cal. yr BP (73Pz2). Subsequently, 1500 cal. yr BP to present (73Pz3) is marked by a more humid climate. However, no evidence for a general decrease in the amount of precipitation or a decrease in the strength of the summer monsoonal system is

available. Indeed the vegetation of southern Iran fluctuates slightly from humid to arid with arid taxa however remaining dominant and percentages of other individual taxa varying throughout. The results show the presence of climatic change over the last 2300 years within the coring region. This thesis indicates that there have been small fluctuations in climate along the Makran coast over the last 2300 years.

6.3.5 'Refuge sites' for the Late Holocene in Arabia and India

It appears that certain records show no evidence for climatic change during the Late Holcene in Arabia and India, suggesting a local expression of the global climatic change. Previous research in regions such as Suwayh in the Omani lowlands (Lézine *et al*., 2010), Hajar Mountains of northern Oman (Fuchs and Buerkert, 2008; Urban and Buerkert, 2009), Karnataka (Fig. 2.17) in western India (Caratini *et al*., 1994) provide additional evidence that numerous localities across the Indian Ocean have remained as desert/semi-desert throughout the Holocene. Lézine *et al.* (2010) conclude that the vegetation of the Arabian lowlands has not changed considerably and has remained of desert/semi-desert type throughout the entire Holocene period. However, perhaps the sampling resolution used in these studies was too low in order to record small-scale fluctuations seen in the OS cores of this study. High-resolution study of a 20 m deep sediment profile within the Hajar Mountains of northern Oman reveals that variations in mollusc shell frequency and periodic peaks of NH_4-N (mineral nitrogen) suggest minor local variations of rainfall throughout the last 2000 years. High concentrations of NH_4-N indicate water logging-induced anaerobic soil conditions occurring whenever temporary water saturation inhibits nitrification (Urban and Buerkert, 2009). Caratini *et al*. (1994) report a reduction in humidity at 2200 cal. yr BP in two marine cores taken from the inner shelf off Karwar (western India) marked by a reduction in forests, an increase in savanna and a decrease in the percentages of mangrove vegetation. After 2200 cal. yr BP pollen assemblages remain stable up to the present day. Enzel *et al*. (1999) suggest that the climate has remained relatively stable for the last 5000 cal. yr BP. The study of Enzel *et al*. (1999) is based on results from Lunkaransar, a small, closed, dry basin at the northeastern margin of the Thar Desert (Fig. 2.17). Results reveal lake level fluctuations throughout the Holocene which are attributed to changes in southeastern Indian monsoon precipitation regimes. The results indicate that the climate over the last 5000 years has remained similar to the present. The low water table has remained constant at around 2.4 m below the lake

surface over the last 5000 years. In addition, the record is punctuated by episodes of sudden inundation caused by short episodes of heavy rainfall represented by thin laminated silt beds dated at 3785 ± 75 and 2325 ± 65 cal. yr BP (Enzel *et al*., 1999).

It can be deduced from these records from the northern Arabian Sea that during the last 2000 years the climate has remained relatively stable and that a climate somewhat similar to present-day conditions was established about 2000 years ago. However, many regions do show climate change over the last 2000 years and the results from this thesis especially support the decrease in precipitation from 1830 - 1500 cal. yr BP (73Pz2) coinciding the end of the Beyşehir Occupation Phase.

6.4 Summary of core OS73

A summary table of the major climatic events in the Arabian Sea region is presented below and compared with signals observed within core OS73 from this study (Table 6.1).

Age	Event/trend	Other Arabian records	Oman Sea Core records
0.16 cal. ka BP present	Spikes in precipitation		Increase in certain dinoflagellate taxa associated with more continental runoff (73Dz4)
0.9 – 0.16 cal. ka BP	Warm SST		Increase in *S. ramosus*
1.5 – 0.12 cal. ka BP	Wet period		Increase in grass percentages (73Pz3)
1.77 – 0.9 cal. ka BP	Decrease in upwelling		Diminished upwelling along Iranian coastline (73Dz2)
1.8 – 1.5 cal. ka BP	Onset of aridification	End of the Beysehir Occupation Phase at 1.5 cal ka BP.	Decrease in grass percentages and onset of aridification (73Pz2)
2.3 – 1.8 cal. ka BP	Wet period	• Dominance of summer monsoonal rains (Lückge *et al*., 2000). • Overall increase in rainfall (Ivory and Lézine, 2009). • Increase in Himalayan vegetation transport into Arabian Sea (Ivory and Lézine, 2009). • Surge in mangrove taxa off Pakistan (Ivory and Lézine, 2009). • Beysehir Occupation Phase – increased anthropogenic activity. • Roman Byzantine period in the Dead Sea region	Decrease of arid adaptive pollen taxa and increase in Poaceae (73Pz1)
2325 ± 65 cal. yr BP	Heavy rainfall	Period of episodic lake inundation, Thar Desert, India (Enzel *et al*., 1999).	General wet period (2300 1820 cal. yr BP)

Table 6.1. Summary table highlighting the major climatic events over the last 2300 years of the study sites surrounding the Arabian Sea. Yellow shading signifies general stages of aridification. Blue shading represents periods of increased humidity. White shading is associated with upwelling and oceanographic conditions. Legend for lithology shown in Fig. 4.7.

6.5 Implications of environmental signals over the last 2300 yr

6.5.1 Terrestrial implications

Overall pollen results indicate general climatic stability over the last 2300 years in the Oman Sea. The results from this study indicate clear minor fluctuations in taxa percentages. Magnetic susceptibility values within core OS73 show little fluctuation, however a slight general increase from 50 cm, 920 cal. yr BP (AD 1000) until present is observed. Grain size within core OS73 remains generally constant throughout, showing little evidence for a change in sedimentation rate or depositional character. At approximately 160 cal. yr BP (AD 1800) a shift in sedimentation is detected at 17 cm, which is possibly due to a recent phenomenon in the region. Explanations for this phenomenon include human impacts associated with the nearby city development of Chabahar, or natural explanations including possible river migrations and diversions in deposition.

Minor fluctuations in pollen percentages provide evidence for three distinct periods of climatic zones within the last 2300 years in southern Iran (Fig. 6.4):

- Wet period (2300 - 1830 cal. yr BP)
  - Coinciding with the increase in moisture at 2000 cal. yr BP in North Africa, Mediterranean and the Middle East during the Roman Classical Period.

- Dry period (1830– 1500 cal. yr BP)
  - Possibly associated with the collapse of the Beyşehir Occupation Phase in southern Turkey, the Roman-Byzantine period in the Dead Sea region and the shift from the cultivation of fields to a more nomadic lifestyle in NW Iran.

- Wet period (1500 - 120 cal. yr BP)

6.5.2 Marine implications

Dinoflagellate percentages show large variability over the last 2300 years. Fluctuations in dinoflagellate percentages provide evidence for three distinct periods of oceanographic conditions within the last 2300 years in southern Iran (Fig. 6.4).

- Increased upwelling (2300 - 1770 cal. yr BP)
- Decreased upwelling (1770 – 920 cal. yr BP)
- Increased upwelling (920 - 160 cal. yr BP)

Changes in upwelling intensity imply fluctuations in the strength of the Indian summer monsoon. Increases in the strength of the monsoon causes winds to induce amplified levels of oceanographic upwelling. As a general trend variations in monsoonal strength follow variations in insolation contrast.

6.6. Final interpretation of core OS73

A summary diagram of the interpreted pollen and dinoflagellate results signals seen in core OS73 is presented in Fig. 6.4. Poaceae has been used to represent fluctuations in rainfall. The pollen indicates three main phases of climate change on the southern Iranian coastline within the last 2300 years. The fourth phase (Fig. 6.4 purple zone) represents changes caused by anthropogenic influences. The dinoflagellates show more variability and *B. spongium* has been chosen in order to represent upwelling fluctuations, which show a period of diminished upwelling intensity between 1770 and 920 cal. yr BP. The wetter period shown by the pollen and the period of increased upwelling indicated by dinocyst assemblages should correspond. However the upwelling only diminishes 60 years after the pollen results indicate aridification. There appears to be a slight time lag in ocean response, but again this could be the result of dating uncertainties.
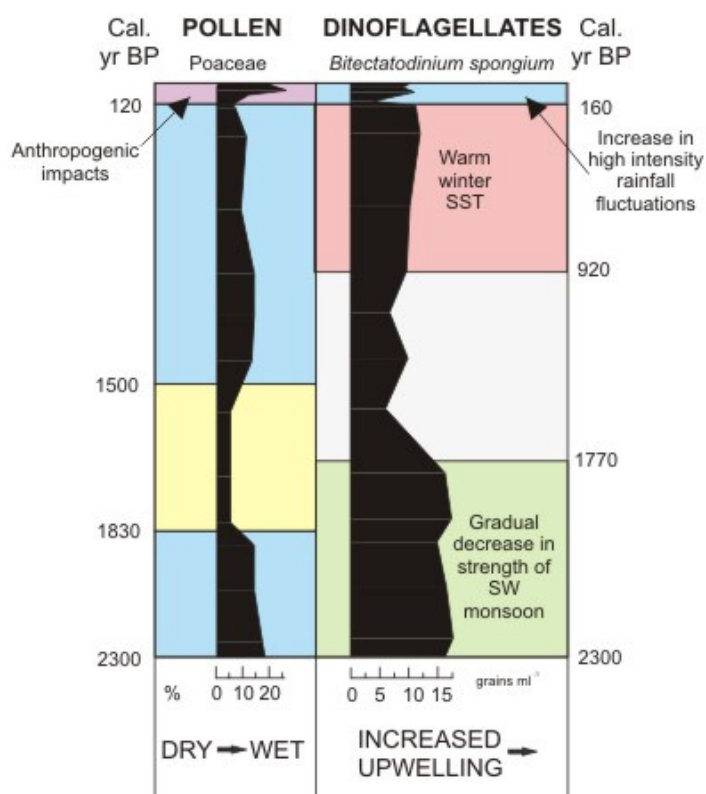
Fig. 6.4. A summary diagram of the interpreted pollen and dinoflagellate results seen in core OS73. Left diagram: Purple = anthropogenic impact, blue = humid, yellow = arid. Right diagram: Blue = wet, red = warm winter SST, grey = decreased upwelling, green = increased upwelling.

7. Conclusions

At the beginning of this thesis in chapter 1, five specific scientific aims were identified (section 1.3). These aims were 1) to use published literature to assess whether tsunamis and/or cyclonic storms have had an effect on sediment accumulation in Pozm and Chabahar Bays in the Late Holocene, 2) to correlate abrupt marine events found in the cores with historical archival data, 3) to reconstruct the vegetation history of the region over the late Holocene, using pollen analysis and a range of sedimentological techniques, 4) to reconstruct the oceanographic history (upwelling intensity fluctuations) of the region over the late Holocene, using dinoflagellate cyst analysis and a range of sedimentological techniques, 5) to relate palaeoenvironmental implications of the thesis to wider-scale studies. In this concluding chapter a synopsis of the key findings is presented and the success to which each of the aims has been met is assessed in section 7.1. Limitations of the study and a brief outline of possible future research are proposed in section 7.2.

7.1 Synopsis of the key findings

7.1.1 Core OS55

Specific scientific aims 1 and 2 (section 1.3) were assessed using core OS55.

Published literature was used to differentiate between storm and tsunami deposits (section 5.1.6). This research highlights the difficulties in distinguishing between different abrupt marine invasions. Unit C consisted of a shell-rich unit rather than arbitrary shell fragments scattered throughout the beds providing some evidence for tsunami source rather than storm. Evidence from palynology provides an identification of the source of sediment, however the mechanism for sediment transport remains slightly controversial, although evidence from palynology suggests the likely mechanism of sediment transport to be a flood. In conclusion, this study was not capable of firmly distinguishing the cause of the abrupt event, nevertheless palynological investigation was able to provide a clear inner-continental source of the sediment.

7.1.1.1 Key findings from core OS55

a. An abrupt marine event at <AD 1808

The varying lithologies of the cores studied for this thesis indicate the complex nature of the sedimentation along the Makran coastline. One of the cores (OS55) was subject to abrupt events which have left a distinct sedimentological and palynological signature within the core. The event was recorded by an increase in grain-size, the level of shell fragmentation and fluctuations within both pollen and dinoflagellate species throughout. We can only be certain of one event within the core (unit C) which has been interpreted as a turbidite deposit with sediment of inner-continental source. The date estimated for the top of Unit B is <AD 1808. This high energy event has its source on the continent. Due to the palynological assemblage the source is clearly not the coast. Therefore a tsunami or cyclone are less likely causes than a river flood (Fig. 5.7).

b. Presence of *Rhizophora* on the southern Iranian coastline

Rhizophora is present throughout core OS55 showing no obvious increase through the event horizon. This finding provides support that the material from the turbidite deposit unit B did not originate from the shore but from a possible sediment pile situated offshore. *Rhizophora* is not present in core OS73. The results of this thesis provide evidence of the local presence of *Rhizophora* growth along the Iranian coastline, possibly related to local variations in salinity or suitable sedimentary environments for the presence of rivers.

7.1.2 Core OS73

Specific scientific aims 3 - 5 (section 1.3) were assessed using core OS73.

Scientific aims 3 - 5 were met using core OS73, with the data able to produce a reconstruction of the vegetation and oceanographic history over the late Holocene. This reconstruction when related to wider-scale studies correlates well with events found elsewhere.

7.1.2.1 Key findings from core OS73

a. Wet period (2300 to 1830 cal. yr BP)

This study indicates the presence of a wet period from 2300 to 1830 cal. yr BP. Supporting evidence for a wet period around this time comes from numerous other studies, although dating in certain studies is difficult to correlate due to their ages being uncalibrated (*e.g.* Lückge *et al*., 2001; Eastwood *et al*., 1998; Reale and

Shukla, 2000; Leroy *et al*., 2002; Djamali *et al*., 2008; Leroy *et al*., 2009; Leroy, 2010; Neumann *et al*., 2010). The wet phase seen in the results of this thesis corresponds with phases of intense agriculture in the archaeological record in Persia, the Mediterranean and in the Middle East. This wet period has been attributed to northward displacement of the ITCZ corresponding to the Beyşehir Occupation Phase and the Roman Byzantine Period.

b. Dry period (1830 – 1500 cal. yr BP)

The collapse of the Sassinid Empire in Iran correslates with the dry period in the OS cores at around 1500 cal. yr BP. This dry period also corresponds well with the end of the Beyşehir occupation phase in southern Turkey.

c. Wet period (1500 - 120 cal. yr BP)

d. Upwelling fluctuations:

- Increased upwelling (2300 - 1770 cal. yr BP)
- Decreased upwelling (1770 – 920 cal. yr BP)
- Increased upwelling (920 - 160 cal. yr BP)

Changes in upwelling intensity imply fluctuations in the strength of the Indian summer monsoon.

e. Pollen and dinocyst correlations

The pollen and dinocyst zones are correlated, with warmer and wetter climates recorded in the pollen assemblages corresponding to increases in upwelling and thus a stronger Indian summer monsoon as recorded in dinocyst assemblages. The dinocyst zones appear to display a lag, implying a delay of around 60 years in the oceanographic response to atmoshpheric changes.

7.2 Limitations and future research possibilities

The research carried out in this study was mainly limited by time. The main concern of the time limitation was the pollen count numbers for each sample. The reliability of concentration calculations and an adequate estimation of diversity have previously been suggested to require count numbers of at least 300 grains (Rull, 1987). With additional time three samples would be counted to 1000 grains to investigate whether counting to 300 grains per sample is sufficient to make the

counts statistically reliable to represent the total population. Species accumulation curves would be constructed in order to assess acceptable count numbers.

An additional limitation is the coring capacity of INCO. If longer cores were to be obtained in close proximity to core OS73, the fluctuations in *Rhizophora* abundance over the last 6000 years could be reconstructed. This may demonstrate the drying event associated with the ecosystem response to the weakening of the Indian monsoon, as recorded by Lézine (2009). Although *Rhizophora* abundance is low at present, with high amounts of rainfall before the drying event when the Indian monsoon was stronger, greater freshwater supply to the mangrove system may have dramatically increased *Rhizophora* abundance.

In light of the results of this study and the difficulties associated with differentiating tsunami from storm deposits in sediment cores, it would be sensible look elsewhere for records of storm and tsunami signals. Taking shallower cores or analysing marine deposits on the coast may provide a way for reconstructing the recurrence times of both tsunamis and storms in the region.

To summarise, if this research was to be continued then: i) species accumulation curves would be constructed to assess accurate count numbers, ii) additional longer cores would be taken to assess fluctuations in mangrove abundance over the last 6000 years and III) shallower cores or marine deposits would be acquired which may help in differentiating tsunami from storm deposits.

References

Allen, C. D., Macalady, A. K., Chenchouni, H., Bachelet, D., McDowell, N., Vennetier, M., Kitzberger, T., Rigling, A., Breshears, D. D., Hogg, E. H., Gonzalez, P., Fensham, R., Zhang, Z., Castro, J., Demidova, N., Lim, J.-H., Allard, G., Running, S. W., Semerci, A., and Cobb, N. (2010). A global overview of drought and heat-induced tree mortality reveals emerging climate change risks for forests. Forest Ecology and Management 259, 660-684.

Alijani, B. (2006). Synoptic climatology, 2nd edition. SAMT, USA, p 258.

Alpar, B., and Yüce, H. (1996). Sea-level variations in the eastern coasts of the Aegean Sea. Estuarine, Coastal and Shelf Science 42, 509-521.

Ambraseys, N. N., and Melville, C. P. (1982). "A History of Persian Earthquakes." Cambridge University Press, Cambridge.

Ansari, M. H., and Vink, A. (2007). Vegetation history and palaeoclimate of the past 30 kyr in Pakistan as inferred from the palynology of continental margin sediments off the Indus Delta. Review of Palaeobotany and Palynology 145, 201-216.

Appleby, P. G., and Oldfield, F. (1978). The calculation of lead-210 dates assuming a constant rate of supply of unsupported ^{210}Pb to the sediment. CATENA 5, 1-8.

Arens, N. C. (2001). Climate and atmosphere interact to drive vegetation change. Trends in Ecology & Evolution 16, 18-18.

Arnaud, F., Lignier, V., Revel, M., Desmet, M., Beck, C., Pourchet, M., Charlet, F., Trentesaux, A., and Tribovillard, N. (2002). Flood and earthquake disturbance of ^{210}Pb geochronology (Lake Anterne, NW Alps). Terra Nova 14, 225-232.

Arpe, K., and Leroy, S. A. G. (2007). The Caspian Sea Level forced by the atmospheric circulation, as observed and modelled. Quaternary International 173-174, 144-152.

Bailey, R. W. (1988). "Records of Oman: 1867-1947." Archive Editions, Buckingham.

Barton, E. D., and Hill, A. E. (1989). Abyssal flow through the Amirante Trench (western Indian Ocean). Deep Sea Research Part A, Oceanographic Research Papers 36, 1121-1126.

Beierle, B. D., Lamoureux, S. F., Cockburn, J. M. H., and Spooner, I. (2002). A new method for visualizing sediment particle size distributions. Journal of Paleolimnology 27, 279-283.

Berger, A. (1978). Long-term variations of daily insolation and Quaternary climatic change. Journal of Atmospheric Science 35, 2362-2367.

Blanford, W.T. (1872). Note on the geological formations seen along the coasts of the Baluchistan and Persia from Karachi to the head of the Persian Gulf and on some of the Gulf Islands. Records of the Geological Survey of India, 41-45.

Bloemendal, J. (1983). Paleoenvironmental implications of the magnetic characteristics of sediments from Deep Sea Drilling Project Site 514, Southeast Argentine Basin. Initial reports DSDP, Leg 71, Valparaiso to Santos, 1980, part 2, 1097-1108.

Blott, S.J., Pye, K. (2001). GRADISTAT: a grain size distribution and statistics package for the analysis of unconsolidated sediments. Earth Surface Processes and Landforms 26, 1237-1248.

Blount, C., Fritz, H. M., and Al-Harthy, A. H. M. (2009). Coastal vulnerability assessment based on historic tropical cyclones in the Arabian Sea. . In "Proceedings of the First International Conference on Indian Ocean Tropical Cyclones and Climatic Change."

Bonnefille, R. (2010). Cenozoic vegetation, climate changes and hominid evolution in tropical Africa. Global and Planetary Change In Press, Corrected Proof.

Bouma, A. H. (1962). Sedimentology of some flysch deposits. Elsevier, 168.

Bouimetarhan, I., Marret, F., Dupont, L., and Zonneveld, K. (2009). Dinoflagellate cyst distribution in marine surface sediments off West Africa (17-6°N) in relation to sea-surface conditions, freshwater input and seasonal coastal upwelling. Marine Micropaleontology 71, 113-130.

Brock, J.C., Luther, M.E., Hay, W.W. (1991). The phytoplankton bloom in the northwestern Arabian Sea during the southwest monsoon of 1979. Journal of Geophysical Research 96, 20623-20642.

Brookfield, M. E., Blechschmidt, I., Hannigan, R., Coniglio, M., Simonson, B., and Wilson, G. (2006). Sedimentology and geochemistry of extensive very coarse deepwater submarine fan sediments in the Middle Jurassic of Oman, emplaced by giant tsunami triggered by submarine mass flows. Sedimentary Geology 192, 75-98.

Bryson, R. A., and Swain, A. M. (1981). Holocene variations of monsoon rainfall in Rajasthan. Quaternary Research 16, 135-145.

Bryson, R. A. (1997). High resolution simulations of regional Holocene climate: North Africa and the Near East. (H. N. Dalfes, G. Kukla, and H. Weiss, Eds.), pp. 565-593.

Burton, W. M., and Stewart, N. G. (1960). Use of long-lived natural radioactivity as an atmospheric tracer. Nature 186, 584-589.

Byrne, D. E., Sykes, L. R., and Davis, D. M. (1992). Great thrust earthquakes and aseismic slip along the plate boundary of the Makran subduction zone. Journal of Geophysical Research 97, 449-478.

Caratini, C., Bentaleb, I., Fontugne, M., Morzadec-Kerfourn, M. T., Pascal, J. P., and Tissot, C. (1994). A less humid climate since ca. 3500 yr B.P. from marine cores off Karwar, western India. Palaeogeography, Palaeoclimatology, Palaeoecology 109, 371-384.

Chao, W.C., Chen, B. (2001). Multiple quasi-equilibria of the ITCZ and the origin of monsoon onset, Part II. Rotational ITCZ attractors. Journal of Atmospheric Science 58, 2820-2831.

Chen, W., and Scawthorn, S. (2002). "Earthquake Engineering Handbook." Kyoto University.

Christensen, A. (1998). Sassanid Persia. The Cambridge Ancient History, Volume XII: The Imperial Crisis and Recovery. Cook, S.A (eds). Cambridge University Press.

Clemens, S. C., and Prell, W. L. (1990). Late Pleistocene variability of Arabian Sea summer monsoon winds and continental aridity: eolian records from the lithogenic component of deep-sea sediments. Paleoceanography 5, 109-145.

Clifton, H. E. (1998). Sedimentological consequences of convulsive geologic events. Geological Society of America 229, 7-22.

Costa, P. (2006). "Geological recognition of abrupt marine invasions in two coastal areas of Portugal." Brunel University, MPhil thesis.

Cowie, G. L., and Levin, L. A. (2009). Benthic biological and biogeochemical patterns and processes across an oxygen minimum zone (Pakistan margin, NE Arabian Sea). Deep Sea Research Part II: Topical Studies in Oceanography 56, 261-270.

Cundy, A. B., and Croudace, I. W. (1996). Sediment accretion and recent sea-level rise in the Solent, Southern England: Inferences from radiometric and geochemical studies. Estuarine, Coastal and Shelf Science 43, 449-467.

Cundy, A. B., Kortekaas, S., Dewez, T., Stewart, I. S., Collins, P. E. F., Croudace, I. W., Maroukian, H., Papanastassiou, D., Gaki-Papanastassiou, P., Pavlopoulos, K., and Dawson, A. (2000). Coastal wetlands as recorders of earthquake subsidence in the Aegean: A case study of the 1894 Gulf of Atalanti earthquakes, central Greece. Marine Geology 170, 3-26.

Cundy, A. B., and Stewart, I. S. (2004). Dating recent colluvial sequences with ^{210}Pb and 137Cs along an active fault scarp, the Eliki Fault, Gulf of Corinth, Greece. Tectonophysics 386, 147-156.

Danne-kar, A. (2005). Status of the Mangrove Forest in Iran. In "Workshop of Mangrove Ecology." Hormozgan University, Bandar Abbass

Dawson, A. G., and Stewart, I. (2007). Tsunami deposits in the geological record. Sedimentary Geology 200, 166-183.

deMenocal, P., Ortiz, J., Guilderson, T., Adkins, J., Sarnthein, M., Baker, L., and Yarusinsky, M. (2000). Abrupt onset and termination of the African Humid Period: rapid climate responses to gradual insolation forcing. Quaternary Science Reviews 19, 347-361.

DeMets, C., Gordon, R.G., Argus, D.F., Stein, S. (1990). Current plate motions. Geophysical Journal International 101, 425-478.

Dinpashoh, Y., Fakher-Fard, A., Moghaddam, M., Jahanbakhsh, S., Mirnia, M. (2004). Selection of variables for the purpose of regionalization of Iran's precipitation climate using multivariate methods. Journal of Hydrology 297, 109-123.

Djamali, M., de Beaulieu, J.-L., Shah-hosseini, M., Andrieu-Ponel, V., Ponel, P., Amini, A., Akhani, H., Leroy, S. A. G., Stevens, L., Lahijani, H., and Brewer, S. (2008). A late Pleistocene long pollen record from Lake Urmia, NW Iran. Quaternary Research 69, 413-420.

Dominey-Howes, D. T. M., Humphreys, G. S., and Hesse, P. P. (2006). Tsunami and palaeotsunami depositional signatures and their potential value in understanding the late-Holocene tsunami record. Holocene 16, 1095-1107.

Donato, S. V., Reinhardt, E. G., Boyce, J. I., Pilarczyk, J. E., and Jupp, B. P. (2009). Particle-size distribution of inferred tsunami deposits in Sur Lagoon, Sultanate of Oman. Marine Geology 257, 54-64.

Drago, M. (2002). A coupled debris flow-turbidity current model. Ocean Engineering 29, 1769-1780.

Dupont, L. M., Behling, H., and Kim, J. H. (2008). Thirty thousand years of vegetation development and climate change in Angola (Ocean Drilling Program Site 1078). Clim. Past 4, 107-124.

Eakins, J. D., and Morrison, R. T. (1978). A new procedure for the determination of lead210 in lake and marine sediments. The International Journal of Applied Radiation and Isotopes 29, 531-536.

Eastwood, W. J., Roberts, N., and Lamb, H. F. (1998). Palaeoecological and Archaeological Evidence for Human Occupance in Southwest Turkey: The BeyÅŸehir Occupation Phase. Anatolian Studies 48, 69-86.

Einsele, G., Chough, S. K., and Shiki, T. (1996). Depositional events and their records- an introduction. Sedimentary Geology 104, 1-9.

El-Daoushy, F. (1988). A summary on the lead-210 cycle in nature and related applications in Scandinavia. Environment International 14, 305-319.

El-Hames, A.S., Richards, K.S. (1998). An integrated, physically based model for arid region flash flood prediction capable of simulating dynamic transmission loss. Hydrological Processes 12, 1219-1232.

Enzel, Y., Ely, L. L., Mishra, S., Ramesh, R., Amit, R., Lazar, B., Rajaguru, S. N., Baker, V. R., and Sandler, A. (1999). High-Resolution Holocene Environmental Changes in the Thar Desert, Northwestern India. Science 284, 125-128.

Faegri, K., and Iversen, J. (1989). "Textbook of pollen analysis." Wiley, Chichester.

Farhoudi, G., and Karig, D. E. (1977). Makran of Iran and Pakistan as an active arc system. Geology 5, 664-668.

Fleitmann, D., Burns, S. J., Mudelsee, M., Neff, U., Kramers, J., Mangini, A., and Matter, A. (2003). Holocene forcing of the Indian monsoon recorded in a stalagmite from Southern Oman. Science 300, 1737-1739.

Fleitmann, D., Burns, S. J., Mangini, A., Mudelsee, M., Kramers, J., Villa, I., Neff, U., Al-Subbary, A. A., Buettner, A., Hippler, D., and Matter, A. (2007). Holocene ITCZ and Indian monsoon dynamics recorded in stalagmites from Oman and Yemen (Socotra). Quaternary Science Reviews 26, 170-188.

Flynn, W. W. (1968). The determination of low levels of polonium-210 in environmental materials. Analytica Chimica Acta 43, 221-227.

Francis, C. W., Chesters, G., and Haskin, L. A. (1970). Determination of ^{210}Pb mean residence time in the atmosphere. Environmental Science and Technology 4, 586-589.

French, P. W., Allen, J. R. L., and Appleby, P. G. (1994). 210-Lead dating of a modern period saltmarsh deposit from the Severn Estuary (Southwest Britain), and its implications. Marine Geology 118, 327-334.

Fritz, H. M., Blount, C. D., Albusaidi, F. B., and Al-Harthy, A. H. M. (2010). Cyclone Gonu storm surge in Oman. Estuarine, Coastal and Shelf Science 86, 102-106.

Fuchs, M., and Buerkert, A. (2008). A 20 ka sediment record from the Hajar Mountain range in N-Oman, and its implication for detecting arid-humid periods on the southeastern Arabian Peninsula. Earth and Planetary Science Letters 265, 546-558.

Furumoto, M., Fukao, Y. (1985). Hierarchy in earthquake size distribution. Physics of the Earth and Planetary Interiors 37, 149-168.

Gadgil, S. (2003). The Indian Monsoon and its variability. Annual Reviews of Earth and Planetary Sciences 31, 429-467.

Gäggeler, H., von Gunten, H. R., and Nyffeler, U. (1976). Determination of ^{210}Pb in lake sediments and in air samples by direct gamma-ray measurement. Earth and Planetary Science Letters 33, 119-121.

Gale, S. J. (2009). Dating the recent past. Quaternary Geochronology 4, 374-377.

Gasse, F., and Van Campo, E. (1994). Abrupt post-glacial climate events in West Asia and North Africa monsoon domains. Earth and Planetary Science Letters 126, 435-456.

Gasse, F. (2000). Hydrological changes in the African tropics since the last glacial maximum. Quaternary Science Reviews 19, 189-211.

Gasse, F., and Van Campo, E. (2001). Late Quaternary environmental changes from a pollen and diatom record in the southern tropics (Lake Tritrivakely, Madagascar). Palaeogeography,Palaeoclimatology,Palaeoecology 167, 287-308.

Gebauer, J., Luedeling, E., Hammer, K., Nagieb, M., and Buerkert, A. (2007). Mountain oases in northern Oman: An environment for evolution and in situ conservation of plant genetic resources. Genetic Resources and Crop Evolution 54, 465-481.

Ghazanfar, S. A. (2003). "Flora of the Sultanate of Oman. Vol. 1: Piperaceae to Primulaceae." Scripta Botanica Belgica.

Godwin, H. (1962). Half-life of radiocarbon. Nature 195, 984.

Gordon, R. G., and Demets, C. (1989). Present-day motion along the Owen fracture zone and Dalrymple trough in the Arabian Sea. Journal of Geophysical Research 94, 5560-5570.

Goudie, A. S., Parker, A. G., Bull, P. A., White, K., and Al-Farraj, A. (2000). Desert loess in Ras Al Khaimah, United Arab Emirates. Journal of Arid Environments 46, 123-135.

Grando, G., and McClay, K. (2007). Morphotectonics domains and structural styles in the Makran accretionary prism, offshore Iran. Sedimentary Geology 196, 157-179.

Gründlingh, M. L. (1985). Occurrence of Red Sea water in the southwester Indian Ocean. Journal of Physical Oceanography 15, 207-212.

Guo, Z., Petit-Maire, N., and Kröpelin, S. (2000). Holocene non-orbital climatic events in present-day arid areas of northern Africa and China. Global and Planetary Change 26, 97-103.

Gupta, A. K., Anderson, D. M., and Overpeck, J. T. (2003). Abrupt changes in the Asian southwest monsoon during the Holocene and their links to the North Atlantic Ocean. Nature 421, 354-357.

Gupta, R. S., and Naqvi, S. W. A. (1984). Chemical oceanography of the Indian Ocean, north of the equator. Deep Sea Research Part A. Oceanographic Research Papers 31, 671-706.

He, Q., and Walling, D. E. (1996). Use of fallout Pb-210 measurements to investigate longer-term rates and patterns of overbank sediment deposition on the floodplains of lowland rivers. Earth Surface Processes and Landforms 21, 141-154.

Hedges, R. E. M. (1992). Sample treatment strategies in radiocarbon dating. In "Radiocarbon After Four Decades: an Interdisciplinary Perspective." (R. E. Taylor, A. Long, and R. S. Kra, Eds.), pp. 165-183. Springer, New York.

Heller, F., Shen, C. D., Beer, J., Liu, X. M., Liu, T. S., Bronger, A., Suter, M., and Bonani, G. (1993). Quantitative estimates of pedogenic ferromagnetic mineral formation in Chinese loess and palaeoclimatic implications. Earth and Planetary Science Letters 114, 385-390.

Heidarzadeh, M., Pirooz, M. D., Zaker, N. H., Yalciner, A. C., Mokhtari, M., and Esmaeily, A. (2008). Historical tsunami in the Makran Subduction Zone off the southern coasts of Iran and Pakistan and results of numerical modeling. Ocean Engineering 35, 774-786.

Hoek, W. Z. (2001). Vegetation response to the ~14.7 and ~11.5 ka cal. BP climate transitions: is vegetation lagging climate? Global and Planetary Change 30, 103-115.

Honjo, S., Weller, R. (1997). Monsoon winds and carbon cycles in the Arabian Sea. Oceanus 40, 24-28.

Hooghiemstra, H., and Agwu, C. O. C. (1988). Changes in the vegetation and trade winds in equatorial northwest Africa 140,000-70,000 yr B.P. as deduced from two marine pollen records. Palaeogeography, Palaeoclimatology, Palaeoecology 66, 173-184, 193-204, 211-213.

Hooghiemstra, H., Lézine, A.-M., Leroy, S. A. G., Dupont, L., and Marret, F. (2006). Late Quaternary palynology in marine sediments: A synthesis of the understanding of pollen distribution patterns in the NW African setting. Quaternary International 148, 29-44.

Hounslow, M. W., and Maher, B. A. (1999). Source of the climate signal recorded by magnetic susceptibility variations in Indian Ocean sediments. Journal of Geophysical Research B: Solid Earth 104, 5047-5061.

Hua, Q. (2009). Radiocarbon: A chronological tool for the recent past. Quaternary Geochronology 4, 378-390.

Ivory, S. J., and Lézine, A.-M. (2009). Climate and environmental change at the end of the Holocene Humid Period: A pollen record off Pakistan. Comptes Rendus Geosciences 341, 760-769.

Jackson, J., and McKenzie, D. (1984). Active tectonics of the Alpine- Himalayan Belt between western Turkey and Pakistan. Geophysical Journal - Royal Astronomical Society 77, 185-264.

Johnson, G. C., Warren, B. A., and Olson, D. B. (1991a). Flow of bottom water in the Somali Basin. Deep Sea Research Part A, Oceanographic Research Papers 38, 637-652.

Johnson, G. C., Warren, B. A., and Olson, D. B. (1991b). A deep boundary current in the Arabian Basin. Deep Sea Research Part A, Oceanographic Research Papers 38, 653-661.

Jull, A. J. T., and Burr, G. S. (2006). Accelerator mass spectrometry: Is the future bigger or smaller? Earth and Planetary Science Letters 243, 305-325.

Kazancı, N., Leroy, S., Ileri, Ö., Emre, Ö., Kibar, M., and Öncel, S. (2004). Late Holocene erosion in NW Anatolia from sediments of Lake Manyas, Lake Ulubat and the southern shelf of the Marmara Sea, Turkey. CATENA 57, 277-308.

Koide, M., Soutar, A., and Goldberg, E. D. (1972). Marine geochronology with ^{210}Pb. Earth and Planetary Science Letters 14, 442-446.

Koide, M., Bruland, K. W., and Goldberg, E. D. (1973). Th-228/Th-232 and Pb-210 geochronologies in marine and lake sediments. Geochimica et Cosmochimica Acta 37, 1171-1187.

Kortekaas, S., (2002). Tsunamis, storms and earthquakes: distinguishing coastal flooding events. Coventry University.

Kortekaas, S., and Dawson, A. G. (2007). Distinguishing tsunami and storm deposits: An example from Martinhal, SW Portugal. Sedimentary Geology 200, 208-221.

Krishna, M. K. (2009). Intensifying tropical cyclones over the North Indian Ocean during summer monsoon--Global warming. Global and Planetary Change 65, 12-16.

Krishnaswamy, S., Lal, D., Martin, J. M., and Meybeck, M. (1971). Geochronology of lake sediments. Earth and Planetary Science Letters 11, 407-414.

Kröpelin, S., Verschuren, D., Lézine, A.-M., Eggermont, H., Cocquyt, C., Francus, P., Cazet, J.-P., Fagot, M., Rumes, B., Russell, J. M., Darius, F., Conley, D. J., Schuster, M., Von Suchodoletz, H., and Engstrom, D. R. (2008). Climate-driven ecosystem succession in the Sahara: The past 6000 years. Science 320, 765-768.

Kuhrt, A., Sherwin-White, S., (1993). From Samarkhand to Sardis. A new approach to the Seleucid empire, London.

Kutzbach, J. E., and Street-Perrott, F. A. (1985). Milankovitch forcing of fluctuations in the level of tropical lakes from 18 to 0 kyr BP. Nature 317, 130-134.

Laane, J. L., and Chen, W. P. (1988). The Makran earthquake of 1983 April 18: A possible analogue to the Puget Sound earthquake of 1965? Geophysical Journal International 98.

Lanfumey, V., (2008). 'Influence des Moussons sur la sedimentation profonde de la marge Pakistanaise'. Bordeux University, MSc thesis.

Lee, H. J., and Clausner, J. E. (1979). Seafloor soil sampling and geotechnical parameter determination-Handbook. In "Civil Engineering Laboratory Report." Port Hueneme, CA

Leonard, J. (1993). On the Plant "Associations" Mentioned in Iran by M. Zohary. Bulletin du Jardin botanique national de Belgique / Bulletin van de National Plantentuin van België 62, 113-118.

Leroy, S.A.G., Kazancı, N., Ileri, Ö., Kibar, M., Emre, O., McGee, E., and Griffiths, H. I. (2002). Abrupt environmental changes within a late Holocene lacustrine sequence south of the Marmara Sea (Lake Manyas, N-W Turkey): possible links with seismic events. Marine Geology 190, 531-552.

Leroy, S.A.G., Marret, F., Gibert, E., Chalié, F., Reyss, J. L., and Arpe, K. (2007). River inflow and salinity changes in the Caspian Sea during the last 5500 years. Quaternary Science Reviews 26, 3359-3383.

Leroy, S.A.G., Boyraz, S., and Gürbüz, A. (2009). High-resolution palynological analysis in Lake Sapanca as a tool to detect recent earthquakes on the North Anatolian Fault. Quaternary Science Reviews 28, 2616-2632.

Leroy, S.A.G. (2010). Pollen analysis of core DS7-1SC (Dead Sea) showing intertwined effects of climatic change and human activities in the Late Holocene. Journal of archaeological science 37, 306-316.

Leroy, S. A. G., Marco, S., Bookman, R., and Miller, C. S. (2010). Impact of earthquakes on agriculture during the Roman-Byzantine period from pollen records of the Dead Sea laminated sediment. Quaternary Research 73, 191-200.

Lézine, A. M., and Hooghiemstra, H. (1990). Land-sea comparisons during the last glacial-interglacial transition: pollen records from West Tropical Africa. Palaeogeography, Palaeoclimatology, Palaeoecology 79, 313-331.

Lézine, A. M., and Vergnaud-Grazzini, C. (1993). Evidence of forest extension in West Africa since 22,000 BP: A pollen record from the eastern tropical Atlantic. Quaternary Science Reviews 12, 203-210.

Lézine, A. M. (1997). Evolution of the West African mangrove during the late Quaternary: a review, . Géographie Physique et Quaternaire.

Lézine, A.-M., Saliège, J.-F., Robert, C., Wertz, F., and Inizan, M.-L. (1998). Holocene Lakes from Ramlat as-Sab'atayn (Yemen) Illustrate the Impact of Monsoon Activity in Southern Arabia. Quaternary Research 50, 290-299.

Lézine, A.-M., Saliège, J.-F., Mathieu, R., Tagliatela, T.-L., Mery, S., Charpentier, V., and Cleuziou, S. (2002). Mangroves of Oman during the late Holocene; climatic implications and impact on human settlements. Vegetation History and Archaeobotany 11, 221-232.

Lézine, A.-M., Tiercelin, J. J., Robert, C., Saliège, J.-F., Cleuziou, S., Inizan, M.-L., and Braemer, F. (2007). Centennial to millennial-scale variability of the Indian monsoon during the early Holocene from a sediment, pollen and isotope record from the desert of Yemen. Palaeogeography, Palaeoclimatology, Palaeoecology 243, 235-249.

Lézine, A.-M. (2009). Timing of vegetation changes at the end of the Holocene Humid Period in desert areas at the northern edge of the Atlantic and Indian monsoon systems. Comptes Rendus Geosciences 341, 750-759.

Lézine, A.-M., Robert, C., Cleuziou, S., Inizan, M.-L., Braemer, F., Saliège, J.-F., Sylvestre, F., Tiercelin, J.-J., Crassard, R., Méry, S., Charpentier, V., and Steimer-Herbet, T. (2010). Climate change and human occupation in the Southern Arabian lowlands during the last deglaciation and the Holocene. Global and Planetary Change.

Lisitzen, E. (1974). "Sea-level changes." (in Heidarzadez et al., 2008).

Lowe, D. R. (1982). Sediment gravity flows: II. Depositional models with special reference to the deposits of high-density turbidity currents. Journal of Sedimentary Petrology 52, 279-297.

Lückge, A., Doose-Rolinski, H., Khan, A. A., Schulz, H., and von Rad, U. (2001). Monsoonal variability in the northeastern Arabian Sea during the past 5000 years: geochemical evidence from laminated sediments. Palaeogeography, Palaeoclimatology, Palaeoecology 167, 273-286.

Lund-Hansen, L.C., (1991). Sedimentation and sediment accumulation rates in a low-energy embayment. Journal of Coastal Research 7(4), 969-980.

Maher, B. A., Thompson, R., and Zhou, L. P. (1994). Spatial and temporal reconstructions of changes in the Asian palaeomonsoon: A new mineral magnetic approach. Earth and Planetary Science Letters 125, 461-471.

Maley, J., Livingstone, D. A., Giresse, P., Brenac, P., Kling, G., Stager, C., Thouveny, N., Kelts, K., Haag, M., Fournier, M., Bandet, Y., Williamson, D., and Zogning, A. (1991). West Cameroon Quaternary lacustrine deposits: preliminary results. Journal of African Earth Sciences 12, 147-157.

Marren, P.M., (1994). Criteria for distinguishing high magnitude flood events in the proglacial fluvial sedimentary record. *he Extremes of the Extremes:*

Extraordinary Floods (Proceedings of a symposium held at Reykjavik. Iceland. July 2000). IAHS Publ. no. 271, 237

Marret, F. (1994). Distribution of dinoflagellate cysts in recent marine sediments from the east Equatorial Atlantic (Gulf of Guinea). Review of Palaeobotany and Palynology 84, 1-22.

Marret, F., and Turon, J.-L. (1994). Paleohydrology and paleoclimatology off Northwest Africa during the last glacial-interglacial transition and the Holocene: Palynological evidences. Marine Geology 118, 107-117.

Marret, F., and Zonneveld, K. A. F. (2003). Atlas of modern organic-walled dinoflagellate cyst distribution. Review of Palaeobotany and Palynology 125, 1-200.

Mazzullo, J. M., Meyer, A., and Kidd, R. (1988). New sediment classification scheme for the Ocean Drilling Program. In "Handbook for Shipboard Sedimentologists, ODP Tech. note." (J. Mazzullo and A.G. Graham, Ed.).

McCarthy, F. M. G., and Mudie, P. J. (1998). Oceanic pollen transport and pollen:dinocyst ratios as markers of late Cenozoic sea level change and sediment transport. Palaeogeography, Palaeoclimatology, Palaeoecology 138, 187-206.

McCreary, J. P., and Kundu, P. K. (1989). A numerical investigation of sea surface temperature variability in the Arabian Sea. Journal of Geophysical Research 94.

McSaveney, M. J., Goff, J. R., Darby, D. J., Goldsmith, P., Barnett, A., Elliott, S., and Nongkas, M. (2000). The 17 July 1998 tsunami, Papua New Guinea: evidence and initial interpretation. Marine Geology 170, 81-92.

Middleton, G. V., and Hampton, M. A. (1973). Sediment gravity flows: mechanics of flow and deposition. In "Turbidites and Deep Water Sedimentation." (G. V. Middleton, Bouma, A.H, Ed.), pp. 1-38. Society of Economic Paleontologists and Mineralogists.

Modarres, R., Rodrigues, V.P. (2007). Rainfall trends in arid and semi-arid regions of Iran. Journal of Arid Environments 70, 344-355.

Morrill, C., Overpeck, J. T., and Cole, J. E. (2003). A synthesis of abrupt changes in the Asian summer monsoon since the last deglaciation. Holocene 13, 465-476.

Morton, R. A., Gelfenbaum, G., and Jaffe, B. E. (2007). Physical criteria for distinguishing sandy tsunami and storm deposits using modern examples. Sedimentary Geology 200, 184-207.

Murty, T., and Bapat, A. (1999). Tsunamis on the coastlines of India. Science of Tsunami Hazards 17, 167-172.

Naidu, P. D. (1993). Distribution patterns of Recent planktonic foraminifera in surface sediments of the western continental margin of India. Marine Geology 110, 403-418.

Neff, U., Burns, S. J., Mangini, A., Mudelsee, M., Fleitmann, D., and Matter, A. (2001). Strong coherence between solar variability and the monsoon in Oman between 9 and 6 kyr ago. Nature 411, 290-293.

Neumann, F. H., Kagan, E. J., Leroy, S. A. G., and Baruch, U. (2010). Vegetation history and climate fluctuations on a transect along the Dead Sea west shore and their impact on past societies over the last 3500 years. Journal of Arid Environments 74, 756-764.

Nevissi, A. E., Shott, G. J., and Crecelius, E. A. (1989). Comparison of two gravity coring devices for sedimentation rate measurement by ^{210}Pb dating techniques. Hydrobiologia 179, 261-269.

New, M., Hulme, M., Jones, P.D. (2000). Representing twentieth century space-time climate variability. Part 2: development of 1901-96 monthly grids of terrestrial surface climate. Journal of Climate 13, 2217-2238.

Norman, W. R., Shayya, W. H., Al-Ghafri, A. S., and McCann, I. R. (1997). Aflaj irrigation and on-farm water management in northern Oman. Irrigation and Drainage Systems 12, 35-48.

Nowaczyk, N. R. (2001). Logging of Magnetic Susceptibility. In "Tracking Environmental Changes Using Lake Sediments, Basin Analysis, Coring, and Chronological Techniques." (W. M. Last, and J. P. Smol, Eds.), pp. 155-170. Kluwer Academic Publishers.

Oatham, M. P., Nicholls, M. K., and Swingland, I. R. (1995). Manipulation of vegetation communities on the Abu Dhabi rangelands. I. The effects of irrigation and release from long-term grazing. Biodiversity and Conservation 4, 696-709.

Overpeck, J., Anderson, D., Trumbore, S., and Prell, W. (1996). The SW Indian Monsoon over the last 18,000 years. Climate Dynamics 12, 213-225.

Page, W. D., Alt, J. N., Cluff, L. S., and Plafker, G. (1979). Evidence for the recurrence of large-magnitude earthquakes along the Makran coast of Iran and Pakistan. Tectonophysics 52, 533-547.

Pak, A., and Farajzadeh, M. (2007). Iran's Integrated Coastal Management plan: Persian Gulf, Oman Sea, and southern Caspian Sea coastlines. Ocean & Coastal Management 50, 754-773.

Parker, A. G., Eckersley, L., Smith, M. M., Goudie, A. S., Stokes, S., Ward, S., White, K., and Hodson, M. J. (2004). Holocene vegetation dynamics in the northeastern Rub' al-Khali desert, Arabian Peninsula: a phytolith, pollen and carbon isotope study. Journal of Quaternary Science 19, 665-676.

Parker, G., Fukushima, Y., and Pantin, H. M. (1986). Self-accelerating turbidity currents. Journal of Fluid Mechanics 171, 145-181.

Pearson, J. E., and Jones, G. E. (1966). Soil concentrations of "emanating radium-226" and the emanation of radon-222 from soils and plants. Tellus 18, 655-662.

Peirson, D. H., Cambray, R. S., and Spicer, S. (1966). Lead-210 and polonium-210 in the atmosphere. Tellus 18, 427-433.

Platt, J. P., Leggett, J. K., Young, J., Raza, H., and Alam, S. (1985). Large-scale sediment underplating in the Makran accretionary prism, southwest Pakistan. Geology 13, 507-511.

Pollastro, R., Persits, F., Steinshouer, D. (1997). Maps showing geology, oil and gas fields and geologic provinces of Iran. U.S Geological Survey open-file report 97-470.

Qasim, S. Z. (1982). Oceanography of the northern Arabian Sea. Deep Sea Research Part A. Oceanographic Research Papers 29, 1041-1068.

Quittmeyer, R. C., and Jacob, K. H. (1979). Historical and modern seismicity of Pakistan, Afghanistan, northwestern India, and southeastern Iran. Bulletin of the Seismological Society of America 69, 773-823.

Quraishee, G. S. (1984). Circulation in the north Arabian Sea at Murray Ridge during S.W. monsoon. Deep Sea Research Part A. Oceanographic Research Papers 31, 651-654, IN1-IN2, 655-664.

Rampen, S. W., Schouten, S., Koning, E., Brummer, G.-J. A., and Sinninghe Damsté, J. S. (2008). A 90 kyr upwelling record from the northwestern Indian Ocean using a novel long-chain diol index. Earth and Planetary Science Letters 276, 207-213.

Rastogi, B. K., and Jaiswal, R. K. (2006). A catalog of tsunamis in the Indian Ocean. Science of Tsunami Hazards 25, 128-143.

Reale, O., and Shukla, J. (2000). Modeling the effects of vegetation on Mediterranean climate during the Roman Classical Period: Part II. Model simulation. Global and Planetary Change 25, 185-214.

Reille, M. (1995). "Pollen et Spores D'Europe et D'Afrique du Nord." Laboratoire de Botanique historique et Palynologie, Marseille.

Reichart, G.J., Lourens, L.J., Zachariasse, W.J. (1998). Temporal variability in the northern Arabian Sea Oxygen Minimum Zone (OMZ) during the last 225,000 years. Palaeoceanography 13, 607-621.

Reimer, P.J, Baillie, M.G.L., Bard, E., Bayliss, A., Warren Beck, J., Bertrang, C.J.H., Blackwell, P.G., Buck, C.E., Burr, G.S., Cutlers, K.B., Damon, P.E., Edwards, R.L., Fairbanks, R.G., Friedrich, M., Guilderson, T.P., Hogg, A.G.,

Hughen, K.A, Kromer, B., McCormac, G., Manning, S, Stuiver, M., Talamo, S., Taylot, F.W., van der Plicht, J., Wayhenmeyer, C.E. (2004). INTCAL04 Terrestrial radiocarbon age calibration, 0-26 cal kyr BP. RADIOCARBON, 46, 1029–1058

Reynolds, M. R. (1993). Physical oceanography of the Gulf, Strait of Hormuz, and the Gulf of Oman--Results from the Mt Mitchell expedition. Marine Pollution Bulletin 27, 35-59.

Ritchie, J. C., and McHenry, J. R. (1990). Application of radioactive fallout cesium-137 for measuring soil erosion and sediment accumulation rates and patterns: A review. Journal of Environmental Quality 19, 215-233.

Robbins, J. A., and Edgington, D. N. (1975). Determination of recent sedimentation rates in Lake Michigan using Pb-210 and Cs-137. Geochimica et Cosmochimica Acta 39, 285-304.

Roberts, N. (1990). Human induced landscape change in south and southwest Turkey during the later Holocene. In "Man's role in the shaping of the eastern Mediterranean landscape." (S. Bottema, G. Entjes-Nieborg, and W. van Zeist, Eds.), pp. 53-67. Balkema, Rotterdam.

Roberts, T. J. (1991). "The birds of Pakistan: Vol 1." Oxford University Press.

Robinson, S. G. (1990). Applications for whole-core magnetic susceptibility measurements of deep-sea sediments: Leg 115 results. Proc., scientific results, ODP, Leg 115, Mascarene Plateau, 737-771.

Robinson, S. G., Maslin, M. A., and McCave, I. N. (1995). Magnetic susceptibility variations in Upper Pleistocene deep-sea sediments of the NE Atlantic: implications for ice rafting and palaeocirculation at the last glacial maximum. Paleoceanography 10, 221-250.

Robinson, W. O. (1927). The determination of organic matter in soil by means of hydrogen peroxide. Journal of Agricultural Research 34, 339-356.

Robson, T. E. I. (1933). Arrian: Anabasis Alexandri: Book VIII (Indica). Courtesy of the Internet Ancient History Sourcebook. .

Rochon, A., Vernal, A., de Turon, J.-L., Matthiessen, J., and Head, M. J. (1999). "Distribution of recent dinoflagellate cysts in surface sediments from the North Atlantic Ocean and adjacent seas in relation to sea-surface parameters."

Rothwell, R. G., and Rack, F. R. (2006). New techniques in sediment core analysis: an introduction. Geological Society, London, Special Publications 267, 1-29.

Rull, V. (1987). A note on pollen counting in palaeoecology. Pollen et Spores XXIX, 471-480.

Sachs, L., and Raymond, S. O. (1965). A new unattached sediment sampler. Journal of Marine Research 23, 44-53.

Sadeghi, A.R., Kamgar-Haghighi, A.A., Sepaskahah, A.R., Khalili, D., Zand-Parsa, S. (2002). Journal of Arid Environments 50, 333-341.

Sandgren, P., and Snowball, I. (2002). Application of Mineral Magnetic Techniques to Paleolimnology. In "Tracking Environmental Change Using Lake Sediments." pp. 217-237.

Schott, F., Swallow, J.C., Fieux, M. (1990). The Somali Current at the equator: annual cycle of currents and transports in the upper 1000 m and connection to neighbouring latitudes. Deep Sea Research 37, 1825-1848.

Schumacher, B. A. (2002). "Methods for the determination of total organic carbon (TOC) in soil and sediments.", Ecological Risk Assessments Support Centre.

Schulz, H., Von Rad, U., Von Stackelberg, U. (1996). Laminated sediments from the oxygen minimum zone of the northeastern Arabian Sea. In: Kemp, A.E.S. Palaeoclimatology and Palaeoceanography from Laminated Sediments. Geological Society Special Publications 116, 185-207.

Schwab, M. J., Werner, P., Dulski, P., McGee, E., Nowaczyk, N. R., Bertrand, S., and Leroy, S. A. G. (2009). Palaeolimnology of Lake Sapanca and identification of historic earthquake signals, Northern Anatolian Fault Zone (Turkey). Quaternary Science Reviews 28, 991-1005.

Seilacher, A. (1973). Biostratinomy: the sedimentology of biologically standardized particles. In "Evolving Concepts in Sedimentology " (R. N. Ginsburg, Ed.), pp. 159-177. John Hopkins University Studies in Geology, Baltimore.

Sen Gupta, R., Naqvi, S.W.A. (1984). Chemical oceanography of the Indian Ocean, north of the equator. Deep-Sea Research 31, 671-706.

Shackleton, N. J., Backman, J., Zimmerman, H., Kent, D. V., Hall, M. A., Roberts, D. G., Schnitker, D., Baldauf, J. G., Desprairies, A., Homrighausen, R., Huddlestun, P., Keene, J. B., Kaltenback, A. J., Krumsiek, K. A. O., Morton, A. C., Murray, J. W., and Westbergsmith, J. (1984). Oxygen isotope calibration of the onset of ice-rafting and history the of glaciation in the North Atlantic region. Nature 307, 620-623.

Shanahan, T. M., Overpeck, J. T., Anchukaitis, K. J., Beck, J. W., Cole, J. E., Dettman, D. L., Peck, J. A., Scholz, C. A., and King, J. W. (2009). Atlantic forcing of persistent drought in West Africa. Science 324.

Shanmugam, G. (1997). The Bouma Sequence and the turbidite mind set. Earth-Science Reviews 42, 201-229.

Shapiro, G. I., and Meschanov, S. L. (1991). Distribution and spreading of Red Sea Water and salt lens formation in the northwest Indian Ocean. Deep Sea Research Part A, Oceanographic Research Papers 38, 21-34.

Shearman, D. J., Walker, G. P. L., Booth, B., and Falcon, N. L. (1976). The Geological Evolution of Southern Iran: The Report of the Iranian Makran Expedition. The Geographical Journal 142, 393-410.

Shichi, K., Kawamuro, K., Takahara, H., Hase, Y., Maki, T., and Miyoshi, N. (2007). Climate and vegetation changes around Lake Baikal during the last 350,000 years. Palaeogeography, Palaeoclimatology, Palaeoecology 248, 357-375.

Shiki, T. (1996). Reading of the trigger records of sedimentary events--a problem for future studies. Sedimentary Geology 104, 249-255.

Shiki, T., Cita, M. B., and Gorsline, D. S. (2000). Sedimentary features of seismites, seismo-turbidites and tsunamiites--an introduction. Sedimentary Geology 135, vii-ix.

Shimmield, G. B., Mowbray, S. R., and Weedon, G. P. (1990). A 350 ka history of the Indian Southwest Monsoon - evidence from deep-sea cores, northwest Arabian Sea. Transactions - Royal Society of Edinburgh: Earth Sciences 81, 289-299.

Singh, G., Joshi, R. D., Chopra, S. K., and Singh, A. B. (1974). Late Quaternary History of Vegetation and Climate of the Rajasthan Desert, India. Philosophical Transactions of the Royal Society of London. B, Biological Sciences 267, 467-501.

Singh, G., Wasson, R. J., and Agrawal, D. P. (1990). Vegetational and seasonal climatic changes since the last full glacial in the Thar Desert, northwestern India. Review of Palaeobotany and Palynology 64, 351-358.

Singh, O. P., Ali Khan, T. M., and Rahman, M. S. (2001). Probable reasons for enhanced cyclogenesis in the Bay of Bengal during July-August of ENSO years. Global and Planetary Change 29, 135-147.

Spalding, M., Blasco, F., and Field, C. (1997). "World Mangrove Atlas." Cambridge Samara Publication Company, Cambridge.

Stein, S., Okal, E.A. (2007). Ultralong period seismic study of the December 2004 Indian Ocean earthquake and implications for regional tectonics and the subduction processes. Bulletin of the Seismological Society of America 97, 279-295.

Stockmarr, J. (1972). Tablets with spores used in absolute pollen analysis. Pollen et Spore XIII, 615-621.

Stoneley, R. (1974). Evolution of the continental margins bounding a former Tethys. In "The geology of continental margins." (C. A. Burk, and C. L. Drake, Eds.), pp. 889-903. Springer, New York.

Stuiver, M. R., P.J. Bard, E. Beck, J.W. Burr, G.S. Hughen, K.A. Kromer, B. McCormac, G. van der Plicht, J. Spurk, M. (1998). INTCAL98 Radiocarbon Age Calibration, 24000-0 cal BP. Radiocarbon 40, 1041-1083

Sun, D., Bloemendal, J., Rea, D.K., Vandenberghe, J., Jiang, Z., An, Z., Su, R. (2002). Grain size distribution function of polymodal sediments in hydraulic and Aeolian environments and numerical partitioning of the sedimentary components. Sedimentary Geology 152, 263-277.

Swain, A. M., Kutzbach, J. E., and Hastenrath, S. (1983). Estimates of holocene precipitation for Rajasthan, India, based on pollen and lake-level data. Quaternary Research 19, 1-17.

Synolakis, C.E. (2003). Tsunami and seiche. In: Chen, W.F., Scawthorn, C., Editors, Earthquake Engineering Handbook, CRS Press.

Synolakis, C. E., and Okal, E. A. (2005). 1992-2002: perspective on a decade of post-tsunami surveys. In "Tsunamis: Case studies and recent developments. ." (K. Satake, Ed.).

Talbot, M. R., Livingstone, D. A., Palmer, P. G., Maley, J., Melack, J. M., Delibrias, G., and Gulliksen, S. (1984). Preliminary results from sediment cores from Lake Bosumtwi, Ghana. Palaeoecology of Africa 16, 173-192.

Tappin, D. R. (2007). Sedimentary features of tsunami deposits -- Their origin, recognition and discrimination: An introduction. Sedimentary Geology 200, 151-154.

Taylor, R. E. (1987). "Radiocarbon Dating an Archaeological Perspective." Academic Press, London

Teasdale, P. (2005). "The Late Holocene evolution of coastal wetlands in Argyll, Western Scotland (radiometric dating and geochemical study)." Brunel University, PhD thesis.

Thamban, M., Purnachandra Rao, V., Schneider, R. R., and Grootes, P. M. (2001). Glacial to Holocene fluctuations in hydrography and productivity along the southwestern continental margin of India. Palaeogeography, Palaeoclimatology, Palaeoecology 165, 113-127.

Tuniz, C., Bird, J. R., Fink, D., and Herzog, G. F. (1998). "Accelerator Mass Spectrometry: Ultrasensitive Analysis for Global Science,." CRC Press.

Urban, B., and Buerkert, A. (2009). Palaeoecological analysis of a Late Quaternary sediment profile in northern Oman. Journal of Arid Environments 73, 296-305.

van Zeist, W., Woldring, H., and Stapert, D. (1975). Late Quaternary vegetation and climate of southwestern Turkey. Palaeohistoria 17, 55-143.

Van Zinderen Bakker Sr, E. M. (1982). African palaeoenvironments 18 000 yrs BP. Palaeoecology of Africa, vol. 15. Proc. 6th conference Southern African Society for Quaternary Research, Pretoria, 1981, 77-99.

Vernant, P., Nilforoushan, F., Hatzfeld, D., Abbasi, M.R., Vigny, C., Masson, F., Nankali, H., Martinod, J., Ashtiani, A., Bayer, R., Tavakoli, F., Chery, J. (2004). Present-day crustal deformation and plate kinematics in the middle east constrained by GPS measurements in Iran and Northern Oman. Geophysical Journal International 157, 381-398.

von Rad, U., Schaaf, M., Michels, K. H., Schulz, H., Berger, W. H., and Sirocko, F. (1999). A 5000-yr Record of Climate Change in Varved Sediments from the Oxygen Minimum Zone off Pakistan, Northeastern Arabian Sea. Quaternary Research 51, 39-53.

Von Rad, U., Schulz, H., Sonne 90 Scientific Party. (1995). Sampling the oxygen minimum zone off Pakistan: glacial-interglacial variations of anoxia and productivity (preliminary results, sonne 90 cruise). Marine Geology 125, 7-19.

Wang, D., and Zhao, H. (2008). Estimation of phytoplankton responses to Hurricane Gonu over the Arabian Sea based on ocean color data. Sensors 8, 4878-4893.

Webster, P. J., Magana, V. O., Palmer, T. N., Shukla, J., Tomas, R. A., Yanai, M., and Yasunari, T. (1998). Monsoons: Processes, predictability, and the prospects for prediction. Journal of Geophysical Research 103, 14451-14510.

Webster, P. J., Holland, G. J., Curry, J. A., and Chang, H.-R. (2005). Changes in Tropical Cyclone Number, Duration, and Intensity in a Warming Environment. Science 309, 1844-1846.

Weedon, G. P., and Shimmield, G. B. (1991). Late Pleistocene upwelling and productivity variations in the Northwestern Indian Ocean deduced from spectral analyses of geochemical data from sites 722 and 724. In "Proceedings of the Ocean Drilling Program, Scientific Results." (W. L. Prell, Ed.), pp. 431-440.

Weiss, H., Courty, M.-A., Wetterstrom, W., Guichard, F., Senior, L., Meadow, R., Curnow, A. (1993). The genesis and collapse of third millennium North Mesopotamian Civilization. Science 261, 295-1004.

White, F. (1983). The vegetation of africa Natural Resources Research. Natural Resources Research 20.

Wilkening, M. H. (1974). Radon-222 from the island of Hawaii: Deep soils are more important than lava fields or volcanoes. Science 183, 413-415.

Wyrtki, K. (1973). Physical oceanography of the Indian Ocean. In "The Biology of the Indian Ocean." (B. Zeitzschel, Ed.), pp. 18-36. Springer, Berlin.

Zachos, J., Pagani, M., Sloan, L., Thomas, E., and Billups, K. (2001). Trends, Rhythms, and Aberrations in Global Climate 65 Ma to Present. Science 292, 686-693.

Zhao, Y., Yu, Z., Chen, F., Zhang, J., and Yang, B. (2009). Vegetation response to Holocene climate change in monsoon-influenced region of China. Earth-Science Reviews 97, 242-256.

Zohary, M. (1973). "Geobotanical foundations of the Middle East: Vol 1." Gustav Fischer Verlag, Berlin.

Zonneveld, K. A. F. (1997a). Dinoflagellate cyst distribution in surface sediments from the Arabian Sea (northwestern Indian Ocean) in relation to temperature and salinity gradients in the upper water column. Deep Sea Research Part II: Topical Studies in Oceanography 44, 1411-1443.

Zonneveld, K. A. F. (1997b). New species of organic walled dinoflagellate cysts from modern sediments of the Arabian Sea (Indian Ocean). Review of Palaeobotany and Palynology 97, 319-337.

Zonneveld, K. A. F., and Jurkschat, T. (1999). Bitectatodinium spongium (Zonneveld, 1997) Zonneveld et Jurkschat, comb. nov. from modern sediments and sediment trap samples of the Arabian Sea (northwestern Indian Ocean): taxonomy and ecological affinity. Review of Palaeobotany and Palynology 106, 153-169.

Zuschin, M., Stachowitsch, M., and Stanton, R. J. (2003). Patterns and processes of shell fragmentation in modern and ancient marine environments. Earth-Science Reviews 63, 33-82.

Appendix I – Core photographs: OS34

Core OS34 (0 – 17 cm)

Core OS34 (18 – 35 cm)

Core OS34 (35 – 54 cm)

Core OS34 (54 – 74 cm)

Core OS34 (72 – 92 cm)

Appendix II – Core photographs: OS55

Core OS55 (0 – 19 cm)

Core OS55 (15 – 35 cm)

Core OS55 (24 – 42 cm)

Core OS55 (39 – 60 cm)

Core OS55 (56 – 77 cm)

Core OS55 (70 – 91 cm)

Appendix III – Core photographs: OS73

Core OS73 (0 – 16 cm)

Core OS73 (17 – 36 cm)

Core OS73 (35 – 55 cm)

Core OS73 (54 – 73 cm)

Core OS73 (71 – 91 cm)

Core OS73 (86 – 106 cm)

Core OS73 (105 – 127 cm)

Core OS73 (120 – 141 cm)

Appendix IV – Core photographs: OS84

Core OS84 (0 – 14 cm)
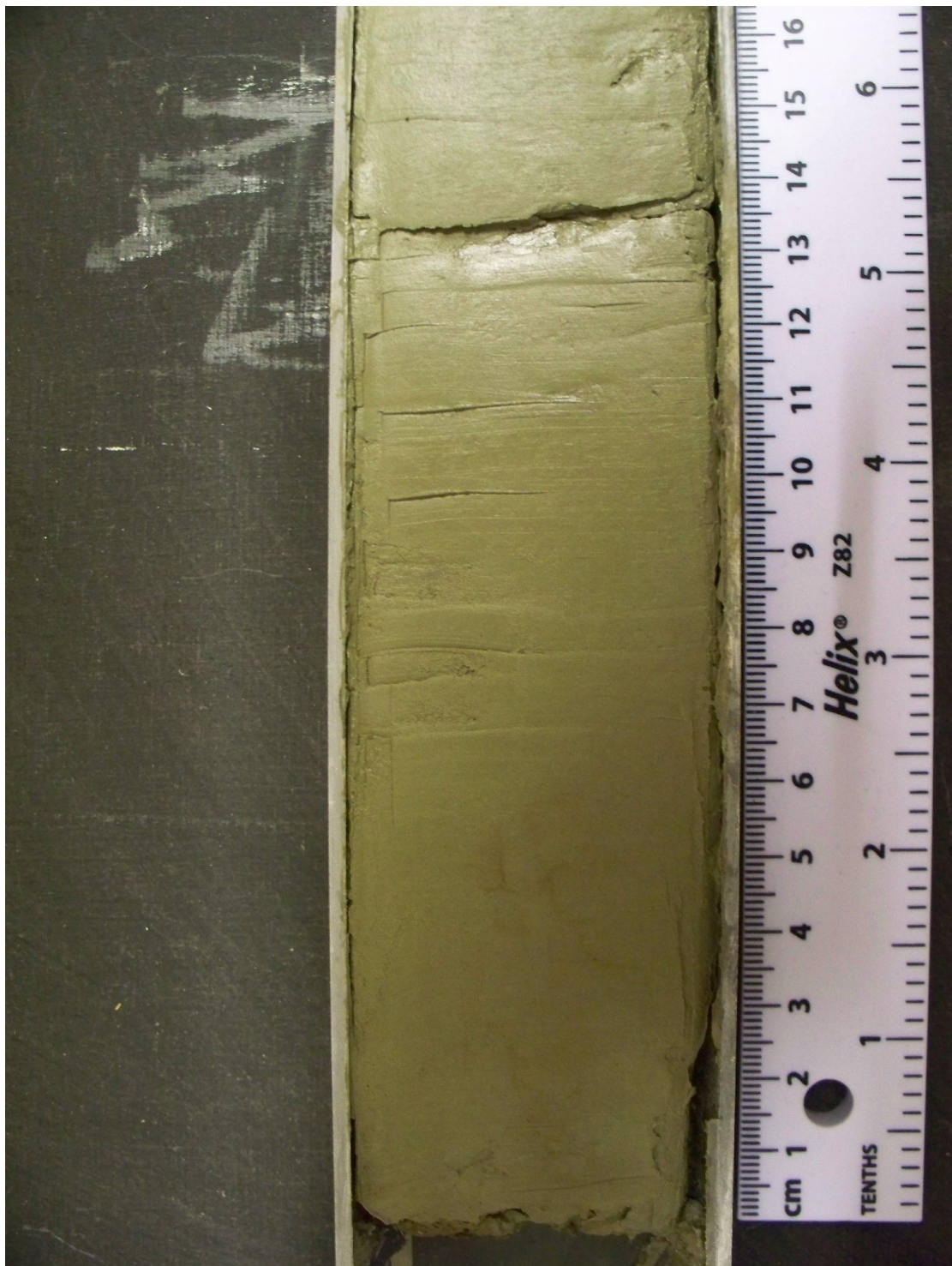
Core OS84 (13 - 32 cm)

Core OS84 (28 – 46 cm)

Core OS84 (40 – 58 cm)

Appendix V – Core photographs: OS94

Core OS94 (0 – 16 cm)

Core OS94 (16 – 35 cm)

Core OS94 (21 – 37 cm)